AGE-DEPENDENT CHANGES IN PROTEIN PHOSPHORYLATION: DIFFERENTIAL PROTEOMIC STUDIES IN RAT TISSUE.

by

G. S. Gerstenecker

B.S. in Chemistry, Southern Illinois University, 1991

M.S. in Pharmaceutical Chemistry, the University of Kansas, 2005

Submitted to the Department of Pharmaceutical Chemistry and the Faculty of the Graduate School of the University of Kansas in partial fulfillment of requirements for the degree of Doctor of Philosophy.

Committee Members(5):

_____
Chairperson

_____

_____

_____

_____

Date Defended: 20 October, 2009

This doctoral dissertation is dedicated to my eldest son Gottlieb.
I was inspired to reach for my goal, so that he might better grasp his own.

ACKNOWLEDGEMENTS

I need to begin by acknowledging several family members, all very close to me, who passed on during the course of this dissertation. While the loss of each person was a considerable setback, I had to honor their memory and complete what they had encouraged me to start. I miss my brother Mike, my father-in-law Frank and my mother Janice very much, but I will always cherish the lessons I learned from them.

I offer my heartfelt thanks to my research advisor, Dr. Christian Schöneich, who never gave up on me and showed considerable patience while I dealt with the aforementioned setbacks as well as others. I certainly learned a great deal working with him, and appreciate the many ways he has made me a better scientist.

I must thank Jim Bostick for introducing me to Professor Stobaugh, who both convinced me to come to the University of Kansas. I would never have taken the first step without their confidence in my success. I also must thank the faculty, staff and students who comprise the Department of Pharmaceutical Chemistry for ensuring that success.

I thank the past and current members of the Schöneich group and all of my collaborators at the University of Kansas including, but not limited to Elena Dremina, Victor Sharov, David Moore, Jianwen Fang, Todd Williams, and Nadya Galeva for their willingness to share their time and knowledge.

I must acknowledge my financial support which came from several sources, the Miriam Rosenfeld Scholarship, a grant from the NIH (AG025350), a grant from Pfizer and a brief tenure on the pre-doctoral training grant of the National Cancer Institute.

Without the members of my family, I never could have succeeded in this endeavor. My father Charles, my brothers Alan and Chuck and my mother-in-law Mary, all never failed to both support and encourage me. Finally, I need to acknowledge the tireless and selfless contributions made by my wife Lauri. She was ever my muse and without her support and devotion, this dissertation would not exist. She is my source of hope and truly the best part of me.

ABSTRACT

Protein phosphorylation is a reversible process that is involved in cellular growth, division and signaling. The mechanisms for protein phosphorylation can be significantly altered during the aging process. These alterations are responsible for various deleterious effects and have been associated with several age-related disease states.

In an effort to elucidate which mechanisms are altered during the aging process we have developed a series of proteomic methods to characterize phosphorylation differences between five month and thirty-four month old rats. Utilizing skeletal muscle and cerebellum tissue extracts from these animals we have performed two-dimensional polyacrylamide gel electrophoresis followed by image analysis of the patterns resulting from staining with both a phosphoprotein stain and a total protein stain and subsequent identification by nanoelectrospray MS/MS. We have also made an effort to understand these phosphorylation differences by exploring the impact of reactive oxygen species on protein phosphorylation in C2C12 myoblast cells.

TABLE OF CONTENTS

INDEX OF FIGURES

SCHEMES

INDEX OF TABLES

NON STANDARD ABBREVIATIONS

2D-PAGE	two- dimensional polyacrylamide gel electrophoresis
ACN	acetonitrile
FT-ICR	Fourier Transform - Ion Cyclotron Resonance
HPLC-MS/MS	high performance liquid chromatography – tandem mass spectrometry
IEF	isoelectric focusing
IMAC	immobilized metal affinity chromatography
IPG	immobilized pH gradient
KEGG	Kyoto Encyclopedia of Genes and Genomes
NSI-MS/MS	nanoelectrospray ionization tandem mass spectrometry
ROS	reactive oxygen species
SDS	sodium dodecyl sulfate
Ser	the amino acid serine
Thr	the amino acid threonine
Tyr	the amino acid tyrosine

Chapter One

A Review of Protein Phosphorylation, Aging Research and the Application to Phosphoproteomic Studies.

1. Introduction

Protein phosphorylation/dephosphorylation is generally accepted in the scientific community as playing a role in nearly every cellular function and drugs targeted at modulating phosphorylation/dephosphorylation events are in development for nearly every class of disease. The purpose of this dissertation is the discovery of proteins undergoing a change in their phosphorylation state due to aging and to provide novel targets for future research into the mechanisms and potential causes.

1.1 Protein Phosphorylation

The activities of many enzymes, membrane channels and other proteins are regulated by phosphorylation. Protein phosphorylation is a reversible process important for cellular signaling[1] and regulation[2] and can be found in virtually every metabolic process in eukaryotic cells including, but not limited to: transcriptional control, apoptosis, protein degradation, nuclear import and export and structural integrity. There are estimates that approximately 30% of all proteins encoded by the human genome are regulated by phosphorylation and dephosphorylation, and that there are more than 100,000 phosphorylation sites in the human proteome[3] making it the most abundant reversible covalent modification to proteins.

This ubiquitous post-translational protein modification is introduced by the catalytic action of protein kinases, which phosphorylate primarily protein serine (Ser) and threonine (Thr), but also tyrosine (Tyr) residues, as observed in **Figure 1**. The occurrence of Ser and Thr phosphorylation is far more frequent than Tyr phosphorylation, with Ser phosphorylation an order of magnitude more abundant than

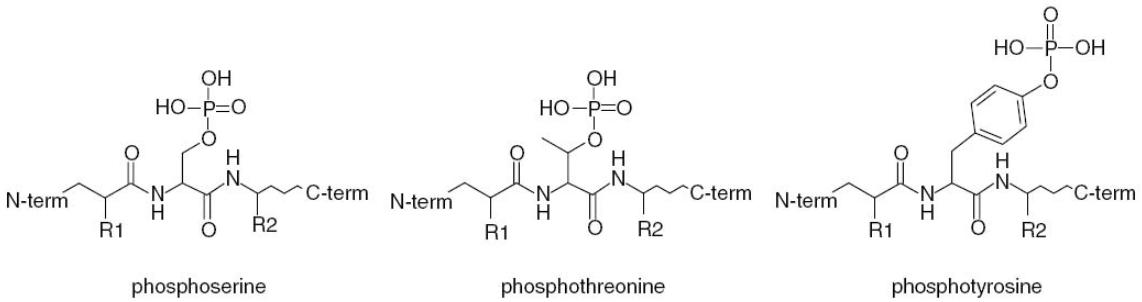

Figure 1. *Phosphorylated amino acid residues.*

Thr phosphorylation which is two orders of magnitude more abundant than Tyr phosphorylation.[4] The human genome encodes more than 500 different protein kinases[5] and at least as many phosphatases, including over 100 tyrosine phosphatases[6]. These enzymes are not only responsible for phosphorylation and dephosphorylation of other proteins, but are also phosphorylation targets. In principle, the extent of phosphorylation at a given site can be regulated by an alteration of the activities of substrate specific kinases and phosphatases.

The addition of the phosphate group can dramatically change the protein's conformation. This can subsequently alter the binding of ligands elsewhere on the protein, dramatically changing its activity through an allosteric effect. Removal of the phosphate group by a phosphatase returns the protein to its original conformation and restores its initial activity[7]. In this way, phosphorylation is an effective way of modulating the activity of proteins. Adding a single phosphoryl group adds two negative charges to a modified protein, since a phosphorylated amino acid is primarily di-basic at biological pH with pK_2 values between 5.5 and 5.9 for phosphoserine (pSer), phosphothreonine (pThr) and phosphotyrosine (pTyr) respectively[8-9]. The structural

implications resulting from the introduction of these negative charges include the possible disruption of the electrostatic interactions in the unmodified protein and the formation of new interactions. Both of these possibilities can potentially alter substrate binding and catalytic activity. A phosphate group can also form multiple hydrogen bonds and these bonds are directional, providing the opportunity for specific interactions with hydrogen-bond donors. Finally, the free energy of phosphorylation is very large; phosphorylation can change the conformational equilibrium between different states by the order of 10^4 making the structural changes seemingly irreversible[10].

An attached phosphate group can also form part of a structure that is directly recognized by binding sites of other proteins. These small domains appear very frequently in larger proteins. A large number of these phosphorylation domains provide binding sites for phosphorylated residues in other protein molecules. An example is the SH2 domain, which binds to a short peptide sequence containing a phosphorylated tyrosine side chain. Several other types of phosphorylation domains recognize phosphorylated serine or threonine side chains. As a result, protein phosphorylation and dephosphorylation events have a major role in driving the regulated assembly and disassembly of protein complexes[7].

The kinetics of phosphorylation and dephosphorylation are highly adaptable and can be changed to meet the timescale of a physiological process. Reactions can occur in seconds or over the course of several hours. The effect of phosphorylation can be highly amplified by the action of a single activated kinase that has the potential to phosphorylate hundreds of target proteins in a very short time. If the target proteins are

enzymes, further amplification can occur as each enzyme catalyzes the transformation of potentially hundreds of different substrates[10].

1.2 Aging

Just over fifty years ago, the prevailing hypothesis concerning aging was 'the rate of living hypothesis'. It was based on the observation that, in general, the animals with the highest metabolic rates had the shortest life expectancy, but the link between metabolism and aging was unknown. In 1957, Denham Hartman speculated that endogenous oxygen radicals caused cumulative damage to biomolecules within every organism and the 'free-radical theory' of aging was postulated[11]. Combining the facts that the mitochondria produce the majority of cellular energy and that they also consume large quantities of intracellular oxygen, the two theories seemed to be nearly interchangeable, but there are exceptions. Certain species, such as birds and primates, tend to have a longer lifespan than would be predicted by their metabolic rate. It was determined that the production of reactive oxygen species (ROS) in the mitochondria of these species is low relative to their metabolic rate, providing evidence that the rate of ROS production correlates more strongly with life span than metabolic rate[12].

ROS include an array of different chemical species including superoxide anions, hydroxyl radicals, peroxynitrite and hydrogen peroxide. There is evidence that suggests that many of these species not only damage biomolecules such as proteins, but also work as specific signaling molecules that may trigger phosphorylation events[13-17]. The primary goals of this research are to determine the age-dependent phosphorylation

differences in specific tissues and to provide evidence of the effect of ROS in protein phosphorylation.

The primary consideration in the design of any experimental study is selection of the correct model. The experiments used to explore age-dependent phosphorylation changes utilized tissues from five month and thirty-four month old Fisher 344/Brown Norwegian F1 hybrid rats. This particular animal model is recommended by the National Institutes on Aging due to a lower rate of pathological conditions than is typically found within the population of inbred rats and its longer lifespan[18-24].

1.3 Phosphoproteomics

A holistic or comprehensive study of phosphorylation requires not only a qualitative identification of phosphoproteins, but also a reliable quantitative method that provides a real measure of the differences in protein phosphorylation levels between biological states. Ideally, one would also want to identify and measure the differences in the concentrations or activities of the protein kinases and phosphatases involved in producing the altered phosphorylation states. It would also be important to elucidate which residues are phosphorylated and any additional post-translational modifications that may be effecting the changes in phosphorylation state, such as nitrotyrosine or chlorotyrosine or any modification that would alter the conformation of the phosphoprotein and prevent phosphorylation or de-phosphorylation. This task is complicated by the fact that many signaling phosphoproteins are expressed at relatively low levels and the stoichiometry of occupied phosphorylation sites can be variable on phosphoproteins where multiple sites are present. This provides a challenge for not

only accurate quantitation, but also for detection, identification and for accurate description of the phosphorylation sites of any particular phosphoprotein[25-27].

Since only a small fraction of proteins are phosphorylated at any given time, our initial strategy pursued enrichment of all phosphoproteins in both skeletal muscle and cerebellum in order to provide the greatest probability of finding unique, low abundant phosphoproteins in these tissues. One of the drawbacks of the most popular enrichment scheme, immobilized metal affinity chromatography (IMAC) is an inability to accurately quantify the phosphorylation differences. Since IMAC targets phosphopeptides based on charge, phosphorylated peptides bearing multiple phosphorylation sites are preferentially retained. In addition, there is non-specific binding of acidic groups (aspartic and glutamic acid) and electron donors such as histidine, and these have been problematic causing non-phosphorylated proteins to be retained. Although higher specificity can be obtained by esterification of acidic residues before the IMAC enrichment, it remains semi-quantitative. With this in mind we first pursued immunoaffinity enrichment using commercially available antibodies.

Following the separation of phosphoproteins from tissue extracts, determination of the identity of the phosphoproteins observed is required. Based on the equipment available, nanoelectrospray mass spectrometry (NSI-MS) was selected for the identification of the phosphoproteins. One requirement in both electrospray and nanoelectrospray mass spectrometry, is that the mass of the analytes must be in the range of the instrument. In order to reduce the size of proteins, they are enyzymatically digested into their corresponding peptides. While NSI-MS is a sensitive method for peptide analysis, it offers its own challenges with respect to phosphopeptides.

Phosphopeptides are negatively charged and the optimal mode for protein identification using electrospray is in positive mode, therefore phosphopeptides are not observed as intense peaks. This is further complicated by the presence of non-phosphorylated peptides in the sample that can cause ionic suppression. With these challenges in mind, the development of methods to determine age-dependent changes in protein phosphorylation began.

The primary goal of our research was the investigation of these changes in the rat cerebellum. In order to achieve this goal the initial method development was conducted using rat skeletal muscle from the same animal model in order to reduce the total number of animals sacrificed.

1.4 References

[1] Hunter T. Protein kinases and phosphatases: the yin and yang of protein phosphorylation and signaling. Cell. 1995 Jan 27;80(2):225-36.

[2] Cohen, P., The origins of protein phosphorylation., Nat. Cell Biol., 2002 May 4(5):E127-130.

[3] Zhang, H., Zha, X., Tan, Y., Hornbeck, P.V., Mastrangelo, A.J., Alessi, D.R., Polakiewicz, R.D., Comb, M.J., Phosphoprotein analysis using antibodies broadly reactive against phosphorylated motifs., J. Biol. Chem. 2002 Oct 18; 277(42):39379-87

[4] Kersten, B., Agrawal, G.K., Iwahashi, H., and Rakwal, R., Plant phosphoproteomics: a long road ahead. Proteomics 2006 Oct;6(20):5517-28

[5] Manning G., Whyte, D.B., Martinez, R., Hunter, T., and Sudarsanam, S., The protein kinase complement of the human genome., Science, 2002 Dec 6; 298(5600):1912-34

[6] Andersen, J.N., Mortensen, O.H., Peters, G.H., Drake, P.G., Iversen, L.F., Olsen, O.H., Jansen, P.G., Andersen, H.S., Tonks, N.K., and Møller, N.P., Structural and evolutionary relationships among protein tyrosine phosphatase domains. Mol. Cell Biol. 2001Nov;21(21):7117-36

[7] Alberts, B; Johnson, A; Lewis, J; Raff, M; Roberts, K; Walter, P. *Molecular Biology of the Cell.* New York and London: Garland Science; c2002

[8] Xie Y, Jiang Y, Ben-Amotz D. Detection of amino acid and peptide phosphate protonation using Raman spectroscopy. Anal Biochem. 2005 Aug 15;343(2):223-30.

[9] Wojciechowski M, Grycuk T, Antosiewicz JM, Lesyng B. Prediction of secondary ionization of the phosphate group in phosphotyrosine peptides. Biophys J. 2003 Feb;84(2 Pt 1):750-6.

[10] Berg, JM.; Tymoczko, JL.; and Stryer, L. *Biochemistry.* New York: W. H. Freeman and Co.; c2002

[11] Harman, D. Aging: a theory based on free radical and radiation chemistry. J Gerontol. 1956 Jul;11(3):298-300.

[12] Ku HH, Brunk UT, Sohal RS. Relationship between mitochondrial superoxide and hydrogen peroxide production and longevity of mammalian species. Free Radic Biol Med. 1993 Dec;15(6):621-7.

[13] Nemoto S, Takeda K, Yu ZX, Ferrans VJ, Finkel T. Role for mitochondrial oxidants as regulators of cellular metabolism. Mol Cell Biol. 2000 Oct;20(19):7311-8.

[14] Finkel T. Oxidant signals and oxidative stress. Curr Opin Cell Biol. 2003 Apr;15(2):247-54.

[15] Starkov AA. The role of mitochondria in reactive oxygen species metabolism and signaling. Ann N Y Acad Sci. 2008 Dec;1147:37-52.

[16] Le Bras M, Clément MV, Pervaiz S, Brenner C. Reactive oxygen species and the mitochondrial signaling pathway of cell death. Histol Histopathol. 2005 Jan;20(1):205-19.

[17] Carmody RJ, Cotter TG. Signalling apoptosis: a radical approach. Redox Rep. 2001;6(2):77-90.

[18] Weindruch R, Masoro EJ. Concerns about rodent models for aging research. *J Gerontol A Biol Sci Med Sci.* 1991;46:B87-B88.

[19] Hazzard DG, Bronson RT, McClearn GE, Strong R. Selection of an appropriate animal model to study aging processes with special emphasis on the use of rat strains. *J Gerontol A Biol Sci Med Sci.* 1992;47:B63-B64.

[20] Coleman GL, Barthold SW, Osbaldiston GW, Foster SJ, Jonas AM. Pathological changes during aging in barrier-reared Fischer 344 male rats. *J Gerontol.* 1977;32:258-278.

[21] Weindruch R. Animal models. In: Masoro EJ, ed. *Handbook of Physiology: Aging.* Section 11. New York: Oxford University Press; 1995:37–52.

[22] Lipman R, Chrisp C, Hazzard D, Bronson R. Pathologic Characterization of Brown Norway, Brown Norway x Fischer 344, and Fischer 344 x Brown Norway Rats with Relation to Age. *J Gerontol Biol Sci.* 1996;51A:B54-B59.

[23] Turturro A, Witt WW, Lewis S, Hass BS, Lipman RD, Hart RW. Growth curves and survival characteristics of the animals used in the biomarkers of aging program. *J Gerontol Biol Sci.* 1999;54A:B492-B501.

[24] Bronson R. Rate of occurrence of lesions in 20 inbred and hybrid genotypes of rats and mice sacrificed at 6 month intervals during the first years of life. In: Harrison DE, ed. *Genetic Effects on Aging II.* Caldwell, NJ: Telford Press; 1990:279–358.

[25] Hjerrild M, Gammeltoft S. Phosphoproteomics toolbox: computational biology, protein chemistry and mass spectrometry. FEBS Lett. 2006 Sep 4;580(20):4764-70.

[26] Morandell S, Stasyk T, Grosstessner-Hain K, Roitinger E, Mechtler K, Bonn GK, Huber LA. Phosphoproteomics strategies for the functional analysis of signal transduction. Proteomics. 2006 Jul;6(14):4047-56.

[27] Preisinger C, von Kriegsheim A, Matallanas D, Kolch W. Proteomics and phosphoproteomics for the mapping of cellular signalling networks. Proteomics. 2008 Nov;8(21):4402-15.

Chapter Two

The Development of Proteomic Methods to Determine Changes in Protein Phosphorylation.

2. Introduction

This chapter focuses on the development of sensitive, robust and reproducible methods for the separation, detection, quantification and identification of the age-dependent differences in protein phosphorylation from tissue samples. The complexity of developing proteomic procedures for tissue samples combined with the level of difficulty in accurately performing this task for a low abundance analyte, which is inherently reversible within the organism itself, cannot be understated. The separation methods must be of the highest quality to ensure reproducibility between replicate samples. Both the sensitivity and precision of the quantitation and the specificity of the identification methods must be very high in order to find low abundant species. These methods must also exhibit a wide dynamic range in order to detect differences at both low and high concentration levels. The majority of these methods and procedures were developed in parallel, as needed, while the actual studies were underway.

Section 2.1 describes the attempts to use immunoaffinity separation as the primary means of enriching phosphoproteins for MS-MS identification. This method was abandoned in favor of a 2D-PAGE methodology as described in section 2.2. The remaining sections describe the procedures which were developed for separating the proteins using 2D-PAGE, the acquisition and analysis of the gel images, the mass spectrometry applied to spots demonstrating two-fold phosphorylation differences and the bioinformatic effort to identify and elucidate structural information about the phosphoproteins of interest, and the distillation of the biological implications of the phosphorylation and the total protein level differences observed in the experiments. **Scheme 1** on page 14 provides an outline of the final process developed.

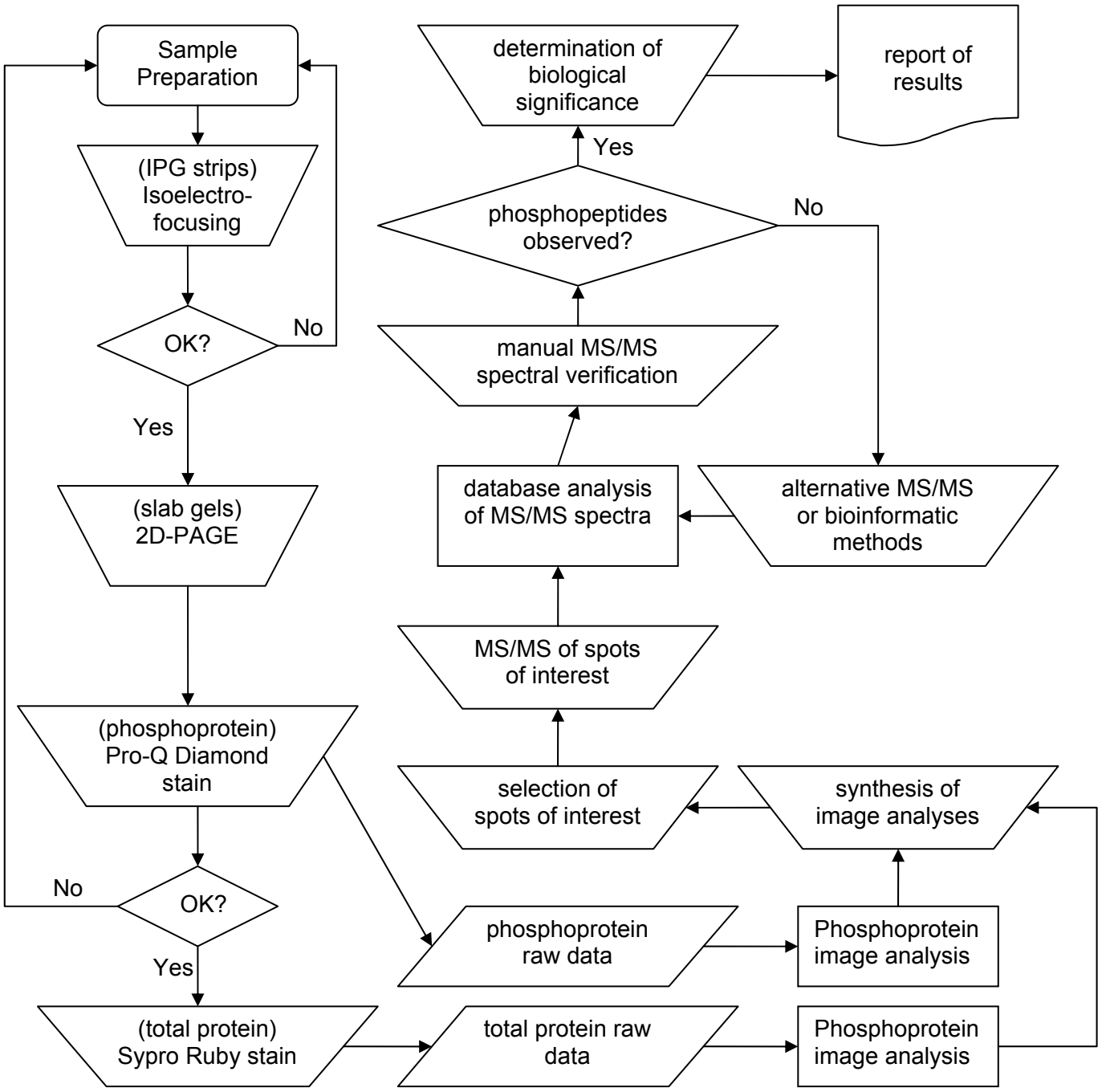

Scheme 1. *Workflow diagram for 2D-PAGE methodology.*

2.1 Immunoaffinity separation

The process of developing the methods to identify proteins showing age-dependent phosphorylation differences began with attempts to enrich phosphoproteins from tissue lysates using immunoprecipitation[1-4]. Anti-phosphoserine/threonine and anti-phosphotyrosine antibodies conjugated to agarose beads were the medium used for enrichment, followed by elution of the proteins with SDS buffer appropriate for SDS-PAGE separation and visualization by Coomassie brilliant blue staining[3, 5].

2.1.1 Materials

Anti-pSer/Thr and anti-pTyr agarose conjugated beads were obtained from Upstate Cell Signaling Solutions [Waltham, MA]. Protease inhibitor cocktail (containing: AEBSF, pepstatin A, E-64, bestatin, leupeptin, and aprotinin), sodium orthovanadate (Na_3VO_4), sodium fluoride (NaF), phenylmethanesulfonyl fluoride (PMSF) and phosphate buffered saline (PBS) were obtained from Sigma-Aldrich [St. Louis, MO]. Novex 4-20% Tris-glycine gradient gels were obtained from Invitrogen [Carlsbad, CA]. All other reagents were obtained from Fisher Scientific [Fairlawn, NJ] at the highest available grade.

2.1.2 Sample Preparation

Three 5-month old and three 34-month old Fisher344/BN F1 rats that were housed in a 12 hour light/dark cycle and had been provided with water and food ad libitum were euthanized by carbon monoxide asphyxiation followed by quick decapitation according to the protocol of the Animal Care Unit of the University of

Kansas. Fast-twitch muscle tissue from the hind legs of the animals was removed immediately and stored at -70º C until further use. The brain was removed and the cerebella were isolated and immediately placed into a cold homogenization buffer containing 0.32 M sucrose, 0.5 mM magnesium sulfate, 10 mM ε-amino caproic acid, 0.1 mM EGTA, 10 mM HEPES, 0.1 mM benzamide, with protease inhibitor cocktail (containing: 4-(2-aminoethyl) benzenesulfonyl fluoride (AEBSF), pepstatin A, E-64, bestatin, leupeptin, and aprotinin), phosphatase inhibitor cocktail 1 (containing: microcystin LR, cantharidin, and (−)-p-bromotetramisole), and phosphatase inhibitor cocktail 2 (containing: sodium vanadate, sodium molybdate, sodium tartrate, and imidazole). The cerebella were minced with scissors and then thoroughly homogenized using a motorized glass-Teflon pestle on ice. The resulting homogenates were aliquoted into 3 mL volumes and stored at -70°C until further use.

The majority of the method development was conducted using the skeletal muscle tissue. With an abundance of skeletal muscle available in comparison to rat cerebellar tissue, using the skeletal muscle for development minimized the number of animals that had to be sacrificed. Slices were cut from the frozen skeletal muscle tissue, ground into a fine powder with mortar and pestle and introduced into a modified RIPA lysis buffer containing: 50mM Tris-HCl, pH 7.4; 1% NP-40; 0.25% sodium deoxycholate; 150mM NaCl; 1mM EDTA; 1mM PMSF; 1µg/mL protease inhibitor cocktail; 1mM NaF and 1mM Na_3VO_4. The lysates (approximate concentration: 8 µg total protein/µL) were then diluted two-fold with the modified RIPA buffer and homogenized with an Ultra-Turrax T8 homogenizer [Fisher, Fair Lawn, NJ]. Following homogenization the samples were briefly sonicated with a Fisher 550 sonic

dismembrator [Fisher, Fair Lawn, NJ] to reduce the level of aggregation. Protein concentrations were determined using the Lowry method[6] and the final protein concentration was adjusted to 1 µg/µL with modified RIPA buffer.

For cerebellar experiments, the homogenates were diluted with the modified RIPA buffer to a final protein concentration of 1 µg/µL.

2.1.3 Immunoaffinity Separation

Fifty microliters of slurry (1 µg/µL antibody) from each anti-phospho, agarose conjugate was separately added to aliquots of each lysate (40 µg total protein) and the samples were allowed to incubate overnight with end over end agitation at 4°C. The supernatant and the agarose beads were subsequently separated by microcentrifugation at 13000 x g. The agarose beads were washed twice with PBS and once with RIPA buffer. The proteins were dissociated from the beads with 30 µL of Tris-glycine-SDS sample buffer and loaded onto Novex 4-20% Tris-glycine gradient gels. Following gel electrophoresis at 200 V for approximately 45 min, the gels were stained with Coomassie Brilliant Blue [BioRad, CA] for visualization of the proteins.

2.1.4 Results

After the procedure had been optimized using skeletal muscle lysates, various total protein levels of skeletal muscle lysates were investigated to determine the dynamic range of the method and to evaluate non-specific binding. Total protein loads of 600 µg, 400 µg, 200 µg and 100 µg for both 5 month old and 34 month old skeletal muscle samples and a constant 50 µg of antibody from each anti-phospho, agarose

conjugate was evaluated separately. The gel images in **Figure 2** show the results from this experiment. The gel image of the SDS-PAGE separation of proteins from the anti-pSer/Thr agarose beads is displayed above the gel image from the SDS-PAGE separation of proteins from the anti-pTyr agarose beads. There are obvious and reproducible age-dependent differences visible between the 5 month and 34 month lanes in the gel images for both anti-phospho conjugates. There are higher amounts of protein visible in the 34 month bands at 120 kD, 80 kD, and 17 kD in the anti-pSer/Thr conjugate image and for the 250 kD band in the anti-pTyr image over the entire concentration range. Several differences only become apparent at discrete concentration levels. While a high concentration is necessary to detect the low abundance bands such as the 30 kD bands in the anti-pTyr image, the lanes with lower protein loads allow the differences between the 5 month and 34 month samples in the 200 and 250 kD bands to be in the anti-pSer/Thr gel image to become discernible. This demonstrates that for this particular enrichment, multiple total protein concentrations

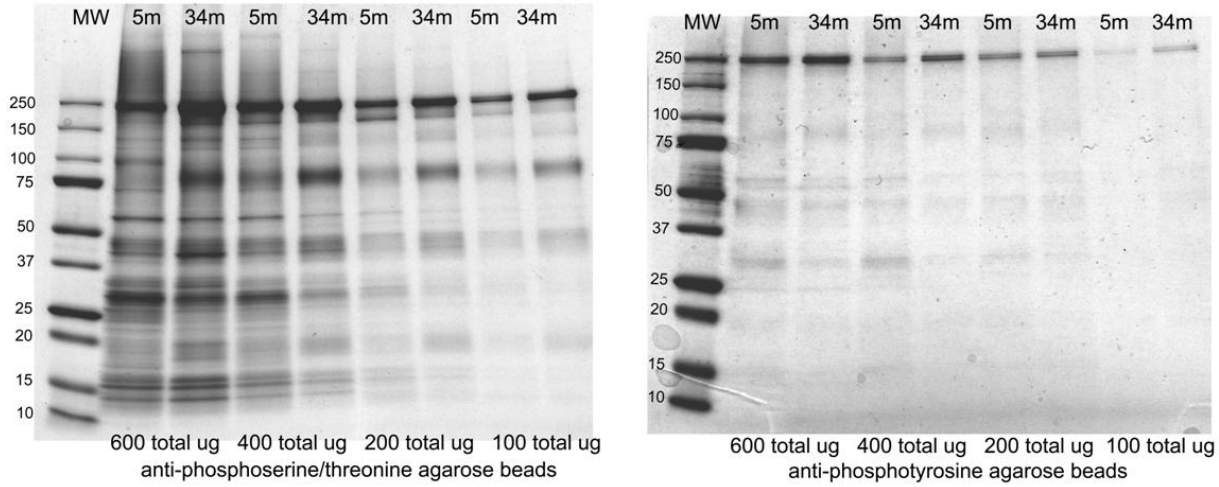

Figure 2. *Gel images of SDS-PAGE separations of various protein loads of both 5 mo and 34 mo rat skeletal muscle lysates against pSer/Thr and pTyr antibodies.*

must be investigated to extend the dynamic range of the separation. While these results looked promising for skeletal muscle, we were equally interested in rat cerebellum and the assay needed to be tested using the cerebellum lysates. These results are displayed in **Figure 3** below.

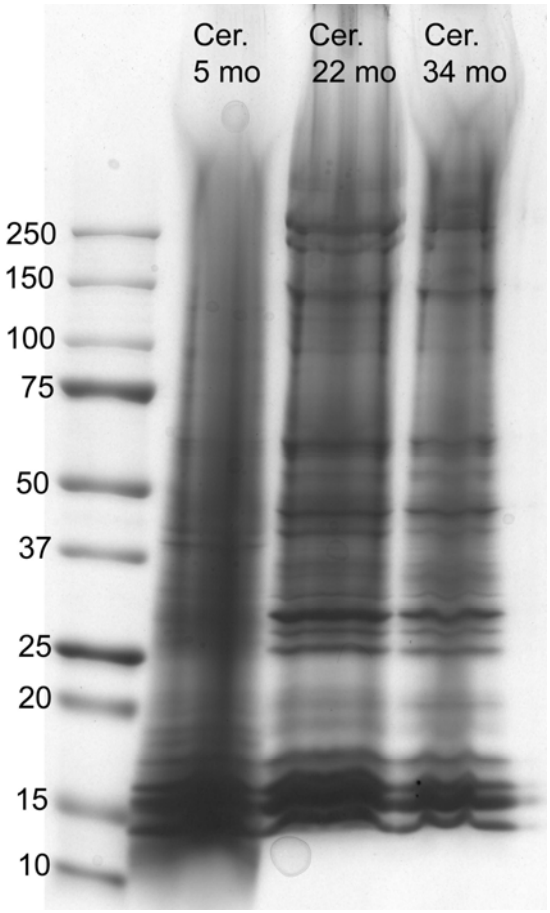

Figure 3. *Gel images of SDS-PAGE separations of 600 µg protein loads of 5 mo, 22 mo and 34 mo rat cerebellum lysates against pSer/Thr antibodies.*

Based on the results shown in **Figure 3**, where we see smearing through all of the gel lanes, there is an obvious need for delipidation of the cerebellum samples that was not required for the skeletal muscle samples. The brain contains approximately 80% (w/w)

lipids in the myelin, 49-66% (w/w) lipids in the white matter and 36-40% (w/w) in the grey matter[7], while skeletal muscle contains 2-4% (w/w)[8]. Several methods of delipidation[9-11] were attempted and none proved viable. The primary difficulty was re-solubilizing the protein pellet post-precipitation using a modified RIPA (Radio-Immunoprecipitation Assay) buffer. Alternative buffers that allowed resolubilization were not compatible with immunoaffinity separation and did not provide any meaningful results.

2.1.5 Conclusions

With the primary focus of our research being the analysis of age-dependent phosphorylation differences in the rat cerebellum, it was obvious that we required a different approach. While the immunoaffinity development had been ongoing, a phosphoprotein specific gel stain, Pro-Q Diamond [Invitrogen, Carlsbad, CA], became commercially available and software for the quantitative analysis of 2D gels, Progenesis PG220 [Nonlinear Dynamics, Newcastle upon Tyne, UK], was acquired by the University of Kansas. In order to achieve the primary goals of our research, the method development moved toward utilizing these newly available tools.

2.1.6 References

[1] Lim YP, Wong CY, Ooi LL, Druker BJ, Epstein RJ. Selective tyrosine hyperphosphorylation of cytoskeletal and stress proteins in primary human breast cancers: implications for adjuvant use of kinase-inhibitory drugs. Clin Cancer Res. 2004 Jun 15;10(12 Pt 1):3980-7.

[2] Di Fiore PP, Fazioli F. Purification of tyrosine-phosphorylated proteins by immunoaffinity chromatography and direct cloning of their cDNAs from bacterial expression libraries. Methods Mol Biol. 2001;124:221-37.

[3] Lewandrowski U, Sickmann A, Cesaro L, Brunati AM, Toninello A, Salvi M. Identification of new tyrosine phosphorylated proteins in rat brain mitochondria. FEBS Lett. 2008 Apr 2;582(7):1104-10.

[4] Davis FM, Tsao TY, Fowler SK, Rao PN. Monoclonal antibodies to mitotic cells. Proc Natl Acad Sci U S A. 1983 May;80(10):2926-30.

[5] Yaffe MB, Schutkowski M, Shen M, Zhou XZ, Stukenberg PT, Rahfeld JU, Xu J, Kuang J, Kirschner MW, Fischer G, Cantley LC, Lu KP. Sequence-specific and phosphorylation-dependent proline isomerization: a potential mitotic regulatory mechanism. Science. 1997 Dec 12;278(5345):1957-60.

[6] Lowry, OH, Rosbrough, NJ, Farr, A.L., and Randall, R.J., Protein measurement with the Folin phenol reagent. J. Biol. Chem. 1951 Nov;193(1):265ND75

[7] O'Brien JS, Sampson EL.. Fatty acid and fatty aldehyde composition of the major brain lipids in normal human gray matter, white matter, and myelin. J Lipid Res. 1965 Oct;6(4):545-51.

[8] Machann J, Bachmann OP, Brechtel K, Dahl DB, Wietek B, Klumpp B, Häring HU, Claussen CD, Jacob S, Schick F. Lipid content in the musculature of the lower leg assessed by fat selective MRI: intra- and interindividual differences and correlation with anthropometric and metabolic data. J Magn Reson Imaging. 2003 Mar;17(3):350-7.

[9] Fu Q, Bovenkamp DE, Van Eyk JE. A rapid, economical, and reproducible method for human serum delipidation and albumin and IgG removal for proteomic analysis. Methods Mol Biol. 2007;357:365-71.

[10] Azzouz N, Shams-Eldin H, Schwarz RT. Removal of phospholipids contaminants through precipitation of glycosylphosphatidylinositols. Anal Biochem. 2005 Aug 1;343(1) 152-8

[11] Wessel, D., and Flügge, U.I., A method for the quantitative recovery of protein in dilute solution in the presence of detergents and lipids. Anal Biochem. 1984 Apr;138(1):141-3.

2.2 Two-dimensional polyacrylamide gel electrophoresis (2D-PAGE)

While the immunoaffinity separation sought to enrich low abundant phosphoproteins, utilizing 2D PAGE required the maximization of protein loading to achieve similar results. In order to achieve this goal, it was necessary to use reagents that quantitatively solubilize both cytosolic and membrane bound proteins yet remain compatible with isoelectric focusing (IEF) and sodium dodecyl sulfate-polyacrylamide gel electrophoresis (SDS-PAGE). The best protein solubilizing agents that meet these criteria contain mixtures of detergents that have different polarities. Several different mixtures of chaotropic compounds, detergents, carrier ampholytes and alcohols were investigated in order to generate high resolution two-dimensional protein patterns in 2D gels that cover the entire pH range from 3 to 10.

Every stage of generating the 2D gels required optimization in order for the individual steps to work in unison. The sample preparation required optimization of the phosphatase inhibitors in order for the phosphoproteins to remain phosphorylated and be detected by the Pro-Q Diamond phosphoprotein gel stain. The phosphatase inhibitors, containing a relatively high salt concentration, caused difficulties in the isoelectric focusing which in turn, required modification. The Pro-Q Diamond stain, which requires an aqueous environment, causes the slab gels to become more porous and therefore more brittle, combined with the remote location of the fluorescent imaging facility (on the main campus) called for optimization of the polyacrylamide gels themselves. The steps taken to address these problems are detailed in the following sections.

2.2.1 Materials and Equipment

Glycerol, Urea, CHAPS, Tween-20, butanol, tris(hydroxymethyl)aminomethane hydrochloride (Tris-HCl), trimethylol aminomethane, tris(hydroxymethyl)aminomethane (Tris base), agarose, and 2-propanol were acquired from Fisher Scientific. [Fairlawn, NJ] Unless otherwise noted, all other chemicals were purchased from Sigma Chemicals [St. Louis, MO] and were of electrophoretic grade or better. An IPGPhor II electrophoresis unit for isoelectric focusing, an Ettan Dalt*six* gel casting apparatus, an Ettan Dalt*six* electrophoresis tank and a Typhoon 9410 variable mode imager, all acquired from GE Healthcare [Piscataway, NJ] were used to conduct the electrophoresis and create the gel images.

2.2.2 Sample solubilization optimization

Rat skeletal muscle samples, stored as described in section 2.1.2, were removed from the -70°C freezer and slices were cut from the frozen tissue, ground into a fine powder with mortar and pestle and introduced into a lysis buffer containing 7M urea, 2M thiourea, 4% (v/v) CHAPS, 1% (v/v) Tween-20, 40 mM Tris, 20 mM DTT, 1mM sodium fluoride, 1 mM sodium orthovanadate, 0.5 mM PMSF, 10 µg/ml of leupeptin, 10 µg/ml apopritin, and homogenized with an Ultra-Turrax T8 homogenizer [Fisher, Fair Lawn, NJ], and briefly sonicated with a Fisher 550 sonic dismembrator [Fisher, Fair Lawn, NJ]. The soluble fractions were transferred and the homogenates were delipidated using chloroform/methanol precipitation [1].

The protein fractions were resolubilized into a buffer amenable to iso-electric focusing (IEF) containing 5M urea, 2M thiourea, 2% (v/v) CHAPS, NJ], 0.5% (v/v) Tween-20, 0.5% (w/v) 3-(decyldimethylammonio)propanesulfonate, 10% (v/v) 2-propanol, 10% (v/v) water saturated butanol, 5% (v/v) glycerol, 0.25% (v/v) carrier ampholytes (50:50 mix of Pharmalyte 3-10 [GE Healthcare, Piscataway, NJ] and Bio-Lyte 3/10 [Bio Rad, Hercules, CA]), 20 mM DTT, 1mM sodium fluoride, and 1mM sodium orthovanadate[2]. In order to maximize dissolution, the sonic dismembrator was utilized until the protein pellets dissipated.

The samples were then centrifuged at 13,000 x g in a microcentrifuge and the supernatant transferred to fresh centrifuge tubes. Protein concentrations were determined using the Lowry method[3] and the samples were reduced using tributylphosphine and alkylated with iodoacetamide using a ReadyPrep Reduction/Alkylation kit [Bio Rad, Hercules, CA] according to manufacturer's procedures prior to final dilution to 1.67µg/µL with the aforementioned IEF buffer.

2.2.3 2D PAGE separation optimization

For the optimization of the first dimension, 150 µL aliquots from each age group's diluted lysates (one 5 month and one 34 month) were applied to 7 cm 'Immobiline' immobilized pH gradient (IPG) strips (pH 3-10 NL) [GE Healthcare, Piscataway, NJ] to load 250 µg of total protein and allowed to rehydrate overnight. The strips were transferred to an IPGPhor II electrophoresis unit and IEF was conducted using a linear gradient from 500 to 5,000 volts to achieve a total of 50,000 volt hours.

While the IEF was running, a set of six 1x200x260mm polyacrylamide gels (12.5% T, 3%C) were cast into individual glass cassettes using an Ettan Dalt*six* gel casting apparatus according to manufacturer's protocols. For the second dimension separation, the focused IPG strips were removed from the IPGphor II and 're-equilibrated' in a solution of 50mM Tris-HCl/Tris base, pH 8.8, 30% (v/v) glycerol, 6M urea, with 2% (w/v) sodium dodecyl sulfate (SDS) [Bio Rad, Hercules, CA] and 0.001% (w/v) bromophenol blue for 20 minutes. Following re-equilibration, the strips were each transferred to one cassette along with a 20x75mm strip of grade 1 Whatman filter paper [Fisher, Fair Lawn, NJ] soaked with a 2uL aliquot of the PeppermintStick phosphoprotein molecular weight marker [Invitrogen, Carlsbad, CA] on the acidic side of the strip, and sealed with 0.5% (w/v) boiling agarose containing 0.001% (w/v) bromophenol blue onto the top of the slab gel in each respective glass cassette. After allowing a few minutes for the agarose to properly cool, the slab gel was transferred to an Ettan Dalt*six* electrophoresis tank with the appropriate buffers and run at 30 W (5 W per gel) for approximately 30 min to effect the transfer of the proteins from the IPG strip to the slab. Once the bromophenol dye front had unequivocally entered the slab gel, the power was increased to 100 W and the gels were allowed to run until the dye front progressed to the bottom of the gels (approximately 6 h).

Immediately following the second dimension SDS-PAGE, the slab gel was removed from its cassette, fixed with a solution of 50% (v/v) methanol and 7% (v/v) acetic acid and stained with Coomassie Brilliant Blue R250 to develop the 2D pattern. The resultant gel image is shown in **Figure 4.**

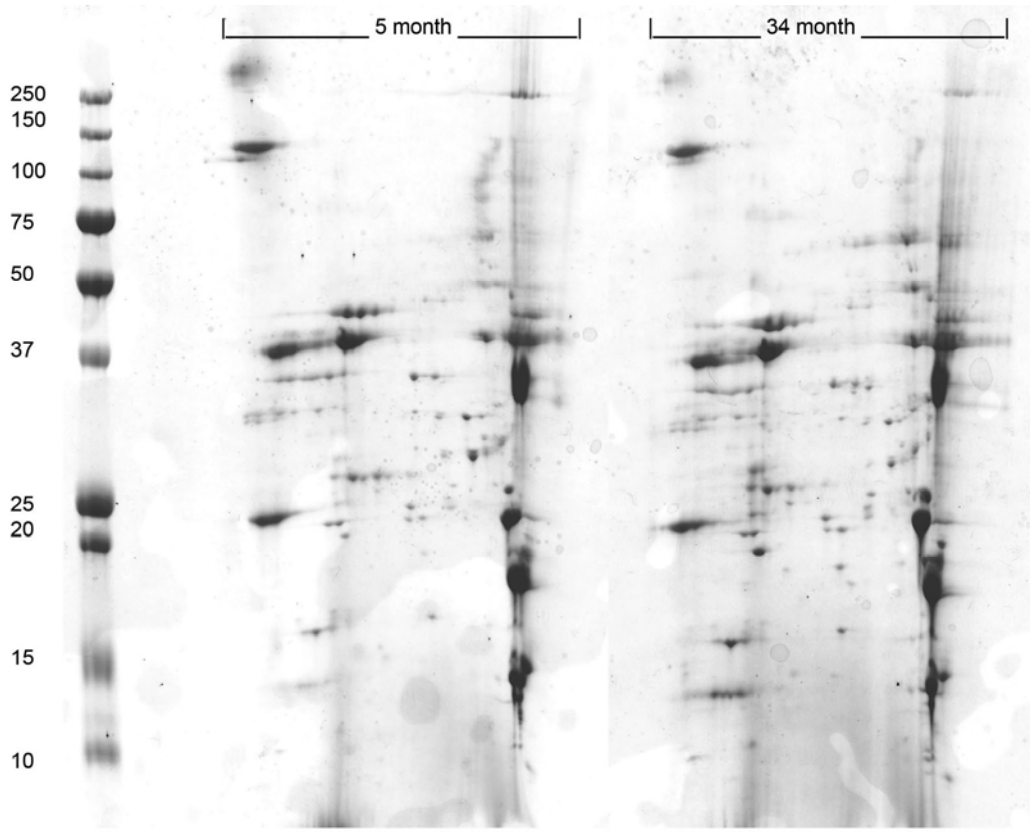

Figure 4. *2D gel image of of 5 month and 34 month rat skeletal muscle samples focused on 7cm IPG stips demonstrating initial results of solubilization and isoelectric focusing.*

Based on these encouraging results, the procedure was repeated using a 450 µL aliquot of a 5 month rat skeletal muscle lysate using an 18 cm 'Immobiline' immobilized pH gradient (IPG) strip (pH 3-10 NL) to load 750 µg of total protein. The isoelectric focusing was modified to use a linear gradient from 500 to 10,000 volts to provide 65,000 total volt hours. Following the SDS-PAGE separation, the slab gel was again fixed but then stained with Pro-Q Diamond Phosphoprotein Gel Stain [Invitrogen, Carlsbad, CA] using the manufacturer's protocol for large 2D gels and transported to the imaging facility where it was imaged using a Typhoon Variable Mode Imager [GE Healthcare, Piscataway, NJ]. The resulting 2D-gel image is shown in **Figure 5**.

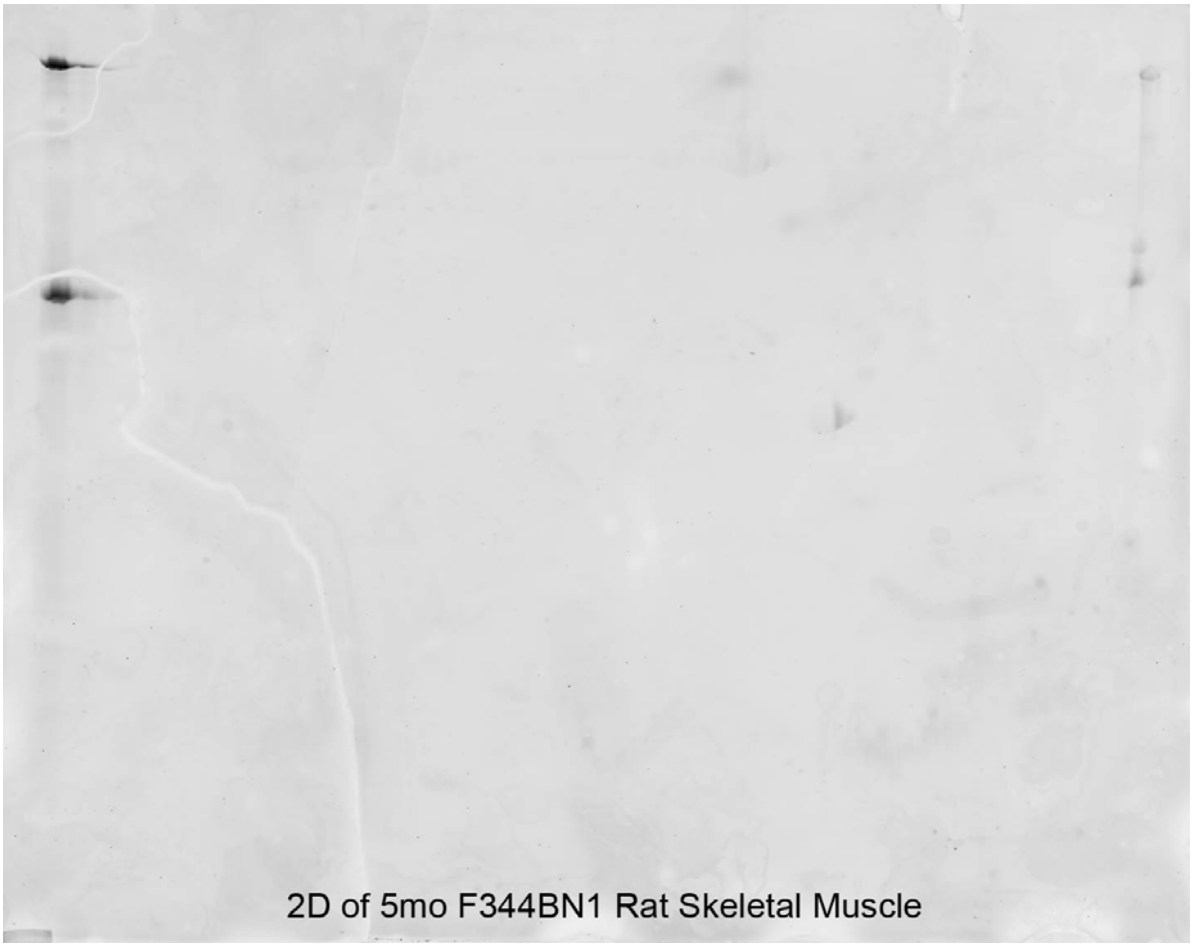

Figure 5. *Initial 2D gel image using the Pro-Q Diamond phosphoprotein gel stain.*

The phosphorylated molecular weight markers on the left hand side of the gel image demonstrated that the Pro-Q Diamond stain was working, but no protein pattern was visible. Assuming that protein was actually loaded onto the gel, the other possibility was that the concentration of phosphatase inhibitors added to the lysate was not sufficient to be effective during room temperature gel loading and subsequent isoelectric focusing. An experiment using fresh lysates with a ten-fold increase in the concentration of the phosphatase inhibitors sodium fluoride and sodium orthovanadate was conducted. **Figure 6** shows the gel image from a control experiment using 200 µg

of rat skeletal muscle lysate containing 1mM NaF and 1mM Na_3VO_4 (phosphatase inhibitors) loaded into a ten well mini-gel. The gel was stained with Pro-Q Diamond Phosphoprotein Gel Stain using the manufacturer's protocol for SDS PAGE mini-gels and subsequently imaged using the Typhoon imager. There are obviously no bands apparent in the gel other than the phosphorylated MW markers.

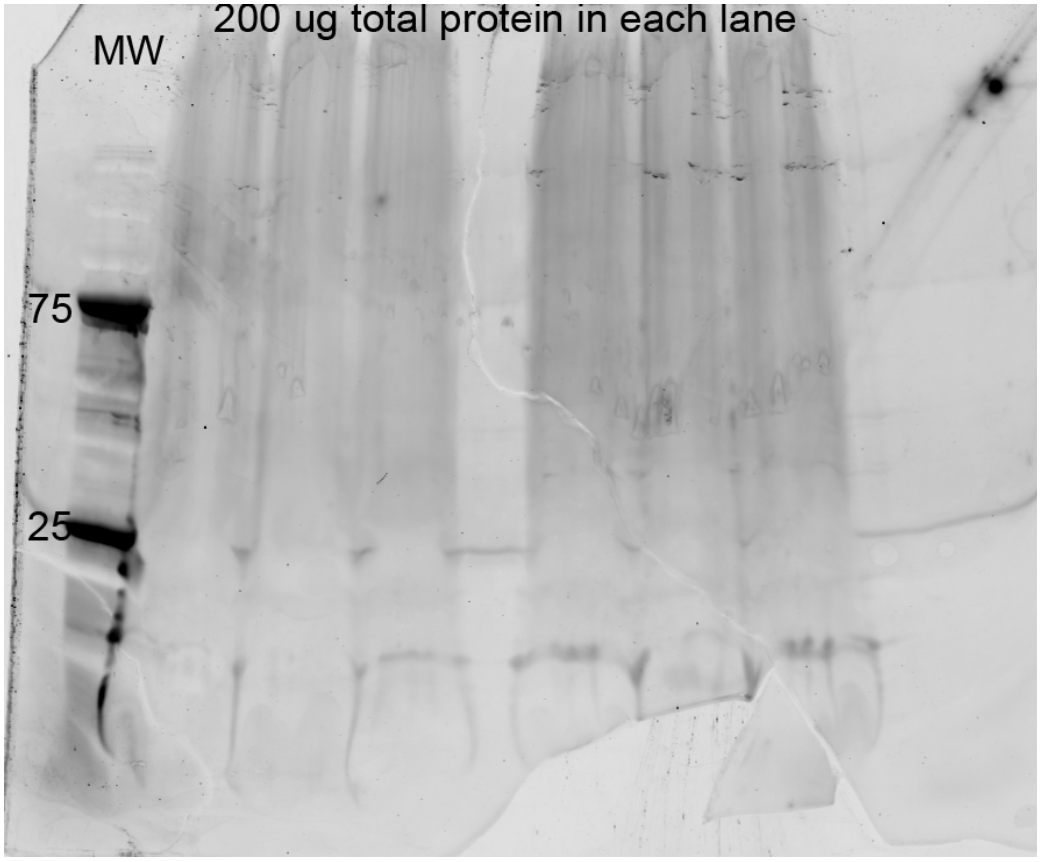

Figure 6. *SDS PAGE of skeletal muscle proteins stained with Pro Q® Diamond Stain with 1mm NaF and 1mm Na_3VO_4 as phosphatase inhibitors.*

The experiment was repeated using 10mM NaF and 10mM Na_3VO_4 as the phosphatase inhibitors during the tissue lysis. **Figure 7** shows the result with 7.5 µg, 15 µg, 30 µg and 60 µg of rat skeletal muscle lysate loaded into each respective lane of a five well mini-gel.

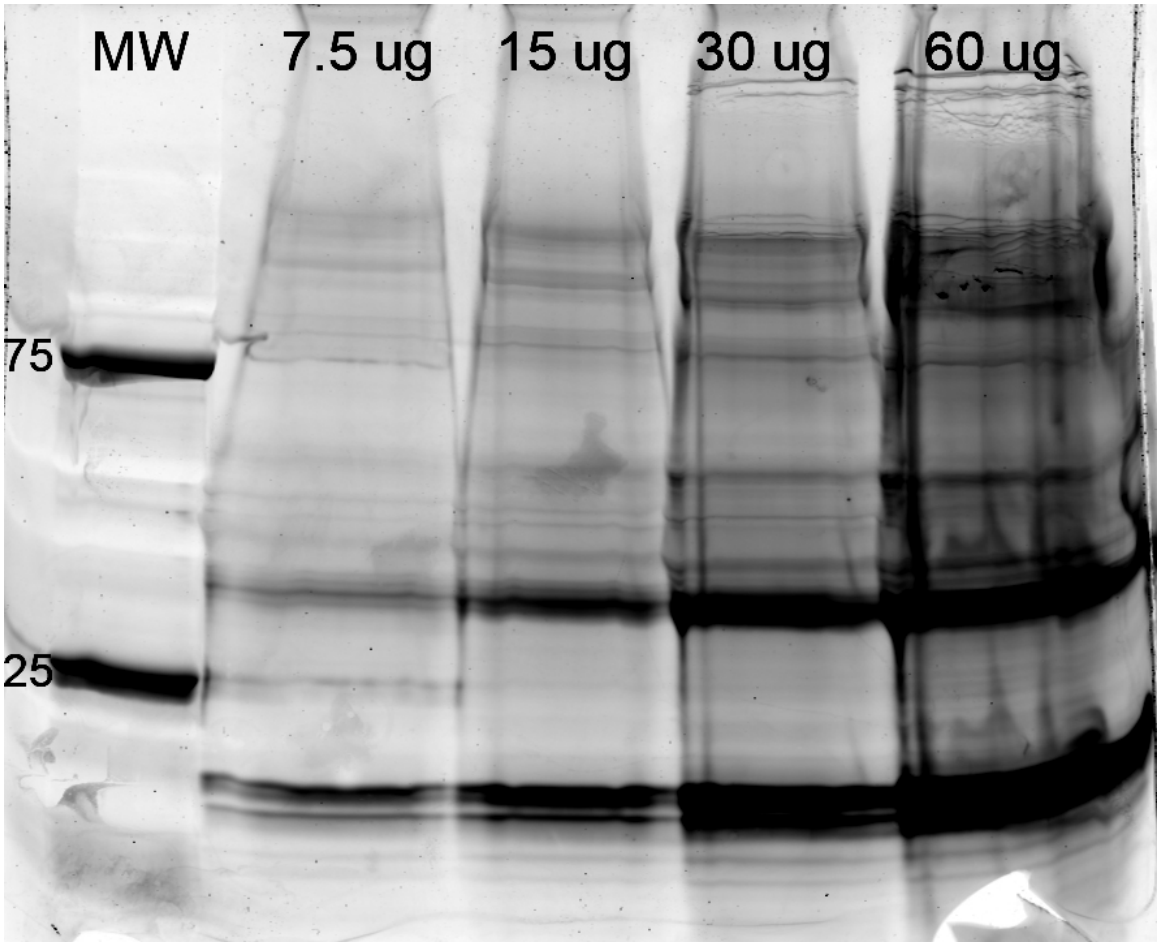

Figure 7. *SDS PAGE of skeletal muscle proteins stained with Pro Q® Diamond Stain with 10mm NaF and 10mm Na_3VO_4 as phosphatase inhibitors.*

Based on this information, the solubilization and IEF buffers were modified to those of increased levels of sodium fluoride and sodium orthovanadate. The initial experiment using two 7cm 'Immobiline' IPG strips was repeated using the new buffers and the resultant 2D gel image is shown in **Figure 8**. During the isoelectric focusing, it was visibly obvious that the samples were not properly focusing and that the increased levels of sodium salts were detrimental to the IEF separation.

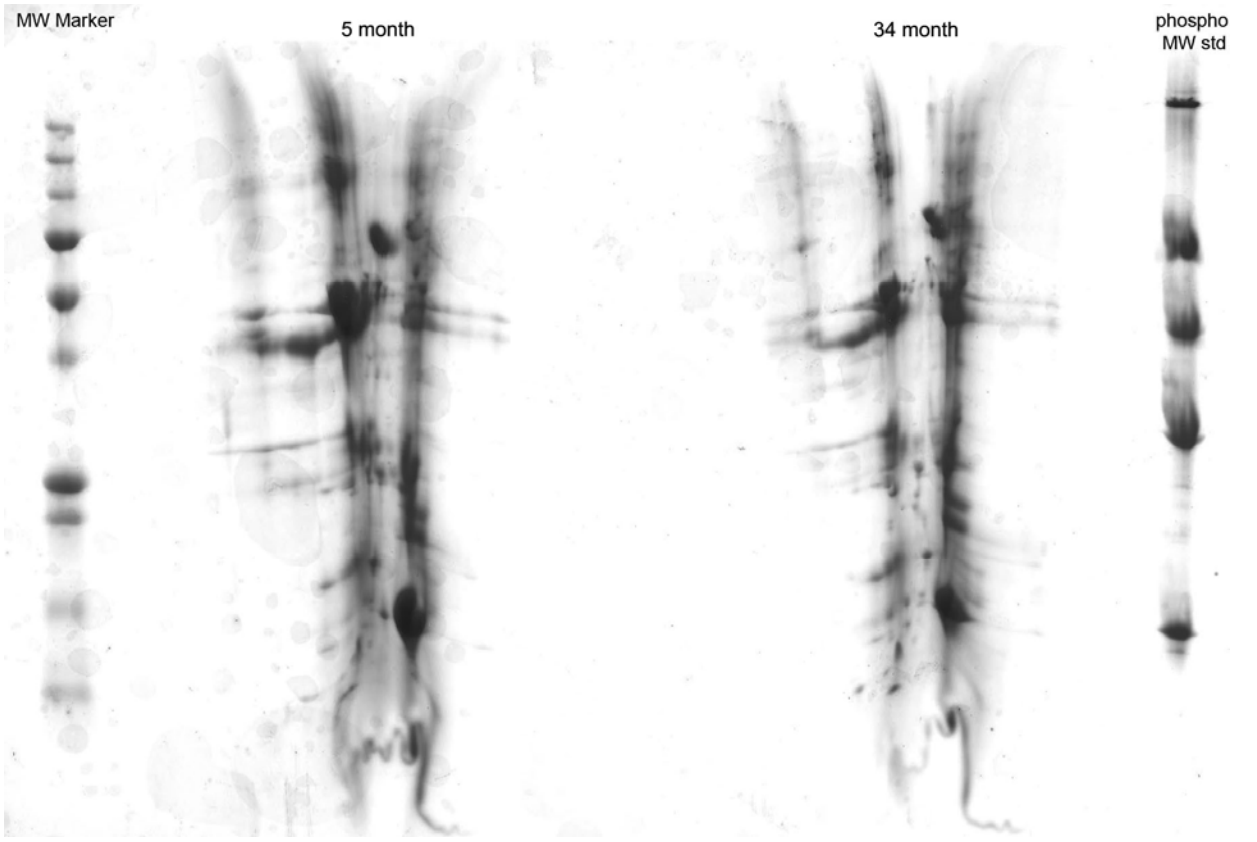

Figure 8. *2D gel image of both a 5 month and 34 month rat skeletal muscle samples focused on 7cm IPG stips with increased phosphatase inhibitor levels.*

This problem had been addressed previously by Görg et al[4] and could be resolved with only minor modifications to the programming for the isoelectric focusing. Subsequent IEF runs were conducted by initially holding the voltage at 50 V for the first 4 h to allow the migration of excess charged species introduced by the various phosphatase inhibitors. The voltage was then increased by stepping to 100 V for 2 h, followed by a step to 500 V for 2 h followed by a linear voltage gradient over 12 h from 500 to 10,000 V in order to achieve a total of 70,000 volt hours. **Figure 9** shows the initial result using this program and the Pro-Q Diamond phosphoprotein gel stain following manufacturer's protocols.

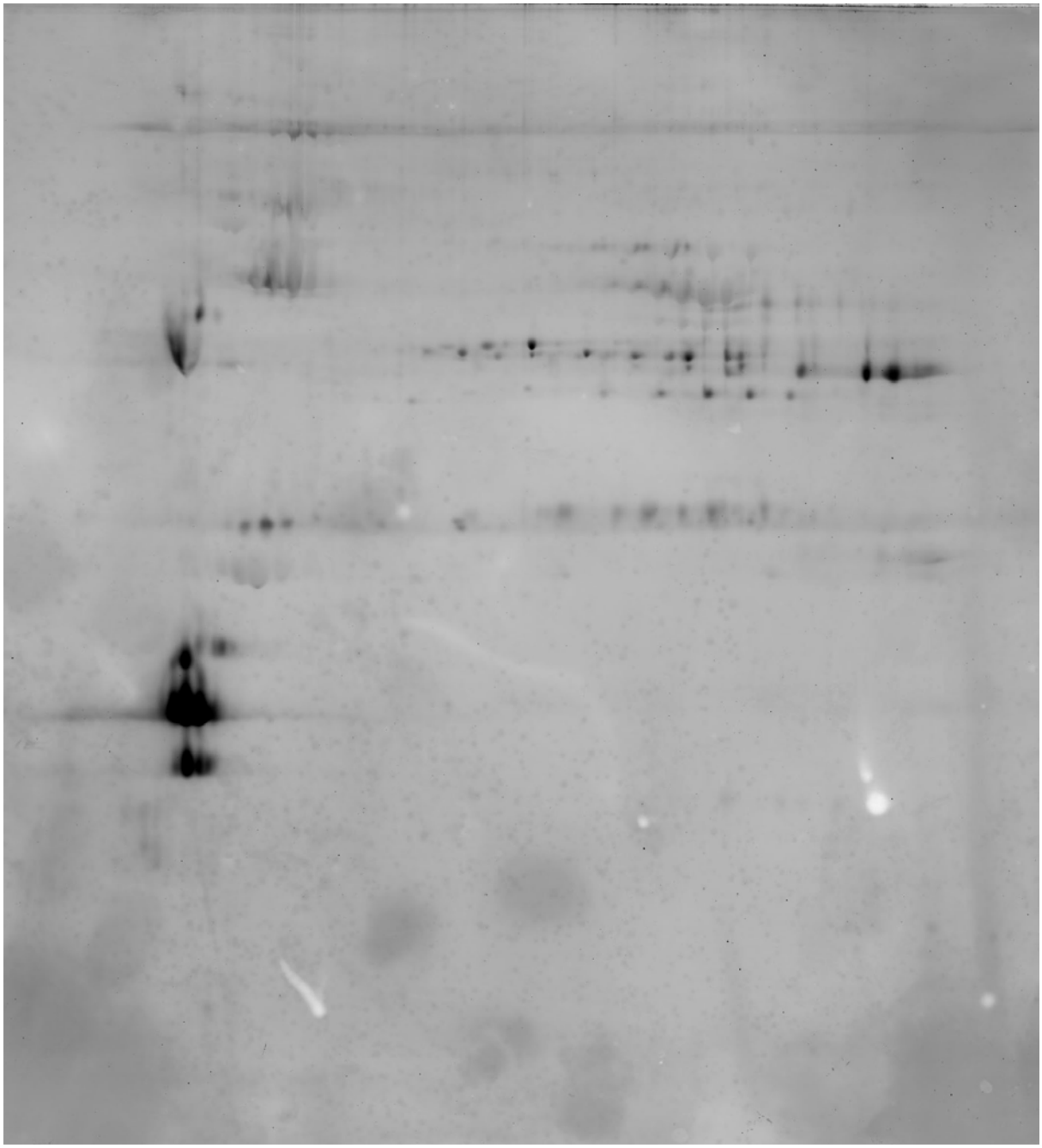

Figure 9. *2D gel image of 5 month old rat skeletal muscle using the Pro-Q Diamond phosphoprotein gel stain using the manufacturer's protocol.*

2.2.4 Polyacrylamide gel optimization

One of the major challenges in achieving quality gel images was a logistical issue. The effectiveness and sensitivity of the Pro-Q Diamond staining requires

numerous water washes which causes the polyacrylamide slab gel to swell and become fragile. In our multi-plexed (multiple fluorescent stains) experiment, the same gel is then stained with a total protein stain, Sypro Ruby, in order to quantitate total protein levels as well as the phosphoprotein levels. To complicate matters, the imaging facility was remote from the actual laboratory space where the samples were prepared and the 2D PAGE separation was performed. Unlike the extremely user-friendly differential in-gel experiments (DIGE) where the flourophores are conjugated to the proteins prior to the 2D PAGE separation allowing the user to transport and image their gels within the glass cassettes without ever physically handling the gel, the use of multi-plexed Pro-Q Diamond with the Sypro Ruby requires that both surfaces of the gel be exposed to the stains and subsequent washes in order to be effective. The difficulty imposed by handling such brittle gels prompted the manufacturer of the stains to create gel additives (Rhinohide) to strengthen the polyacrylamide gels[5]. Numerous attempts were made to increase the mechanical durability of the polyacrylamide gels while retaining resolution and reproducibility without success. The Rhinohide additives significantly improved the mechanical durability of the gels, but the gel matrix proved to be irreproducible showing a high gel-to-gel variability in the protein patterns. Increasing the thickness of the gels, without Rhinohide, from 1 mm to 1.5 mm caused a corresponding increase in the background signal by reducing the ability of the wash solutions to remove excess stain. This could not be resolved by extending the number of washes or in extending the wash times. In the end, the only way to minimize mechanical damage to the gels was by performing the gel staining and washing procedures at the imaging facility. This eliminated transportation as one source of damage to the gels.

2.2.5 Gel Imaging

One unintended consequence of moving the gel staining and washing procedures to the imaging lab was an improvement in the sensitivity of the Pro-Q Diamond stain. This occurred due to an initial lack of physical access to the facility to complete the manufacturer's protocol in the recommended time constraints and resulted in the first wash of the Pro-Q Diamond stain to be extended from 30 minutes to 12 hours. The result was a greatly reduced background as evidenced in **Figure 10** in comparison to **Figure 9**; otherwise manufacturer's protocols were followed.

Optimization of the Typhoon scanner settings was required for every batch of gels due to the variability of protein spot composition in each separate experiment. Low resolution (200 µm) test scans were conducted and the power to the laser was increased incrementally until pixel saturation was achieved in the most concentrated region of the gel pattern. Pixel saturation is determined by the Typhoon acquisition software and indicated by red pixilation. The energy was then gradually lowered so that maximum sensitivity could be obtained with no pixel saturation. In order to prevent photo-bleaching by the laser, it was necessary to keep the number and duration of the test scans to a minimum.

The optimal signal for the analytical scans was achieved at 25 µm resolution, using the Typhoon's incorporated 20 mW solid-state doubled frequency SYAG laser (wavelength: 532 nm) with a 560 nm long pass emission filter for the Pro-Q Diamond stain (green-excited fluorescence) and using the Typhoon's 30 mW Argon ion laser (wavelength: 488 nm) with a 610 +/- 35 nm emission filter for the Sypro Ruby stain (blue-excited fluorescence).

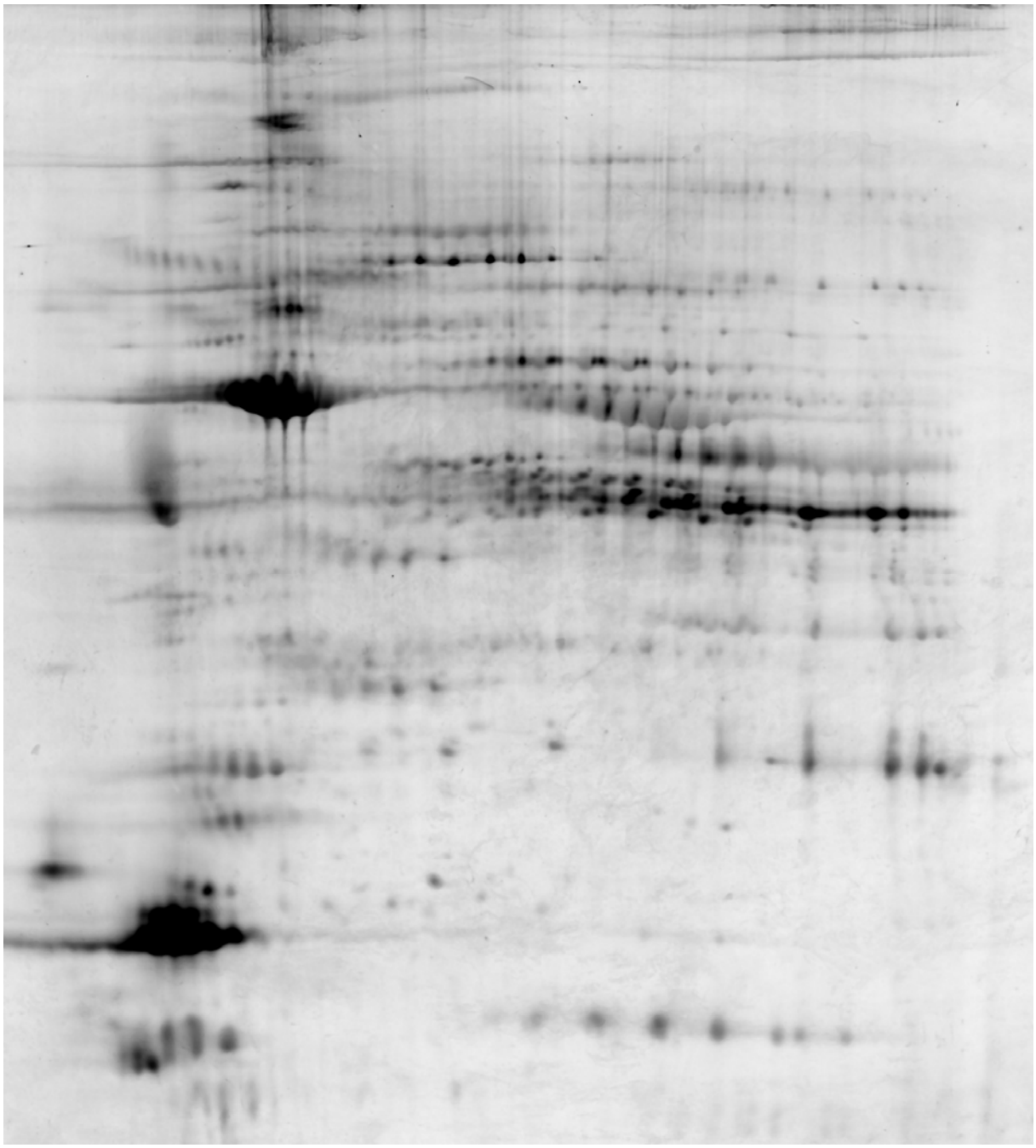

Figure 10. *2D gel image of 5 month old rat skeletal muscle using an optimized Pro-Q Diamond phosphoprotein gel stain protocol.*

2.2.6 Conclusions

The final conditions for the sample preparation, separation, staining and imaging resulted in reproducible, high resolution images which were appropriate for image analysis through an experiment containing six individual gels. By the end of the method development, the sodium fluoride concentration had been reduced to 1mM and the sodium orthovanadate in the IEF solution had been replaced by phosphatase inhibitor cocktail 1 (containing: microcystin LR, cantharidin, and (−)-p-bromotetramisole), and phosphatase inhibitor cocktail 2 (containing: sodium vanadate, sodium molybdate, sodium tartrate, and imidazole), both acquired from Sigma [St. Louis, MO]. This small change helped to improve phosphoprotein detection by targeting a wider variety of phosphatases.

2.2.7 References

[1] Wessel, D., and Flügge, U.I., A method for the quantitative recovery of protein in dilute solution in the presence of detergents and lipids. Anal Biochem. 1984 Apr;138(1):141ND3.

[2] Leimgruber, R.M., Malone, J.P., Radabaugh, M.R., LaPorte, M.L., Violand, B.N. and Monahan, J.B. Development of improved cell lysis, solubilization and imaging approaches for proteomic analyses. Proteomics 2002 Feb;2(2):135ND44.

[3] Lowry, O.H., Rosbrough, N.J., Farr, A.L., and Randall, R.J., Protein measurement with the Folin phenol reagent. J. Biol. Chem. 1951 Nov;193(1):265ND75

[4] Görg A., Boguth, G., Obermaier, C., Posch, A. and Weiss, W., Two-dimensional polyacrylamide gel electrophoresis with immobilized pH gradients in the first dimension (IPG-Dalt): the state of the art and the controversy of vertical versus horizontal systems. Electrophoresis 1995 Jul;16(7):1079ND86.

[5] Schulenberg B, Arnold B, Patton WF. An improved mechanically durable electrophoresis gel matrix that is fully compatible with fluorescence-based protein detection technologies. Proteomics. 2003 Jul;3(7):1196-205.

2.3 Image Analysis

To perform relevant quantitative proteomic experiments and generate reliable reproducible results, the separation is only the beginning. Software to match and quantitate the several hundred or potentially several thousand protein spots found in replicates of controls and a given disease state and between disease states themselves is necessary. Ideally, the software would be able to perform these functions automatically and therefore objectively, but there are fundamental problems that require trained user intervention. Primary among the problems with 2D gel image analysis software is that even in gels with the best resolution there are co-migrating spots. Depending on the particular set of spots, the algorithm used, and the settings applied, the software might resolve the spots into their distinct areas in one gel image and combine the spot areas in another. This leads to errors in quantification, mismatched spots and unmatched spots. Minor gel-to-gel variations such as artifacts from dust and positional warping can cause similar problems. User intervention can ameliorate many of these issues but at a cost of bias. The authors of the software provide a number of tools in order to reduce bias and allow the user to make consistent decisions to generate the most reliable and reproducible data set. In this section, the tools used to perform image analysis of 2D gels will be discussed.

2.3.1 Equipment

Image analysis of the gel images was conducted using the Progenesis PG220 software produced by Nonlinear Dynamics [Newcastle upon Tyne, UK] on a Pentium IV 3.2 MHz PC equipped with 4GB of RAM and a 265MB ATI Radeon 9600 video card.

2.3.2 Procedures

Due to the drastically different extinction coefficients between the multiplexed gel stains, Pro-Q Diamond and Sypro Ruby, the image analysis required separating the images into two discrete image sets based on the stain: one set of images from the Pro-Q Diamond stain with the 5 and 34 month old animals to determine phosphoprotein levels and one set of images from the Sypro Ruby stain with the 5 and 34 month old animals to determine total protein levels. Our experiments included three images for each set; the software was used to combine the images in each set to create an averaged image with matched spots in each set and their respective location and averaged spot density. These averaged images were matched to a master image to provide a reference between different sets of gels. The final quantitative analysis consisted of four averaged gel images, one for each age group depicting phosphoprotein levels and one for each age group depicting total protein levels. The spots of interest were determined from the differences between the 5 month averaged phosphoprotein gel image and the 34 month averaged phosphoprotein gel image. These spots were then referenced against an identical analysis containing total protein images in order to normalize the difference in phosphorylation values by the expression values in each protein spot.

2.3.2.1 Spot Elucidation

To ensure unequivocal identification of phosphoproteins in the Pro-Q Diamond analysis, the grayscale adjustment was set using the PeppermintStick phosphoprotein molecular weight marker as a reference[1]. The marker contains equal amounts of

phosphorylated and unphosphorylated proteins. Optimizing the grayscale so that only the phosphorylated bands were visible was critical throughout this procedure.

In order reduce errors in quantitation and matching, the user must first perform extensive spot editing to separate co-migrating spots. An example of the result of the software's automatic spot detection is shown in **Figure 11.** All of the spot borders in the image were automatically determined. The individual spots in the spot

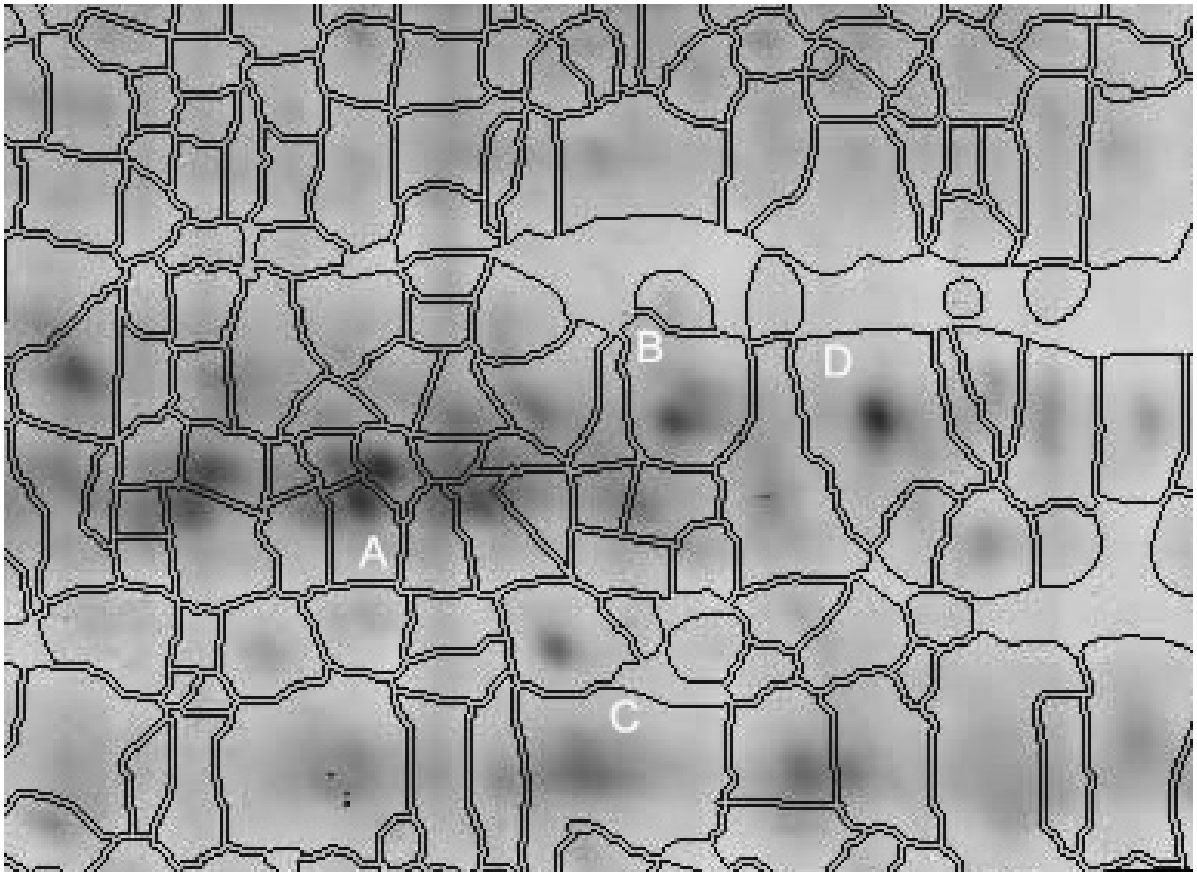

Figure 11. *Automatic spot detection in Progenesis PG220. .*

clusters near (A) in the figure were automatically isolated, but these spots are well resolved with similar intensities. The spots (B), (C) and (D) in **Figure 11** were

determined as single spots where they are in fact, spot clusters. The spots in these clusters are not so well defined and are of variable intensities leading to the poor spot assignment. A slight alteration in the intensities of one of the spots in these clusters in one of the replicate gels could potentially cause the cluster to be separated into distinct spots causing a mismatch and inaccurate quantitation for multiple spots in and around the cluster. One of the primary means used to delineate spots from spot clusters was the 3D image tool to visualize the spot terrain as shown in **Figure 12.**

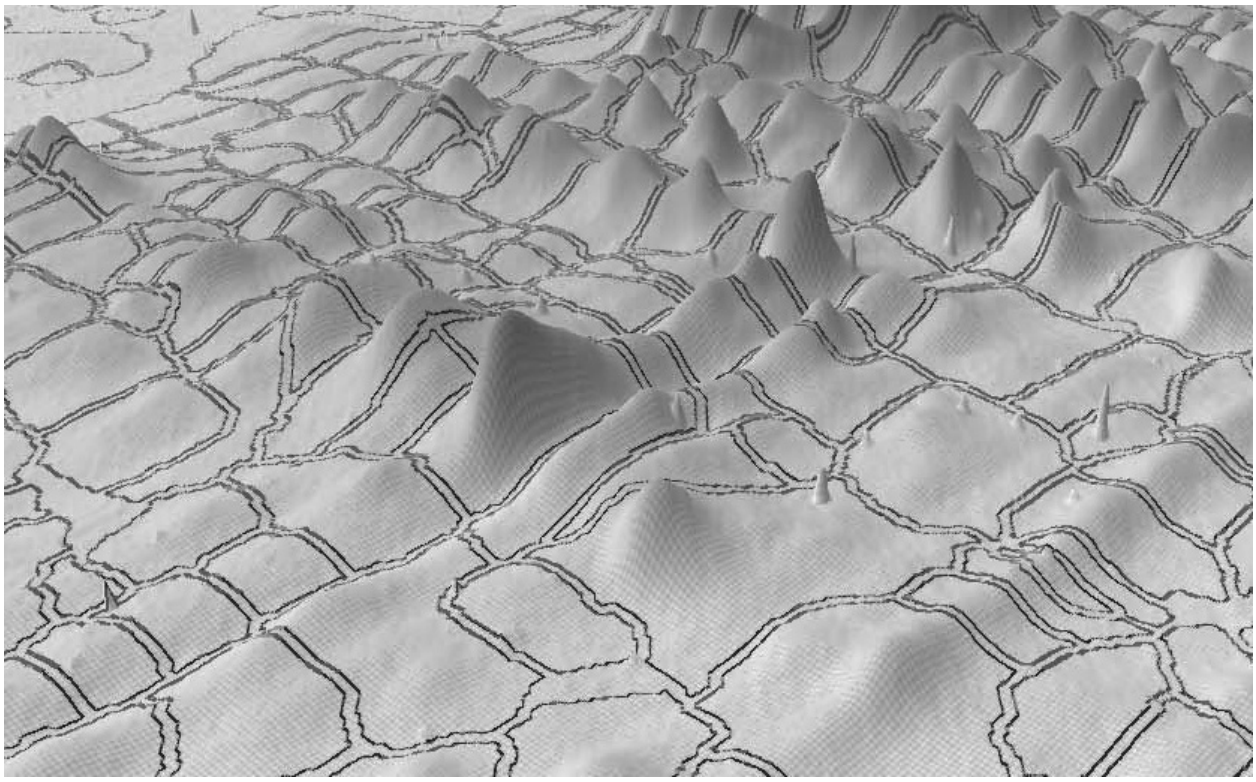

Figure 12. *An example of spot terrain from the 3D image tool.*

2.3.2.2 Spot Matching and Gel Warping

Once all of the spots in an entire data set had been clearly elucidated, spot matching and gel warping throughout the entire data set could take place. This procedure consisted of identifying easily recognizable spots as landmarks and using the software to mark these landmarks as the same spot in each individual gel image. Several spots in each region of the gel were required to maximize the efficiency of the automatic matching and gel warping. The software then utilized the seeded matches to warp the x and y coordinates in each gel image to a predefined master image and then automatically matched the spots based on these coordinates. An example of match vectors is displayed in **Figure 13.** The green and magenta spots in **Figure 13** show the

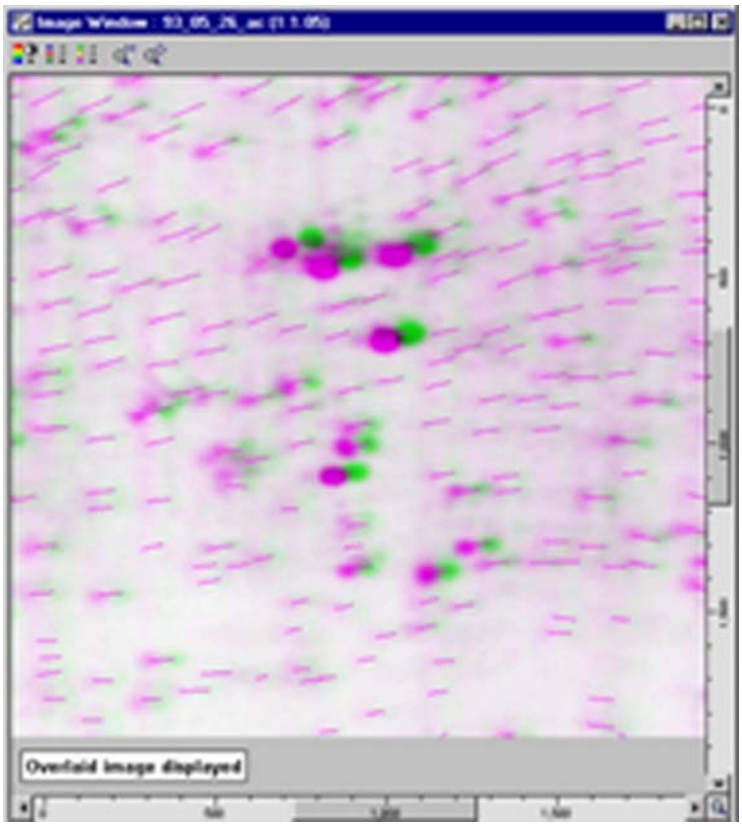

Figure 13. *Image analysis match vectors.*

spot patterns between individual gel images undergoing matching. The magenta line vectors should all flow in the same direction to show that the warping is homogeneous throughout the gel. Regional discrepancies in the motion of the match vectors required repeating the procedure if not resulting from an obvious cause such as a torn gel. The match vectors reduced but did not eliminate the number of mismatches. Individual spots still required verification and those failing verification were added to the seeded matches as new landmark spots. The procedure was repeated for each new landmark. Following dozens of iterations and failing to find any mismatched spots, the image analysis was complete and comparative quantitative data could be ascertained.

2.3.3 Conclusions

A methodology for producing reliable and reproducible image analysis was developed using the available tools and minimal training. One of the claims of the Progenesis software programmers is that their algorithm produces the same results irrespective of the operator using the same data set. With reproducibility achieved, the programmers must now seek accuracy and precision. Much work still needs to be done in the future to provide both reproducible and correct results this type of software[2].

2.3.4 References

[1] Schulenberg B, Aggeler R, Beechem JM, Capaldi RA, Patton WF. Analysis of steady-state protein phosphorylation in mitochondria using a novel fluorescent phosphosensor dye. J Biol Chem. 2003 Jul 18;278(29):27251-5.

[2] Clark BN, Gutstein HB. The myth of automated, high-throughput two-dimensional gel analysis. Proteomics. 2008 Mar;8(6):1197-203.

2.4 Mass Spectrometry

Numerous attempts have been made to utilize the available Finnigan LCQ MS ion traps combined with various Microtech HPLC systems to perform nanoelectrospray high performance liquid chromatography tandem mass spectrometry (NSI HPLC-MS/MS) using the methodology previously established within the group for identifying proteins from in-gel digests of protein spots from 2D gels. Attempts at modifying and extending the gradient using this instrumentation were not successful and a very limited number of identifications were made. The primary hypothesis offered to explain this failure was that not enough peptide mass from the in-gel digests was present to accommodate the detection range of the instrument. To investigate this possibility, ten replicate spots were excised from ten separate 2D gels to increase the protein mass for each sample by an order of magnitude. With 110 spots of interest in the cerebellum study, this translated into 1100 spots manually excised. Twenty samples were initially submitted for NSI HPLC-MS/MS analysis using the LCQ MS. This resulted in only a 5% identification rate or one sample out of twenty samples submitted. An example of the ion chromatogram for the successful ID and the resultant database search from the spectra obtained can be seen in **Figure 14.** Aliquots of these twenty samples were simultaneously submitted to the Analytical Proteomics Lab (APL) where they were analyzed by MALDI using the Applied Biosystems 4700 Proteomics Analyzer (MALDI tandem TOF-TOF mass spectrometer). The results for the MALDI analysis can be seen in **Figure 15**, and show improved coverage for creatine kinase B (Ckb) with three additional peptides observed. These samples were also analyzed by electrospray

capillary HPLC- MS/MS (ESI HPLC-MS/MS) on the Thermo-Finnigan hybrid LTQ FT-ICR mass spectrometer, **Figure 16**, where an even greater improvement in coverage

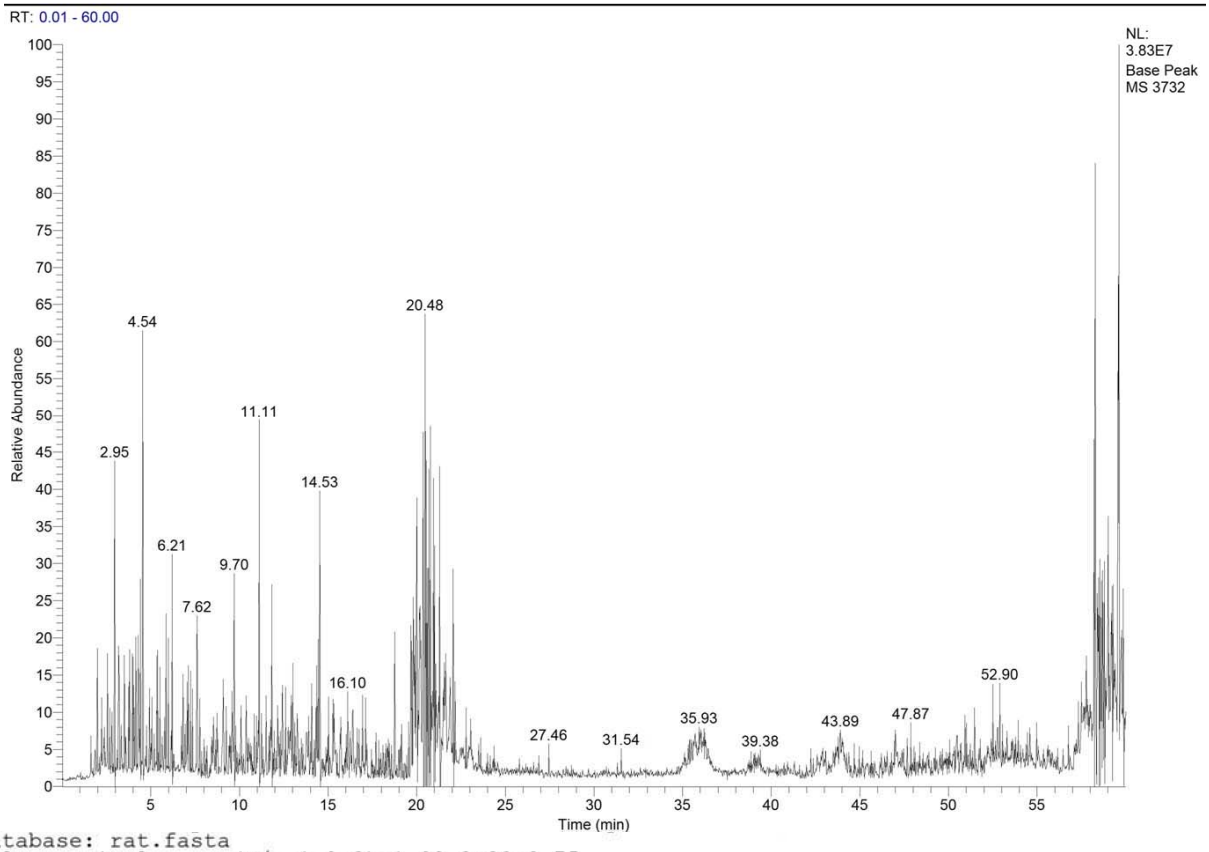

Database: rat.fasta
Filter: single, xc (+/- 1,2,3)=1.90,2.20,3.75

	Reference Scan(s)	Sequence	MH+	z	XC	DeltaCn	Sp	RSp	Score Ions	Accession Count
#1		**creatine kinase brain isoform [Rattus nor**					**28.2**			**31322101**
	813	R.FC#TGLTKIETLFK.E	1558.81	2	2.891	0.483	1335.5	1	18/24	
	813	R.FC@TGLTKIETLFK.E	1557.81	2	3.217	0.000	1335.5	1	18/24	
	834	R.FCTGLTKIETLFK.E	1500.81	2	4.005	0.387	1356.1	1	20/24	

#1

Figure 14. Top: *Ion chromatogram of spot 3732 from NSI HPLC-MS/MS on a Thermo-Finnigan LCQ ion trap MS using a 5 µL injection volume and a linear gradient of 5-80% ACN/0.1% FA (v/v) over the first 45 minutes holding at 80% ACN/0.1% FA (v/v) for the last 15 minutes at ~300 nL/min.* **Bottom:** *Result of SEQUEST database searching of spectra obtained for sample 3732.*

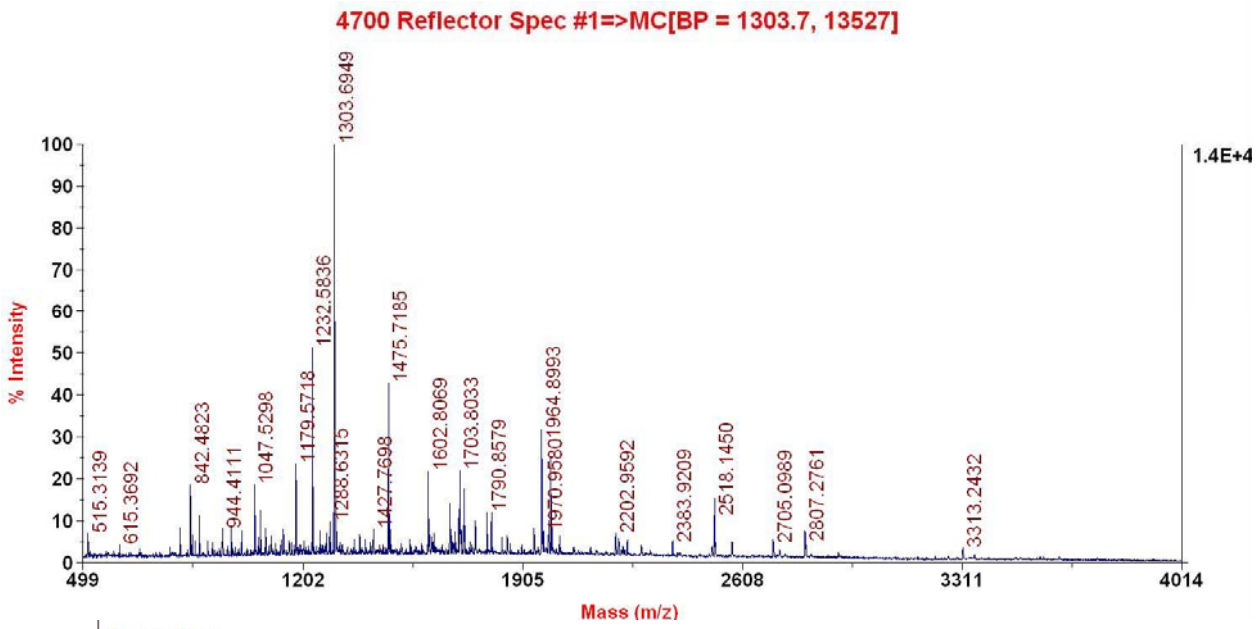

Protein View

Match to: P07335|KCRB_RAT Score: 117
Creatine kinase B-type (EC 2.7.3.2) (Creatine kinase B chain) (B-CK) - Rattus norvegicus (Rat)
Found in search of ppw_B17_117621670802.txt

Nominal mass (M_r): 42988; Calculated pI value: 5.39
NCBI BLAST search of P07335|KCRB_RAT against nr
Unformatted sequence string for pasting into other applications

Taxonomy: Rattus norvegicus

Fixed modifications: Carboxymethyl (C)
Cleavage by Trypsin: cuts C-term side of KR unless next residue is P
Sequence Coverage: 9%

Matched peptides shown in Bold Red

```
     1 MPFSNSHNTQ KLRFPAEDEF PDLSSHNNHM AKVLTPELYA ELRAKCTPSG
    51 FTLDDAIQTG VDNPGHPYIM TVGAVAGDEE SYDVFKDLFD PIIEDRHGGY
   101 QPSDEHKTDL NPDNLQGGDD LDPNYVLSSR VRTGRSIRGF CLPPHCSRGE
   151 RRAIEKLAVE ALSSLDGDLS GRYYALKSMT EAEQQQLIDD HFLFDKPVSP
   201 LLLASGMARD WPDARGIWHN DNKTFLVWIN EEDHLRVISM QKGGNMKEVF
   251 TRFCTGLTQI ETLFKSKNYE FMWNPHLGYI LTCPSNLGTG LRAGVHIKLP
   301 HLGKHEKFSE VLKRLRLQKR GTGGVDTAAV GGVFDVSNAD RLGFSEVELV
   351 QMVVDGVKLL IEMEQRLEQG QPIDDLMPAQ K
```

Show predicted peptides also

Sort Peptides By ◉ Residue Number ○ Increasing Mass ○ Decreasing Mass

Start - End	Observed	Mr(expt)	Mr(calc)	Delta	Miss	Sequence
33 - 43	1303.7704	1302.7631	1302.7183	0.0448	0	K.VLTPELYAELR.A (Ions score 33)
87 - 96	1232.6526	1231.6453	1231.6084	0.0369	0	K.DLFDPIIEDR.H (Ions score 47)
157 - 172	1602.9087	1601.9014	1601.8260	0.0754	0	K.LAVEALSSLDGDLSGR.Y (Ions score 37)

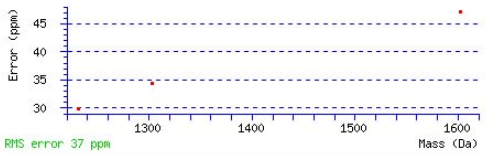

Figure 15. Top: *MS spectrum from MALDI 4700 analysis of spot 3732.* **Bottom:** *Result of Mascot database search of MALDI spectrum.*

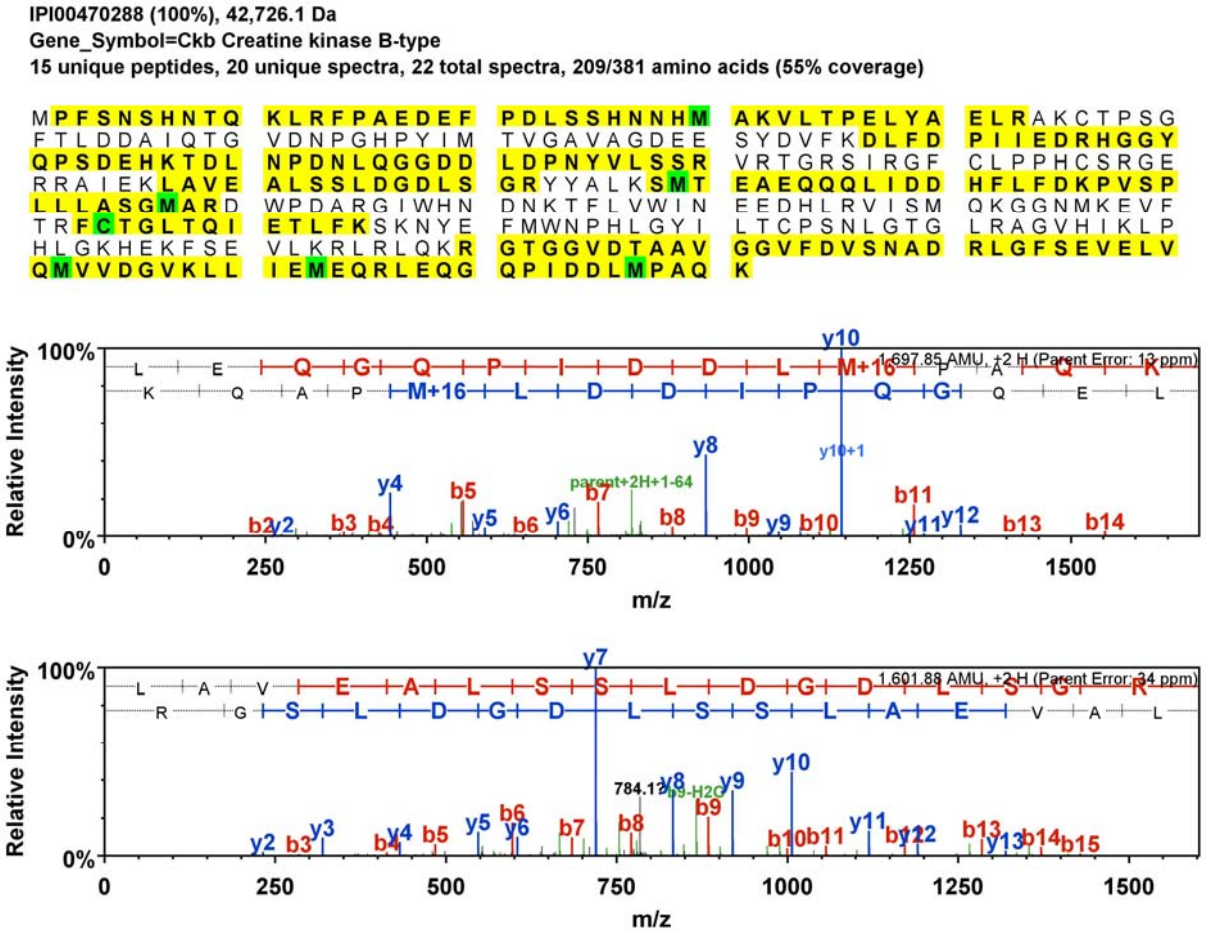

Figure 16. *The sequence coverage and representative MS spectra from ESI HPLC-MS/MS analysis of spot 3732 using FT-ICR MS. Database search conducted using both SEQUEST and Mascot with results combined in the program Scaffold.*

was observed for the same sample (spot 3732), but the remaining samples were still not identified. With only a marginal improvement in the overall identification of the proteins utilizing existing methods within the APL, the process of initiating and developing NSI HPLC-MS/MS utilizing the LTQ FT-ICR began in earnest.

2.4.1 Materials and Equipment

The chromatography system either consisted of a MicroTech Ultra-Plus II capillary LC [Micro-Tech Scientific, Vista, CA] or a FAMOS Capillary and Nano HPLC Autosampler, a Switchos loading pump and switching valve and an ULTIMATE Capillary and Nano HPLC Pump [Dionex/LC Packings, Sunnyvale, CA]. A 1mm C-18 PepTrap column [Dionex, Sunnyvale, CA] was utilized to trap the peptides and a standard coated PicoFrit® column, 360µm/75µm OD/ID, 15µm tip, 15 cm long [New Objective, Woburn, MA], packed in house with 5 µm particles of 300 Å pore-size Bio-Basic C18 material [Thermo-Scientific, Waltham, MA] was used for the separation of the peptides. The mass spectrometer used for peptide identification was a Thermo-Finnigan hybrid LTQ FT [Thermo-Scientific, Waltham, MA]. MS-grade modified trypsin [Promega, Madison WI] was used to perform the in-gel digests and all other reagents and solvents were acquired from Fisher Scientific [Fairlawn, NJ].

2.4.2 Chromatographic Conditions

The optimization of the chromatography began by attempting to duplicate the NSI HPLC system in place within the Schöneich group using the Microtech/LCQ instruments and the Microtech HPLC was transported to the Structural Biology Center. The same pre-column/pre-injection split was installed and the same capillary tubing diameters (25 µm ID) and lengths were employed. A 5 µL injection loop was utilized on the integrated injection port of the MicroTech Ultra-Plus II capillary LC and the same linear gradient of 5-80% ACN/0.1% FA (v/v) over the first 45 minutes and then holding at 80% ACN/0.1% FA (v/v) for 15 minutes for a total run time of 60 minutes was programmed. The flow

rate was regulated in the program and measured using a volumetric capillary to be between 250 and 300 nL/min from the PicoFrit column. After applying a voltage and establishing a spray, the first goal with the newly assembled system was to tune the FT-ICR for nanospray which was not possible by conventional means (infusion) due to the extremely low flow rates and design of the system. Typically, one of the disadvantages of a highly sensitive system such as an FT-ICR MS are background contaminants in the mobile phase, primarily from phthalates in even the highest grade commercial water. Turning this disadvantage into an advantage, the instrument was tuned using a low level laboratory water contaminant, diisooctyl phthalate (m/z: 391) found in the mobile phase[2]. With the detector tuned, the next priority was to establish the elution and detection of a test mixture of peptides.

Using a mixture of angiotensin and other standard peptides provided by the APL, several manual injections were made in series with no reproducible result. After extensive troubleshooting with no observable faults in the system, the run time was extended to 120 minutes by holding at 80% ACN/0.1% FA (v/v) for an additional 60 minutes and the peptides were clearly and reproducibly observed at 100 minutes. This experiment was repeated using the Microtech/LCQ instruments within the group and the same results were observed explaining nearly a year of difficulties in submitting samples to be analyzed by the established methods.

In designing a new system and the corresponding chromatographic methods, the primary concern was in minimizing the void volume introduced by the extremely low flow rates. To accomplish this goal, a system of column switching utilizing a 1mm C-18 PepTrap column and two separate LC pumps was employed. The first pump was a

Switchos loading pump, in line to a FAMOS autosampler followed by the PepTrap column plumbed into an integrated switching valve in the Switchos (blue arrows in **Figure 17**). The flow for the pre-concentration step was set at 20 µL/min using 0.1% TFA in water (v/v). The increased flow rate (from 200 nL/min) along with a reduction to 15 cm of 25 µm capillary tubing between the switching valve and the PicoFrit column compared to 50 cm of the same tubing with the Microtech pump reduced the overall runtime by 50 minutes. This pre-concentration step also allowed the incorporation of a larger 10 µL sample loop with no change in runtime increasing the absolute mass of peptides presented to the MS.

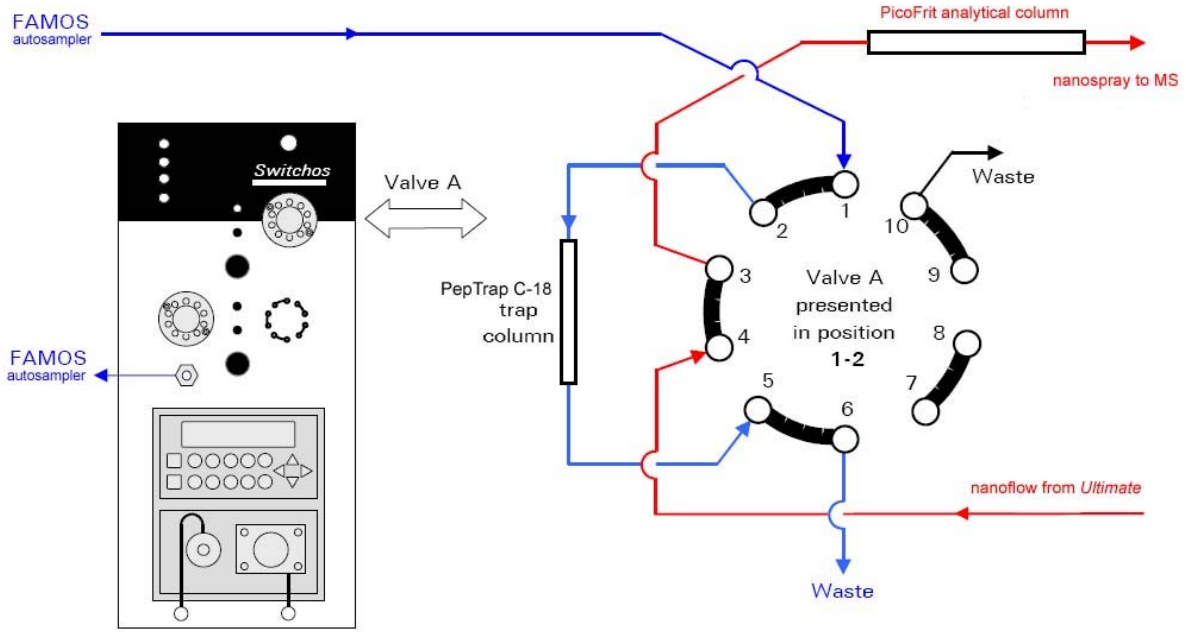

Figure 17. *Modified schematic from Ultimate nano HPLC User Guide[1] demonstrating setup of pre-concentration valve switching. Here the valve is shown in position (1-2) [sample loading] showing flow (in blue) from the loading pump to the autosampler through the trap column to waste (5-6). In red, nanoflow from the Ultimate pump enters the valve and is directed to the PicoFrit analytical column (4-3). When the valve switches to 1-10, flow from the loading pump/autosampler is directed to waste (1-10) and nanoflow from the Ultimate is transferred through the trap column (4-5) to the analytical column (2-3).*

Five minutes were allowed for the Switchos pump to trap the peptides on the PepTrap column before the switching valve was engaged to change the mobile phase flow through the PepTrap column from the Switchos to the Ultimate Nano pump which then flowed through the PepTrap column at 200 nL/min into the PicoFrit column and, subsequently, the mass spectrometer. Several different gradients were applied with the Ultimate pump in a delicate balance between maximizing the peptide separation and allowing ample time for the mass spectrometer to perform CID on individual peaks.

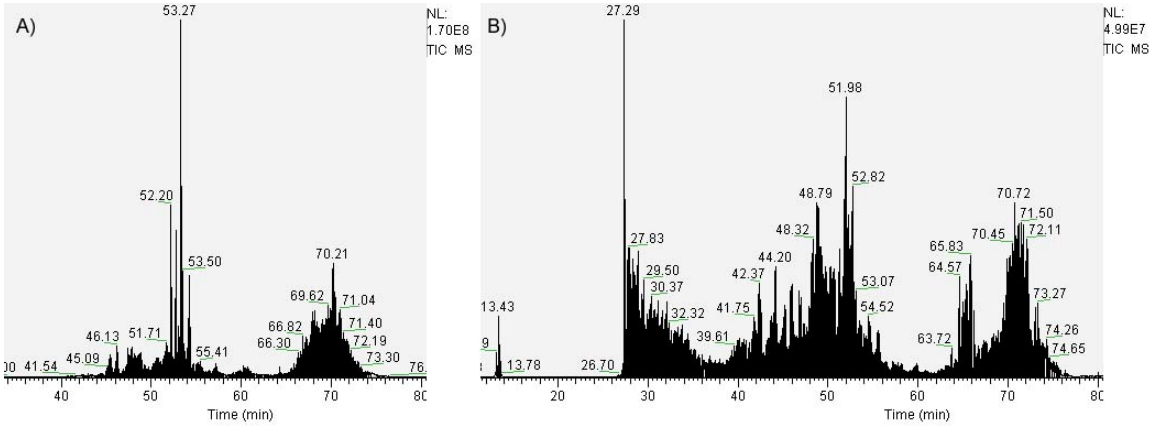

Figure 18. *Comparison of Total Ion Current (TIC) chromatograms for 100 total nanomole of trypsin digested bovine serum albumin (BSA). The linear gradient in chromatogram A) consists of 5-90% solvent B over 60 minutes and the linear gradient in chromatogram B) consists of 10-90% solvent B over 60 minutes. Solvent A consisted of 10% ACN/89.9% H_2O/0.1% FA (v/v/v) and solvent B consisted of 10% H_2O/89.9% ACN/0.1% FA (v/v/v).*

To demonstrate this point, in **Figure 18**, chromatogram B provided more quality MS/MS spectral data for BSA than the conditions found in chromatogram A and also provided faster re-equilibration for subsequent injections by starting at a higher organic concentration. The peak at 27.29 minutes in chromatogram B is indicative of very hydrophilic peptides which are not retained on the PicoFrit analytical column after the

switching of the valve and introduction of the low organic mobile phase from the Ultimate pump. With a reasonable optimized separation, the next step before sample analysis was to test the detection/identification limits of the integrated system.

The BSA digest used above was serially diluted with 0.1% FA in H_2O to 5 fmol/µL, 500 amol/µL and 50 amol/µL and 10 µL of each were injected in inverse order using the gradient program B in order to establish the detection limits of the system. The TIC chromatograms are provided in **Figure 19** below and the linear decrease in ion

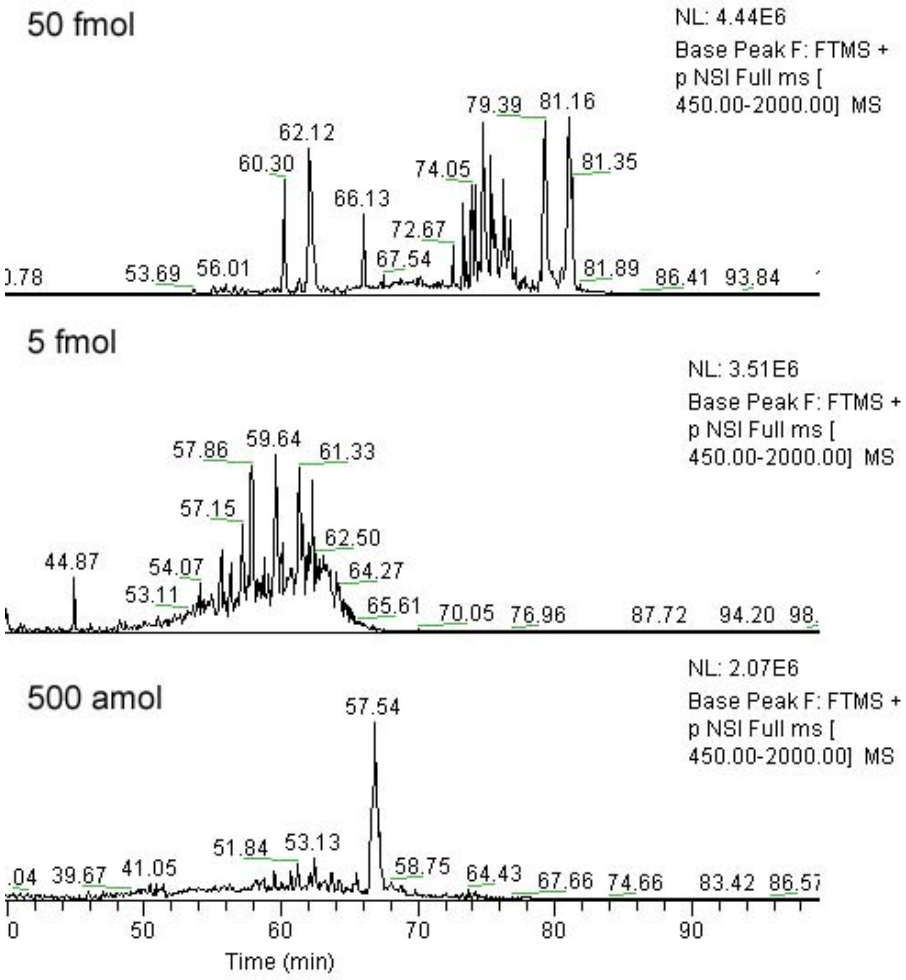

Figure 19. *Several concentrations of BSA were tested to estimate the mass needed for database identification.*

intensity does not necessarily translate into lower quality MS/MS spectra. Only one of the three samples showed BSA peptides. A total mass of 50 fmol showed three unique BSA spectra, while neither 5 fmol nor 500 amol sample showed any BSA spectra. All of the samples were dominated by exogenous interference peaks from keratins and trypsin auto-digest peptides. The data acquisition system for the FT-ICR MS was programmed to ignore any subsequent trypsin peptide ions, by creating an exclusion list with the appropriate mass to charge ratios for the known interfering species.

2.4.3 Survey Scanning

The first experiment applied to all samples was designed for the general identification of peptides. In this experiment the LTQ-ICR FT mass spectrometer was programmed to use a data-dependent survey scan in the positive mode where a full range mass spectrum (m/z 400-2000) was collected and the three most abundant ions were scanned using selected ion monitoring by the Fourier transform ion cyclotron resonance mass spectrometer (FT-ICR) and accumulated in the linear quadrupole ion trap (LTQ) mass spectrometer prior to conducting MS/MS on the accumulated ions.

The automatic gain control (AGC) target values were set to $1X10^6$ ions for the survey MS, $1X10^5$ ions for the selected ion monitoring (SIM) and $1X10^4$ for the MS/MS experiments. The maximum accumulation time was set at 200 ms for all modes. The resolution at 400 *m/z* was set to $1X10^4$ for the FT-ICR scans and isolation widths were set at ± 2 *m/z* for the SIM experiments, and ± 1 *m/z* for the MS/MS experiments. Ions were selected for MS/MS when their respective intensities reached 1000 counts. The normalized collision energy was set to 35% and three microscans were acquired for

each spectrum. The mass spectrometer was programmed to ignore singly charged species for fragmentation and was set to dynamically exclude precursors that had already been selected during the first minute after their respective fragmentations.

2.4.4 Neutral Loss Scanning

One feature of phosphorylated peptides is that the phosphate group provides a low-energy pathway in competition with peptide backbone fragmentation resulting in a potential loss of 98 Daltons for phosphoserine and phosphothreonine residues from the parent mass and a potential loss of 80 Daltons from the parent mass for phosphotyrosine residues. Proposed mechanisms for phosphoserine losses are shown in **Scheme 2.**

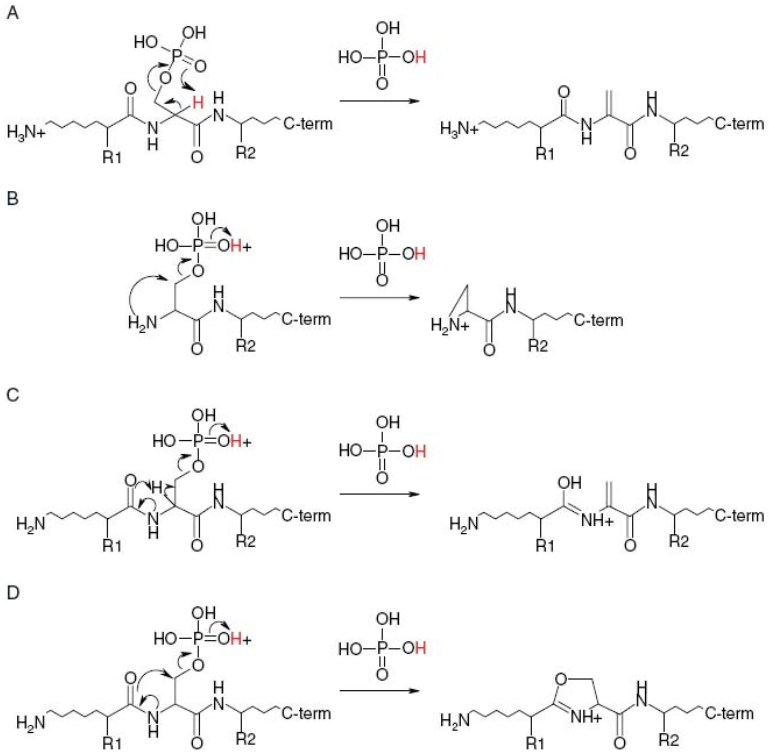

Scheme 2. *Proposed neutral loss pathways for phosphoserine (from Boersema et al[3]).*

In reaction **A**, a charge-remote β-elimination produces dehydroalanine with the loss of the phosphate group. The remainder of the reactions are charge-directed pathways with intermediates to the dehydroalanine. In reactions **B** and **D** we find S_N2 neighboring group participation and reaction **C** represents an E2 elimination.

Due to the difficulty in observing phosphopeptides while optimally determining protein ID in the positive mode and to enhance our ability to localize the exact phosphorylation site, a second experiment was conducted for each sample with similar parameters as the first experiment. An additional step was added, that of monitoring neutral losses by scanning for fragment ions that had suffered a loss of 98 Daltons from the parent. Additional tandem mass spectra (MS^3) were collected on these fragments[3,4].

2.4.5 Hypothesis-based mass spectrometry

This third and final MS experiment was conducted after data analysis had confirmed an identity for an in-gel digest of a given spot, but where a quality mass spectrum for a phosphopeptide was not obtained. Utilizing information from PhosphoSitePlus (www.phosphosite.org) about previously reported phosphorylation sites and phosphoproteins among the identified proteins, an extensive list of hypothetical phosphopeptides was created in-silica by manually cross-referencing the results from the MS-Digest tool from ProteinProspector (http://prospector.ucsf.edu/mshome.htm) for each known phosphoprotein without a quality phosphopeptide tandem mass spectrum. (see section **2.5.4**) This information

was used to program the FT-ICR employing SIM to look for these specific ions. Each sample had its own exclusive ion list containing the hypothetical peptides in their most probable charge states. The AGC target value was lowered to 1 $X10^4$ for the SIM experiment and the maximum accumulation time was increased to 300 ms; all other features of the mass spectrometer programming were left static.

2.4.6 Experimental

The mass spectrometer programming for subsequent experiments was applied as described in each relevant section. The resultant chromatographic conditions and the sample preparation methods which were the result of the method development are summarized here.

Protein spots demonstrating differential phosphorylation were excised manually from the gels using a 1.5 mm spot picker and disposable tips using a blue-light LED gel imager and Sypro Ruby gel stain to visualize the spots. The gel plugs were dehydrated with acetonitrile, dried and subjected to in-gel digestion with MS-grade modified trypsin in 50 mM NH_4HCO_3 overnight at 37°C. The supernatant was removed and analyzed via nanospray ionization (NSI) HPLC-MS/MS using a Thermo-Finnigan hybrid LTQ FT mass spectrometer.

The chromatography for all mass spectrometric experiments was kept consistent with injection volumes of 10 µL for all peptide digests. The final chromatography system consisted of the FAMOS Autosampler, the Switchos loading pump and switching valve and the ULTIMATE Capillary and Nano HPLC Pump. The Switchos Loading pump, in-line to the autosampler, trapped the digests on a 1mm C-18 PepTrap column (5 µm

particle size, 300 Á pore size) at a flow rate of 20µL/min of 0.1% (v/v) TFA. After 5 minutes, the switching valve, integral to the Switchos pump, changed sample flow through the PepTrap column from the Switchos to the ULTIMATE Nano pump which then flowed through the PepTrap column into a PicoFrit column, 360µm/75µm OD/ID, 15µm tip, 15 cm long, packed in house with 5 µm particles of 300 Á pore-size Bio-Basic C18 material. The flow rate was approximately 200 nL/min, utilizing a 90 minute linear gradient from 90% (v/v) solvent A to 90% (v/v) solvent B and held at 90% B for 30 minutes. Solvent A consisted of 10% ACN/89.9% H_2O/0.1% FA (v/v/v) and solvent B consisted of 10% H_2O/89.9% ACN/0.1% FA (v/v/v). The PepTrap column and the PicoFrit column were allowed to re-equilibrate to aqueous conditions (0.1% TFA and 90% solvent A respectively) for 60 minutes between analytical runs.

2.4.7 Results and Conclusions

The use of nanoelectrospray ionization coupled with the FT-ICR MS provided a substantial improvement in the identification of the in-gel digests. Where prior to this method development successful identification was staggeringly low at a level of 5%, the sensitivity afforded by the resultant methods produced an identification level on the order of 150% since many single spot digests resulted in multiple proteins identified for many of the spots. In the following experiments using C2C12 cells, rat cerebellum and rat skeletal muscle, the additional peptide mass provided by cutting ten replicate spots (in the cerebellum study) versus three replicate spots (in the skeletal muscle and C2C12 studies) provided better peptide coverage and improved the overall protein identifications, but at the same time presented a hazard introduced by operator error in

the manual spot excision. These errors could be ameliorated by using a robotic spot picker and the advantages of the extra mass would be combined with a large reduction in errant spot excision.

2.4.8 References

[1] 'Ultimate Nano User Guide.' Dionex. http://www.dionex.com/en-us/webdocs/64684_D970R3_Users_Manual_UltiMate.pdf

[2] 'Optimizing Mobile Phase Solvent Purity of LC-MS." Fisher Scientific. http://www.fishersci.com/wps/downloads/segment/Scientific/pdf/Literature/LCMS_OptimizeMobilePhase.pdf

[3] Boersema PJ, Mohammed S, Heck AJ. Phosphopeptide fragmentation and analysis by mass spectrometry. J Mass Spectrom. 2009 Jun;44(6):861-78.

[4] Mann, M., Ong, S.E., Grønborg, M., Steen, H., Jensen, O.N. and Pandey, A., Analysis of protein phosphorylation using mass spectrometry: deciphering the phosphoproteome. Trends Biotechnol. 2002 Jun;20(6):261-8

2.5 Bioinformatics

The bottleneck of proteomic studies has been and will continue to be, the increasingly large volume of data produced by these studies. The key components in reducing the lag time of data analysis are computing power, task automation, and the quality of data[1]. Computing power is a fairly straightforward consideration, the faster the processor can cycle and the more data the processor has available to process at peak speed, the faster the result. Task automation is also straightforward; it involves queuing the data processing in an intelligent fashion to minimize the loss of processor cycles. Both of these variables are dependent on data quality, which describes a number of factors beyond experimental design. Not only does data quality represent the mass spectral quality, but it is also influenced by the quality and appropriateness of the data reduction algorithm which transforms the mass spectra into reduced data sets that can be used to search the appropriate database[1]. A poor translation of the mass spectra leads directly to incorrect data being searched. The next factor in data quality is the searching algorithm, which is specific for a particular instrument or set of conditions therefore introducing an inherent bias to each algorithm. The database itself can also play an important role, impacting the quality of the data or the relative speed of data analysis in many ways. Is it current? Is it redundant? Are there sequencing errors present? The final component in data quality is a statistical validation in the assignment of mass spectra to peptide sequences. What is the estimated rate of false positive or false negative assignments? This section of the dissertation will describe measures that were taken to ensure the quality of the data and to mine the data for additional information.

2.5.1 Software and Equipment

The computer hardware used for the data analysis consisted of a matched pair of Dell Intel 64-bit Xeon dual-core workstations with 32 GB of RAM. The software used for the data reduction and analysis consisted of XCalibur and Bioworks v.3.3.1 utilizing the SEQUEST[32] database searching algorithm [Thermo-Scientific, Waltham, MA], GPS Explorer utilizing the Mascot searching algorithm[33] [Matrix Science, Boston MA], and Scaffold utilizing the X!Tandem[34] searching algorithm [Proteome Software, OR].

2.5.2 Tandem MS protein and phosphopeptide identification

Prior to the projects described in this dissertation consisting of hundreds of samples, the Analytical Proteomics Laboratory at KU had no need to develop the batch processing capabilities required to reduce this volume of data. In order to speed the process and minimize the impact of our projects on the limited computational power available, several previously unused tools were utilized in automating the tasks involved in obtaining protein and phosphopeptide identifications.

To maintain the quality of the data and minimize the amount of bias applied in the database searches, all available database searching algorithms were utilized. The Scaffold program is designed to verify the peptide assignments made by SEQUEST[2] and Mascot[3] with its X!Tandem[4] algorithm and then performs a statistical validation on the peptide assignments using the PeptideProphet[5] and then derives corresponding protein probabilities using ProteinProphet[6].

Search parameters for all algorithms were matched to include static mass modifications to cysteine due to alkylation by iodoacetamide, and differential mass modifications to methionine from oxidation. Parameters specific to the modification of Ser, Thr and Tyr from phosphorylation were also utilized including the possibility of neutral losses from these residues. The time to perform a database search increases nearly exponentially with each additional modification parameter, but in order to identify unknown phosphoproteins the additional time was necessary.

The process of transforming the mass spectral data into peptide identifications began with the software and algorithm designed for the instrument on which it was acquired. For the data from the FT-ICR MS, this software was XCalibur and Bioworks. The batch processing tool incorporated into Bioworks allowed queuing ten analytical runs for database searching using the SEQUEST algorithm and sending the peptide hit results to distinct result directories. A Perl script written for the APL was in use to create data files usable by Mascot from the SEQUEST result directories. This function was automated to create the Mascot-friendly data files as the SEQUEST result directories were generated. Next, a batch processing tool within GPS Explorer was discovered and utilized to automate the Mascot searches and generate Mascot result files. Both the SEQUEST and Mascot batch searches took at least one and possible two or three days to complete. When a complete set of result files from both Mascot and SEQUEST for a given batch of analytical runs was available, they were presented to Scaffold for verification and compilation of peptide and protein assignments. A typical analysis of ten samples required over a week of computational time to process and is diagrammed in aiming for the bull's-eye in **Figure 20.**

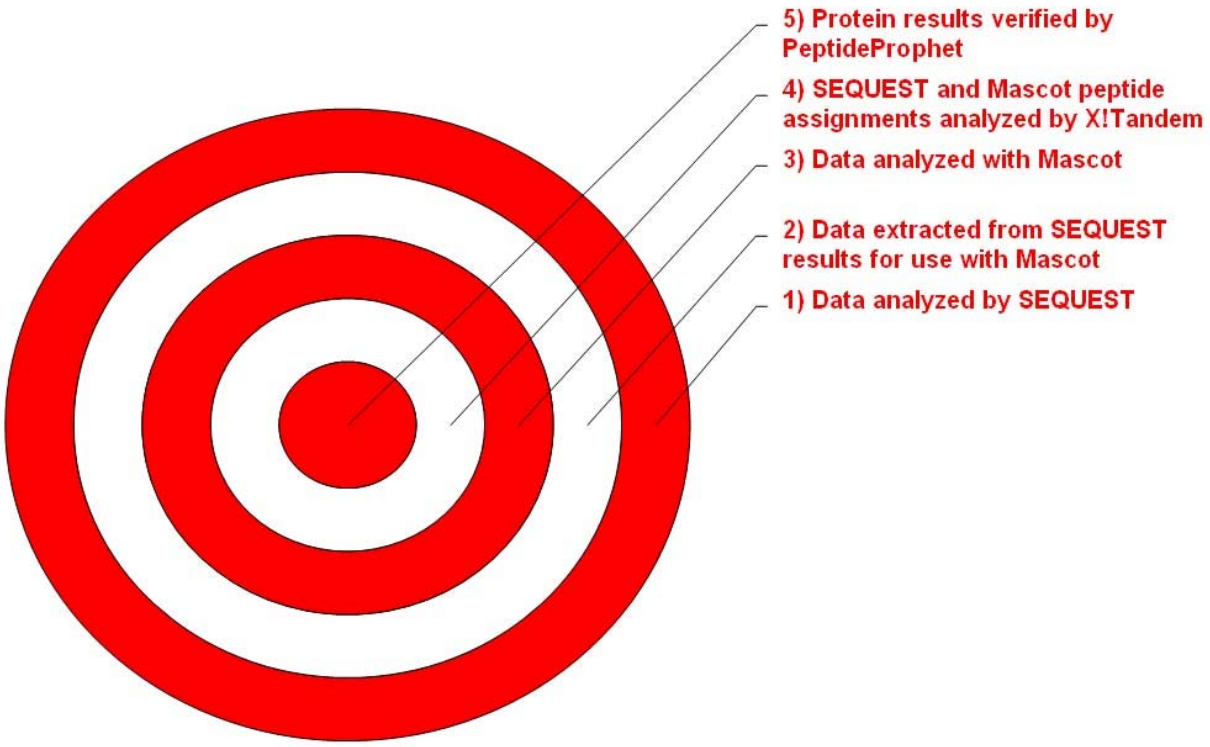

Figure 20. *Bull's-eye diagram of data refinement from mass spectra (outer ring) to protein identification (bull's eye).*

2.5.3 MS Extract phosphopeptide mapping

For the initial data set, less than 20% of the suspected phosphoproteins yielded MS/MS spectra of phosphopeptides meeting the requisite standards of quality. In an attempt to mine additional phosphopeptides from the existing data, an add-on program, MS Extract, was acquired from Thermo-Scientific to extract the MS1 spectra from the raw analytical run data where it is not readily available. This was an onerous manual exercise calling for opening each individual file, highlighting the area in the TIC chromatogram of interest, applying the MS Extract filter, and then renaming the data file to distinguish the extracted file from the original. Over 300 data files were manipulated in this fashion. Once the extracted files had been collected they were individually

searched using the peptide mass fingerprinting functionality of Mascot typically used for the identification of proteins by MALDI. The highest quality result is found in **Figure 21.**

Match to: IPI00231302.5 Score: 3 Expect: 89
NEUROFILAMENT LIGHT POLYPEPTIDE.
Found in search of 988.txt

Nominal mass (M_r): 61355; Calculated pI value: 4.63
NCBI BLAST search of IPI00231302.5 against nr
Unformatted sequence string for pasting into other applications

Fixed modifications: Carbamidomethyl (C)
Variable modifications: Oxidation (M),Phospho (ST),Phospho (Y)
Cleavage by Trypsin: cuts C-term side of KR unless next residue is P
Number of mass values searched: 610
Number of mass values matched: 29
Sequence Coverage: 51%

Matched peptides shown in Bold Red

```
     1 MSSFSYEPYF STSYKRRYVE TPRVHISSVR SGYSTARSAY SSYSAPVSSS
    51 LSVRRSYSSS SGSLMPSLEN LDLSQVAAIS NDLKSIRTQE KAQLQDLNDR
   101 FASFIERVHE LEQQNKVLEA ELLVLRQKHS EPSRFRALYE QEIRDLRLAA
   151 EDATNEKQAL QGEREGLEET LRNLQARYEE EVLSREDAEG RLMEARKGAD
   201 EAALARAELE KRIDSLMDEI AFLKKVHEEE IAELQAQIQY AQISVEMDVS
   251 SKPDLSAALK DIRAQYEKLA AKNMQNAEEW FKSRFTVLTE SAAKNTDAVR
   301 AAKDEVSESR RLLKAKTLEI EACRGMNEAL EKQLQELEDK QNADISAMQD
   351 TINKLENELR STKSEMARYL KEYQDLLNVK MALDIEIAAY RKLLEGEETR
   401 LSFTSVGSIT SGYSQSSQVF GRSAYSGLQS SSYLMSARAF PAYYTSHVQE
   451 EQSEVEETIE ATKAEEAKDE PPSEGEAEEE EKEKEEGEEE EGAEEEEAAK
   501 DESEDAKEEE GGEGEEEDTK ESEEEEKKEE SAGEEQAAKK KD
```

Show predicted peptides also

Sort Peptides By (•) Residue Number ( ) Increasing Mass ( ) Decreasing Mass

Start - End	Observed	Mr(expt)	Mr(calc)	ppm	Miss	Sequence
1 - 15	1902.8300	1902.8300	1902.7423	46	0	-.MSSFSYEPYFSTSYK.R Phospho (Y)
1 - 16	2458.5900	2458.5900	2458.6750	-35	1	-.MSSFSYEPYFSTSYKR.R 3 Phospho (ST); 3 Phospho (Y)
17 - 23	919.4800	919.4800	919.4875	-8	1	R.RYVETPR.V
56 - 87	3368.8000	3368.8000	3368.6769	37	1	R.SYSSSSGSLMPSLENLDLSQVAAISNDLKSIR.T
85 - 91	1020.4400	1020.4400	1020.4042	35	1	K.SIRTQEK.A 2 Phospho (ST)
88 - 91	504.2600	504.2600	504.2544	11	0	R.TQEK.A
117 - 126	1153.7400	1153.7400	1153.7070	29	0	K.VLEAELLVLR.Q
129 - 134	711.3100	711.3100	711.3300	-28	0	K.HSEPSR.F
148 - 157	1060.4800	1060.4800	1060.5036	-22	0	R.LAAEDATNEK.Q
158 - 164	800.4100	800.4100	800.4140	-5	0	K.QALQGER.E
158 - 172	1807.9200	1807.9200	1807.8465	41	1	K.QALQGEREGLEETLR.N Phospho (ST)
173 - 177	600.3400	600.3400	600.3343	9	0	R.NLQAR.Y
186 - 196	1291.7100	1291.7100	1291.5826	99	1	R.EDAEGRLMEAR.K Oxidation (M)
192 - 196	634.3600	634.3600	634.3108	78	0	R.LMEAR.K Oxidation (M)
197 - 206	1000.5400	1000.5400	1000.5301	10	1	R.KGADEAALAR.A
273 - 282	1295.6300	1295.6300	1295.5604	54	0	K.NMQNAEEWFK.S
304 - 310	820.4200	820.4200	820.3563	78	0	K.DEVSESR.R
304 - 310	980.3500	980.3500	980.2889	62	0	K.DEVSESR.R 2 Phospho (ST)
333 - 354	2547.2800	2547.2800	2547.2122	27	1	K.QLQELEDKQNADISAMQDTINK.L Oxidation (M)
355 - 360	772.3900	772.3900	772.4079	-23	0	K.LENELR.S
361 - 368	908.4100	908.4100	908.4385	-31	1	R.STKSEMAR.Y
361 - 368	1164.3500	1164.3500	1164.3324	15	1	R.STKSEMAR.Y Oxidation (M); 3 Phospho (ST)
364 - 371	1092.5400	1092.5400	1092.4675	66	1	K.SEMARYLK.E Oxidation (M); Phospho (Y)
381 - 391	1360.7200	1360.7200	1360.6098	81	0	K.MALDIEIAAYR.K Oxidation (M); Phospho (Y)
393 - 400	945.4600	945.4600	945.4767	-18	0	K.LLEGEETR.L
423 - 438	1706.6900	1706.6900	1706.7933	-61	0	R.SAYSGLQSSSYLMSAR.A
439 - 463	2885.4800	2885.4800	2885.3243	54	0	R.AFPAYYTSHVQEEQSEVEETIEATK.A
469 - 484	1910.9100	1910.9100	1910.7306	94	1	K.DEPPSEGEAEEEEKEK.E Phospho (ST)
501 - 520	2210.7800	2210.7800	2210.8458	-30	1	K.DESEDAKEEEGGEGEEEDTK.E

Figure 21. *Peptide mass fingerprint result for an MS Extract file of spot 988. The tolerance factor was set to 100ppm for peptide matching.*

In the initial assessment of this result, credence must be given to the fact that the protein assignment seems to be sound based on the pI and molecular weight compared to the location of spot 988 within the 2D gel. In the 2D gel, spot 988 is found at an estimated pI of approximately 4 and an estimated molecular weight of approximately 70 kD. If the protein in the spot was modified at multiple phosphorylation sites, the pI could reasonably be shifted from 4.63 to 4 and a MW of 61 kD is within a reasonable range of the spot within the gel. The primary factors influencing the lack of confidence in this result is that there are nine phosphopeptides out of twenty-one matches, approximately 40% of the total number. From these nine phosphopeptides, four have multiple phosphorylation sites, six have missed cleavages, and one is a known phosphopeptide. One factor that would seem to support this result is that there is evidence to support the presence of this protein in the spot with MS/MS evidence as shown in **Figure 22**.

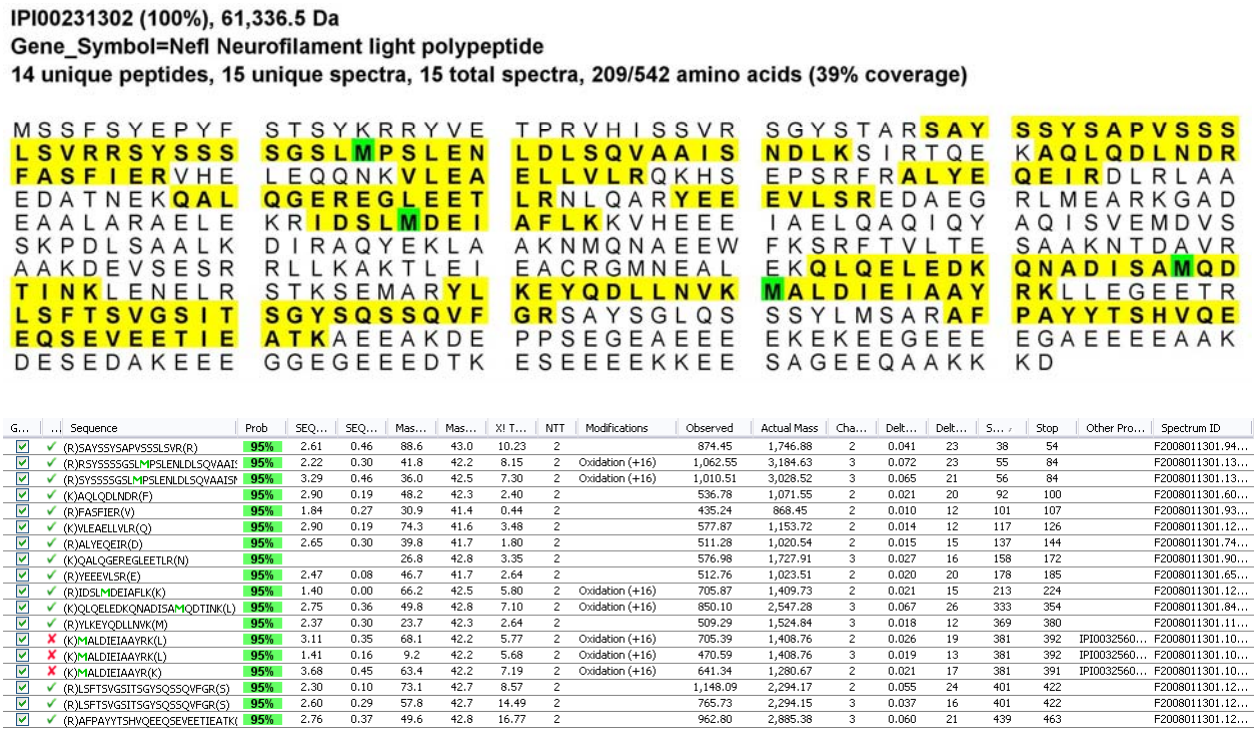

IPI00231302 (100%), 61,336.5 Da
Gene_Symbol=Nefl Neurofilament light polypeptide
14 unique peptides, 15 unique spectra, 15 total spectra, 209/542 amino acids (39% coverage)

MSSFSYEPYF STSYKRRYVE TPRVHISSVR SGYSTARSAY SSYSAPVSSS
LSVRRSYSSS SGSLMPSLEN LDLSQVAAIS NDLKSIRTQE KAQLQDLNDR
FASFIERVHE LEQQNKVLEA ELLVLRQKHS EPSRFRALYE QEIRDLRLAA
EDATNEKQAL QGEREGLEET LRNLQARYEE EVLSREDAEG RLMEARKGAD
EAALARAELE KRIDSLMDEI AFLKKVHEEE IAELQAQIQY AQISVEMDVS
SKPDLSAALK DIRAQYEKLA AKNMQNAEEW FKSRFTVLTE SAAKNTDAVR
AAKDEVSESR RLLKAKTLEI EACRGMNEAL EKQLQELEDK QNADISAMQD
TINKLENELR STKSEMARYL KEYQDLLNVK MALDIEIAAY RKLLEGEETR
LSFTSVGSIT SGYSQSSQVF GRSAYSGLQS SSYLMSARAF PAYYTSHVQE
EQSEVEETIE ATKAEEAKDE PPSEGEAEEE EKEKEEGEEE EGAEEEEAAK
DESEDAKEEE GGEGEEEDTK ESEEEEKKEE SAGEEQAAKK KD

G...	...	Sequence	Prob	SEQ...	SEQ...	Mas...	Mas...	X! T...	NTT	Modifications	Observed	Actual Mass	Cha...	Delt...	Delt...	S...	Stop	Other Pro...	Spectrum ID
☑	✓	(R)SAYSSYSAPVSSSLSVR(R)	95%	2.61	0.46	88.6	43.0	10.23	2		874.45	1,746.88	2	0.041	23	38	54		F2008011301.94...
☑	✓	(R)RSYSSSSGSLMPSLENLDLSQVAAIS	95%	2.22	0.30	41.8	42.2	8.15	2	Oxidation (+16)	1,062.55	3,184.63	3	0.072	23	55	84		F2008011301.13...
☑	✓	(R)SYSSSSGSLMPSLENLDLSQVAAISN	95%	3.29	0.46	36.0	42.5	7.30	2	Oxidation (+16)	1,010.51	3,028.52	3	0.065	21	56	84		F2008011301.13...
☑	✓	(K)AQLQDLNDR(F)	95%	2.90	0.19	48.2	42.3	2.40	2		536.78	1,071.55	2	0.021	20	92	100		F2008011301.60...
☑	✓	(R)FASFIER(V)	95%	1.84	0.27	30.9	41.4	0.44	2		435.24	868.45	2	0.010	12	101	107		F2008011301.93...
☑	✓	(K)VLEAELLVLR(Q)	95%	2.90	0.19	74.3	41.6	3.48	2		577.87	1,153.72	2	0.014	12	117	126		F2008011301.12...
☑	✓	(R)ALYEQEIR(D)	95%	2.65	0.30	39.8	41.7	1.80	2		511.28	1,020.54	2	0.015	15	137	144		F2008011301.74...
☑	✓	(K)QALQGEREGLEETLR(N)	95%			26.8	42.8	3.35	2		576.98	1,727.91	3	0.027	16	158	172		F2008011301.90...
☑	✓	(R)YEEEVLSR(E)	95%	2.47	0.08	46.7	41.7	2.64	2		512.76	1,023.51	2	0.020	20	178	185		F2008011301.65...
☑	✓	(R)IDSLMDEIAFLK(K)	95%	1.40	0.00	66.2	42.5	5.80	2	Oxidation (+16)	705.87	1,409.73	2	0.021	15	213	224		F2008011301.12...
☑	✓	(K)QLQELEDKQNADISAMQDTINK(L)	95%	2.75	0.36	49.8	42.8	7.10	2	Oxidation (+16)	850.10	2,547.28	3	0.067	26	333	354		F2008011301.84...
☑	✓	(R)YLKEYQDLLNVK(M)	95%	2.37	0.30	23.7	42.3	2.64	2		509.29	1,524.84	3	0.018	12	369	380		F2008011301.11...
☑	✗	(K)MALDIEIAAYRK(L)	95%	3.11	0.35	68.1	42.2	5.77	2	Oxidation (+16)	705.39	1,408.76	2	0.026	19	381	392	IPI0032560...	F2008011301.10...
☑	✗	(K)MALDIEIAAYRK(L)	95%	1.41	0.16	9.2	42.2	5.68	2	Oxidation (+16)	470.59	1,408.76	3	0.019	13	381	392	IPI0032560...	F2008011301.10...
☑	✗	(K)MALDIEIAAYR(K)	95%	3.68	0.45	63.4	42.2	7.19	2	Oxidation (+16)	641.34	1,280.67	2	0.021	17	381	391	IPI0032560...	F2008011301.10...
☑	✓	(R)LSFTSVGSITSGYSQSSQVFGR(S)	95%	2.30	0.10	73.1	42.7	8.57	2		1,148.09	2,294.17	2	0.055	24	401	422		F2008011301.12...
☑	✓	(R)LSFTSVGSITSGYSQSSQVFGR(S)	95%	2.60	0.29	57.8	42.7	14.49	2		765.73	2,294.15	3	0.037	16	401	422		F2008011301.12...
☑	✓	(R)AFPAYYTSHVQEEQSEVEETIEATK(	95%	2.76	0.37	49.6	42.8	16.77	2		962.80	2,885.38	3	0.060	21	439	463		F2008011301.12...

Figure 22. *Scaffold results for spot 988. The green for methionine denotes oxidation.*

Confounding the apparent agreement between the two searches is that only two peptides are found in both series. One of the peptides, mALDIEIAAYRK is homologous to other proteins and fails validation by PeptideProphet and is therefore denoted by a red *X* in the Scaffold results. The other peptide common to the two searches, QALQGEREGLEETLR is only found by the Mascot algorithm and not the SEQUEST algorithm. The primary reason for invalidating the peptide mass fingerprinting results is the fact that with a high quality protein assignment resulting from Scaffold, there were no phosphopeptide MS/MS spectra observed at all.

The low protein score of 6 found in the peptide mass fingerprinting result was characteristic of all of the peptide mass fingerprinting results. In the case provided, it is to be expected with only 29 of 610 MS1 ion masses being matched. A number of parameters for this experiment were varied in an attempt to improve the results; the filter applied to the MS Extract was modified to select only the fifty most intense peaks, the ppm tolerance range for assignments was varied from 500 ppm down to 10 ppm. After numerous iterations, it was decided that the extracted MS1 spectra were far too complex due to the sensitivity of the FT-ICR and the likelihood of multiple proteins in the sample for the MS extract-peptide mass fingerprinting approach to provide any meaningful results.

2.5.4 Hypothetical phosphopeptide generation

In a final attempt to elucidate phosphorylation information from the 2DPAGE differential phosphoprotein staining experiments, assistance was requested from the Bioinformatics group to generate a list of the potential phosphorylation sites in the

identified proteins for which no phosphopeptides were found in the survey or neutral-loss scanning experiments. A total of 4195 human phosphoproteins were downloaded from http://kinase.bioinformatics.tw/. All Pfam domains existing in these proteins were identified using software program hmmpfam (http://pfam.sanger.ac.uk/), where **Pfam** is a database of protein families that includes their annotations and multiple sequence alignments generated using hidden Markov models[7,8]. Overall 14893 domains were found (p-value <= 0.1), among them 1860 were distinct. Among these domains, 263 (146 distinct) were found out of the total number of 182 identified proteins. Known phosphoproteins were found in 110 out of the 146 distinct domains, and 152 out of the 182 proteins had one or more these 110 domains. From the 150 identified proteins for which no phosphopeptide mass spectra were obtained, 263 potential phosphorylation sites were elucidated by this method.

The assumption had been made prior to this analysis, that the majority of these phosphorylation sites would be conserved between human and rat protein sequences. This assumption was true in regards to the relative homology being preserved; unfortunately, in the practical application the absolute location was not preserved. A manual inspection of 20 randomly selected theoretical phosphorylation sites in the phosphopeptide deficient proteins showed some absolute correlation, but there were a surprising number of examples where this did not hold true. For example, the neurofilament light polypeptide (Nefl) from the previous section, for which no phosphorylated peptides were found, is a known phosphoprotein. There are nine known phosphorylation sites and a comparison between the known absolute phosphorylation sites in rat versus human shows that only one, pSer472, is at the same

location. For the others, pSer2 in rat correlates with pSer3 in human, pSer26 in rat correlates with pSer27 in human, etc. For other proteins, the change in absolute location could be even greater, or could be a mutation. For Heat shock 27 kDa protein (Hsp27), pThr147 in rat correlates to pThr143 in human and pSer65 in the rat is replaced by a glycine residue in human. This information, combined with the absolute number of potential phosphopeptides generated from the hypothetical domain search, led us to restrict the phosphopeptide investigation to documented phosphopeptides in rat tissue.

The sequence for each identified protein lacking a quality phosphopeptide MS/MS spectrum was searched against the MS-Digest tool from ProteinProspector (http://prospector.ucsf.edu/mshome.htm) to generate the potential peptides. For example, a truncated list of the peptides produced from the sequence of Nefl and the search parameters used is supplied in **Figure 23.** The information in these lists were exported to Excel were they were sorted by start-end sequence and manually compared against the known phosphorylation sites of Nefl from PhosphoSitePlus (www.phosphosite.org), shown in **Figure 24**. The hypothetical peptides were converted into hypothetical ions within Excel by applying the simple calculation $(m + z_1)/z_1 = (m/z)_1$ and $(m + z_2)/z_2 = (m/z)_2$, where m is the mass of the protein and z is the number of charges. This was done for singly through triply charged ions for each hypothetical phosphopeptide. The resultant ions were organized into ion lists for each protein undergoing the additional analysis. These lists were used in the MS experiment described in section 2.4.5.

MS-Digest Search Results

[–] Parameters

Database: **User Protein**
Considered modifications: | **Carbamidomethyl (C)** | **Oxidation (M)** | **Phospho (ST)** | **Phospho (STY)** |
Digest Used: **Trypsin**
Max. # Missed Cleavages: **1**
User AA Formula 1: **C2 H3 N1 O1**
Minimum Digest Fragment Mass: **800**
Maximum Digest Fragment Mass: **4000**
Minimum Digest Fragment Length: **5**

Index Number: **1**
pI of Protein: **5.7**
Protein MW: **30277**
Amino Acid Composition: **A27 D17 E27 F7 G11 H5 I4 K23 L38 M2 N4 P8 Q23 R16 S15 T9 V18 W5 Y6**

```
1   MKAVVLTLAV LFLTGSQARH FWQQDDPQSS WDRVKDFATV YVEAIKDSGR DYVAQFEASA LGKQLNLKLL DNWDTLASTL
81  SKVREQLGPV TQEFWDNLEK ETASLRQEMH KDLEEVKQKV QPYLDEFQKK WHEEVEIYRQ KVAPLGEEFR EGARQKVQEL
161 QDKLSPLAQE LRDRARAHVE TLRQQLAPYS DDLRQRLTAR LEALKEGGGS LAEYHAKASE QLKALGEKAK PVLEDLRQGL
241 LPVLESLKVS ILAAIDEASK KLNAQ
```

Number	m/z (mi)	m/z (av)	Modifications	Start	End	Missed Cleavages	Sequence
1	824.4138	824.8569	1Phospho	195	200	1	(R)QRLTAR(L)
1	825.4577	825.9485		177	183	0	(R)AHVETLR(Q)
1	836.2951	836.7115	2Phospho	101	106	0	(K)ETASLR(Q)
1	859.4520	859.9602		157	163	0	(K)VQELQDK(L)
1	905.4241	905.9284	1Phospho	177	183	0	(R)AHVETLR(Q)
1	988.5310	989.1201		112	119	1	(K)DLEEVKQK(V)
1	1014.6306	1015.2485		197	205	1	(R)LTARLEALK(E)
1	1017.5364	1018.1645		142	150	0	(K)VAPLGEEFR(E)
1	1026.5942	1027.2160		164	172	0	(K)LSPLAQELR(D)
1	1040.6099	1041.2430		229	237	0	(K)AKPVLEDLR(Q)
1	1052.5960	1053.2165		175	183	1	(R)ARAHVETLR(Q)
1	1094.5969	1095.2284	1Phospho	197	205	1	(R)LTARLEALK(E)
1	1106.5606	1107.1958	1Phospho	164	172	0	(K)LSPLAQELR(D)
1	1115.6055	1116.2670		155	163	1	(R)QKVQELQDK(L)
1	1132.5623	1133.1963	1Phospho	175	183	1	(R)ARAHVETLR(Q)
1	1173.6474	1174.3475		218	228	1	(K)ASEQLKALGEK(A)
1	1196.7249	1197.4694		238	248	0	(R)QGLLPVLESLK(V)
1	1216.6783	1217.4134		249	260	0	(K)VSILAAIDEASK(K)
1	1218.5749	1219.3040		206	217	0	(K)EGGGSLAEYHAK(A)
1	1253.6137	1254.3274	1Phospho	218	228	1	(K)ASEQLKALGEK(A)
1	1255.6569	1256.4500		36	46	0	(K)DEATVYVEAIK(D)

Figure 23. *Truncated list of hypothetical peptides for Nefl created by MS-Digest. Depending on the size of the protein and number of arginine and lysine residues, this list could contain several hundred potential peptides.*

Link to reference	location	Rat	location	Human
1	S2-p	SsFSYEPYF	S3	MSsFSYEPYY
2	S12-p	YEPYFSTsYKRRYVE	S13	YEPYYSTsYKRRYVE
1	T20	YKRRYVEtPRVHISS	T21-p	YKRRYVEtPRVHISS
1	T20-g	YKRRYVEtPRVHISS	T21	YKRRYVEtPRVHISS
1	S26	ETPRVHIsSVRSGYS	S27	ETPRVHIsSVRSGYS
1	S26-g	ETPRVHIsSVRSGYS	S27	ETPRVHIsSVRSGYS
1	S27	TPRVHISsVRSGYST	S28	TPRVHISsVRSGYST
1	S33	SSVRSGYsTARSAYS	S34	SSVRSGYsTARSAYS
1	S33-g	SSVRSGYsTARSAYS	S34	SSVRSGYsTARSAYS
2	S41-p	TARSAYSsYSAPVSS	S42	TARSAYSsYSAPVSS
1	Y42	ARSAYSSySAPVSSS	Y43	ARSAYSSySAPVSSS
3	S47-g	SSYSAPVsSSLSVRR	S48	SSYSAPVsSSLSVRR
1	S48	SYSAPVSsSLSVRRS	S49	SYSAPVSsSLSVRRS
1	S49-p	YSAPVSSsLSVRRSY	S50	YSAPVSSsLSVRRSY
1	S49	YSAPVSSsLSVRRSY	S50	YSAPVSSsLSVRRSY
1	S51	APVSSSLsVRRSYSS	S52	APVSSSLsVRRSYSS
1	S51	APVSSSLsVRRSYSS	S52	APVSSSLsVRRSYSS
3	S55-p	SSLSVRRsYSSSSGS	S56	SSLSVRRsYSSSSGS
3	S57-p	LSVRRSYsSSSGSLM	S58	LSVRRSYsSSSGSLM
1	S58	SVRRSYSsSSGSLMP	S59	SVRRSYSsSSGSLMP
1	S59	VRRSYSSsSGSLMPS	S60	VRRSYSSsSGSLMPS
1	S60	RRSYSSSsGSLMPSL	S61	RRSYSSSsGSLMPSL
2	S62	SYSSSSGsLMPSLEN	S63	SYSSSSGsLMPSLEN
3	S66	SSGSLMPsLENLDLS	S67	SSGSLMPsLENLDLS
1	N69	SLMPSLEnLDLSQVA	N70	SLMPSLEnLDLSQVA
1	S73	SLENLDLsQVAAISN	S74	SLENLDLsQVAAISN
1	S413	GSITSGYsQSSQVFG	S413	GSITSGYsQSSQVFG
1	Y424	QVFGRSAySGLQSSS	Y424	QVFGRSAyGGLQTSS
1	Y432	SGLQSSSyLMSARAF	Y432	GGLQTSSyLMSTRSF
1	S435-p	QSSSYLMsARAFPAY	S435	QTSSYLMsTRSFPSY

Figure 24. *List of known phosphopeptide sites for Nefl from PhosphoSitePlus. The locations highlighted in red are links to the references for the previously identified phosphorylation site in the given species.*

2.5.5 KEGG pathway analysis

With additional assistance from the Bioinformatics group, KEGG pathway analyses were conducted on all identified proteins including those for which no phosphopeptides were detected by MS/MS sequencing. KEGG, which stands for Kyoto Encyclopedia of Genes and Genomes, has become a major resource for pathway analysis and contains a wealth of data associated with pathways, genes, genomes, chemical compounds and reaction information, in addition to links to outside resources such as PubMed[9]. The pathways in KEGG are manually drawn and derived from textbooks, literature and expert knowledge. Genomic information is derived from publicly available resources such as RefSeq data from the NCBI (National Center for Biotechnology Information). KEGG contains completely sequenced genomes in addition to draft genome sequences and ESTs (expressed sequence tags). All available genome sequences and their sources are listed at (http://www.genome.jp/kegg/catalog/org_list.html).

The KEGG Automatic Annotation Server (KAAS)[10] was utilized to perform the analysis and is available at http://www.genome.jp/kegg/kaas/. KAAS can automatically reconstruct pathways using a set of amino-acid query sequences derived from a complete genome. For our purposes, the amino-acid query sequences were derived from the results of our MS/MS experimental data. The ability to add the quantitative information from the 2D-PAGE studies enhanced the quality of the KEGG analyses was instrumental in drawing biological inferences from our data. Graphical representations of the results of the KEGG analyses for the rat cerebellum data are provided in **Figures 25 and 26.**

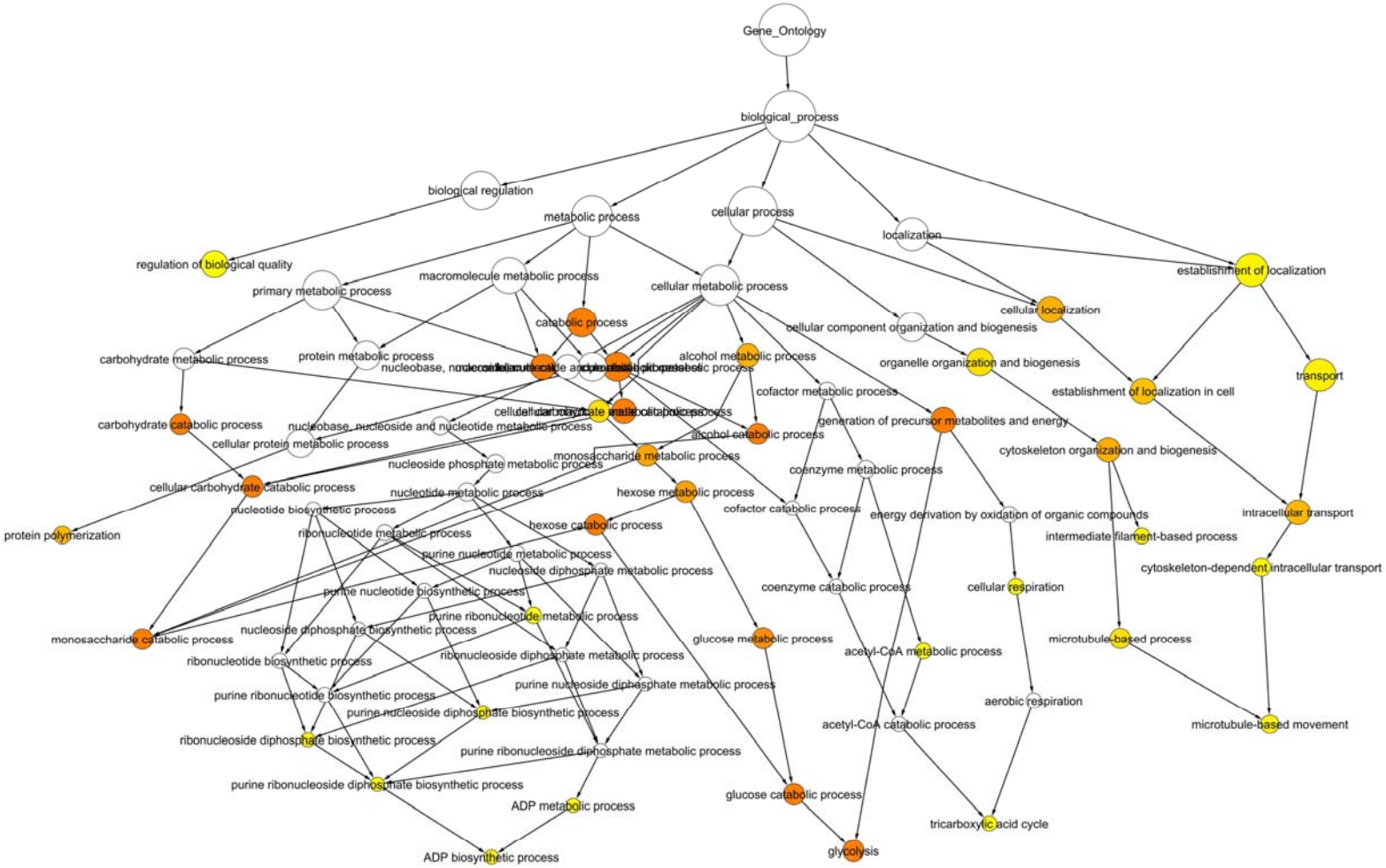

Figure 25. *Gene ontology results from KEGG pathway analysis of age-dependent differentially phosphorylated proteins in rat cerebellum relevant to biological processes. Yellow indicates an effect and increasing coloration through orange to red shows an increasing effect.*

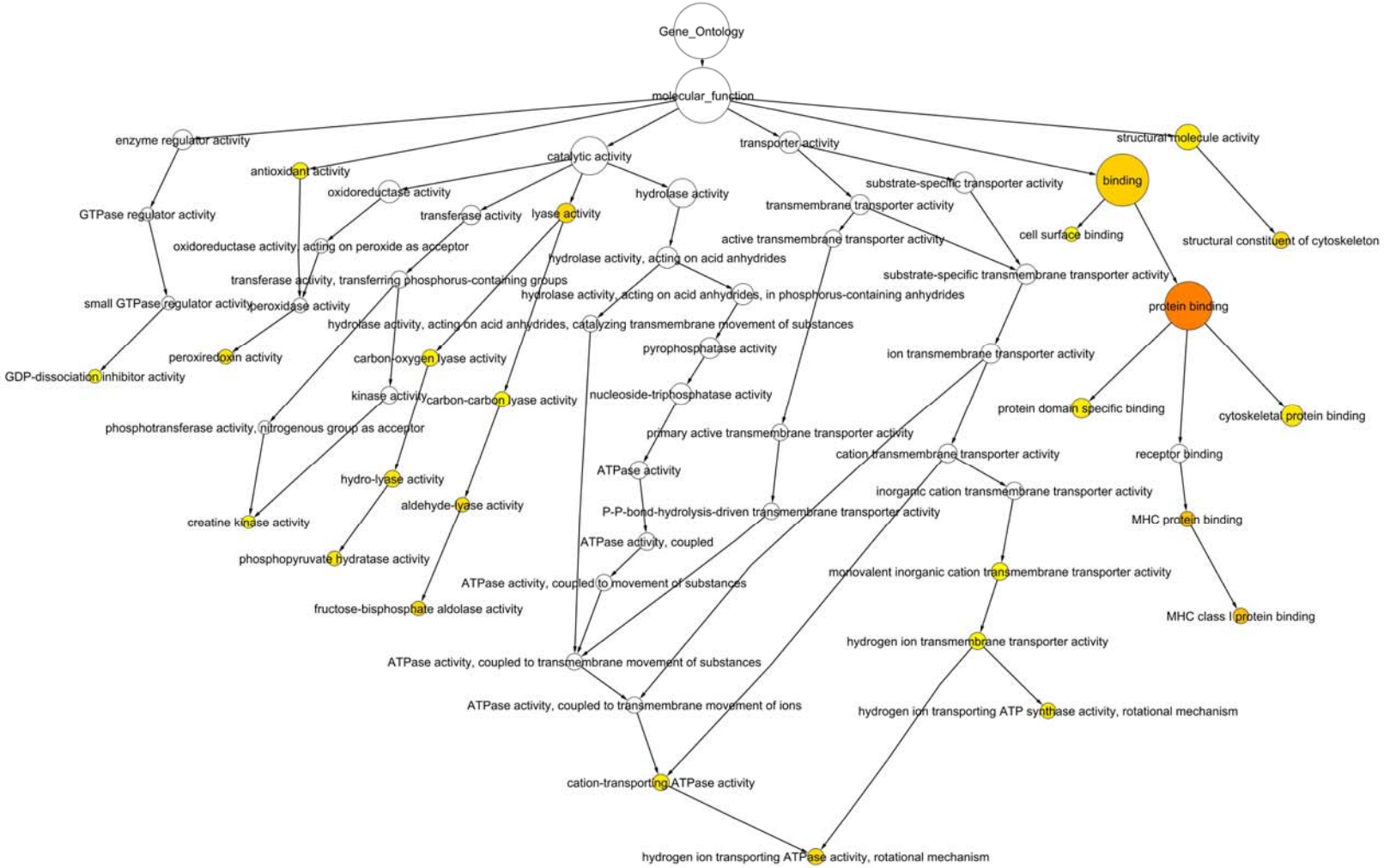

Figure 26. *Gene ontology results from KEGG pathway analysis of age-dependent differentially phosphorylated proteins in rat cerebellum relevant to molecular function. Yellow indicates an effect and increasing coloration through orange to red shows an increasing effect.*

2.5.6 Conclusions

All of the available resources were utilized in assuring the data was handled with the utmost care. Extraordinary effort went into developing many of the methods described in this section. These methods meant to extract information from data that was already difficult to acquire. Even though most of these methods were unsuccessful or only marginally successful, they were necessary in order to perform due diligence. Partially as a result of the effort applied in streamlining the data analysis and primarily due to demonstrating the negative impact of such a large data set on the resources available, significant improvements in the equipment and data analysis methodology within the APL were observed over the course of the experiments described in this dissertation.

2.5.7 References

[1] Domon B, Aebersold R. Challenges and opportunities in proteomics data analysis. Mol Cell Proteomics. 2006 Oct;5(10):1921-6.

[2] Eng, J., McCormack, A.L., and Yates, J.R. An approach to correlate tandem mass spectral data of peptides with amino acid sequences in a protein database. J. Am. Soc. Mass Spectrom. 5, 976ND989 (1994).

[3] Perkins, D.N., Pappin, D.J., Creasy, D.M., and Cottrell, J.S., ProbabilityNDbased protein identification by searching sequence databases using mass spectrometry data. Electrophoresis 1999 Dec;20(18) 3551ND67

[4] Craig, R. and Beavis, R.C., A method for reducing the time required to match protein sequences with tandem mass spectra. Rapid Commun. Mass Spectrom. 2003;17(20):2310ND16

[5] Keller, A., Nesvizhskii, A.I., Kolker, E., and Aebersold, R., Empirical statistical model to estimate the accuracy of peptide identifications made by MS/MS data search. Anal. Chem. 2002 Oct 15;74(20):5383–92.

[6] Nesvizhskii, A.I., Keller, A., Kolker, E., and Aebersold, R. A statistical model for identifying proteins by tandem mass spectrometry. Anal Chem. 2003 Sep 2;75(17):4646–58.

[7] Finn RD, Tate J, Mistry J, Coggill PC, Sammut SJ, Hotz HR, Ceric G, Forslund K, Eddy SR, Sonnhammer EL, Bateman A. The Pfam protein families database. Nucleic Acids Res. 2004 Jan 1;32(Database issue):D138-41.

[8] Bateman A, Coin L, Durbin R, Finn RD, Hollich V, Griffiths-Jones S, Khanna A, Marshall M, Moxon S, Sonnhammer EL, Studholme DJ, Yeats C, Eddy SR. Pfam: clans, web tools and services. Nucleic Acids Res. 2006 Jan 1;34(Database issue):D247-51.

[9] Kanehisa M. The KEGG database. Novartis Found Symp. 2002;247:91-101; discussion 101-3, 119-28, 244-52.

[10] Moriya Y, Itoh M, Okuda S, Yoshizawa AC, Kanehisa M. KAAS: an automatic genome annotation and pathway reconstruction server. Nucleic Acids Res. 2007 Jul;35(Web Server issue):W182-5.

Chapter Three

Oxidation effects on protein phosphorylation in C2C12 myoblasts treated with hydrogen peroxide.

3.1 Introduction

Subsequent chapters will deal with finding the phosphorylation differences in targeted age-dependent studies in specific tissues. The overarching hypothesis behind these studies is that reactive oxygen species (ROS) cause modifications to various biomolecules and either directly or indirectly cause differential changes in protein phosphorylation in aged subjects. This chapter attempts to directly demonstrate phosphorylation changes in cultured C2C12 myoblasts using physiological levels[1] of hydrogen peroxide. Mouse-derived C2C12 myoblasts are a model system for investigating the basis of skeletal muscle cellular specification and development[2].

3.2 Experimental

3.2.1 Materials

Tissue culture media, serum and media supplements were obtained from Invitrogen [Invitrogen, Carlsbad, CA]. Glycerol, urea, CHAPS, Tween-20, butanol, phosphate-buffered saline (PBS), tris(hydroxymethyl)aminomethane hydrochloride (Tris-HCl), trimethylol Aminomethane, tris(hydroxymethyl)aminomethane (Tris base), agarose, hydrogen peroxide (30%) and 2-propanol were acquired from Fisher Scientific. [Fairlawn, NJ] Unless otherwise noted, all other chemicals were purchased from Sigma Chemicals [St. Louis, MO] and were of electrophoretic grade or better.

3.2.2 Cell Culture

Mitotic C2C12 mouse myoblasts from the American Type Culture Collection (ATCC) (Manassas, VA) were grown as monolayers in Dulbecco's modified Eagle's

medium (DMEM) supplemented with 20% fetal bovine serum, 200 mM L-glutamine, 10 units/mL penicillin, and 10 µg/mL streptomycin in an incubator at 37°C in a 5% humidified atmosphere[2].

3.2.3 Sample Treatment and Preparation

Once the cells had reached ~90% confluency, the myoblasts were removed from the incubator, the DMEM solution was removed and the myoblasts were washed (3X) with PBS. One set was then 'fed' once more with DMEM, but instead of going back to the incubator, it was transferred to the -70°C freezer to arrest any cellular processes and act as a control set. The remaining sets of myoblasts were treated with a confluent layer of 8 µM hydrogen peroxide and returned to the incubator. After 30 minutes, half of the peroxide treated myoblasts were removed from the incubator, the peroxide was removed and they were washed (3X) with PBS. All of the myoblasts were given DMEM, but half of the 30 min peroxide-treated myoblasts went to the -70°C freezer while the remaining sets were returned to the incubator. After 120 minutes the remaining myoblast sets (still exposed to peroxide) were removed from the incubator and washed (3X) with PBS. Again, all of the myoblasts were given DMEM, but half of the 120 min peroxide-treated myoblasts went to the -70°C freezer while the remaining sets were returned to the incubator. After 22 hours, the myoblast sets in the freezer were removed and allowed to thaw. After 24 hours, the myoblasts in the incubator were removed. All sets of myoblasts were washed (3X) with PBS, and then harvested into separate 15 mL centrifuge tubes after lysis with a buffer of 7M urea, 2M thiourea, 4% (v/v) CHAPS, 1% (v/v) Tween-20, 40 mM Tris, 20 mM DTT, 1mM sodium fluoride, 1

μg/mL phosphatase inhibitor cocktail 1, 1 μg/mL phosphatase inhibitor cocktail 2, 0.5 mM PMSF, 10 μg/mL of leupeptin, 10 μg/mL apopritin, where they were homogenized with an Ultra-Turrax T8 homogenizer [Fisher, Fair Lawn, NJ], and then briefly sonicated with a Fisher 550 sonic dismembrator [Fisher, Fair Lawn, NJ]. The homogenates were delipidated using chloroform/methanol precipitation[3] and re-solubilized in a solubilization buffer amenable to iso-electric focusing (IEF) containing 5M urea, 2M thiourea, 2% (v/v) CHAPS, 0.5% (v/v) Tween-20, 0.5% (w/v) 3-(decyldimethylammonio)propanesulfonate, 10% (v/v) 2-propanol, 10% (v/v) water saturated butanol, 5% (v/v) glycerol, 0.25% (v/v) carrier ampholytes (50:50 mix of Pharmalyte 3-10 [GE Healthcare, Piscataway, NJ] and Bio-Lyte 3/10 [Bio Rad, Hercules, CA]), 1mM sodium fluoride, 1 μg/mL phosphatase inhibitor cocktail 1 and 1 μg/mL phosphatase inhibitor cocktail 2[4]. Again, they were briefly sonicated with the sonic dismembrator followed by centrifugation at 13,000 x g in a microcentrifuge. The supernatant was transferred to fresh centrifuge tubes. Protein concentrations were determined using the Lowry method[5] and the samples were reduced using tributylphosphine and alkylated with iodoacetamide using a ReadyPrep Reduction/Alkylation kit [Bio Rad, Hercules, CA] according to manufacturer's procedures prior to final dilution to 1.67μg/μL with the aforementioned IEF buffer.

3.2.4 2D-PAGE Separation

Due to the size limitations of the SDS PAGE equipment (six gel maximum), the myoblast samples were broken into two batches of six samples each. Performing this experiment with two separate gel castings, and two independent IEF and SDS-PAGE requires a great deal of care to ensure reproducibility between the batches. To reduce

the amount of bias toward any particular set of treatments due to procedural inconsistencies, each batch of six consisted of two control samples and one of each of the treated samples (30 min fed, 30 min unfed, 120 min fed and 120 min unfed).

Isoelectric Focusing (IEF)

For each batch, 450 µL aliquots of each sample in the batch were applied to 18 cm 'Immobiline' immobilized pH gradient (IPG) strips (pH 3-10 NL) [GE Healthcare, Piscataway, NJ] to load 750 µg of total protein and allowed to re-hydrate overnight. The strips were transferred to an IPGPhor II electrophoresis unit [GE Healthcare, Piscataway, NJ] and IEF was conducted by initially holding the voltage at 50 V for the first 4 h to allow the migration of excess charged species introduced by the various phosphatase inhibitors[6], the voltage was then increased by stepping to 100 V for 2 hours, followed by a step to 500 V for the subsequent 2 hours and then a linear voltage gradient over 12 hours from 500 to 10,000 V was created in order to achieve a total of 70,000 volt hours.

SDS-PAGE

For each separate batch, during the isoelectric focusing, a set of six 1x200x260mm polyacrylamide gels (12.5% T, 3%C) were cast into individual glass cassettes using an Ettan Dalt*six* gel casting apparatus [GE Healthcare, Piscataway, NJ] according to manufaturer's protocols. All gels were used within 12 h of casting. For the second dimension separation, the focused IPG strips were removed from the IPGphor II and 're-equilibrated' in a solution of 50mM Tris-HCl/Tris base, pH 8.8, 30% (v/v)

glycerol, 6M urea, with 2% (w/v) sodium dodecyl sulfate (SDS) [Bio Rad, Hercules, CA] and 0.001% (w/v) bromophenol blue for 20 minutes. Following re-equilibration, the strips were each transferred to individual cassettes with 20x75mm strips of grade 1 Whatman filter paper [Fisher, Fair Lawn, NJ] soaked with 2uL aliquots of the PeppermintStick™ phosphoprotein molecular weight marker [Invitrogen, Carlsbad, CA] on the acidic side of the strip, and sealed with 0.5% (w/v) boiling agarose containing 0.001% (w/v) bromophenol blue onto the top of the slab gel in each respective glass cassette. After allowing a few minutes for the agarose to properly cool, the six slab gels were transferred to an Ettan Dalt*six* electrophoresis tank [GE Healthcare, Piscataway, NJ] with the appropriate buffers and run at 30 W (5 W per gel) for approximately 30 min to effect the transfer of the proteins from the IPG strip to the slab. Once the bromophenol dye front had unequivocally entered the slab gels, the power was increased to 100 W and the gels were allowed to run until the dye front progressed to the bottom of the gels (approximately 6 hours).

Imaging

For each batch, immediately following the second dimension SDS-PAGE, the slab gels were transported to the MAI facility where they were removed from their respective cassettes and fixed in a solution of 50% (v/v) methanol and 7% (v/v) acetic acid. The first batch remained in the fixing solution until the separation of the second batch was complete and the gels from the experiment had been fixed overnight. The gels were then stained with Pro-Q Diamond Phosphoprotein Gel Stain [Invitrogen, Carlsbad, CA] using the manufacturer's protocol for large 2D gels with the following

modifications: The gels were fixed for 24 hours in each fixation step (48 hours for the first fixation step of the first batch). 2) The first destaining step was for 12 h. The gels were subsequently imaged using a Typhoon™ Variable Mode Imager [GE Healthcare, Piscataway, NJ] thus creating phosphoprotein gel images for each slab gel. Following imaging, each gel was immersed in a fixation solution (50% (v/v) methanol, 7% (v/v) acetic acid) and left overnight prior to staining with Sypro Ruby [Invitrogen, Carlsbad, CA]. The Sypro Ruby stained gels were then imaged with the Typhoon Imager to create images of total protein for each slab gel.

3.2.5 Image Analysis

Analysis of the resultant gel images was conducted using the Progenesis PG220 software [Nonlinear Dynamics, Newcastle upon Tyne, UK]. This analysis required separating the images into two discrete image analysis sets based on the gel dye: one set of images from the Pro-Q Diamond stain with both the control and treated samples to determine phosphoprotein levels and one set of images from the Sypro Ruby stain to determine total protein levels. This experiment included 12 images for each stain; the software was used to combine the images in each set to create an averaged image with matched spots in each set and their respective location and averaged spot density. These averaged images were matched to a master image to provide a reference between different sets of gels. The final quantitative analysis consisted of ten averaged gel images, one for each treatment or control depicting phosphoprotein levels and one for each treatment or control depicting total protein levels. The spots of interest were determined from the differences between the averaged phosphoprotein gel images of

each treatment. These spots were then referenced against an identical analysis containing total protein images in order to normalize the difference in phosphorylation values by the expression values in each protein spot.

3.2.6 FT-ICR MS analysis

Spots demonstrating normalized differential phosphorylation were excised manually from the gels using a 1.5 mm spot picker utilizing disposable tips to ameliorate cross contamination. The spots of interest were dehydrated with acetonitrile, dried and subjected to in-gel digestion with MS-grade modified trypsin [Promega, Madison, WI] in 50 mM NH_4HCO_3 overnight at 37º C[7]. The supernatant was removed and analyzed via nanoelectrospray ionization (NSI) HPLC-MS/MS using a Thermo-Finnigan hybrid LTQ-FT mass spectrometer. Two separate experiments were conducted; the first focused primarily on identifying the proteins in the in-gel digests, while the second was focused on locating phosphopeptides for structural information. In all cases the instrument was run in the positive mode. In the first experiment for identification, the LTQ-FT mass spectrometer was programmed to use a data-dependent survey scan where a full range mass spectrum (m/z 400-2000) was collected and the three most abundant ions were scanned using selected ion monitoring (SIM) by the Fourier transform ion cyclotron resonance mass spectrometer (FT-ICR) prior to an MS/MS experiment in the linear quadrupole ion trap (LTQ) mass spectrometer. The ions accumulated in the linear ion trap for both the MS and MS/MS scans. The AGC target values were set to $1X10^6$ ions for the survey MS, $1X10^5$ ions for the SIM and $1X10^4$ for the MS/MS experiments. The maximum accumulation time was set at 200 ms for all modes. The resolution at 400

m/z was set to $1X10^4$ for the FT-ICR scans and isolation widths were set at ± 2 *m/z* for the SIM experiments and ± 1 *m/z* for the MS/MS experiments and ions were selected for MS/MS when their respective intensities reached 1000 counts. The normalized collision energy was set to 35% and three microscans were acquired for each spectrum. The mass spectrometer was programmed to ignore singly charged species for fragmentation and was set to dynamically exclude precursors that had already been selected for 1 minute after their respective fragmentations. The second experiment was conducted with the same parameters as the first experiment, but an additional step was added, which monitored neutral losses by scanning for fragment ions that had suffered a loss of 98 Daltons from the precursor and collecting an additional tandem mass spectrum on these fragments[8]. The chromatography for both experiments was kept consistent with 10 µL injection volumes of the peptide digests injected into a chromatography system consisting of a FAMOS Capillary and Nano HPLC Autosampler, a Switchos loading pump and switching valve and an ULTIMATE Capillary and Nano HPLC Pump [Dionex/LC Packings, Sunnyvale, CA]. The Switchos loading pump, in-line with the autosampler, trapped the digests on a 1mm C-18 PepTrap column [Dionex, Sunnyvale, CA] at a flow rate of 20µL/min of 0.1% (v/v) TFA. After 5 minutes the switching valve, integral to the Switchos, changed the flow to the ULTIMATE Nano pump which was set to flow through the PepTrap column into a standard coated PicoFrit® column, 360µm/75µm OD/ID, 15µm tip, 15 cm long [New Objective, Woburn, MA], packed in house with 5 µm particles of 300 Á pore-size Bio-Basic C18 material [Thermo-Scientific, Waltham, MA] at a flow rate of approximately 200 nL/min, utilizing a 90 minute linear gradient from 90% (v/v) solvent A to 90% (v/v)

solvent B and held at 90% B for 30 minutes. Solvent A consisted of 10% ACN/89.9% H_2O/0.1% FA (v/v/v) and solvent B consisted of 10% H_2O/89.9% ACN/0.1% FA (v/v/v). The PepTrap column and the PicoFrit column were allowed to re-equilibrate to aqueous conditions (0.1% TFA and 90% solvent A respectively) for 60 minutes between analytical runs.

3.2.7 Tandem MS Protein Identification

The resultant spectra obtained from all MS experiments were first analyzed via Bioworks v.3.3.1 [Thermo-Scientific, Waltham, MA] which uses the SEQUEST[9] algorithm against the most recent version of the International Protein Index (IPI) database. The DTA files generated by SEQUEST for each mass spectrum were concatenated into a single data file and then analyzed using Mascot v.2.2[10] [Matrix Science, Boston MA] with the same database as the SEQUEST analysis. Search parameters for both programs included static mass modifications to cysteine due to alkylation by iodoacetamide, differential mass modifications to methionine due to oxidation and modifications to serine, threonine and tyrosine from phosphorylation. Parameters specific to neutral losses from phosphorylated peptides were also included. The Scaffold [Proteome Software, OR] program was used to validate protein identifications derived from the MS/MS sequencing results. Scaffold verifies peptide identifications assigned by SEQUEST and Mascot using the X!Tandem database searching program[11]. Scaffold then probabilistically validates these peptide identifications using PeptideProphet[12] and derives corresponding protein probabilities using ProteinProphet[13].

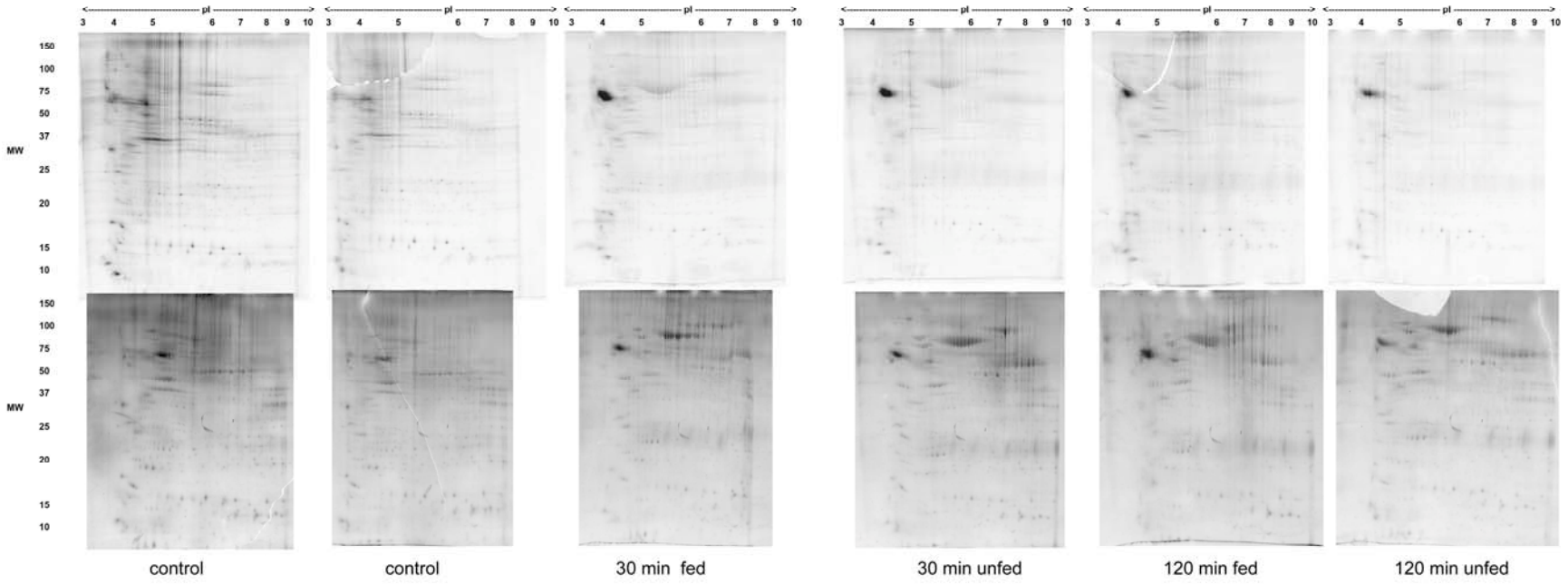

Figure 27. *Pro-Q Diamond images of C2C12 myoblast samples. Batch 1 is on the top and batch 2 on the bottom. The 30 min fed and 120 min fed samples were samples returned to the incubator after exposure to H_2O_2 and the 30 min unfed and 120 min unfed were the samples placed in the freezer after exposure to H_2O_2.*

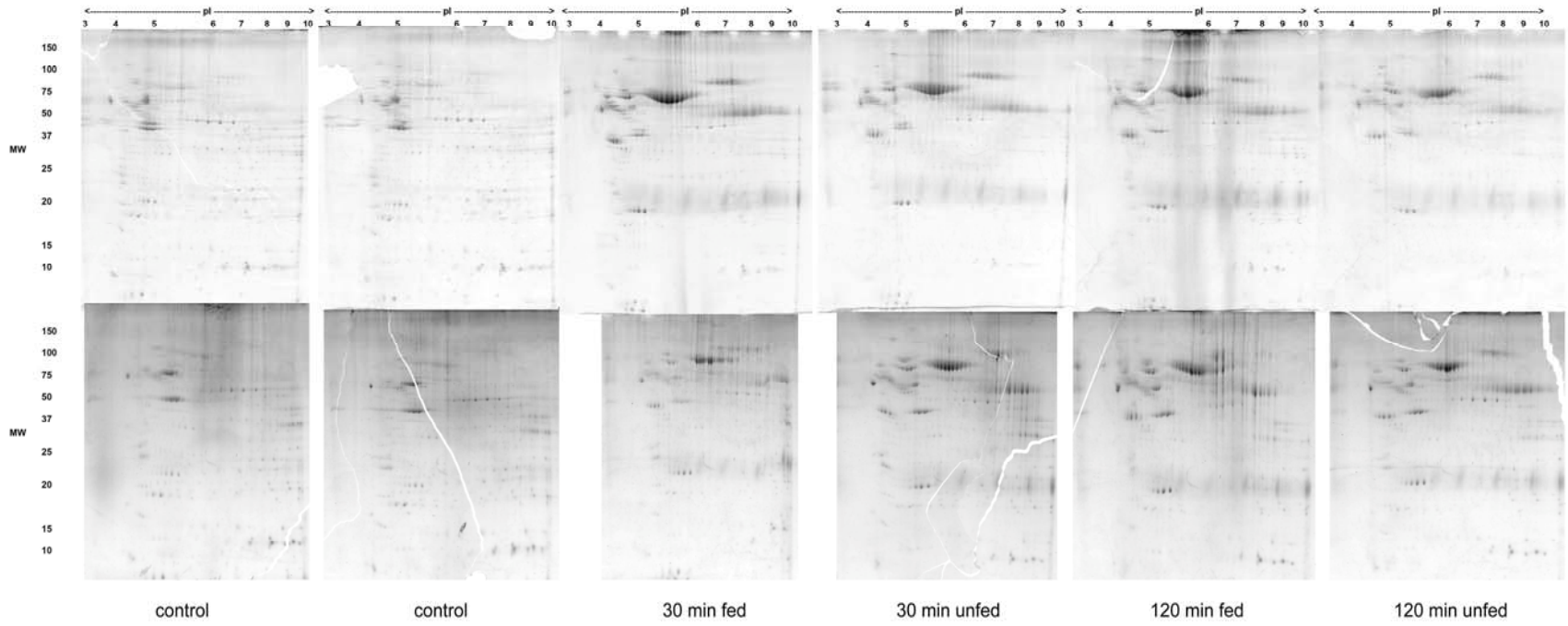

Figure 28. *Sypro Ruby images of C2C12 myoblast samples. Batch 1 is on the top and batch 2 on the bottom. The 30 min fed and 120 min fed samples were samples returned to the incubator after exposure to H_2O_2 and the 30 min unfed and 120 min unfed were the samples placed in the freezer after exposure to H_2O_2.*

3.3 Results

Figures 27 and **28** display images of the individual gels run for C2C12 myoblast samples treated with hydrogen peroxide. There seemed to be good reproducibility for both the Sypro Ruby and Pro-Q Diamond staining for the duplicate samples, although a higher background is evident for batch 2 with both dyes possibly due to the extended fixation for batch one. A significant amount of gel tearing occurred with such a large set of gels. This complicated the image analysis, but could be remedied by tools available within the Progenesis software. Simply from casual observation, there were significant total protein and phosphorylation differences between the data sets from the various treatments.

The image analysis identified approximately 35 phosphoprotein spots which demonstrated at least a two-fold difference between the averages of gels from the various treatments when normalized to total protein content. Spots meeting this criterion are annotated in **Figure 29** and the quantitative data for the spot volumes of phosphorylated species were obtained from the optical density of the spots in the images from the Pro-Q Diamond staining. The quantitative data are displayed in **Table 1**, while the data for the spot volumes of the total proteins derived from the Sypro Ruby stained images are displayed in **Table 2**. These tables, though not immediately identifying proteins, are important for the statistical analysis of our data. Due to the design of the study, the statistics for samples other than the controls only demonstrate the agreement between two replicates. The statistics for the controls in **Tables 1** and **2**, provide some measure of the reproducibility between batches. The covariances (CV) in the spots of interest for these four gels ranged between 4% and 113%. Approximately

63% of the control sample spots showed CVs less than 50% and approximately 35% of these spots had CVs less than 20%.

The MS/MS analysis of 33 spots of interest yielded 3 phosphoproteins which were identified by peptide sequences and for which MS/MS spectra of specific phosphopeptides were obtained. These are listed in **Table 3**. In this table, the observed phosphopeptides are listed with the modified amino acid residues in lower case. In addition to phosphorylation of Ser, Thr and Tyr residues, oxidized methionine residues are also noted in lower case.

Among the IDs, the serum albumin IDs for spots 1106 and 1123 are the most surprising and may also have a significant impact on the study. The DMEM media used to feed the cells is supplemented with serum and is the obvious source of the contamination. The proteins representing the charge train from which these spots were excised represents a fairly large contributor to the total amount of protein within each of the affected gels. A comparison of the average total spot density for this charge train compared to the total spot density in the gel shows differential levels between fed and unfed, but not a significant difference between exposure times to H_2O_2. The 30 min and 120 min unfed samples (placed in the freezer) contained 7.6% and 6.5% albumin respectively, while the 30 min fed and 120 min fed (returned to the incubator for 24 hours) contained 11.9% and 10.3% albumin. **Figures 30** and **31** demonstrate the tandem MS information for one of the observed phosphopeptides, EGRIC-53-like GLSPsLCLLsLLLVLHGAERSQPPPR peptide. **Figure 30** contains the sequence coverage for the peptide, the MS/MS spectrum and the associated errors with the assignments. **Figure 31** shows the fragmentation coverage for the peptide.

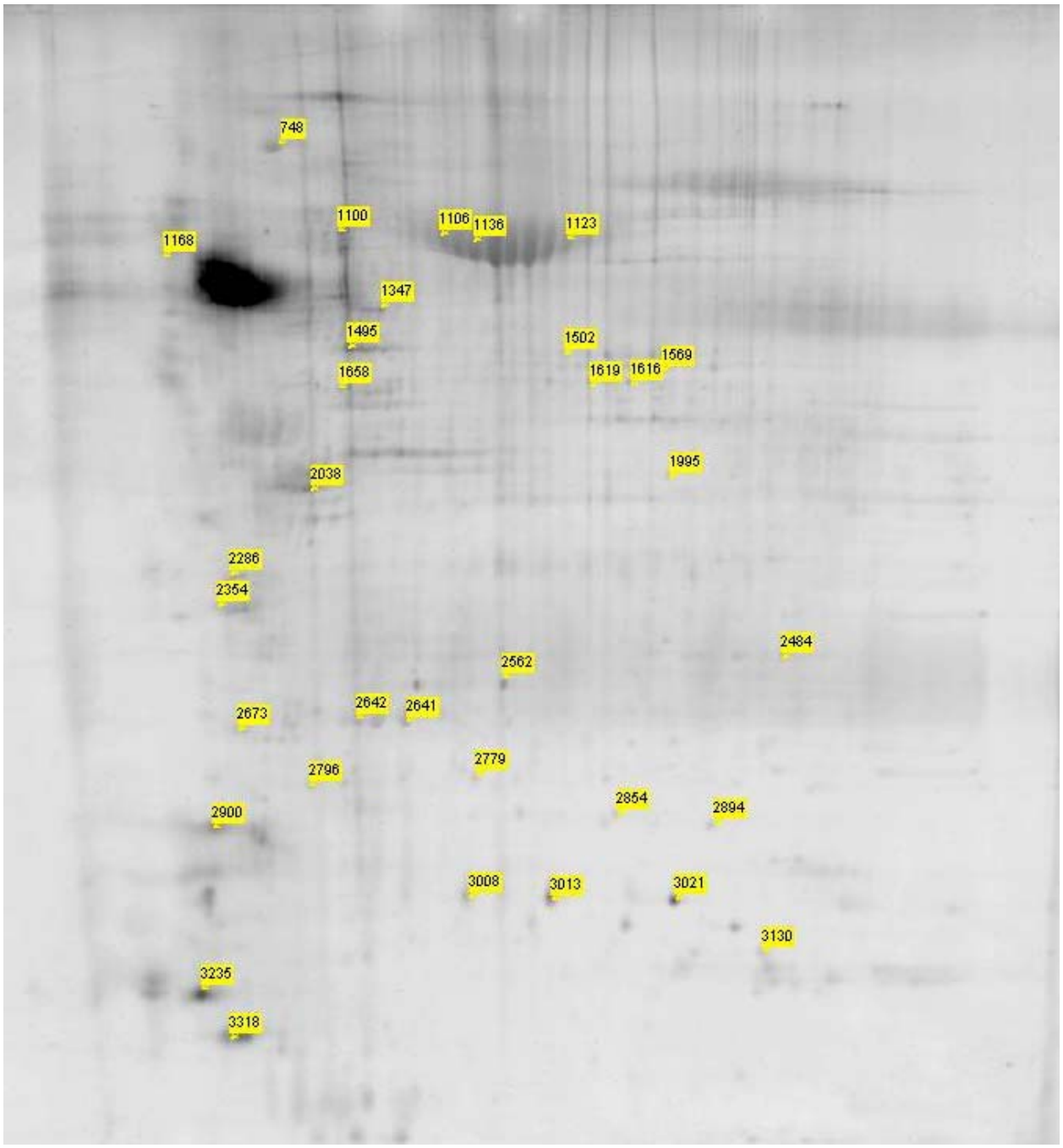

Figure 29. *Spots demonstrating phosphorylation differences in peroxide treated C2C12 myoblasts. The image displayed is a 30 min fed gel image which displayed the highest number of matching spots. The annotations on this image were generated using Progenesis PG220 following image analysis.*

Spot	Control Volume (CV)	120 min H_2O_2 exposure - unfed Volume (CV)	Ratio vol/ control	120 min H_2O_2 exposure - fed 24hrs Volume (CV)	Ratio vol/ control	30 min H_2O_2 exposure - unfed Volume (CV)	Ratio vol/ control	30 min H_2O_2 exposure - fed 24 hrs Volume (CV)	Ratio vol/ control
748	ND	3,456,415.2 (--)	691.28	608,844.0 (124%)	121.77	ND	0.00	ND	0.00
852	192,819.3 (11%)	1,797,188.5 (64%)	9.32	540,259.4 (82%)	2.80	463,606.4 (50%)	2.40	ND	0.00
1100	2,196,194.9 (6%)	846,439.2 (--)	0.39	ND	0.00	1,999,290.8 (119%)	0.91	ND	0.00
1106	ND	103,782.1 (129%)	20.76	934,854.8 (29%)	186.97	5,385,965.9(134%)	1077.19	2,989,983.8(111%)	598.00
1123	ND	1,196,023.6 (137%)	239.20	427,975.3 (--)	85.60	374,080.5 (141%)	74.82	3,199,679.4 (41%)	639.94
1136	ND	15,558,386.7 (14%)	3111.68	2,843,898.7 (65%)	568.78	13,444,771.4 (104%)	2689	4,687,520.0 (22%)	937.5
1168	2,065,524.0 (15%)	68,430.7 (--)	0.03	592,883.0 (31%)	0.29	ND	0.00	4,683,562.5(138%)	2.27
1347	8,163,818.2 (33%)	4,407,560.9 (92%)	0.54	1,883,748.4 (48%)	0.23	3,085,907.4 (120%)	0.04	11,684,973.5 (63%)	1.43
1495	743,443.5 (8%)	4,760,270.3 (98%)	6.40	765,279.8 (88%)	1.03	ND	0.00	69,141.2 (3%)	0.09
1502	109,751.2 (26%)	618,546.1 (16%)	5.64	ND	0.00	332,224.6 (28%)	3.03	6,323,184.0 (135%)	57.61
1569	ND	123,018.1 (--)	24.60	1,285,157.0 (36%)	257.03	23,565.2 (128%)	4.71	2,957,919.4 (141%)	591.58
1616	ND	584,536.3 (123%)	116.91	1,111,368.8 (6%)	222.27	483,740.1 (110%)	96.75	303,853.3 (19%)	60.77
1619	7,489,296.3 (7%)	620,898.0 (61%)	0.08	848,620.9 (7%)	0.11	273,983.3 (131%)	0.04	611,220.1 (6%)	0.08
1658	1,700,346.1 (16%)	116,098.5 (131%)	0.07	90,040.0 (95%)	0.05	852,314.1 (71%)	0.50	566,066.8 (79%)	0.33
1662	1,659,970.3 (58%)	209,854.3 (45%)	0.13	ND	0.00	370,184.9 (99%)	0.22	827,752.1 (122%)	0.50
1995	ND	529,435.4 (--)	105.89	15,559.7 (15%)	3.11	213,352.9 (114%)	42.67	124,399.7 (44%)	24.88
2038	1,867,398.5 (17%)	352,350.0 (49%)	0.19	267,890.7 (104%)	0.14	9,369,416.2 (11%)	5.02	3,801,486.7(123%)	2.04
2286	ND	1,795,014.9 (91%)	359.00	608,877.1 (99%)	121.78	ND	0.00	128,809.3 (75%)	25.76
2354	ND	ND	0.00	182,002.4 (7%)	36.40	ND	0.00	673,923.3 (50%)	134.78
2484	672,418.4 (58%)	125,191.5 (3%)	0.19	257,088.7 (--)	0.38	ND	0.00	407,455.3 (14%)	0.61
2562	ND	2,433,260.8 (8%)	486.65	2,051,610.6 (83%)	410.32	366,874.9 (107%)	73.37	ND	0.00
2641	ND	98,193.3 (114%)	19.64	164,475.5 (92%)	32.90	372,249.3 (17%)	74.45	ND	0.00
2642	ND	3,577,911.6 (32%)	715.58	1,396,863.5 (--)	279.37	ND	0.00	992,879.2 (82%)	198.58
2673	374,444.6 (10%)	102,050.1 (8%)	0.27	ND	0.00	17,730.4 (106%)	0.05	ND	0.00
2685	ND	512,852.2 (54%)	102.57	ND	0.00	ND	0.00	568,857.1 (122%)	113.77
2779	ND	1,012,110.4 (25%)	202.42	68,472.3 (--)	13.69	ND	0.00	ND	0.00
2796	ND	1,699,582.2 (44%)	339.92	242,631.5 (71%)	48.53	2,697,654.8 (11%)	539.53	ND	0.00
2854	ND	871,796.1 (--)	174.36	70,461.2 (2%)	14.09	ND	0.00	ND	0.00
2894	110,014.5 (64%)	555,025.1 (83%)	5.05	73,660.5 (124%)	0.67	877,693.3 (104%)	7.98	92,172.4 (94%)	0.84
3000	ND	107,436.0 (88%)	21.49	909,273.8 (98%)	181.85	46,977.2 (99%)	9.40	422,572.2 (110%)	84.51
3013	ND	6,363,863.9 (10%)	1272.77	1,694,552.0(126%)	338.91	372,944.6 (29%)	74.59	ND	0.00
3021	ND	2,922,671.3 (87%)	584.53	37,999.2 (72%)	7.60	28,993.9 (24%)	5.80	59,310.114679 (67%)	11.86
3130	ND	1,634,617.5 (19%)	326.92	55,443.3 (126%)	11.09	ND	0.00	1,738,143.575827 (52%)	347.63
3235	ND	12,398,667.3 (--)	2479.73	ND	0.00	13,487.9 (25%)	2.70	ND	0.00
3318	ND	12,365,470.7 (54%)	2473.09	399,533.4 (--)	79.91	ND	0.00	ND	0.00

Table 1. *Observed phosphorylation volumes for peroxide treated C2C12 myoblasts. Ratios are the observed volume vs. the control volume. In the case where no spot was observed (ND), a value of 5000 was used to represent the background staining level. A CV value of (--)indicates that the spot was observed in only one replicate.*

Spot	Control Volume (CV)	120 min H_2O_2 exposure ND unfed Volume (CV)	Ratio vol/ control	120 min H_2O_2 exp ND fed 24hrs Volume (CV)	Ratio vol/ control	30 min H_2O_2 exp ND unfed Volume (CV)	Ratio vol/ control	30 min H_2O_2 exp ND fed 24 hrs Volume (CV)	Ratio vol/ control
748	210,167.6 (113%)	238,626.8 (81%)	1.14	167,966.7 (92%)	0.80	ND	0.00	ND	0.00
852	733,093.1 (72%)	1,797,188.5 (64%)	2.45	655,834.3 (--)	0.89	348,689.3 (32%)	0.48	111,031.5 (--)	0.15
1100	1,403,029.8 (67%)	84,439.2 (--)	0.06	31,132.4 (43%)	0.02	15,345.7 (58%)	0.01	153,268.0 (--)	0.11
1106	ND	99,103,782.1 (19%)	9910.38	68,542,103.6 (12%)	6854.21	80,264,965.6 (29%)	8026.5	75,303,958 (19%)	7530.40
1123	ND	11,196,023.6 (13%)	1119.60	8,685,113.9 (17%)	868.51	10,325,611.4 (137%)	1032.6	7,823,714.2 (37%)	782.37
1136	ND	15,558,386.7 (14%)	1555.84	12,249,758.3 (42%)	1224.98	16,249,102.4 (14%)	1624.9	10,574,116 (14%)	1057.41
1168	369,187.0 (26%)	103,487.0 (34%)	0.28	199,623.2 (19%)	0.54	425,136.6 (39%)	1.15	280,198.2 (--)	0.76
1347	65,121.4 (64%)	41,257.6 (30%)	0.63	32,456.1 (45%)	0.50	68,606.6 (23%)	1.05	31,810.4 (67%)	0.49
1495	77,401.6 (15%)	43,368.7 (--)	0.56	38,815.0 (41%)	0.50	53,046.7 (17%)	0.69	15,725.5 (--)	0.20
1502	182,621.5 (4%)	127,855.5 (4%)	0.70	367,430.1 (91%)	2.01	543,889.0 (106%)	2.98	451,243.2 (30%)	2.47
1569	ND	236,237.3 (19%)	23.62	180,237.6 (10%)	18.02	144,170.4 (64%)	14.42	175,897.7 (90%)	17.59
1616	112,716.6 (23%)	79,940.1 (39%)	0.71	84,603.2 (--)	0.75	55,973.3 (--)	0.50	69,761.8 (--)	0.62
1619	1,067,985.0 (31%)	620,898.0 (61%)	0.58	469,646.1 (120%)	0.44	593,712.2 (--)	0.56	451,421.9 (96%)	0.42
1658	203,520.7 (15%)	116,098.5 (131%)	0.57	373,979.3 (121%)	1.84	167,420.9 (71%)	0.82	235,153.2 (--)	1.16
1662	489,678.2 (37%)	209,854.3 (45%)	0.43	ND	0.00	73,396.5 (66%)	0.15	58,997.3 (134%)	0.12
1995	ND	52,435.4 (--)	5.24	26,536.9 (--)	2.65	79,945.5 (--)	7.99	92,895.2 (--)	9.29
2038	84,492.9 (36%)	352,350.0 (49%)	4.17	87,575.2 (139%)	1.04	129,245.3 (44%)	1.53	65,317.1 (8%)	0.77
2286	421,075.2 (51%)	395,014.9 (91%)	0.94	160,267.3 (103%)	0.38	ND	0.00	256,054.9 (--)	0.61
2354	63,791.8 (17%)	ND	0.00	41,682.7 (--)	0.65	ND	0.00	12,907.8 (--)	0.20
2484	87,436.7 (68%)	125,191.5 (3%)	1.43	127,285.6 (--)	1.46	187,580.0 (90%)	2.15	153,869.0 (40%)	1.76
2562	31,546.4 (51%)	33,260.8 (8%)	1.05	31,479.7 (24%)	1.00	20,737.4 (9%)	0.66	ND	0.00
2641	381,737.7 (22%)	98,193.3 (114%)	0.26	139,572.8 (59%)	0.37	47,376.5 (3%)	0.12	ND	0.00
2642	1,046,083.0 (75%)	77,911.6 (32%)	0.07	20,211.9 (--)	0.02	17,209.1 (51%)	0.02	75,292.9 (--)	0.07
2673	45,235.2 (18%)	102,050.1 (8%)	2.26	139,358.4 (--)	3.08	17,730.9 (106%)	0.39	ND	0.00
2685	60,435.8 (30%)	512,852.2 (54%)	8.49	ND	0.00	ND	0.00	93,892.2 (42%)	1.55
2779	781,673.4 (16%)	1,012,110.4 (25%)	1.29	1,047,068.2 (50%)	1.34	ND	0.00	ND	0.00
2796	1,340,811.0 (98%)	1,699,582.2 (44%)	1.27	976,772.7 (62%)	0.73	2,083,259.7 (--)	1.55	ND	0.00
2854	2,906,912.5 (10%)	871,796.1 (--)	0.30	1,190,427.7 (134%)	0.41	ND	0.00	ND	0.00
2894	927,540.6 (27%)	555,025.1 (83%)	0.60	432,530.0 (--)	0.47	877,693.2 (104%)	0.95	365,470.7 (54%)	0.39
3000	2,490,624.2 (31%)	107,436.0 (88%)	0.04	69,527.7 (--)	0.03	46,977.6 (99%)	0.02	58,201.3 (--)	0.02
3013	2,355,853.9 (14%)	33,863.9 (10%)	0.01	26,238.3 (--)	0.01	29,485.8 (--)	0.01	ND	0.00
3021	274,601.1 (77%)	222,671.3 (87%)	0.81	103,072.1 (--)	0.38	183,086.3 (129%)	0.67	114,700.6 (126%)	0.42
3130	2,256,568.4 (80%)	1,634,617.5(19%)	0.72	606,287.5 (103%)	0.27	ND	0.00	332,307.9 (--)	0.15
3235	1,294,552.7 (36%)	128,667.9 (--)	0.10	ND	0.00	139,572.7 (59%)	0.11	132,745.7 (--)	0.10
3318	220,622.7 (32%)	65,470.7 (54%)	0.30	42,091.9 (41%)	0.19	ND	0.00	ND	0.00

.

Table 2. *Observed total protein volumes for peroxide treated C2C12 myoblasts. Ratios are the observed vs. the control volume. In the case where no spot was observed, a value of 10000 was used to represent the background staining level.*

Spot #	Protein ID	Primary IPI Accession Number	SEQUEST XCorr (charge)	MW (kDa)	Phosphopeptide Sequence	Normalized Phosporylation Levels			
						120m unfed fold change	120m fed fold change	30m unfed fold change	30m fed fold change
1100	Vim Vimentin	IPI00227299.6	3.22 (+2)	54	ND	6.4	-9.7	83.2	-48.0
1106	Alb Serum albumin	IPI00131695.3	2.59 (+3)	68	ND	-477.5	-36.7	-7.5	-12.6
1123	Alb Serum albumin	IPI00131695.3	2.82 (+3)	68	ND	-4.7	-10.1	-13.8	-1.2
1347	Atp5b ATP synthase subunit beta, mito	IPI00468481.2	2.87 (+2)	56	ND	-1.2	-2.2	-2.8	2.9
1495	Mtrf1l mitochondrial chain release factor 1-like	IPI00222491	2.01 (+3)	42	HAs$_{175}$ASVGGPEAYRH NDmK	11.4	2.1	-101.9	-2.2
1619	Protein ERGIC-53 like	IPI00122028	2.39 (+3)	41	GLSPs$_{10}$LCLLs$_{15}$LLLVL NDHGAERSQPPPR	-7.0	-3.9	-15.2	-5.2
2286	Ywhaz 14-3-3 protein zeta/delta	IPI00116498.1	3.52 (+2)	28	ND	382.7	319.9	42.1	42.4
2354	Ywhae 14-3-3 protein epsilon	IPI00118384.1	2.54 (+3)	29	ND	6.4	55.7	6.4	666.1
2641	similar to pol protein	IPI00850309	2.26 (+2)	18	s$_{29}$NALEVIRTQIWDQLK	76.3	90.0	599.9	38.2
2854	LOC100048522 similar to CofilinND1	IPI00848816.1	2.63 (+2)	19	ND	581.4	34.4	290.7	290.7
2894	Fabp5 Fatty acid-binding, epidermal	IPI00114162.3	2.70 (+2)	15	ND	8.4	1.4	8.4	2.1
3000	2900073G15Rik myosin light chain, reg. BNDlike	IPI00109044.8	3.38 (+2)	22	ND	498.1	6514.4	498.1	3616.6
3013	Ppia Peptidyl-prolyl cis-trans isomerase	IPI00554989.3	2.21 (+3)	18	ND	88545	30429	5959.5	235.6
3235	Hist2h2ac Histone H2A type 2C	IPI00272033.3	2.39 (+2)	14	ND	24949	129.5	25.0	9.8
3318	Lgals1 Galectin-1	IPI00229517.5	3.01 (+2)	15	ND	8333.8	418.8	22.1	22.1

Table 3. *Tandem MS/MS results and normalized phosphorylation change, where a negative value is a decrease in phosphorylation and a positive value is an increase in phosphorylation compared to the control per the Pro-Q Diamond/Sypro Ruby staining data.*

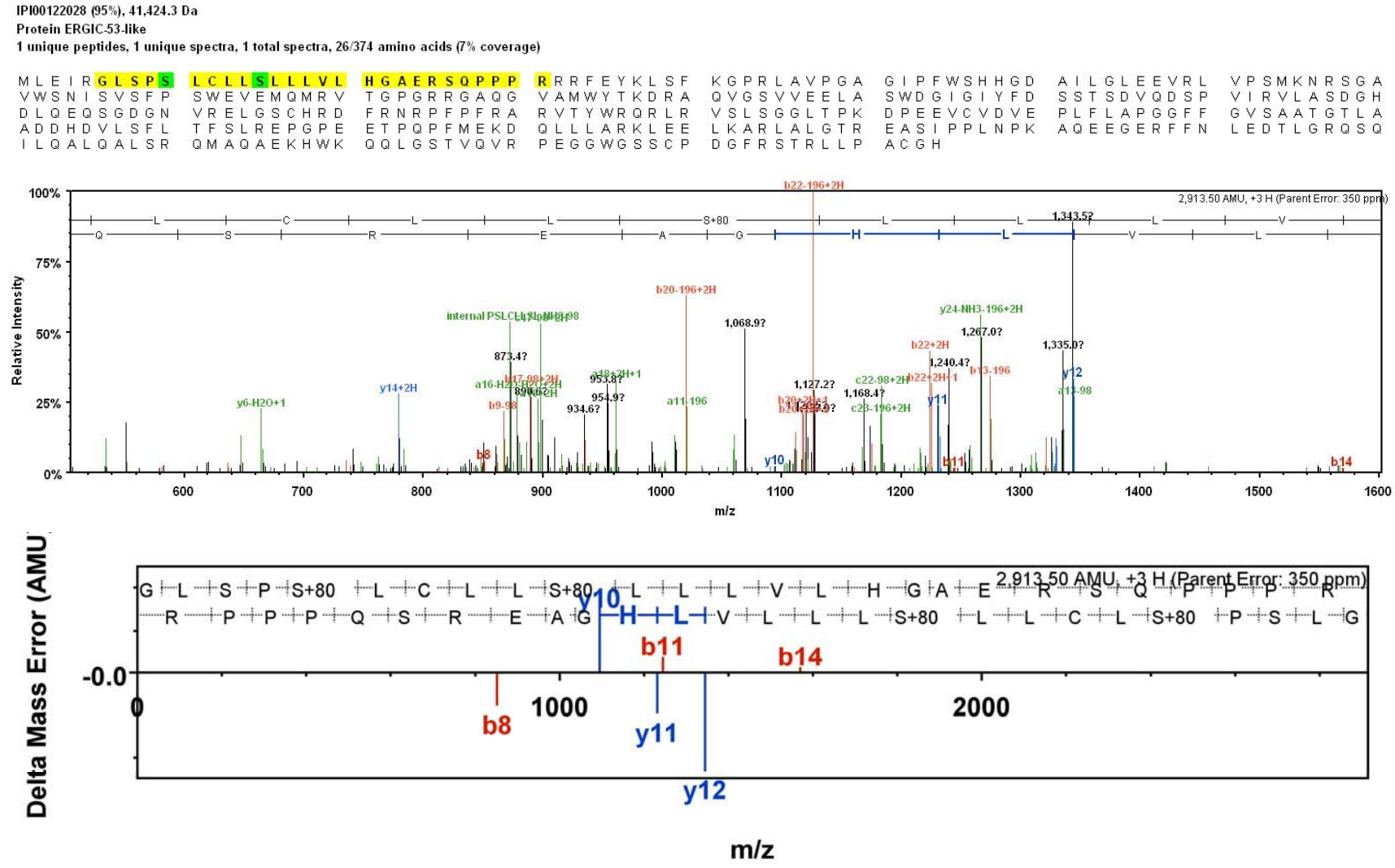

Figure 30. *Sequence coverage, spectrum and spectrum/model error for EGRIC-53-like GLSPsLCLLsLLLVLHGAERSQPPPR phosphopeptide.*

...	B Ions	B+2H	B-NH3	B-H2O	AA	Y Ions	Y+2H	Y-NH3	Y-H2O	...
1	58.0				G	2,913.5	1,457.2	2,896.5	2,895.5	26
2	171.1				L	2,856.5	1,428.7	2,839.4	2,838.5	25
3	258.1			240.1	S	2,743.4	1,372.2	2,726.4	2,725.4	24
4	355.2			337.2	P	2,656.3	1,328.7	2,639.3	2,638.3	23
5	522.2			504.2	S+80	2,559.3	1,280.2	2,542.3	2,541.3	22
6	635.3	318.1		617.3	L	2,392.3	1,196.7	2,375.3	2,374.3	21
7	738.3	369.6		720.3	C	2,279.2	1,140.1	2,262.2	2,261.2	20
8	851.4	426.2		833.4	L	2,176.2	1,088.6	2,159.2	2,158.2	19
9	964.5	482.7		946.4	L	2,063.1	1,032.1	2,046.1	2,045.1	18
10	1,131.5	566.2		1,113.4	S+80	1,950.0	975.5	1,933.0	1,932.0	17
11	1,244.5	622.8		1,226.5	L	1,783.0	892.0	1,766.0	1,765.0	16
12	1,357.6	679.3		1,339.6	L	1,670.0	835.5	1,652.9	1,651.9	15
13	1,470.7	735.9		1,452.7	L	1,556.9	778.9	1,539.8	1,538.9	14
14	1,569.8	785.4		1,551.8	V	1,443.8	722.4	1,426.8	1,425.8	13
15	1,682.9	841.9		1,664.9	L	1,344.7	672.9	1,327.7	1,326.7	12
16	1,819.9	910.5		1,801.9	H	1,231.6	616.3	1,214.6	1,213.6	11
17	1,876.9	939.0		1,858.9	G	1,094.6	547.8	1,077.5	1,076.6	10
18	1,948.0	974.5		1,930.0	A	1,037.5	519.3	1,020.5	1,019.5	9
19	2,077.0	1,039.0		2,059.0	E	966.5	483.8	949.5	948.5	8
20	2,233.1	1,117.1	2,216.1	2,215.1	R	837.5	419.2	820.4	819.5	7
21	2,320.2	1,160.6	2,303.1	2,302.1	S	681.4	341.2	664.3	663.4	6
22	2,448.2	1,224.6	2,431.2	2,430.2	Q	594.3		577.3		5
23	2,545.3	1,273.1	2,528.2	2,527.3	P	466.3		449.3		4
24	2,642.3	1,321.7	2,625.3	2,624.3	P	369.2		352.2		3
25	2,739.4	1,370.2	2,722.3	2,721.4	P	272.2		255.1		2
26	2,913.5	1,457.2	2,896.5	2,895.5	R	175.1		158.1		1

Figure 31. *Fragmentation table for EGRIC-D53-like GLSPsLCLLsLLLVLHGAERSQPPPR phosphopeptide.*

3.4 Discussion

The impact of the albumin contamination on the study affects the total protein ratios and potentially the phosphorylation ratios, exacerbating an overall lack of confidence in the results. Several potential explanations for this contamination seem readily apparent: the C2C12 myoblasts were damaged by the H_2O_2 treatment and trapped albumin within the remaining structure, the H_2O_2 treatment modified/signaled unknown membrane proteins on the cell surface causing adhesion of albumin and finally, that the C2C12 myoblasts continued to differentiate into myotubes and trapped albumin within as they formed.

The apparent correlation between the fed and frozen samples, with a slightly higher amount of albumin for the samples treated for 30 minutes with H_2O_2, and an elevated value for the samples returned to the incubator compared to the samples placed in the freezer seems to support the case for continued myotube formation. If the C2C12 myoblasts were damaged by the H_2O_2 treatment, a longer exposure time should cause more damage and therefore an increased concentration of albumin would be observed. Without an extensive study to elucidate the effects of H_2O_2 on the protein-protein interactions of albumin with cell-surface proteins it is not possible to rule out a potential effect, but with the evidence that after 24 hours without the H_2O_2 exposure the concentration of albumin continued to increase, leaves the most likely explanation to be the continued formation of myotubes.

Without fully understanding the cause of the albumin contamination, it is difficult to assess its influence on the study. The remainder of the discussion will assume that it only had a minor effect on the observed phosphorylation differences.

More important to the results of the study are the lack of quality tandem MS results. The results shown in **Figures 30** and **31** demonstrate the highest quality phosphopeptide evidence that was obtained. There is a significantly high parent mass value error of 350 ppm, which is very likely due to a parent charge misalignment caused by poor resolution of the isotopic envelope for the parent as happens most frequently in high charge states like the (+3) charge state observed in our example[14]. Another possible cause of charge misalignment is due to poor signal intensity for the given parent ion, common for phosphorylated peptides. Nevertheless, this result meets our error tolerance criteria and requires further inspection. There is one missed cleavage site, which is within reason, and a number of a-series fragments, but a-series fragments are not rare in tandem MS resulting from a parent bearing multiple charges and show higher than expected intensity due to the neutral losses associated with them. Looking at the spectrum/model error, the most significant error is observed in the y_{12} ion which is over 300 ppm. This error is easily explained as not a matching error, but a modeling error and from manual interpretation (**Figure 32**) we see the error is much reduced if we consider multiple losses, which are also common for fragments of multiply-charged parents. The y_{12} fragment would be more appropriately assigned at an m/z of 1344.9

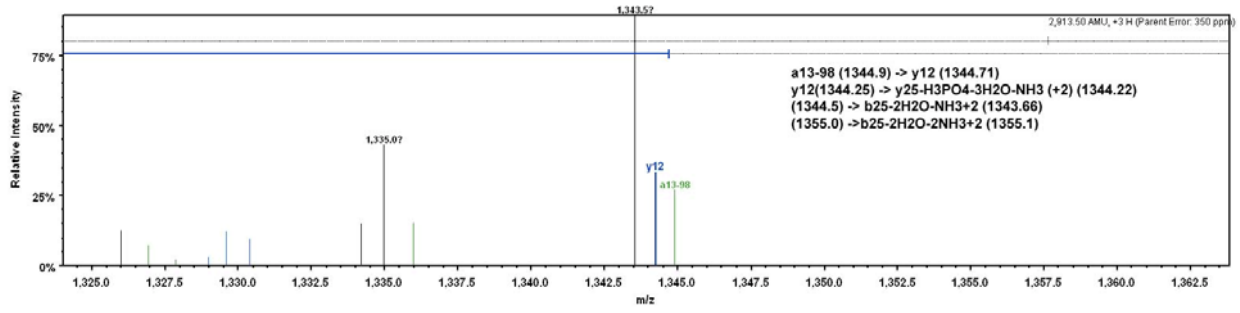

Figure 32. *Modeling errors with potential corrections and assignments.*

which is closer to the theoretical value of 1344.71 than in the assignment by Scaffold of 1344.25. This ion is more likely to represent the relatively large y_{25} fragment suffering multiple losses and the unassigned peaks in the window are also readily explained by multiple losses to the large b_{25} fragment.

The normalized phosphorylation levels given in **Table 3** do not stand alone, and must be referenced against the data in **Tables 1** and **2** to infer any potential biological implications of the results. From this data, vimentin (Vim) is a known phosphoprotein and there is evidence that its phosphorylation state plays a role in the assembly and disassembly dynamics of intermediate filaments within the cell[15-17]. Vim has been characterized as playing a role in mitosis when phosphorylated[18] yet shows decreased phosphorylation relative to the control after H_2O_2 treatment and a return to the incubator, with no phosphorylated spots detected. There were increases in phosphorylation observed from the 30 min and 120 min treatment samples that were placed in the -70°C freezer, suggesting that the effects from the H_2O_2 treatment were not necessarily arrested by freezing. The exaggerated differences between the 30 min and 120 min treatments suggest that the H_2O_2 treatment influenced the results, but without a targeted study these results are merely suggestive.

ATP synthase subunit beta, mitochondrial precursor (Atp5b) produces ATP from ADP in the presence of a proton gradient across the mitochondrial membrane. The beta chain is the catalytic subunit and there is evidence that it is phosphorylated[19]. The phosphorylation level for the spot identified as Atp5b undergoes changes that seem to correlate with the duration of exposure to H_2O_2. The H_2O_2 treatment demonstrated a 2-fold decrease in phosphorylation for most of the samples, suggesting possible activation

of the phosphatase, but showed an increase in the normalized phosphorylation level after feeding in the 30 min exposure sample. The total protein levels of the spot show that there was at most a two-fold change for any given treatment. The phosphorylation increase observed after feeding for the 30 min exposure sample and the relative decrease in phosphorylation in the fed 120 min exposure sample suggests an effect from exposure time, but requires further elucidation. This may be meaningful since a reduction in the phosphorylated isoform of ATP synthase subunit beta has been implicated in type-2 diabetes as a possible source of insulin resistance.[20] and the potential correlation with ROS may be noteworthy.

The normalized phosphorylation numbers for the 14-3-3 proteins zeta and epsilon both showed a remarkable correlation within the specific treatments although no such correlation was evident from the spot phosphorylation or spot total protein levels alone. The spot identified as 14-3-3 zeta showed an increase in phosphorylation for both of the 120 m exposures (>300-fold) that was almost an order of magnitude higher than for the 30 m exposures (~40-fold) showing an exposure time dependence and no subsequent response after 24 hours in the incubator. 14-3-3 zeta is a protein of the 14-3-3 family of proteins which mediate signal transduction by binding to phosphoserine-containing proteins and is a multifunctional regulator of the cell signaling processes. There is evidence that phosphorylation of 14-3-3 zeta disrupts homo-dimerization and its phosphorylation state has been implicated in the activation of apoptosis signal-regulating kinase 1 (ASK1) initiating oxidant stress-induced cell death[21]. The protein 14-3-3 epsilon is an adapter protein implicated in the regulation of a large spectrum of both general and specialized signaling pathways and binds to a large number of

partners, usually by recognition of a phosphoserine or phosphothreonine motif. The binding of 14-3-3 epsilon generally results in the modulation of the activity of the binding partner. Similar to 14-3-3 zeta, 14-3-3 epsilon has also been implicated in oxidative stress-induced apoptosis[22], although the link to its phosphorylation status has not been established.

3.5 Conclusions

The overall results of the experiment suggest a correlation between oxidative stress and changes in phosphorylation state of certain proteins and several results warrant further investigation. Further experiments would require that the contamination from albumin be remediated, possibly through a method of sample preparation such as protein depletion[23]. The danger of inadvertently forming myotubes from confluent cell cultures could also be avoided by using an alternative cell line.

3.6 References

[1] Schröder E, Eaton P. Hydrogen peroxide as an endogenous mediator and exogenous tool in cardiovascular research: issues and considerations. Curr Opin Pharmacol. 2008 Apr;8(2):153-9.

[2] Kislinger T, Gramolini AO, Pan Y, Rahman K, MacLennan DH, Emili A. Proteome dynamics during C2C12 myoblast differentiation. Mol Cell Proteomics. 2005 Jul;4(7):887-901.

[3] Wessel, D., and Flügge, U.I., A method for the quantitative recovery of protein in dilute solution in the presence of detergents and lipids. Anal Biochem. 1984 Apr;138(1):141ND3.

[4] Leimgruber, R.M., Malone, J.P., Radabaugh, M.R., LaPorte, M.L., Violand, B.N. and Monahan, J.B. Development of improved cell lysis, solubilization and imaging approaches for proteomic analyses. Proteomics 2002 Feb;2(2):135ND44.

[5] Lowry, O.H., Rosbrough, N.J., Farr, A.L., and Randall, R.J., Protein measurement with the Folin phenol reagent. J. Biol. Chem. 1951 Nov;193(1):265ND75

[6] Görg A., Boguth, G., Obermaier, C., Posch, A. and Weiss, W., Two-dimensional polyacrylamide gel electrophoresis with immobilized pH gradients in the first dimension (IPG-Dalt): the state of the art and the controversy of vertical versus horizontal systems. Electrophoresis 1995 Jul;16(7):1079ND86.

[7] Olsen, J.V., Ong, S.E. and Mann, M. Trypsin cleaves exclusively C-terminal to arginine and lysine residues. Mol. Cell. Proteomics 2004 Jun;3(6):608ND14

[8] Mann, M., Ong, S.E., Grønborg, M., Steen, H., Jensen, O.N. and Pandey, A., Analysis of protein phosphorylation using mass spectrometry: deciphering the phosphoproteome. Trends Biotechnol. 2002 Jun;20(6):261ND8

[9] Eng, J., McCormack, A.L., and Yates, J.R. An approach to correlate tandem mass spectral data of peptides with amino acid sequences in a protein database. J. Am. Soc. Mass Spectrom. 5, 976ND989 (1994).

[10] Perkins, D.N., Pappin, D.J., Creasy, D.M., and Cottrell, J.S., ProbabilityNDbased protein identification by searching sequence databases using mass spectrometry data. Electrophoresis 1999 Dec;20(18) 3551ND67

[11] Craig, R. and Beavis, R.C., A method for reducing the time required to match protein sequences with tandem mass spectra. Rapid Commun. Mass Spectrom. 2003;17(20):2310ND16

[12] Keller, A., Nesvizhskii, A.I., Kolker, E., and Aebersold, R., Empirical statistical model to estimate the accuracy of peptide identifications made by MS/MS data search. Anal. Chem. 2002 Oct 15;74(20):5383–92.

[13] Nesvizhskii, A.I., Keller, A., Kolker, E., and Aebersold, R. A statistical model for identifying proteins by tandem mass spectrometry. Anal Chem. 2003 Sep 2;75(17):4646–58.

[14] Creasy DM, Cottrell JS. Error tolerant searching of uninterpreted tandem mass spectrometry data. Proteomics. 2002 Oct;2(10):1426-34.

[15] Eriksson JE, He T, Trejo-Skalli AV, Härmälä-Braskén AS, Hellman J, Chou YH, Goldman RD. Specific in vivo phosphorylation sites determine the assembly dynamics of vimentin intermediate filaments. J Cell Sci. 2004 Feb 29;117(Pt 6):919-32.

[16] Cheng TJ, Tseng YF, Chang WM, Chang MD, Lai YK. Retaining of the assembly capability of vimentin phosphorylated by mitogen-activated protein kinase-activated protein kinase-2. J Cell Biochem. 2003 Jun 1;89(3):589-602.

[17] Ando S, Tanabe K, Gonda Y, Sato C, Inagaki M. Domain- and sequence-specific phosphorylation of vimentin induces disassembly of the filament structure. Biochemistry. 1989 Apr 4;28(7):2974-9.

[18] Dephoure N, Zhou C, Villén J, Beausoleil SA, Bakalarski CE, Elledge SJ, Gygi SP. A quantitative atlas of mitotic phosphorylation. Proc Natl Acad Sci U S A. 2008 Aug 5;105(31):10762-7.

[19] Lee J, Xu Y, Chen Y, Sprung R, Kim SC, Xie S, Zhao Y Mitochondrial phosphoproteome revealed by an improved IMAC method and MS/MS/MS. Mol Cell Proteomics. 2007 Apr;6(4):669-76.

[20] Højlund, K., Wrzesinski, K., Larsen, P.M., Fey, S.J., Roepstorff, P., Handberg, A., Dela, F., Vinten, J., McCormack, J.G., Reynet, C., and BeckNDNielsen, H., Proteome analysis reveals phosphorylation of ATP synthase beta subunit in human skeletal muscle and proteins with potential roles in type 2 diabetes. J. Biol. Chem. 2003 Mar 21;278(12):10436ND42

[21] Zhou J, Shao Z, Kerkela R, Ichijo H, Muslin AJ, Pombo C, Force T. Serine 58 of 14-3-3 zeta is a molecular switch regulating ASK1 and oxidant stress-induced cell death. Mol Cell Biol. 2009 Aug;29(15):4167-76. Epub 2009 May 18.

[22] Nielsen MD, Luo X, Biteau B, Syverson K, Jasper H. 14-3-3epsilon antagonizes FoxO to control growth, apoptosis and longevity in Drosophila. Aging Cell. 2008 Oct;7(5):688-99.

[23] Rieux L, Bischoff R, Verpoorte E, Niederländer HA. Restricted-access material-based high-molecular-weight protein depletion coupled on-line with nano-liquid chromatography-mass spectrometry for proteomics applications. J Chromatogr A. 2007 May 18;1149(2):169-77.

Chapter Four

Age-Dependent Changes of Protein Phosphorylation in Rat Skeletal Muscle: a Proteomic Study.

4.1 Introduction

In 1999, the United States Centers for Disease Control and Prevention listed sarcopenia (muscle atrophy) in the top five major health risks facing the US population[1]. Sarcopenia has been demonstrated to develop in the aged population[2], primarily through a decrease in number of muscle fibers, but also in a degradation of existing muscle fibers[3] and has been linked to various dysfunctions in the aged population including impaired thermoregulation, glucose intolerance and the loss of mobility and contractility[4-8].

While sarcopenia has been shown to be ameliorated by weight training exercise[9], it has been directly associated with an age-dependent increase in oxidative stress in movement-restricted animals[10]. There are numerous sources of reactive oxygen species (ROS) within any organism. The vast majority of ROS are endogenous and are the result of normal metabolism within the mitochondria and peroxisomes. But there are also exogenous sources for ROS such as environmental toxins. One example of such a potential toxin is unbound or free iron. While iron is necessary for the normal function of an organism, it has the potential to accumulate over time until it becomes toxic, causing damage as the concentration level increases. There is direct evidence that there is an increasing level of free iron present in skeletal muscle during the aging process and that free iron can enhance the reaction of reactive oxygen species with some biomolecules[11,12]. One potential effect of these reactions is an altered phosphoproteome. These reactions have the potential to damage both kinases and phosphatases and result in abnormal protein phosphorylation. The phosphorylation

sites on the kinase and phosphatase substrates themselves could even be functionally damaged by reactions with reactive oxygen species. In turn, downstream expression levels could be altered in response to oxidative damage[13-15].

There are estimates that approximately 30% of all proteins encoded by the human genome are regulated by phosphorylation/ dephosphorylation. Phosphorylation represents a reversible process important for cellular signaling and regulation[16]. It has been estimated that there are more than 100,000 phosphorylation sites in the human proteome, and recent work has shown that multiple phosphorylation sites can be present on any given protein[17,18]. The targeted residues for phosphorylation are primarily serine and threonine, but tyrosine and other residues can also be phosphorylated and various phosphorylation motifs have been elucidated[19,20]. Protein kinases and protein phosphatases work in concert to provide a dynamic balance between the two protein states and thus regulate function[21,22]. These enzymes are not only responsible for phosphorylation and dephosphorylation, but represent phosphorylation targets themselves. Any perturbation of this system could influence the onset and degree of sarcopenia.

A comprehensive study of phosphorylation requires not only identification of phosphoproteins, but also a quantitative method that provides a real measure of the differences in phosphorylation between biological states. Ideally, one would also want to identify and measure differences in the protein kinases and phosphatases involved in producing those differences and also elucidate the phosphorylation sites and any additional post-translational modifications that may be effecting the changes. This task is complicated by the fact that many signaling phosphoproteins are expressed at

relatively low levels and the stoichiometry of occupied phosphorylation sites is variable on phosphoproteins where multiple sites are present. This provides a challenge for not only for accurate quantitation, but also for detection, identification and accurate description of the phosphorylation site of any particular phosphoprotein.

In order to characterize differences in protein phosphorylation between the skeletal muscle of aged and young animals, a differential phosphoproteomic study on skeletal muscle homogenates of 34-month versus 5-month-old Fisher344/BN F1 rats was conducted using 2D-PAGE followed by mass spectrometric identification. In order to determine protein spots of interest and to normalize phosphorylation differences to protein expression differences, Pro-Q Diamond images demonstrating a change of two-fold or greater were cross-referenced against images of the same gels stained with a total protein stain, Sypro Ruby. The spots of interest were then subsequently digested with trypsin and analyzed via mass spectrometry to determine their identities and potential phosphorylation sites.

4.2 Experimental

4.2.1 Materials

Unless otherwise noted, all chemicals were purchased from Sigma Chemicals (St. Louis, MO) and were of electrophoretic grade or better.

4.2.2 Tissue Preparation

Three 5-month old and three 34-month old Fisher344/BN F1 rats housed in a 12 hour light/dark cycle, that had been provided with water and food ad libitum, were

euthanized by carbon monoxide asphyxiation followed by quick decapitation according to the protocol of the Animal Care Unit of the University of Kansas. Fast-twitch muscle tissue from the hind legs of the animals was removed immediately and stored at -80º C until further use.

4.2.3 Sample Preparation

Small samples were cut from the frozen skeletal muscle tissue, ground into a fine powder with mortar and pestle and introduced into a 15 mL centrifuge tube containing a lysis buffer consisting of: 7M urea [Fisher, Fair Lawn, NJ], 2M thiourea, 4% (v/v) CHAPS [Fisher, Fair Lawn, NJ], 1% (v/v) Tween-20 [Fisher, Fair Lawn, NJ], 40 mM Tris, 20 mM DTT, 1mM sodium fluoride, phosphatase inhibitor cocktail 1, and phosphatase inhibitor cocktail 2, 0.5 mM PMSF, 10 µg/ml of leupeptin, 10 µg/ml apopritin, and homogenized with an Ultra-Turrax T8 homogenizer [Fisher, Fair Lawn, NJ], and then briefly sonicated with a Fisher 550 sonic dismembrator [Fisher, Fair Lawn, NJ]. The soluble fraction was transferred to a fresh 15 mL centrifuge tube and the homogenates were delipidated using chloroform/methanol precipitation.[23] The protein fraction was resolubilized into a buffer amenable to iso-electric focusing (IEF) containing 5M urea [Fisher, Fair Lawn, NJ], 2M thiourea, 2% (v/v) CHAPS [Fisher, Fair Lawn, NJ], 0.5% (v/v) Tween-20 [Fisher, Fair Lawn, NJ], 0.5% (w/v) 3-(decyldimethylammonio)propanesulfonate, 10% (v/v) 2-propanol [Fisher, Fair Lawn, NJ], 10% (v/v) water- saturated butanol [Fisher, Fair Lawn, NJ], 5% (v/v) glycerol, 0.25% (v/v) carrier ampholytes (50:50 mix of Pharmalyte 3-10 [GE Healthcare, Piscataway, NJ] and Bio-Lyte 3/10 [Bio Rad, Hercules, CA]), 1mM sodium fluoride, phosphatase inhibitor cocktail 1 and phosphatase inhibitor cocktail 2.[24]

In order to maximize dissolution, a sonicator probe was utilized where the samples were kept in an ice bath and 3 second bursts were applied until the protein pellets dissipated. The samples were then centrifuged at 13000 x g in a microcentrifuge and the supernatant transferred to fresh centrifuge tubes. Protein concentrations were determined using the Lowry method[25] and the samples were reduced using tributylphosphine and alkylated with iodoacetamide using a ReadyPrep Reduction/Alkylation kit [Bio Rad, Hercules, CA] according to manufacturer's procedures prior to final dilution to 1.67µg/µL with the aforementioned IEF buffer.

4.2.4 2D-PAGE Separation

Isoelectric Focusing

For the first dimension separation, 450 µL aliquots of six samples prepared from the rat skeletal muscle tissue (3 young, 3 old) were applied to 18 cm 'Immobiline' immobilized pH gradient (IPG) strips (pH 3-10 NL) [GE Healthcare, Piscataway, NJ] to load 750 µg of total protein and allowed to rehydrate overnight. The strips were transferred to an IPGPhor II [GE Healthcare, Piscataway, NJ] electrophoresis unit where the IEF was conducted by first holding the voltage at 50 volts for the first four hours to allow the migration of excess charged species introduced by the various phosphatase inhibitors[26], then stepping to 100 volts for two hours followed by a step to 500 volts for two hours and then using a linear gradient over 12 hours from 500 to 10,000 volts to achieve a total of 70,000 volt hours.

SDS-PAGE

During the isoelectric focusing, a set of six 1x200x260mm polyacrylamide gels (12.5% T, 3%C) were cast into individual glass cassettes using an Ettan Dalt*six* gel casting apparatus [GE Healthcare, Piscataway, NJ] following manufaturer's protocols and used within twelve hours of casting.

For the second dimension separation, the focused IPG strips were removed from the IPGPhor II and 're-equilibrated' in a solution of 50mM Tris-HCl [Fisher, Fair Lawn, NJ], pH 8.8, 30% (v/v) glycerol [Fisher, Fair Lawn, NJ], 6M urea [Fisher, Fair Lawn, NJ], with 2% (w/v) sodium dodecyl sulfate (SDS) [Bio Rad, Hercules, CA] and 0.001% (w/v) bromophenol blue for 20 minutes. Following re-equilibration, the strips were each transferred to individual cassettes with 20x75mm strips of grade 1 Whatman filter paper [Fisher, Fair Lawn, NJ] soaked with 2uL aliquots of the PeppermintStick™ phosphoprotein molecular weight marker [Invitrogen, Carlsbad, CA] on the acidic side of the strip, and sealed with 0.5% (w/v) boiling agarose [Fisher, Fair Lawn, NJ] containing 0.001% (w/v) bromophenol blue onto the top of the slab gel in each respective glass cassette. After allowing a few minutes for the agarose to properly cool, the six slab gels were transferred to an Ettan Dalt*six* electrophoresis tank [Fisher, Fair Lawn, NJ] with the appropriate buffers and run at 30 total watts (5 watts per gel) for approximately 30 minutes to effect the transfer of the proteins from the IPG strip to the slab gel noting the progress of the bromphenol blue dye front onto the slab gel.

Once the dye front had unequivocally entered the slab gels, the power was increased to 100 total Watts and the gels were allowed to run until the dye front progressed to the bottom of the gels which required approximately six hours.

Imaging

Immediately following the second dimension SDS-PAGE, the slab gels were removed from their respective cassettes, fixed and stained according to the Pro-Q Diamond Phosphoprotein Gel Stain [Invitrogen, Carlsbad, CA] following the manufacturer's protocol for large 2D gels with the following modifications: 1) The first fixation step was conducted for 12 hours and the second fixation step for 24 hours. 2) The first destaining step was conducted for 12 hours. The gels were then imaged using a Typhoon Imager [GE Healthcare, Piscataway, NJ] creating phosphoprotein gel images for each slab gel.

Following imaging, each gel was then returned to a fixation solution (50% (v/v) methanol, 7% (v/v) acetic acid) and left overnight prior to staining with Sypro Ruby [Invitrogen, Carlsbad, CA], following the manufacturer's protocol. The Sypro Ruby stained gels were then imaged with the Typhoon Imager to create total protein gel images for each slab gel.

4.2.5 Image Analysis

Analysis of the resultant gel images was conducted using the Progenesis PG220 software [Nonlinear Dynamics, Newcastle upon Tyne, UK]. This analysis required separating the images into the following base sets: Images of phosphoproteins from 5 and 34 month old animals, images of total protein from 5 and 34 month old animals. Our experiment included three images for each set; the software combines these images in each set to create an averaged image and matched spots in each set with

location and averaged spot density for each spot. These averaged images are matched to a master image to provide a reference between the sets of gels.

Several attempts were made to create a complete overall analysis by combining the phosphoprotein gel images with the total protein gel images to generate ratiometric phosphorylation difference values corrected for expression differences. This proved to be an untenable exercise with this version of the software due to the large number of spots present in the gel images and differences in spot visibility between the two dyes. A number of spots evident in the phosphoprotein gel images were not found in the total protein gel images, and, as expected, many of the spots detected in the total protein images were not observed in the phosphoprotein gel images. The spot matching algorithm in the software would force matches between spots that were nearby and not necessarily the correct match. To overcome this problem, the analysis was broken into two separate parts with a phosphoprotein gel image analysis to determine the spots of interest and a total protein analysis to be referenced for each spot of interest to normalize the phosphorylation difference values to expression differences.

4.2.6 FT-ICR MS Analysis

Spots demonstrating normalized differential phosphorylation were excised manually from the gels using a 1.5 mm spot picker utilizing disposable tips to ameliorate cross contamination. The spots of interest were dehydrated with acetonitrile, dried and subjected to in-gel digestion with MS-grade modified trypsin [Promega, Madison, WI] in 50 mM NH_4HCO_3 overnight at 37º C.[27] The supernatant was removed and analyzed via nanoelectrospray ionization (NSI) HPLC-MS/MS using a Thermo-Finnigan hybrid LTQ-

FT mass spectrometer. Two separate experiments were conducted; the first focused primarily on identifying the proteins in the in-gel digests, while the second was focused on locating phosphopeptides for structural information. In all cases the instrument was run in the positive mode.

In the first experiment for identification, the LTQ-FT mass spectrometer was programmed to use a data-dependent survey scan where a full range mass spectrum (m/z 400-2000) was collected and the three most abundant ions were scanned using selected ion monitoring (SIM) by the Fourier transform ion cyclotron resonance mass spectrometer (FT-ICR) prior to an MS/MS experiment in the linear quadrupole ion trap (LTQ) mass spectrometer. The ions accumulated in the linear ion trap for both the MS and MS/MS scans. The AGC target values were set to $1X10^6$ ions for the survey MS, $1X10^5$ ions for the SIM and $1X10^4$ for the MS/MS experiments. The maximum accumulation time was set at 200 ms for all modes. The resolution at 400 *m/z* was set to $1X10^4$ for the FT-ICR scans and isolation widths were set at ± 2 *m/z* for the SIM experiments and ± 1 *m/z* for the MS/MS experiments and ions were selected for MS/MS when their respective intensities reached 1000 counts. The normalized collision energy was set to 35% and three microscans were acquired for each spectrum. The mass spectrometer was programmed to ignore singly charged species for fragmentation and was set to dynamically exclude precursors that had already been selected for 1 minute after their respective fragmentations.

The second experiment was conducted with the same parameters as the first experiment, but an additional step was added, which monitored neutral losses by

scanning for fragment ions that had suffered a loss of 98 Daltons from the precursor and collecting an additional tandem mass spectrum on these fragments.[28]

The chromatography for both experiments was kept consistent. Ten uL injection volumes of the peptide digests injected into a chromatography system consisting of a FAMOS Capillary and Nano HPLC Autosampler, a Switchos loading pump and switching valve and an ULTIMATE Capillary and Nano HPLC Pump [Dionex/LC Packings, Sunnyvale, CA]. The Switchos loading pump, in-line to the autosampler, trapped the digests on a 1mm C-18 PepTrap column [Dionex, Sunnyvale, CA] at a flow rate of 20μL/min of 0.1% (v/v) TFA. After 5 minutes the switching valve, integral to the Switchos, changed the flow to the ULTIMATE Nano pump which was set to flow through the PepTrap column into a standard coated PicoFrit® column, 360μm/75μm OD/ID, 15μm tip, 12 cm long [New Objective, Woburn, MA], packed in house with 5 μm particles of 300 Á pore-size Bio-Basic C18 material [Thermo-Scientific, Waltham, MA] at a flow rate of approximately 200 nL/min, utilizing a 90 minute linear gradient from 90% (v/v) solvent A to 90% (v/v) solvent B and held at 90% B for 30 minutes. Solvent A consisted of 10% ACN/89.9% H_2O/0.1% FA (v/v/v) and solvent B consisted of 10% H_2O/89.9% ACN/0.1% FA (v/v/v). The PepTrap column and the PicoFrit column were allowed to re-equilibrate to aqueous conditions (0.1% TFA and 90% solvent A respectively) for 60 minutes between analytical runs.

4.2.7 Tandem MS Protein Identification

The resultant spectra obtained from all MS experiments were first analyzed via Bioworks v.3.3.1 [Thermo-Scientific, Waltham, MA] which uses the SEQUEST[29]

algorithm against the most recent version of the International Protein Index (IPI) database. The DTA files generated by SEQUEST for each mass spectrum were concatenated into a single data file and then analyzed using Mascot v.2.2[30] [Matrix Science, Boston MA] with the same database as the SEQUEST analysis. Search parameters for both programs included static mass modifications to cysteine due to alkylation by iodoacetamide, and differential mass modifications to methionine from oxidation, and to serine, threonine and tyrosine from phosphorylation. Parameters specific to neutral losses and the formation of dehydroalanine, the result of a neutral loss from serine, were available within the Mascot program and were used in addition to the aforementioned parameters. The Scaffold [Proteome Software, OR] program was used to validate protein identifications derived from the MS/MS sequencing results. Scaffold verifies peptide identifications assigned by SEQUEST and Mascot using the X!Tandem database searching program[31]. Scaffold then probabilistically validates these peptide identifications using PeptideProphet[32] and derives corresponding protein probabilities using ProteinProphet[33].

4.3 Results

Figures 33 and **34** display images of the individual gels run for skeletal muscle samples from the three 5-month old and three 34-month old Fisher 344/BN1 rats. There is excellent reproducibility for both the Sypro Ruby and Pro-Q Diamond staining for each set of three animals, but there are significant age-dependant differences between the data sets from the 5-month and 34-month old animals. The image analysis identified approximately 75 phosphoprotein spots which demonstrate nearly a two-fold

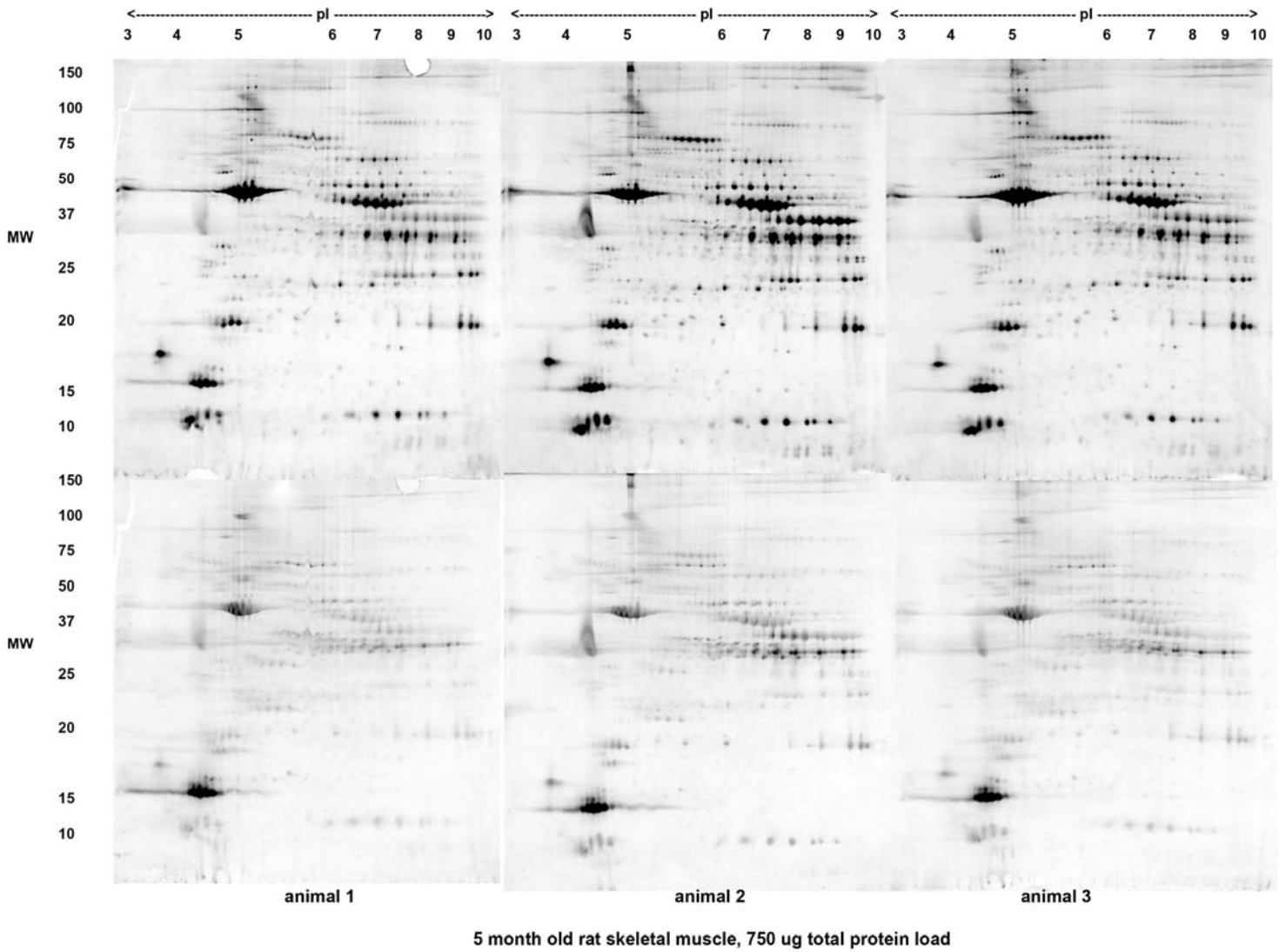

Figure 33. *Gel images of soluble skeletal muscle proteins of 5 month old animals. Top panel: total protein imaging, bottom panel: phosphoprotein imaging.*

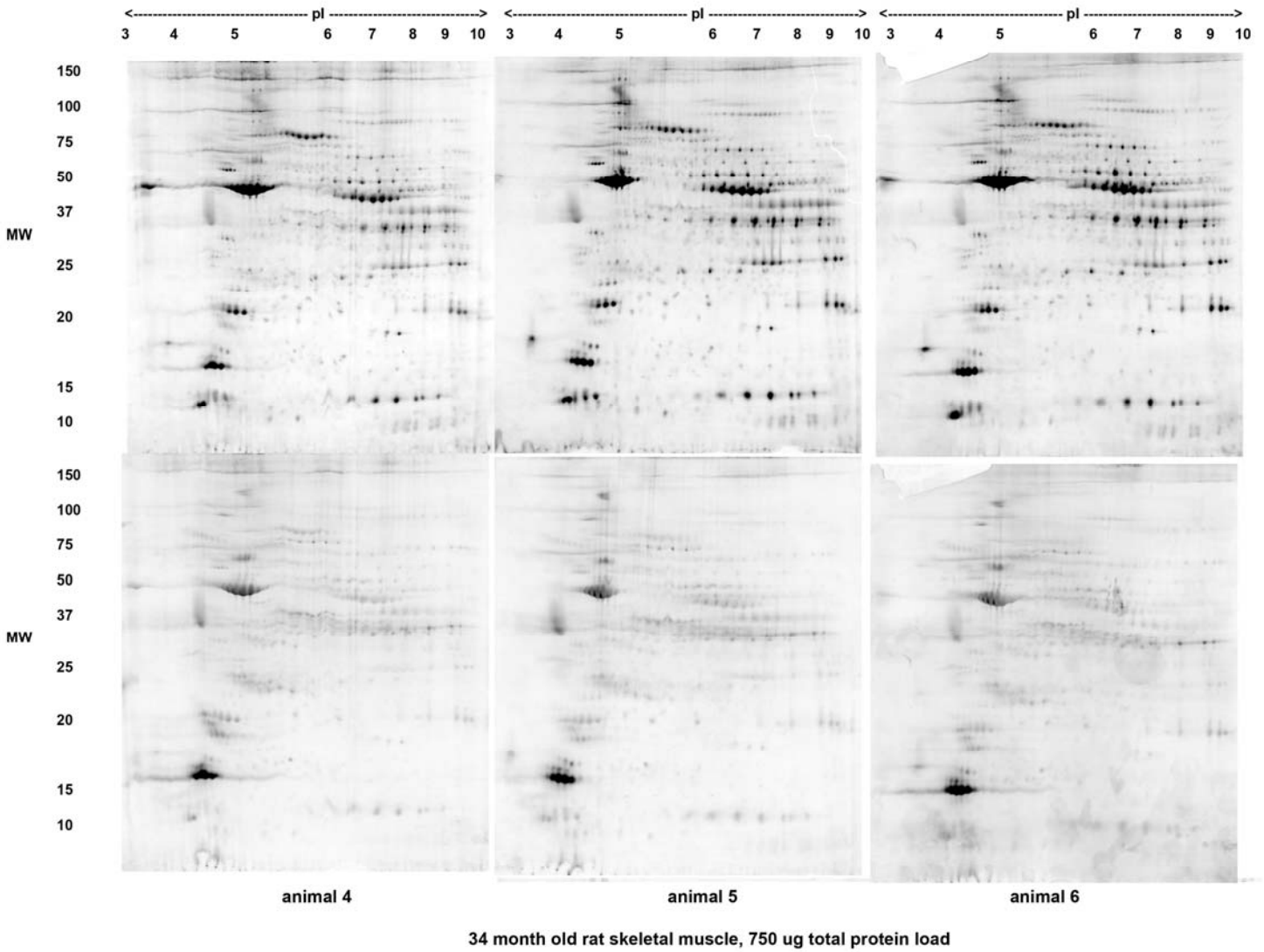

Figure 34. *Gel images of soluble skeletal muscle proteins of 34 month old animals. Top panel: total protein imaging, bottom panel: phosphoprotein imaging.*

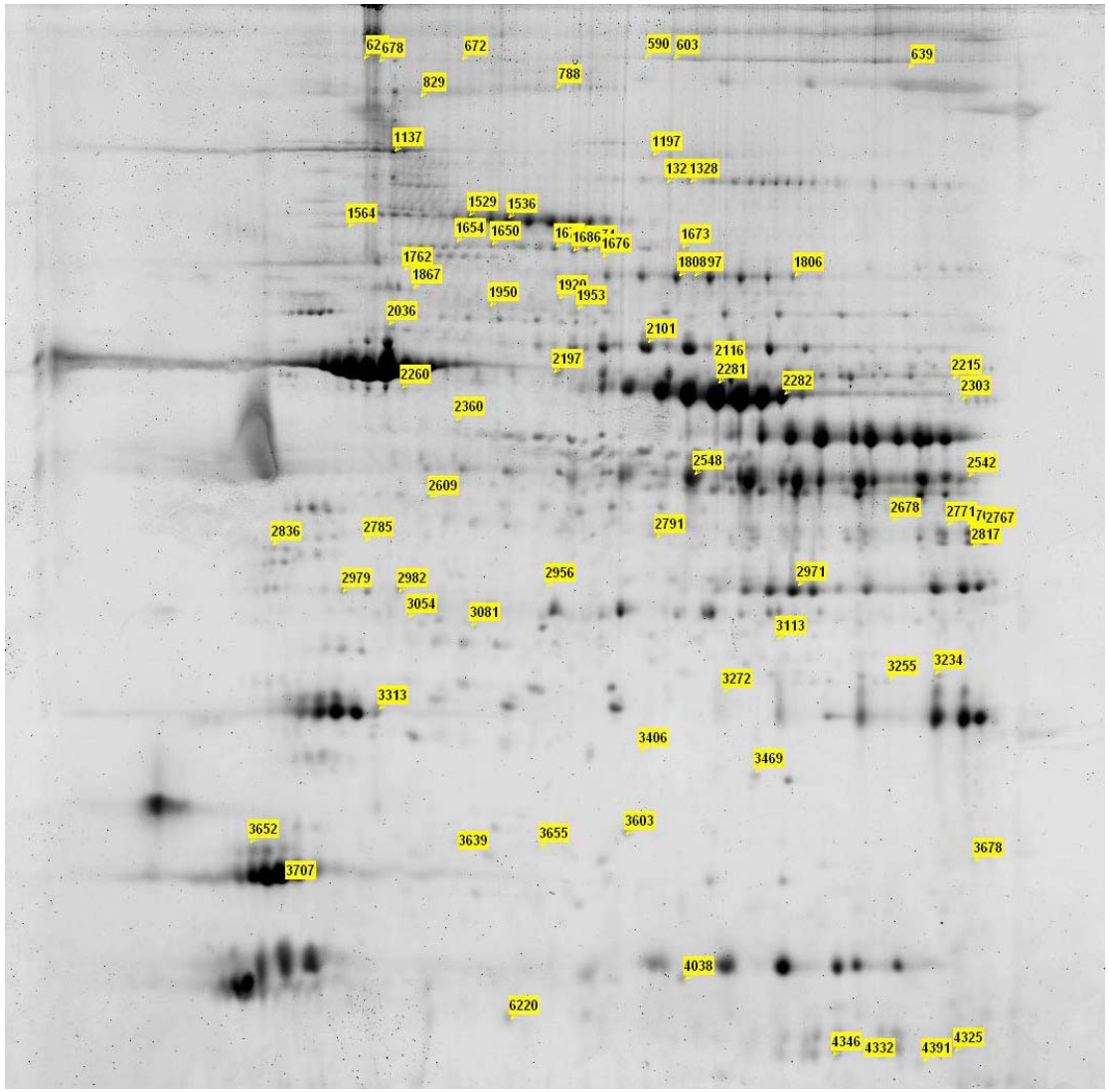

Figure 35. *Spots demonstrating age-dependent phosphorylation differences in aging rat skeletal muscle. Image generated by Progenesis PG220.*

difference between the 5-month and 34-month old animals when normalized to protein expression. Spots meeting this criterion are annotated in **Figure 35** and the quantitative data for the optical density for the spots in the images obtained from both the Pro-Q Diamond and the Sypro Ruby stained images are displayed in **Table 4.** This table, while not immediately identifying proteins, is important for the statistical analysis of our data. In the Pro-Q Diamond columns on the left hand side of the table, we see the biological variability of a reversible modification like protein phosphorylation demonstrated with statistics. The covariance (CV) for the phosphoprotein stained gel triplicates varies from 0% to 144%, with the majority above 50%. These covariances seem to be attributable to biological variability and not due to the quality of the gels, since the variability is reduced in the columns reporting the Sypro Ruby image analysis results. Here, the covariances are much tighter with 65% of the spots showing a CV of 50% or less and 30% showing a CV of 25% or less compared to 37% and 18% respectively for the Pro-Q Diamond staining. When a spot was absent in one of the replicate gels, no CV could be determined. Examples where this is the case, are spots 1762, 1867, 2956, and 6220. The difficulty in finding these spots in the Sypro Ruby stained images highlights the inherent difference in dynamic range between the gel stains. The ratios between 5 month and 34 month volumes for both image analyses are shown and it is apparent that the more the value diverges from unity the more extreme the difference is between the values. The P ratio values from the Pro-Q Diamond image analysis (quantifying phosphorylation) that approach unity are made much more meaningful when normalized with the E ratio values from the Sypro Ruby image analysis (quantifying expression).

Ref.	5 Month Diamond	34 Month Diamond	P ratio	5 Month Ruby	34 Month Ruby	E ratio
Spot	Volume (CV)	Volume (CV)	5/34	Volume (CV)	Volume (CV)	5/34
590	43,847.399253 (71%)	105,651.248993 (19%)	0.4	313,401.457867 (37%)	179,368.895268 (15%)	1.7
603	31,822.445213 (75%)	182,783.794094 (99%)	0.2	647,403.859311 (52%)	749,885.861113 (98%)	0.9
620	161,644.411911 (69%)	368,881.224841 (88%)	0.4	2,100,800.162475 (97%)	946,307.468021 (105%)	2.2
639	97,427.370148 (35%)	315,698.138553 (82%)	0.3	506,126.682846 (49%)	519,505.049576 (121%)	1.0
672	30,638.297571 (99%)	117,119.103965 (103%)	0.3	84,142.680031 (69%)	100,190.588386 (51%)	0.8
678	116,917.362848 (21%)	369,492.808795 (85%)	0.3	1,528,097.328971 (80%)	742,917.117895 (75%)	2.1
788	371,498.847987 (25%)	130,744.529433 (29%)	2.8	870,848.870754 (40%)	761,100.019468 (86%)	1.1
829	190,000.222528 (54%)	364,515.883801 (50%)	0.5	2,190,137.401653 (46%)	458,048.858072 (113%)	4.8
1137	401,780.134210 (51%)	924,231.826705 (45%)	0.4	4,900,951.538197 (80%)	653,937.350325 (30%)	7.5
1197	129,887.916217 (43%)	383,261.048242 (79%)	0.3	782,451.001952 (10%)	543,780.813356 (29%)	1.4
1323	35,082.557642 (52%)	156,584.164987 (4%)	0.2	1,169,499.746977 (22%)	1,403,973.936161 (7%)	0.8
1328	230,495.398617 (11%)	81,510.221830 (68%)	2.8	1,206,719.839379 (74%)	1,675,812.912470 (24%)	0.7
1529	121,212.630949 (41%)	950,856.628167 (0%)	0.1	7,003,525.380540 (45%)	7,205,834.832507 (22%)	1.0
1536	776,057.627726 (67%)	312,324.316352 (67%)	2.5	12,148,064.622397 (39%)	11,940,023.130459 (52%)	1.0
1564	73,490.848079 (57%)	212,756.889703 (144%)	0.3	404,886.933401 (48%)	629,874.926129 (60%)	0.6
1650	220,588.487390 (1%)	549,310.743561 (83%)	0.4	1,748,956.904001 (28%)	679,459.424979 (72%)	2.6
1654	580,422.699596 (45%)	136,181.524616 (62%)	4.3	808,649.649942 (30%)	789,348.214554 (41%)	1.0
1671	387,964.921792 (65%)	1,054,925.623948 (10%)	0.4	2,781,567.287678 (3%)	1,723,538.399154 (16%)	1.6
1673	143,148.751837 (12%)	27,805.142853 (12%)	5.1	493,632.580474 (20%)	363,153.116419 (20%)	1.4
1674	431,569.410734 (22%)	909,862.813358 (18%)	0.5	2,621,304.205747 (14%)	1,507,967.288977 (29%)	1.7
1676	805,271.689927 (134%)	158,696.381326 (73%)	5.1	2,514,122.894325 (5%)	2,451,568.325736 (51%)	1.0
1686	1,792,335.854534 (11%)	224,196.625446 (39%)	8.0	2,378,217.539442 (11%)	2,373,672.082606 (26%)	1.0
1762	91,469.515278 (121%)	824,883.515369 (18%)	0.1	320,992.855661 (40%)	5641.354878 (-)	56.9
1797	731,398.458695 (86%)	102,038.620831 (16%)	7.2	2,265,974.198867 (14%)	1,023,218.158345 (48%)	2.2
1806	346,225.425737 (54%)	62,164.306484 (23%)	5.6	2,910,454.941941 (7%)	1,303,478.931678 (20%)	2.2
1808	329,102.500780 (52%)	600,832.034834 (10%)	0.5	8,765,634.382612 (15%)	5,187,608.953262 (19%)	1.7
1867	412,691.126078 (35%)	1,161,985.389965 (48%)	0.4	839,436.049708 (14%)	9857.235646 (-)	85.2
1920	408,296.527273 (103%)	151,999.730467 (81%)	2.7	576,847.766117 (12%)	742,441.185191 (39%)	0.8
1950	223,825.116474 (42%)	392,217.834729 (107%)	0.6	1,096,898.281842 (44%)	910,924.311778 (75%)	1.2
1953	135,364.618722 (103%)	417,111.240342 (39%)	0.3	1,041,599.940344 (27%)	1,005,931.953563 (49%)	1.0
2036	341,405.678238 (35%)	669,711.523646 (15%)	0.5	2,313,792.643533 (22%)	1,344,433.921868 (83%)	1.7
2101	166,289.125047 (50%)	941,590.482825 (66%)	0.2	15,427,529.542639 (28%)	9,212,624.497150 (26%)	1.7
2116	1,139,883.447537 (49%)	348,670.659977 (121%)	3.3	16,910,376.042506 (30%)	6,623,617.132141 (53%)	2.6
2197	262,122.662238 (79%)	799,156.069746 (83%)	0.3	3,528,327.207529 (1%)	2,409,237.724436 (53%)	1.5
2215	47,243.992384 (69%)	88,460.973864 (72%)	0.5	656,994.580948 (30%)	363,492.786679 (14%)	1.8
2260	109,801.599138 (33%)	204,336.585565 (29%)	0.5	3,011,830.706323 (41%)	3,132,254.777500 (12%)	1.0
2281	2,866,916.064370 (118%)	584,169.324791 (76%)	4.9	77,509,443.381092 (50%)	26,205,376.603509 (75%)	3.0
2282	982,009.710502 (80%)	269,196.612053 (46%)	3.6	19,766,017.602462 (72%)	9,082,914.857522 (50%)	2.2
2303	26,460.483590 (63%)	90,514.290363 (11%)	0.3	1,251,593.472573 (40%)	1,402,817.265018 (32%)	0.9
2360	113,912.442945 (42%)	185,524.488074 (113%)	0.6	208,385.623545 (48%)	558,408.047915 (35%)	0.4

Table 4. *Spot Volumes from 2D PAGE Image Analysis.*

Ref.	5 Month Diamond	34 Month Diamond	P ratio	5 Month Ruby	34 Month Ruby	E ratio
Spot	Volume (CV)	Volume (CV)	5/34	Volume (CV)	Volume (CV)	5/34
2542	1,631,552.759223 (90%)	466,176.317656 (38%)	3.5	5,853,520.307312 (50%)	2,736,688.525322 (33%)	2.1
2548	5,250,253.798702 (53%)	1,830,977.097158 (5%)	2.9	37,688,297.413846 (25%)	21,655,553.510410 (34%)	1.7
2609	174,886.064622 (41%)	386,700.597343 (63%)	0.5	299,836.854942 (24%)	213,056.016592 (35%)	1.4
2678	136,252.263943 (66%)	28,509.697228 (73%)	4.8	447,172.230922 (61%)	329,411.066053 (51%)	1.4
2766	299,250.083170 (70%)	19,494.230211 (69%)	15.4	3,558,691.152479 (87%)	1,136,596.518130 (35%)	3.1
2767	221,921.955822 (32%)	69,329.379310 (20%)	3.2	1,902,355.513059 (62%)	864,302.445568 (40%)	2.2
2771	575,357.521073 (87%)	145,024.511220 (20%)	4.0	4,262,563.913570 (46%)	2,574,526.657884 (25%)	1.7
2785	116,860.732502 (28%)	28,385.890439 (31%)	4.1	307,919.788641 (35%)	231,675.085755 (100%)	1.3
2791	38,536.886259 (50%)	177,375.547019 (38%)	0.2	879,315.954126 (33%)	1,244,164.122076 (39%)	0.7
2817	131,988.642669 (74%)	25,041.310874 (84%)	5.3	2,216,974.140890 (39%)	1,001,269.923329 (45%)	2.2
2836	191,191.737593 (53%)	338,346.897470 (29%)	0.6	1,189,738.884705 (12%)	374,446.293666 (22%)	3.2
2956	22,455.344632 (75%)	76,716.821278 (120%)	0.3	240,586.960315 (110%)	8654.546895 (-)	27.8
2971	990,470.530645 (54%)	328,732.531804 (23%)	3.0	15,138,336.330696 (32%)	10,751,778.721344 (24%)	1.4
2979	138,398.918018 (26%)	302,273.449530 (47%)	0.5	1,862,168.651049 (20%)	504,944.402825 (21%)	3.7
2982	501,401.259827 (64%)	1,156,958.859723 (105%)	0.4	1,802,108.353720 (1%)	545,578.397272 (30%)	3.3
3054	123,355.798951 (90%)	1,768,820.920592 (20%)	0.1	175,650.452760 (32%)	320,596.636110 (37%)	0.5
3081	94,751.364269 (104%)	1,468,014.223193 (135%)	0.1	487,463.149297 (14%)	271,191.934496 (65%)	1.8
3113	16,518.812254 (63%)	48,666.148876 (120%)	0.3	309,791.923848 (9%)	291,818.441522 (22%)	1.1
3234	825,501.437185 (31%)	132,352.970622 (72%)	6.2	1,062,301.563606 (44%)	788,585.862178 (19%)	1.3
3255	11,352.876930 (56%)	22,604.810365 (91%)	0.5	299,982.562062 (7%)	165,943.121331 (7%)	1.8
3272	177,692.117029 (45%)	9,626.149248 (3%)	18.5	596,122.709848 (26%)	237,270.895649 (48%)	2.5
3313	403,152.740847 (13%)	1,903,526.999934 (22%)	0.2	4,249,582.873321 (12%)	2,637,717.153794 (18%)	1.6
3406	23,566.010193 (53%)	57,653.356818 (57%)	0.4	103,724.326399 (11%)	68,621.545821 (36%)	1.5
3469	176,691.014089 (37%)	485,716.410132 (19%)	0.4	1,359,573.836591 (33%)	3,625,290.270972 (4%)	0.4
3603	98,511.230495 (62%)	220,503.584054 (56%)	0.4	1,232,368.795104 (4%)	1,165,671.569420 (88%)	1.1
3639	86,251.632003 (50%)	239,836.209377 (13%)	0.4	133,128.435329 (154%)	78,209.809195 (41%)	1.7
3652	5,620,177.216471 (17%)	411,501.569408 (137%)	13.7	4,839,313.505068 (14%)	1,766,326.907393 (78%)	2.7
3655	14,322.501814 (86%)	84,776.072673 (78%)	0.2	92,489.837711 (105%)	51,309.232828 (88%)	1.8
3678	57,134.564072 (88%)	190,491.594513 (41%)	0.3	235,477.657410 (56%)	427,328.535576 (60%)	0.6
3707	23,058,625.080626 (10%)	37,897,830.406906 (19%)	0.6	35,993,546.865386 (14%)	33,014,042.970972 (13%)	1.1
4038	107,044.159595 (53%)	41,019.538859 (61%)	2.6	1,036,456.745564 (48%)	921,930.458904 (68%)	1.1
4325	27,427.059550 (28%)	202,931.450692 (49%)	0.1	1,429,631.631170 (39%)	2,348,831.647386 (42%)	0.6
4332	210,579.061161 (52%)	64,426.502894 (51%)	3.3	2,105,688.035433 (22%)	2,096,895.642129 (32%)	1.0
4346	175,734.396410 (76%)	62,251.085343 (71%)	2.8	1,768,845.528224 (56%)	1,659,739.709299 (53%)	1.1
4391	40,391.435959 (88%)	84,218.797424 (130%)	0.5	503,152.879505 (25%)	379,925.823715 (49%)	1.3
6220	20,888.810417 (23%)	325,519.116644 (145%)	0.1	7898.239865 (-)	8514.746593 (-)	0.9

Table 4. *Spot Volumes from 2D PAGE Image Analysis (continued).*

The MS/MS analysis of 75 spots of interest yielded 14 phosphoproteins, which were not only identified but for which MS/MS spectra of specific phosphopeptides were also obtained. From these numbers it is obvious that the majority of the spots for which we observed phosphorylation differences by Pro-Q Diamond staining did not provide sufficient material for MS/MS sequencing of phosphopeptides. A true quantitative analysis of the specific proteins in each spot is difficult as many spots contain more than one protein. We assume that the phosphopeptides showing MS/MS are likely to be the most abundant phosphoprotein in the spot, suggesting that the protein from which they originate may represent the most abundant phosphoprotein in the spot. Hence, the following discussion is based on the assumption that the Pro-Q Diamond staining in the spot predominantly quantifies the phosphoprotein of which we obtained MS/MS data and that we can quantitate the phosphoprotein. Targeted purification and analysis of each phosphoprotein would be required to establish a more reliable quantitative analysis.

The phosphoproteins for which we have found direct MS/MS evidence of a phosphopeptide are listed in **Table 5.** Spots that were unambiguously identified, but for which sufficient material for MS/MS sequencing of phosphopeptides was not available, are listed in **Table 6.** Included in both of these tables are specific references to previous work done with 2D PAGE that provide corroborating evidence of the protein ID for the given spot. Also shown in both tables are the normalized phosphorylation difference between the 5 month and 34 month spots, derived from the P ratios and E ratios. These will be referenced in the discussion. To provide an example of the quality

spot #	Protein ID	Primary IPI Accession number	Phosphopeptide sequence	MW (kD)	SEQUEST XCorr (charge)	Scaffold Protein Probability	reference	P ratio 5m/34m	E ratio 5m/34m	Normalized P fold change
672	Pcdh12 similar to Protocadherin 12 precursor	IPI00194383.5	GESs_{927}PHQILRSLVR	128	2.54 (+2)	95%	-	0.3	0.8	-3.2
1564	Hspa4 Heat shock 70 kDa protein 4	IPI00387868.2	KLMSANAs_{282}DLPLs_{287}IECFMNDI-DVSGTMNR	94	2.81 (+3)	94%	-	0.3	0.6	-1.9
2282	Ckm Creatine kinase M-type	IPI00211053.6	GQs_{372}IDDmIPAQK	43	5.22 (+2)	100%	34,35,36,37,38	3.6	2.2	1.7
2303	Kmo Kynurenine 3-monooxygenase	IPI00213422.1	GRSINLALSy_{60}R	54	2.90 (+2)	94%	-	0.3	0.9	-3.1
2767	Rogdi Protein rogdi homolog	IPI00369213.1	LcLTVYQLHt_{208}LQPTSTK	32	2.50 (+2)	95%	-	3.2	2.2	1.5
2836	Slc39a11 36 kDa protein	IPI00557477.1	IGs_{145}Ts_{147}VLLt_{151}NK	36	2.90 (+2)	95%	-	0.6	3.2	-5.6
2956	Pid1 23 kDa protein	IPI00776803.1	s_{184}KLNVLt_{190}LK	23	2.23 (+2)	95%	-	0.3	27.8	-95
2979	Spock1 similar to Testican-1 precursor	IPI00782288.1	KQVt_{6}KNVLEDLLCVGGFVGK	36	3.49 (+2)	95%	-	0.5	3.7	-8.1
2982	Akr1a1 Alcohol dehydrogenase [NADP+]	IPI00230859.5	y_{298}IVPMITVDGK	37	2.59 (+2)	94%	-	0.4	3.3	-7.6
3054	Prdx6 Peroxiredoxin-6	IPI00231260.5	GVFt_{208}KELPs_{213}GKK	25	2.11 (+3)	95%	35	0.1	0.5	-7.9
3255	Pop7 processing of precursor 7, ribonuclease P family	IPI00194491.1	PNDIYVNMKt_{43}DFK	16	2.82 (+2)	94%	-	0.5	1.8	-3.6
SEQUEST XCorr values are for listed phosphopeptide.										

Table 5. *Phosphoprotein IDs from MS/MS analysis.*

spot #	Protein ID	Primary IPI Accession number	Phosphopeptide sequence	MW (kD)	SEQUEST XCorr (charge)	Scaffold Protein Probability	reference	P ratio 5m/34m	E ratio 5m/34m	Normalized P fold change
1536	Alb Serum albumin	IPI00191737.6	ND	69	3.19 (+2)	100%	34,35,36,37,38	2.5	1.0	2.4
1650	Hspa5 78 kDa glucose-regulated protein	IPI00206624.1	ND	72	3.76 (+2)	100%	-	0.4	2.6	-6.4
1673	Ckb Creatine kinase B-type	IPI00470288.4	ND	43	4.08 (+2)	100%	-	5.1	1.4	3.8
1674	Jup Junction plakoglobin	IPI00421429.3	ND	82	2.26 (+2)	100%	-	0.5	1.7	-3.7
1676	Pgm1 phosphoglucomutase 1	IPI00780332.1	ND	61	4.92 (+2)	100%	-	5.1	1.0	4.9
1762	Vim Vimentin	IPI00230941.5	ND	54	4.71 (+2)	100%	39*	0.1	56.9	-513
1808	Pkm2 Isoform M1 of Pyruvate kinase isozymes M1/M2	IPI00231929.6	ND	58	3.16 (+2)	100%	34,35,36	0.5	1.7	-3.1
1920	Trim72 Tripartite motif-containing protein 72	IPI00361208.4	ND	53	3.41 (+2)	100%	-	2.7	0.8	3.5
1950	Eno1 Alpha-enolase	IPI00464815.11	ND	47	4.63 (+2)	100%	34,36	0.6	1.2	-2.1
1953	Eno1 Alpha-enolase	IPI00464815.11	ND	47	5.20 (+2)	100%	34,36	0.3	1.0	-3.2
2101	Eno3 Beta-enolase	IPI00231631.13	ND	47	3.89 (+2)	94%	34,35,36,37,38	0.2	1.7	-9.5
2215	Atp5a1 ATP synthase subunit alpha, mitochondrial	IPI00396910.1	ND	60	3.55 (+2)	100%	-	0.5	1.8	-3.4
2260	Acta1 Actin, alpha skeletal muscle	IPI00189813.1	ND	42	3.08 (+2)	94%	34,36	0.5	1.0	-1.8
2281	Ckm Creatine kinase M-type	IPI00211053.6	ND	43	5.27 (+2)	100%	34,35,36,37,38	4.9	3.0	1.7
2542	Hnrnpa1 Heterogeneous nuclear ribonucleoprotein A1	IPI00421500.9	ND	34	4.27 (+2)	100%	-	3.5	2.1	1.6
2771	Vdac1 Voltage-dependent anion-selective channel protein 1	IPI00421874.4	ND	31	3.29 (+2)	100%	34,36	4.0	1.7	2.4
2791	Gpd1 Glycerol-3-phosphate dehydrogenase [NAD+], cytoplasmic	IPI00231148.8	ND	37	2.37 (+2)	100%	36,37,38	0.2	0.7	-3.3
2817	Ldb3 Ldb3 protein	IPI00566392.2	ND	31	3.52 (+2)	100%	-	5.3	2.2	2.4
2971	Car3 Carbonic anhydrase 3	IPI00230788.6	ND	29	3.14 (+2)	100%	35,36	3.0	1.4	2.1
3081	Hbb Hemoglobin subunit beta-1	IPI00230897.5	ND	16	3.02 (+2)	100%	-	0.1	1.8	-27.8
3234	Tnni2 Troponin I, fast skeletal muscle	IPI00231700.5	ND	21	4.28 (+2)	95%	-	6.2	1.3	4.6

ND: not detected. *: this reference is to a previously identified phosphorylation site, the remaining references are to spot identifications from 2D-PAGE maps. SEQUEST XCorr values are for the best peptide of identifying series. Scaffold Protein Probability determined by PeptideProphet[32,33]

Table 6. *Skeletal Muscle Protein IDs from MS/MS analysis.*

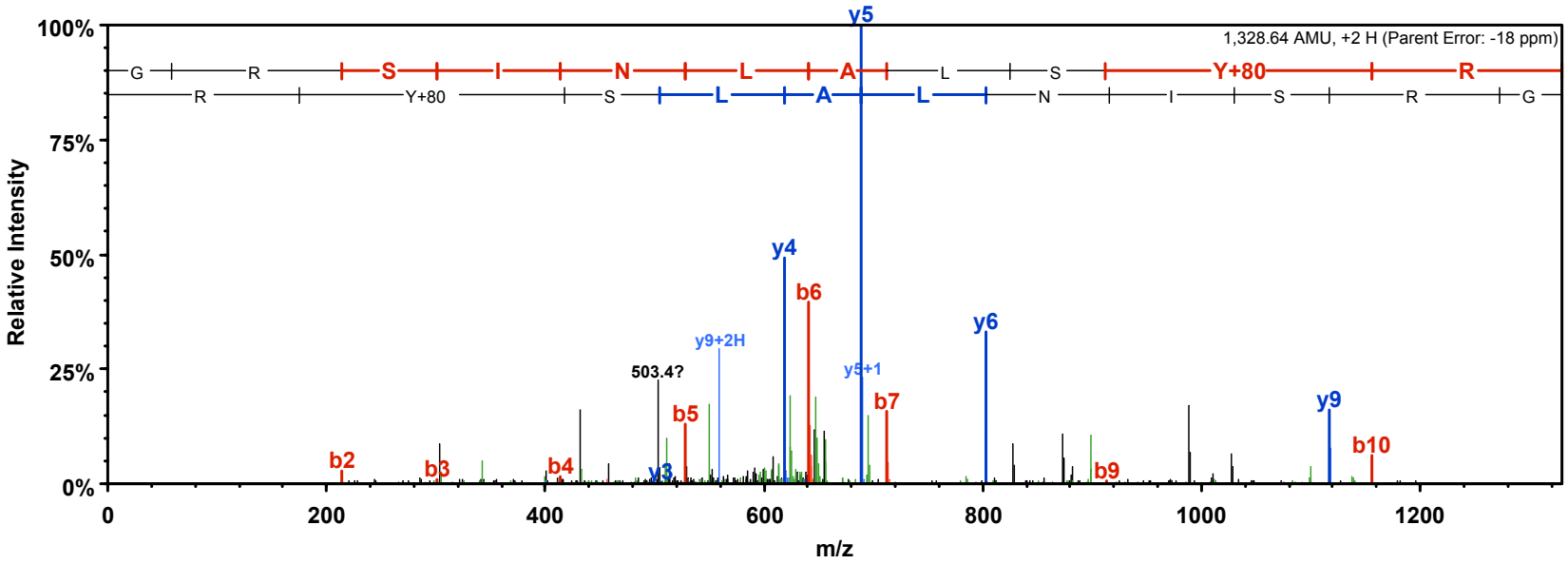

Figure 36. *Tandem mass spectrum of GRSINLALSyR phosphopeptide from Kynurenine 3-monooxygenase.*

...	B Ions	B+2H	B-NH3	B-H2O	AA	Y Ions	Y+2H	Y-NH3	Y-H2O	...
1	58.0				G	1,329.7	665.3	1,312.6	1,311.7	11
2	214.1	107.6	197.1		R	1,272.6	636.8	1,255.6	1,254.6	10
3	301.2	151.1	284.1	283.2	S	1,116.5	558.8	1,099.5	1,098.5	9
4	414.2	207.6	397.2	396.2	I	1,029.5	515.3	1,012.5	1,011.5	8
5	528.3	264.6	511.3	510.3	N	916.4	458.7	899.4	898.4	7
6	641.4	321.2	624.3	623.4	L	802.4	401.7	785.4	784.4	6
7	712.4	356.7	695.4	694.4	A	689.3		672.3	671.3	5
8	825.5	413.3	808.5	807.5	L	618.3		601.2	600.3	4
9	912.5	456.8	895.5	894.5	S	505.2		488.2	487.2	3
10	1,155.6	578.3	1,138.5	1,137.5	Y+80	418.1		401.1		2
11	1,329.7	665.3	1,312.6	1,311.7	R	175.1		158.1		1

Figure 37. *Fragmentation table for GRSINLALSyR phosphopeptide from Kynurenine 3-monooxygenase.*

for of the mass spectra obtained, **Figure 36** shows the tandem mass spectrum and model error for the doubly charged, phosphorylated peptide GRSINLALSyR from kynurenine-3 monooxygenase with the fragmentation table for the same phosphopeptide displayed in **Figure 37**.

4.4 Discussion

The process of aging appears to produce a number of changes in the phosphorylation status of skeletal muscle proteins. Since there has been extensive work done on this subject, we will restrict our discussion to comparisons against previous work, where we have corroborating evidence of spot identity and quantitative data, but otherwise limit our discussion to phosphoproteins where we have MS/MS evidence of a phosphopeptide. The vast majority of identified proteins seem to be involved in some manner with metabolism, but we also observe structural proteins, transporter proteins, catabolic proteins and proteins responsive to oxidative stress. A few of the age-dependent changes in expression levels observed by Doran et al[40] are confirmed in our study. Much of the previous work was conducted either in humans or with alternative animal models, thus the modest amount of correlation is not surprising and our work should be viewed as complementary to previous work.

Among the identified metabolic proteins, we observe that the enzymes alpha-enolase, beta-enolase, creatine kinase type M, kynurenine 3-monooxygenase, isoform M1 of pyruvate kinase, alcohol dehydrogenase, glycerol-3-phosphate dehydrogenase and mitochondrial ATP synthase subunit alpha all appear to have differential phosphorylation levels between muscle from young and old animals, with some proteins

demonstrating stable and some showing differential expression levels. In the context of skeletal muscle, Kmo is involved in the metabolism of tryptophan and while the spot identified in our study shows little change in expression level, it demonstrates a three-fold increase in phosphorylation level in the aged animal. Such a drastic change in phosphorylation level has the potential to drastically affect the structural integrity of an enzyme. Creatine kinase (Ckm) is another enzyme involved in the metabolism of amino acids. Ckm metabolizes arginine and proline and catalyzes the phosphorylation of creatine to phosphocreatine using ATP. Phosphocreatine is an important energy reservoir in skeletal muscle, due to availability of fast ATP generation via the reverse reaction.[41] The two spots from a protein charge train were identified in our study as Ckm. These spots, 2281 and 2282 showed a decrease in expression for the aged animals of three-fold and approximately two-fold, respectively. These values are slightly higher than observations made in previous studies[34,37,38] conducted using Wistar rats, LOU/c/jall rats and human samples and may be the result of model/biological variation. Interestingly, the phosphorylation levels for these spots, when normalized to expression, show the same approximate two-fold decrease in the aged samples. A recent study in frog skeletal muscle has demonstrated that the activity of Ckm is dependent on its phosphorylation state, with the phosphorylated form showing the higher level of activity.[42]

Among the proteins involved in glycolysis, the spot associated with the glycolytic enzyme glycerol-3-phosphate dehydrogenase (Gpd1) demonstrates a similar age-dependent increase in expression level of approximately one and one-half fold as reported in the review by Doran et al[40] and observed by Gelfi et al[38] for human tissue.

However, in our study the increase in phosphorylation level was even more dramatic. When the phosphorylation value is normalized to expression, it demonstrates a three-fold increase. Glycerol-3-phosphate dehydrogenase is a critical component of the glycerol-3-phosphate shuttle and an increased activity for this enzyme has been demonstrated in aged mice[41]. Whether this increase in activity is solely related to increased expression, or if the increase in expression is related to the increase in phosphorylation state remains to be determined. The spot for another glycolytic protein, isoform M1 of pyruvate kinase (Pkm2), shows a 1.5 fold reduction in expression based on the Sypro Ruby staining, which correlates well to the numbers reviewed by Doran et al[40]. While the expression level may be lower for the aged sample, this same spot shows a two-fold increase in Pro-Q Diamond staining, yielding a normalized (to expression) three-fold increase in phosphorylation level. Doran et al[40] elucidate the relevance of this finding, highlighting the change to a 'more oxidative metabolism in the sarcopenia of old age' since Pkm2 is essential for the final stage of the glycolytic pathway, where it is responsible for the conversion of phosphoenolpyruvate to pyruvate and ATP. In support of this argument we have additional evidence of differential phosphorylation and differential expression for the enolases, which are involved in the catalysis of the interconversion of 2-phosphoglycerate and phosphoenolpyruvate. Structural perturbations due to hyperphosphorylation of these enzymes are likely to hamper the effectiveness of the alpha-enolase and greatly affect beta-enolase which appears to also suffer from a reduced level of expression. This, in turn would impact the production of phosphoenolpyruvate and the subsequent need for pyruvate kinase. The protein spot charge train where alpha-enolase was identified, spots 1950 and 1953,

shows an age-dependent increase in phosphorylation level, while the expression level appears to remain stable. When normalized for the expression level, a two-fold and three-fold age-dependent increase in phosphorylation for the respective spots is observed. While the alpha-enolase spots were not selected in previous phosphoproteomic studies, presumably due to a lack of difference between the expression levels between young and old rat skeletal muscle, the spot identified in our study as beta-enolase (2101 in Figure 3) was previously characterized by Gannon et al[34], and our observed reduction in the expression levels in the aged samples appears to correlate. The expression level of beta-enolase appears to suffer nearly a two-fold reduction paralleled by a five-fold decrease in phosphorylation. The difficulty in comparing this data against the work by Gannon et al[34], is that the observed loss in phosphorylation level with the Pro-Q Diamond stain for this particular spot is much higher in our experiment and does not change linearly with the expression level, whereas in their study the change in phosphorylation level mirrors the change in expression level. Although both studies used the same stain and similar procedures, in our gel images the spot is a single isoform in what appears to be an extended charge train for this protein and it is one of the more acidic isoforms, meaning that it very likely contains multiple phosphorylation sites, thus increasing the response of the gel stain. Post-translational modifications other than phosphorylation may be complicating the comparison, but the lack of resolution for this spot in the previous work also makes the comparison difficult.

Downstream in the glycolysis pathway, we identified alcohol dehydrogenase (Akr1a1), which shows an age-dependent pattern similar to Pkm2. The observed

expression level for the spot associated with Akr1a1 decreases by a factor of three while the phosphorylation level for the spot more than doubled providing a normalized 7-fold age-dependent increase in phosphorylation. The expression levels and potentially the phosphorylation state of the proteins observed in our study that are involved in the glycolytic pathway seem to support the hypothesis of a metabolic shift in sarcopenia[40]. It seems logical that there should be a corresponding change in the proteins involved in oxidative phosphorylation to support this hypothesis; we did detect the alpha subunit of the mitochondrial protein ATP synthase (Atp5a1) but our results do not offer any firm conclusion. If there is indeed a shift to the oxidative pathway we would expect an increase in the level of Atp5a1, but the expression level in the spot associated with Atp5a1 showed nearly a two-fold age-dependent reduction. Similar reductions in the level of ATP synthase in aged tissues have been observed elsewhere.[44,45] The phosphorylation level of Atp5a1 displayed an approximate two-fold age-dependent increase, which, when combined with the apparent age-dependent decrease in expression level, yields an overall normalized phosphorylation increase of 3.4 fold. Although Atp5a1 is a known phosphoprotein[46,47], we could not find any quantitative evaluation of the effect of phosphorylation on Atp5a1.

Several other proteins involved in various functions such as skeletal muscle function, cell cycle, maintenance and stress response were also observed to be differentially phosphorylated. These proteins include actin alpha 1 (Acta1), caprin 1, carbonic anhydrase III (Car3), heat shock 70 kD protein 4 (Hspa4), and peroxiredoxin 6 (Prdx6). The spot associated with Acta1 (spot 2036) did not show any change in total protein level while demonstrating a two-fold loss in phosphorylation level. Whether this

change in phosphorylation level suggests a direct loss in function remains to be determined. This protein was observed in the rat phosphoproteomic study by Gannon et al[34], and in the human proteomic study by Gelfi et al[38]. The change in phosphorylation level observed in our study agrees with the phosphoproteomic study[34] (a two-fold increase), while the level of total protein observed does not agree with either study: where Gannon et al[34] found a 2.7-fold increase and Gelfi et al[38] found a 1.5 fold increase, we observed no change in protein expression level. Again these differences are likely to be rationalized by the 2D PAGE resolution. In our study we have selected a spot representing a single isoform, whereas in the studies by Gannon et al[34] and Gelfi et al[38] there is no resolution of the distinct isoforms. Carbonic anhydrase III (Car3) is involved in removing carbon dioxide from tissues and in maintaining the pH balance of blood and tissue by converting carbon dioxide to bicarbonate. The spot associated with Car3 showed a 50% age-dependent decrease in expression level and a three-fold decrease in phosphorylation level. Finally, it is not surprising to see heat shock 70 kD protein 4 (Hspa4) and peroxiredoxin 6 (Prdx6) to show elevated expression levels and correspondingly elevated phosphorylation levels. Hspa4 is a known phosphoprotein and the phosphorylation state of prdx6 has been directly implicated in regulating its activity level, with an increased level of phospholipase activity in the phosphorylated state.[48] Both proteins show an approximate two-fold increase in total protein levels, but whereas Hspa4 shows a two-fold normalized increase in phosphorylation level, Prdx6 exhibits an apparent eight-fold increase in phosphorylation when normalized for expression.

4.5 Conclusion

The objective of the study was to catalogue proteins that show distinct differential phosphorylation in the skeletal muscle of 5 month compared to 34 month old rats, which could potentially be correlated to sarcopenia. This objective was achieved for several classes of proteins with numerous metabolic, functional and stress response proteins identified as differentially phosphorylated. The potential implications of the change in function of these proteins due to changes in phosphorylation state have been individually outlined in the discussion. Taken as a whole, these age-dependent changes can be seen as potentially contributing to the development of sarcopenia. There are obvious implications in energy production and storage which have been highlighted in this study that require further research while the phosphorylation and expression level differences observed in the catabolic, functional and stress-response proteins could potentially offer targets to explain the degeneration of muscle fiber known as sarcopenia.

4.6 References

[1] Kamimoto LA, Easton AN, Maurice E, Husten CG, Macera CA. Surveillance for five health risks among older adults--United States, 1993-1997. MMWR CDC Surveill Summ. 1999 Dec 17;48(8):89-130

[2] Doherty TJ. Invited review: Aging and sarcopenia. J Appl Physiol 2003 Oct;95(4):1717-27

[3] Lexell J. Human aging, muscle mass, and fiber type composition. J Gerontol A Biol Sci Med Sci. 1995 Nov;50 Spec No:11-6.

[4] Bendall MJ, Bassey EJ, Pearson MB. Factors affecting walking speed of elderly people. Age Ageing. 1989 Sep;18(5):327-32.

[5] Morley JE. A fall is a major event in the life of an older person. J Gerontol A Biol Sci Med Sci. 2002 Aug;57(8):M492-5.

[6] Vellas B, Baumgartner RN, Wayne SJ, Conceicao J, Lafont C, Albarede JL, Garry PJ. Relationship between malnutrition and falls in the elderly. Nutrition. 1992 Mar-Apr;8(2):105-8

[7] Kenney WL, Buskirk ER. Functional consequences of sarcopenia: effects on thermoregulation. J Gerontol A Biol Sci Med Sci. 1995 Nov;50 Spec No:78-85

[8] Kamel HK. Sarcopenia and aging. Nutr Rev. 2003 May;61(5 Pt 1):157-67

[9] Melov S, Tarnopolsky MA, Beckman K, Felkey K, Hubbard A. Resistance exercise reverses aging in human skeletal muscle. PLoS One. 2007 May 23;2(5):e465

[10] Siu PM, Pistilli EE, Alway SE. Age-dependent increase in oxidative stress in gastrocnemius muscle with unloading. J Appl Physiol. 2008 Dec;105(6):1695-705. Epub 2008 Sep 18

[11] Hofer T, Marzetti E, Xu J, Seo AY, Gulec S, Knutson MD, Leeuwenburgh C, Dupont-Versteegden EE. Increased iron content and RNA oxidative damage in skeletal muscle with aging and disuse atrophy. Exp Gerontol. 2008 Jun;43(6):563-70. Epub 2008 Feb 29

[12] Miura, Y., Kano, M., Abe, K., Urano,S., Suzuki, S., and Toda, T., Age-dependent variations of cell response to oxidative stress: proteomic approach to protein expression and phosphorylation. Electrophoresis 2005 Jul;26(14):2786-96

[13] Kanski J, Alterman MA, Schoneich C. Proteomic identification of age-dependent protein nitration in rat skeletal muscle. Free Radic Biol Med. 2003 Nov 15;35(10):1229-39

[14] Gow, A.J., Duran, D., Malcolm, S. and Ischiropoulos, H. Effects of peroxynitrite-induced protein modifications on tyrosine phosphorylation and degradation. FEBS Lett. 1996 Apr 29;385:63-6

[15] Di Stasi, A.M., Mallozzi, C., Macchia, G., Petrucci, T.C., and Minetti, M. Peroxynitrite induces tyrosine nitration and modulates tyrosine phosphorylation of synaptic proteins. J. Neurochem. 1999 Aug; 73(2):727-35.

[16] Cohen, P., The origins of protein phosphorylation., Nat. Cell Biol., 2002 May 4(5):E127-130

[17] Zhang, H., Zha, X., Tan, Y., Hornbeck, P.V., Mastrangelo, A.J., Alessi, D.R., Polakiewicz, R.D., Comb, M.J., Phosphoprotein analysis using antibodies broadly reactive against phosphorylated motifs., J. Biol. Chem. 2002 Oct 18; 277(42):39379-87

[18] Olsen J.V., Blagoev B., Gnad F., Macek B., Kumar C., Mortensen P., Mann M. Global, in vivo, and site-specific phosphorylation dynamics in signaling networks. Cell. 2006 Nov 3;127(3):635-48.

[19] Sickmann A., Meyer H.E. Phosphoamino acid analysis. Proteomics. 2001 Feb;1(2):200-6.

[20] Amanchy R., Periaswamy B., Mathivanan S., Reddy R., Tattikota S.G., Pandey A.. A curated compendium of phosphorylation motifs. Nat Biotechnol. 2007 Mar;25(3):285-6.

[21] Manning G., Whyte, D.B., Martinez, R., Hunter, T., and Sudarsanam, S., The protein kinase complement of the human genome., Science, 2002 Dec 6; 298(5600):1912-34

[22] Andersen, J.N., Mortensen, O.H., Peters, G.H., Drake, P.G., Iversen, L.F., Olsen, O.H., Jansen, P.G., Andersen, H.S., Tonks, N.K., and Møller, N.P., Structural and evolutionary relationships among protein tyrosine phosphatase domains. Mol. Cell Biol. 2001Nov;21(21):7117-36

[23] Wessel, D., and Flügge, U.I., A method for the quantitative recovery of protein in dilute solution in the presence of detergents and lipids. Anal Biochem. 1984 Apr;138(1):141-3.

[24] Leimgruber, R.M., Malone, J.P., Radabaugh, M.R., LaPorte, M.L., Violand, B.N. and Monahan, J.B. Development of improved cell lysis, solubilization and imaging approaches for proteomic analyses. Proteomics 2002 Feb;2(2):135-44.

[25] Lowry, O.H., Rosbrough, N.J., Farr, A.L., and Randall, R.J., Protein measurement with the Folin phenol reagent. J. Biol. Chem. 1951 Nov;193(1):265-75

[26] Görg A., Boguth, G., Obermaier, C., Posch, A. and Weiss, W., Two-dimensional polyacrylamide gel electrophoresis with immobilized pH gradients in the first dimension (IPG-Dalt): the state of the art and the controversy of vertical versus horizontal systems. Electrophoresis 1995 Jul;16(7):1079-86.

[27] Olsen, J.V., Ong, S.E. and Mann, M. Trypsin cleaves exclusively C-terminal to arginine and lysine residues. Mol. Cell. Proteomics 2004 Jun;3(6):608-14

[28] Mann, M., Ong, S.E., Grønborg, M., Steen, H., Jensen, O.N. and Pandey, A., Analysis of protein phosphorylation using mass spectrometry: deciphering the phosphoproteome. Trends Biotechnol. 2002 Jun;20(6):261-8

[29] Eng, J., McCormack, A.L., and Yates, J.R. An approach to correlate tandem mass spectral data of peptides with amino acid sequences in a protein database. J. Am. Soc. Mass Spectrom. 5, 976-989 (1994).

[30] Perkins, D.N., Pappin, D.J., Creasy, D.M., and Cottrell, J.S., Probability-based protein identification by searching sequence databases using mass spectrometry data. Electrophoresis 1999 Dec;20(18) 3551-67

[31] Craig, R. and Beavis, R.C., A method for reducing the time required to match protein sequences with tandem mass spectra. Rapid Commun. Mass Spectrom. 2003;17(20):2310-16

[32] Keller, A., Nesvizhskii, A.I., Kolker, E., and Aebersold, R., Empirical statistical model to estimate the accuracy of peptide identifications made by MS/MS data search. Anal. Chem. 2002 Oct 15;74(20):5383–92.

[33] Nesvizhskii, A.I., Keller, A., Kolker, E., and Aebersold, R. A statistical model for identifying proteins by tandem mass spectrometry. Anal Chem. 2003 Sep 2;75(17):4646–58.

[34] Gannon J, Staunton L, O'Connell K, Doran P, Ohlendieck K. Phosphoproteomic analysis of aged skeletal muscle. Int J Mol Med. 2008 Jul;22(1):33-42.

[35] Yan JX, Harry RA, Wait R, Welson SY, Emery PW, Preedy VR, Dunn MJ. Separation and identification of rat skeletal muscle proteins using two-dimensional gel electrophoresis and mass spectrometry. Proteomics. 2001 Mar;1(3):424-34.

[36] Gelfi C, Viganò A, De Palma S, Ripamonti M, Begum S, Cerretelli P, Wait R. 2-D protein maps of rat gastrocnemius and soleus muscles: a tool for muscle plasticity assessment. Proteomics. 2006 Jan;6(1):321-40.

[37] Piec I, Listrat A, Alliot J, Chambon C, Taylor RG, Bechet D. Differential proteome analysis of aging in rat skeletal muscle. FASEB J. 2005 Jul;19(9):1143-5.

[38] Gelfi C, Vigano A, Ripamonti M, Pontoglio A, Begum S, Pellegrino MA, Grassi B, Bottinelli R, Wait R, Cerretelli P. The human muscle proteome in aging. J Proteome Res. 2006 Jun;5(6):1344-53.

[39] Oguri T, Inoko A, Shima H, Izawa I, Arimura N, Yamaguchi T, Inagaki N, Kaibuchi K, Kikuchi K, Inagaki M. Vimentin-Ser82 as a memory phosphorylation site in astrocytes. Genes Cells. 2006
May;11(5):531-40.

[40] Doran P, Donoghue P, O'Connell K, Gannon J, Ohlendieck K. Proteomics of skeletal muscle aging. Proteomics. 2009 Feb;9(4):989-1003.

[41] Wallimann T, Wyss M, Brdiczka D, Nicolay K, Eppenberger HM. Intracellular compartmentation, structure and function of creatine kinase isoenzymes in tissues with high and fluctuating energy demands: the 'phosphocreatine circuit' for cellular energy homeostasis. Biochem J. 1992 Jan 1;281 (Pt 1):21-40.

[42] Dieni CA, Storey KB. Creatine Kinase Regulation by Reversible Phosphorylation in Frog Muscle. Comp Biochem Physiol B Biochem Mol Biol. 2009 Apr;152 (4), p.405-412

[43] Hagopian K, Ramsey JJ, Weindruch R. Enzymes of glycerol and glyceraldehyde metabolism in mouse liver: effects of caloric restriction and age on activities. Biosci Rep. 2008 Apr;28(2):107-15.

[44] Dencher NA, Frenzel M, Reifschneider NH, Sugawa M, Krause F. Proteome alterations in rat mitochondria caused by aging. Ann N Y Acad Sci. 2007 Apr;1100:291-8.

[45] Lombardi A, Silvestri E, Cioffi F, Senese R, Lanni A, Goglia F, de Lange P, Moreno M. Defining the transcriptomic and proteomic profiles of rat ageing skeletal muscle by the use of a cDNA array, 2D- and Blue native-PAGE approach. J Proteomics. 2009 May 2;72(4):708-21.

[46] Villén J, Beausoleil SA, Gerber SA, Gygi SP. Large-scale phosphorylation analysis of mouse liver. Proc Natl Acad Sci U S A. 2007 Jan 30;104(5):1488-93.

[47] Vosseller K, Hansen KC, Chalkley RJ, Trinidad JC, Wells L, Hart GW, Burlingame AL. Quantitative analysis of both protein expression and serine / threonine post-translational modifications through stable isotope labeling with dithiothreitol. Proteomics. 2005 Feb;5(2):388-98.

[48] Wu Y, Feinstein SI, Manevich Y, Chowdhury I, Pak JH, Kazi A, Dodia C, Speicher DW, Fisher AB. Mitogen-activated protein kinase-mediated phosphorylation of peroxiredoxin 6 regulates its phospholipase A(2) activity. Biochem J. 2009 May 1;419(3):669-79.

Chapter Five

Age-Dependent Changes of Protein Phosphorylation in Rat Cerebellum: a Proteomic Study.

5.1 Introduction

The cerebellum is the brain region primarily responsible for vestibular function and fine motor control[1], regulating the timing, range, accuracy and force of movement. Since the cerebellum is responsible for integrating sensory perceptions with motor output, age-related abnormalities in cerebellar function are manifested through varieties of ataxia such as essential tremor[2], postural instability[3], and a modified gait[4]. In part, these signs of cerebellar dysfunction could be the result of an age dependent increase in oxidative stress, which is specifically associated with several age-related disease states such as adult-onset diabetes, atherosclerosis, Alzheimer's disease (AD), Parkinson's disease (PD), amyotrophic lateral sclerosis (ALS), and cancer.[5-9]

Genomic, biochemical and cellular studies have shown marked differential sensitivity of cerebellar granule cells, the major neuronal population in the cerebellum, to oxidative stress.[10] Reactive oxygen species in the central nervous system can lead to damage of neuronal mitochondria as a result of the high metabolic demand for oxygen. There is also evidence that free iron present in the cerebrospinal fluid can enhance the reaction of some reactive oxygen species with biomolecules.[11] These reactions could potentially damage kinases and phosphatases or even directly impact the phosphorylation sites on the respective target proteins, producing abnormal protein phosphorylation and potentially abnormal protein expression in response to oxidative damage.[12-16]

Protein phosphorylation is a reversible process important for cellular signaling and regulation[17]. Protein phosphorylation and dephosphorylation events also play a crucial role in learning and memory formation, and both processes suffer during

aging.[18,19] There are estimates that approximately 30% of all proteins encoded by the human genome are regulated by phosphorylation/ dephosphorylation, and that there are more than 100,000 phosphorylation sites in the human proteome.[20] Phosphorylation and dephosphorylation events are involved in almost every cellular activity including but not limited to: transcriptional control, apoptosis, protein degradation, nuclear import and export and structural integrity. This ubiquitous post-translational protein modification is introduced by the catalytic action of protein kinases, which phosphorylate primarily protein serine (Ser) and threonine (Thr), but also tyrosine (Tyr) residues. The occurrence of Ser and Thr phosphorylation is far more frequent than Tyr phosphorylation, with Ser phosphorylation an order of magnitude more abundant than Thr phosphorylation which is two orders of magnitude more abundant than Tyr phosphorylation.[21] The action of protein kinases is balanced by the counter action of protein phosphatases, which are responsible for the dephosphorylation of proteins at the same residues and it is the delicate balance between the two protein states that regulate function. The human genome encodes more than 500 different protein kinases[22] and at least as many phosphatases, including over 100 tyrosine phosphatases[23]. These enzymes are not only responsible for phosphorylation and dephosphorylation of other proteins, but are also phosphorylation targets themselves. Any perturbation of this system could produce many of the effects associated with the previously mentioned neurodegenerative diseases and/or the aforementioned effects on the cerebellum evidenced in an aging population.

As an example of the potential effects, a recent study of the phosphorylation state of DARPP-32, an intermediary protein of neuronal signal transduction showed that

the effects of various psychotomimetic drugs (D-amphetamine, LSD and PCP) could be traced to the phosphorylation of specific Ser and Thr residues on DARPP-32, thus controlling the downstream effects in the signaling cascade. Transgenic mice lacking these Ser and Thr residues, did not experience the behavioral effects such as repetitive behavior and a reduction in sensorimotor gating (i.e. information processing and stimulus filtering) that is observed in the wild type mice under the influence of the psychomimetics, demonstrating one potential effect of abnormal protein phosphorylation.[24]

A holistic or comprehensive study of phosphorylation requires not only a qualitative identification of phosphoproteins, but also a reliable quantitative method that provides a real measure of the differences in phosphorylation between biological states. Ideally, one would also want to identify and measure the differences in the levels or activities of the protein kinases and phosphatases involved in producing the altered phosphorylation states. It would also be important to elucidate the phosphorylation sites and any additional post-translational modifications that may be effecting the changes in phosphorylation state. This task is complicated by the fact that many signaling phosphoproteins are expressed at relatively low levels and the stoichiometry of occupied phosphorylation sites is variable on phosphoproteins where multiple such sites are present. This provides a challenge for not only accurate quantitation, but also for detection, identification and for accurate description of the phosphorylation sites of any particular phosphoprotein.

In order to characterize differences in protein phosphorylation between the cerebella of aged and young animals, a differential phosphoproteomic study on

cerebellar homogenates of 34-month versus 5-month-old Fisher 344/BN F1 rats was conducted using 2D-PAGE followed by mass spectrometric identification. To determine phosphoprotein spots of interest and to avoid selecting differentially expressed protein spots, Pro Q Diamond images of phosphoproteins exhibiting a change of two-fold or greater, were cross referenced against images of the same gels stained with a total protein stain, Sypro Ruby. In addition to 2D-PAGE analysis an effort was made to enrich phosphopeptides using an immobilized metal affinity column (IMAC) using a method previously described.[25] The spots of interest were subsequently digested with trypsin and, along with the samples from the IMAC purification, were analyzed via mass spectrometry to determine their identities as well as relevant structural information.

5.2 Experimental

5.2.1 Materials

Glycerol, Urea, CHAPS, Tween-20, butanol, tris(hydroxymethyl)aminomethane hydrochloride (Tris-HCl), trimethylol Aminomethane, tris(hydroxymethyl)aminomethane (Tris base), agarose, and 2-propanol were acquired from Fisher Scientific. [Fairlawn, NJ] Unless otherwise noted, all other chemicals were purchased from Sigma Chemicals [St. Louis, MO] and were of electrophoretic grade or better.

5.2.2 Tissue Preparation

Three 5-month old and three 34-month old Fisher 344/BN F1 rats were euthanized by carbon monoxide asphyxiation followed by quick decapitation according to the protocol of the Animal Care Unit of the University of Kansas. After the removal of the brain, the cerebella were dissected and immediately placed into a cold homogenization buffer containing 0.32 M sucrose, 0.5 mM magnesium sulfate, 10 mM ε-amino caproic acid, 0.1 mM EGTA, 10 mM HEPES, 0.1 mM benzamide, with protease inhibitor cocktail (containing: 4-(2-aminoethyl) benzenesulfonyl fluoride (AEBSF), pepstatin A, E-64, bestatin, leupeptin, and aprotinin), phosphatase inhibitor cocktail 1 (containing: microcystin LR, cantharidin, and (−)-p-bromotetramisole), and phosphatase inhibitor cocktail 2 (containing: sodium vanadate, sodium molybdate, sodium tartrate, and imidazole). The cerebella were first minced with scissors then thoroughly homogenized by a motorized glass-Teflon pestle on ice. The resulting homogenates were aliquoted and stored at -70°C until further use.

5.2.3 Sample Preparation

To ensure quality separations the homogenates were delipidated using chloroform/methanol precipitation[26] and the protein fraction was resolubilized into a buffer amenable to iso-electric focusing (IEF) containing 5M urea [Fisher, Fair Lawn, NJ], 2M thiourea, 2% (v/v) CHAPS, 0.5% (v/v) Tween-20, 0.5% (w/v) 3-(decyldimethylammonio)propanesulfonate, 10% (v/v) 2-propanol, 10% (v/v) water saturated butanol, 5% (v/v) glycerol, 0.25% (v/v) carrier ampholytes (50:50 mix of Pharmalyte 3-10 [GE Healthcare, Piscataway, NJ] and Bio-Lyte 3/10 [Bio Rad, Hercules, CA]), 1mM sodium fluoride, phosphatase inhibitor cocktail 1 and phosphatase inhibitor cocktail 2.[27] In order to maximize dissolution, all samples were kept in an ice bath and subjected to 3 second bursts of a Fisher 550 sonic dismembrator [Fisher, Fair Lawn, NJ] until the protein pellets dissipated. The samples were then centrifuged at 13,000 x g in a microcentrifuge and the supernatant transferred to fresh centrifuge tubes. Protein concentrations were determined using the Lowry method[28] and the samples were reduced using tributylphosphine and alkylated with iodoacetamide using a ReadyPrep Reduction/Alkylation kit [Bio Rad, Hercules, CA] according to manufacturer's procedures prior to final dilution to 1.67µg/µL with the aforementioned IEF buffer.

5.2.4 2D-PAGE Separation

Isoelectric Focusing (IEF)

For the first dimension separation of proteins, 450 µL aliquots of six samples prepared from the six rat cerebella (3 young, 3 old) were applied to 18 cm 'Immobiline'

immobilized pH gradient (IPG) strips (pH 3-10 NL) [GE Healthcare, Piscataway, NJ] to load 750 µg of total protein and allowed to rehydrate overnight. The strips were transferred to an IPGPhor II electrophoresis unit [GE Healthcare, Piscataway, NJ] and IEF was conducted by initially holding the voltage at 50 V for the first 4 h to allow the migration of excess charged species introduced by the various phosphatase inhibitors[29], the voltage was then increased by stepping to 100 V for 2 h, followed by a step to 500 V for the subsequent 2 h and then a linear voltage gradient over 12 h from 500 to 10,000 V was created in order to achieve a total of 70,000 volt hours.

SDS-PAGE

During the isoelectric focusing, a set of six 1x200x260mm polyacrylamide gels (12.5% T, 3%C) were cast into individual glass cassettes using an Ettan Dalt*six* gel casting apparatus [GE Healthcare, Piscataway, NJ] according to manufaturer's protocols. All gels were used within 12 h of casting.

For the second dimension separation, the focused IPG strips were removed from the IPGphor II and 're-equilibrated' in a solution of 50mM Tris-HCl/Tris base, pH 8.8, 30% (v/v) glycerol, 6M urea, with 2% (w/v) sodium dodecyl sulfate (SDS) [Bio Rad, Hercules, CA] and 0.001% (w/v) bromophenol blue for 20 minutes. Following re-equilibration, the strips were each transferred to individual cassettes with 20x75mm strips of grade 1 Whatman filter paper [Fisher, Fair Lawn, NJ] soaked with 2uL aliquots of the PeppermintStick™ phosphoprotein molecular weight marker [Invitrogen, Carlsbad, CA] on the acidic side of the strip, and sealed with 0.5% (w/v) boiling agarose containing 0.001% (w/v) bromophenol blue onto the top of the slab gel in each

respective glass cassette. After allowing a few minutes for the agarose to properly cool, the six slab gels were transferred to an Ettan Dalt*six* electrophoresis tank [GE Healthcare, Piscataway, NJ] with the appropriate buffers and run at 30 W (5 W per gel) for approximately 30 m to effect the transfer of the proteins from the IPG strip to the slab. Once the bromophenol dye front had unequivocally entered the slab gels, the power was increased to 100 W and the gels were allowed to run until the dye front progressed to the bottom of the gels (approximately 6 h).

Imaging

Immediately following the second dimension SDS-PAGE, the slab gels were removed from their respective cassettes, fixed and stained with Pro-Q Diamond Phosphoprotein Gel Stain [Invitrogen, Carlsbad, CA] using the manufacturer's protocol for large 2D gels with the following modifications: 1) The first fixation step was conducted for 12 h and the second fixation step for 24 h. 2) The first destaining step was for 12 h. The gels were subsequently imaged using a Typhoon™ Variable Mode Imager [GE Healthcare, Piscataway, NJ] thus creating phosphoprotein gel images for each slab gel.

Following imaging, each gel was immersed in a fixation solution (50% (v/v) methanol, 7% (v/v) acetic acid) and left overnight prior to staining with Sypro Ruby [Invitrogen, Carlsbad, CA] using the manufacturer's protocol. The Sypro Ruby stained gels were then imaged with the Typhoon Imager to create images of total protein for each slab gel.

5.2.5 Image Analysis

Analysis of the resultant gel images was conducted using the Progenesis PG220 software [Nonlinear Dynamics, Newcastle upon Tyne, UK]. This analysis required separating the images into two discrete image analysis sets based on the gel dye: one set of images from the Pro-Q Diamond stain with the 5 and 34 month old animals to determine phosphoprotein levels and one set of images from the Sypro Ruby stain with the 5 and 34 month old animals to determine total protein levels.

Our experiment included three images for each set; the software was used to combine the images in each set to create an averaged image with matched spots in each set and their respective location and averaged spot density. These averaged images were matched to a master image to provide a reference between different sets of gels. The final quantitative analysis consisted of four averaged gel images, one for each age group depicting phosphoprotein levels and one for each age group depicting total protein levels. The spots of interest were determined from the differences between the 5 month averaged phosphoprotein gel image and the 34 month averaged phosphoprotein gel image. These spots were then referenced against an identical analysis containing total protein images in order to normalize the difference in phosphorylation values by the expression values in each protein spot.

5.2.6 FT-ICR Analyses

Spots demonstrating normalized differential phosphorylation were excised manually from the gels using a 1.5 mm spot picker and disposable tips to avoid cross contamination. The gel plugs were dehydrated with acetonitrile, dried and subjected to

in-gel digestion with MS-grade modified trypsin [Promega, Madison WI] in 50 mM NH_4HCO_3 overnight at 37°C[30]. The supernatant was removed and analyzed via nanospray ionization (NSI) HPLC-MS/MS using a Thermo-Finnigan hybrid LTQ FT mass spectrometer.

Three separate experiments were conducted; the first focused primarily on identifying the proteins in the in-gel digests, while the second two were focused on locating phosphopeptides for structural information. In all cases the instrument was run in the positive mode. In the first experiment, designed for the identification of peptides, the LTQ FT mass spectrometer was programmed to use a data-dependent survey scan where a full range mass spectrum (m/z 400-2000) was collected and the three most abundant ions were scanned using selected ion monitoring by the Fourier transform ion cyclotron resonance mass spectrometer (FT-ICR) and accumulated in the linear quadrupole ion trap (LTQ) mass spectrometer prior to conducting MS/MS on the accumulated ions. The AGC target values were set to $1X10^6$ ions for the survey MS, $1X10^5$ ions for the selected ion monitoring (SIM) and $1X10^4$ for the MS/MS experiments. The maximum accumulation time was set at 200 ms for all modes. The resolution at 400 *m/z* was set to $1X10^4$ for the FT-ICR scans and isolation widths were set at ± 2 *m/z* for the SIM experiments, and ± 1 *m/z* for the MS/MS experiments. Ions were selected for MS/MS when their respective intensities reached 1000 counts. The normalized collision energy was set to 35% and three microscans were acquired for each spectrum. The mass spectrometer was programmed to ignore singly charged species for fragmentation and was set to dynamically exclude precursors that had already been selected during the first minute after their respective fragmentations

The second experiment was conducted with the same parameters as the first experiment, but an additional step was added, that of monitoring neutral losses by scanning for fragment ions that had suffered a loss of 98 Daltons from the precursor and collecting an additional tandem mass spectrum on these fragments.[31]

The third and final experiment was conducted after data analysis had confirmed an identity for a given gel spot digest but where a quality phosphopeptide was not observed. Utilizing information about the known phosphorylation sites for these identified proteins from PhosphoSitePlus (www.phosphosite.org) and the MS-Digest tool from ProteinProspector at UCSF (http://prospector.ucsf.edu/mshome.htm) the potential phosphopeptides for each protein were generated in-silica. This information was used to program the FT-ICR employing SIM to look for these specific ions, exclusively, prior to collecting a tandem mass spectrum for each respective spot where a phosphopeptide was not observed.

The chromatography for all experiments was kept consistent. The injection volume of the peptide digests was 10 µL. The chromatography system consisted of a FAMOS Capillary and Nano HPLC Autosampler, a Switchos loading pump and switching valve and an ULTIMATE Capillary and Nano HPLC Pump [Dionex/LC Packings, Sunnyvale, CA]. The Switchos Loading pump, in-line to the autosampler, trapped the digests on a 1mm C-18 PepTrap column [Dionex, Sunnyvale, CA] at a flow rate of 20µL/min of 0.1% (v/v) TFA. After 5 minutes, the switching valve, integral to the Switchos pump, changed sample flow through the PepTrap column from the Switchos to the ULTIMATE Nano pump which then flowed through the PepTrap column into a standard coated PicoFrit® column, 360µm/75µm OD/ID, 15µm tip, 12 cm long [New

Objective, Woburn, MA], packed in house with 5 µm particles of 300 Á pore-size Bio-Basic C18 material [Thermo-Scientific, Waltham, MA]. The flow rate was approximately 200 nL/min, utilizing a 90 minute linear gradient from 90% (v/v) solvent A to 90% (v/v) solvent B and held at 90% B for 30 minutes. Solvent A consisted of 10% ACN/89.9% H_2O/0.1% FA (v/v/v) and solvent B consisted of 10% H_2O/89.9% ACN/0.1% FA (v/v/v). The PepTrap column and the PicoFrit column were allowed to re-equilibrate to aqueous conditions (0.1% TFA and 90% solvent A respectively) for 60 minutes between analytical runs.

5.2.7 Immobilized Metal Affinity Chromatography (IMAC) Analysis

Solution digestion of sample aliquots containing 1.5 mg of cerebellum homogenate from both 5 month and 34 month old animals was achieved with overnight digestions using MS-grade modified trypsin [Promega, Madison WI] at 37º C, following the protocol supplied by Promega. The digestion solution was then adjusted to contain 30% (v/v) acetonitrile and 250 mM acetic acid at a final volume of 500 µL in 2 mL capped centrifuge tubes. Approximately 250 µL of slurry (125 µL of gel) of PHOS-Select™ iron affinity gel beads was added to the digest solution and the tubes were incubated by mixing end-over-end for 2 hours. The tubes were then centrifuged for 30 seconds at 9000 x g in a microcentrifuge. The supernatant solution was removed from the centrifuge tubes and discarded, the gel beads washed by adding 1 mL of 18 MΩ deionized water, mixing end-over-end for 5 minutes, centrifuging at 9000 x g, and removing the supernatant. The phosphopeptides were eluted once with 50 mM and once with 100 mM phosphate buffer, pH 8.9, and the eluent was quickly adjusted to pH

2.75. The IMAC solutions were analyzed with the same equipment and methods as the gel spot digests with the only modification being that the gradient was extended from 90 minutes to 4 hours to maximize ion sampling. The trapping column used prior to gradient elution, performs in-line desalting and ameliorates the need for a desalting procedure to remove the excess phosphate from the sample preparation.

5.2.8 Tandem MS Protein Identification

The resultant spectra obtained from all MS experiments were first analyzed via Bioworks v.3.3.1 [Thermo-Scientific, Waltham, MA] which uses the SEQUEST[32] algorithm against the most recent version of the International Protein Index (IPI) database. The DTA files generated by SEQUEST for each mass spectrum were concatenated into a single data file and then analyzed using Mascot v.2.2[33] [Matrix Science, Boston MA] with the same database as the SEQUEST analysis. Search parameters for both programs included static mass modifications to cysteine due to alkylation by iodoacetamide, and differential mass modifications to methionine from oxidation, and to Ser, Thr and Tyr from phosphorylation. Parameters specific to neutral losses from phosphorylated peptides were also included. The Scaffold [Proteome Software, OR] program was used to validate protein identifications derived from the MS/MS sequencing results. Scaffold verifies peptide identifications assigned by SEQUEST and Mascot using the X!Tandem database searching program[34]. Scaffold then probabilistically validates these peptide identifications using PeptideProphet[35] and derives corresponding protein probabilities using ProteinProphet[36].

5.2.9 Target Validation

Aliquots of the homogenates of both 5 month and 34 month old samples, from the tissue preparations previously stored at -70°C, were delipidated as previously described under sample preparation, and the protein fraction was re-solubilized into a buffer amenable to immunoprecipitation, a modified RIPA buffer containing 50mM Tris-HCl, pH 7.4, 1% (v/v) of Igepal CA-630, 0.25% sodium deoxycholate, 150 mM sodium chloride, 1mM sodium fluoride, and 1 mM phosphatase inhibitor cocktails 1 and 2. The protein pellets were dispersed by sonicating according to the procedure described above, the samples were centrifuged at 13000 x g in a microcentrifuge, and the supernatant transferred to fresh centrifuge tubes. Protein concentrations were determined using the Lowry method and diluted appropriately with the RIPA buffer for immunoprecipitation to a concentration of 0.05 µg/µL total protein.

Phosphoproteins were immunoprecipitated using Dynabeads® Protein A [Invitrogen, Carlsbad, CA] according to manufacturers protocols, initially with a rabbit polyclonal antibody broadly engineered for all phosphoamino acids (pS/pT/pY), [Invitrogen, Carlsbad, CA] and subsequently with individual antibodies specific for phosphoserine, phosphothreonine and phosphotyrosine [Calbiochem, Gibbstown, NJ]. The phosphoproteins were eluted from the magnetic beads with Tris-glycine-SDS sample buffer and loaded onto Novex 4-20% Tris-glycine gradient gels [Invitrogen, Carlsbad, CA]. Following gel electrophoresis at 200 V for approximately 45 min, the protein bands on the gels were transferred to polyvinyl difluoride (PVDF) membranes [Millipore, Billerica, MA] for Western Blot analysis.

Primary antibodies for Western Blotting [Santa Cruz Biotechnology, Santa Cruz, CA] included homer-3 (C-18), synapsin IIa (R-20), PARG (M-13), MARK2 (C-16) and β-synuclein (C-20). The blots were visualized using the Western Breeze® Chemiluminescent Kit-anti-goat [Invitrogen, Carlsbad, CA] as described in the manufacturer's protocol.

5.3 Results

Figures 38 and **39** display images of the individual gels run for cerebellar samples from the three 5-month old and three 34-month old Fisher 344/BN1 rats. There was excellent reproducibility for both the Sypro Ruby and Pro-Q Diamond staining for each set of three animals. However, there were significant age-dependent differences between the data sets from the 5-month and 34-month old animals.

Several attempts were made to create a complete overall analysis by combining the phosphoprotein gel images with the total protein gel images to generate ratiometric phosphorylation difference values corrected for expression differences. This proved to be an untenable exercise with this version of the software due to the large number of spots present in the gel images and the differences in spot visibility between the two dyes. A number of spots evident in the phosphoprotein gel images were not found in the total protein gel images, and, as expected, many of the spots detected in the total protein images were not observed in the phosphoprotein gel images. The spot matching algorithm in the software would force matches between spots that were nearby and not necessarily the correct match. To overcome these difficulties, the image analysis was split into two distinct parts, one for the phosphoprotein levels using the

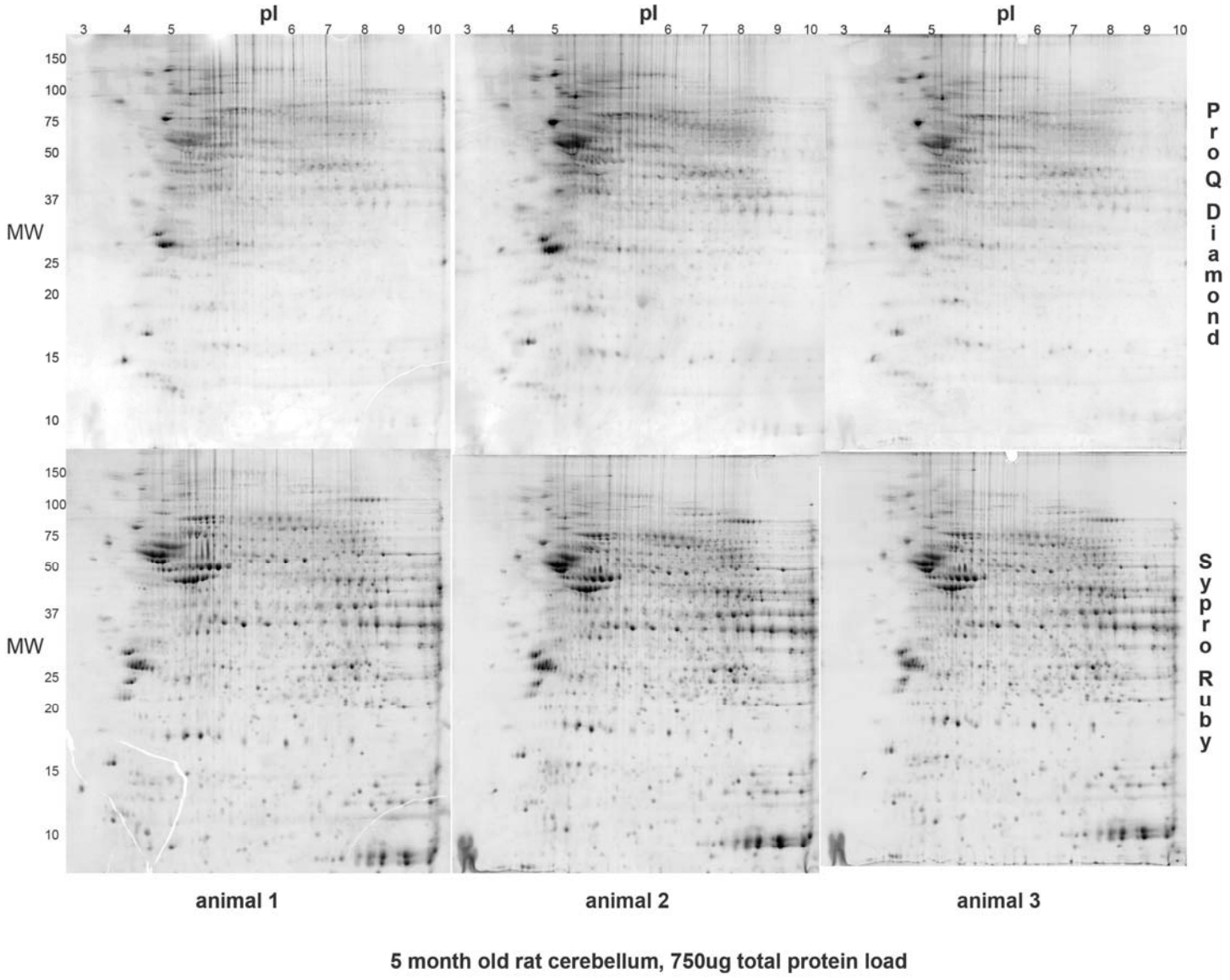

Figure 38. *Gel images of cerebellar proteins of 5 month old animals. Top panel: Pro-Q Diamond. Bottom panel: Sypro Ruby.*

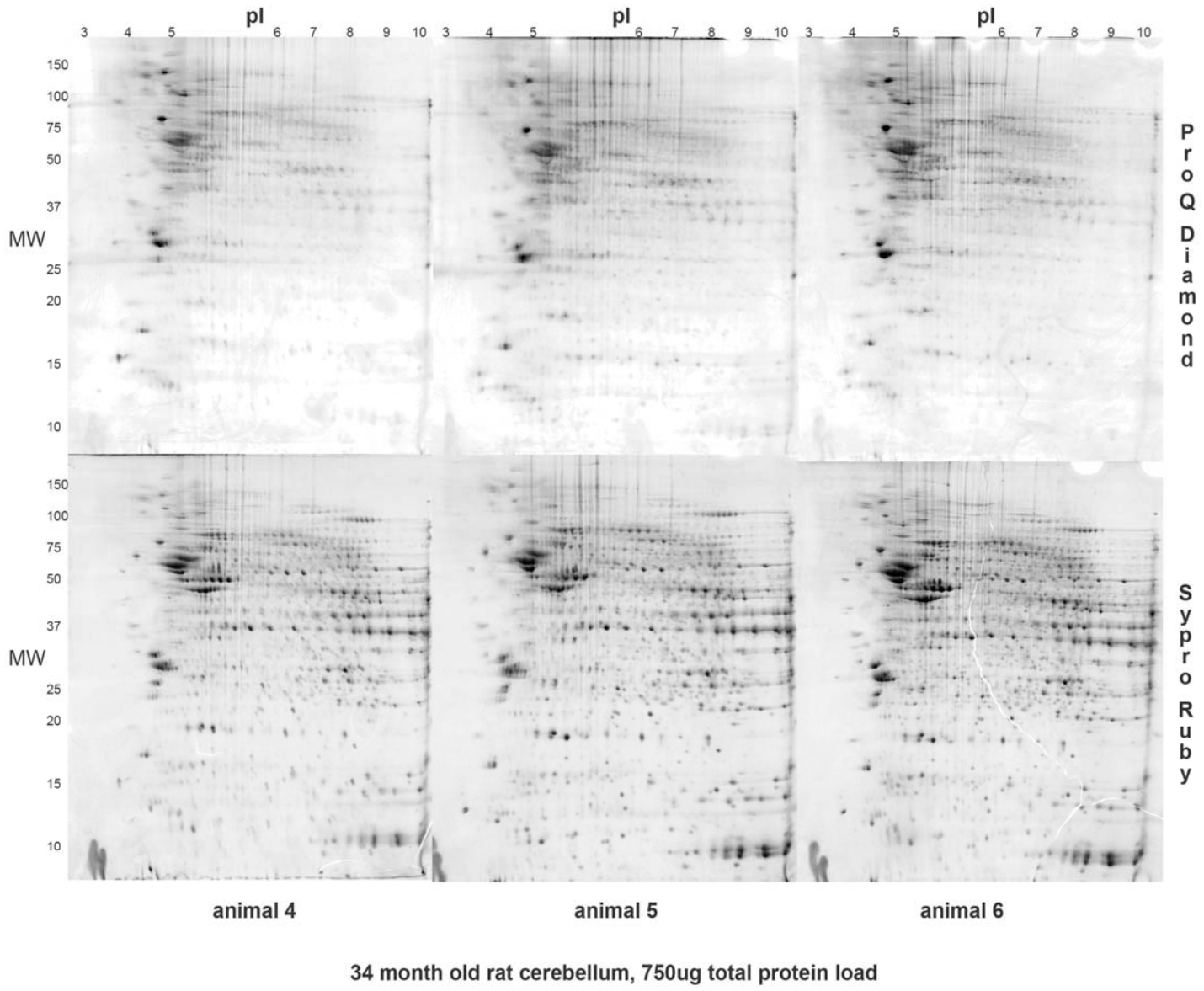

Figure 39. *Gel images of cerebellar proteins of 34 month old animals. Top panel: Pro-Q Diamond. Bottom panel: Sypro Ruby.*

Pro-Q Diamond gel images and one for the total protein using the Sypro Ruby gel images. Spots from the phosphoprotein analysis exhibiting a two-fold change were manually referenced against the total protein image analysis and spots from the total protein analysis exhibiting a two-fold change were cross referenced against the phosphoprotein analysis in order to normalize the data.

The image analysis identified approximately 110 phosphoprotein spots which demonstrate at least a two-fold difference between the averages of gels from the 5-month and 34-month old animals when normalized to total protein content. Spots meeting this criterion are annotated in **Figure 40** and the quantitative data for the spot volumes of phosphorylated species were obtained from the optical density of the spots in the images from the Pro-Q Diamond staining. The quantitative data are displayed in **Table 7**, while the data for the spot volumes of the total proteins derived from the Sypro Ruby stained images are displayed in **Table 8**.

These tables, though not immediately identifying proteins, are important for the statistical analysis of our data. In **Table 7**, we see the biological variability of a reversible modification like protein phosphorylation demonstrated as statistical variability. The covariance (CV) for the gel triplicates ranged between 2% and 154%, but the variance can actually be far more extreme in some cases where spots were only detected in two of the three triplicate gels. For these spots, no covariance was determined, denoted in the tables as (--) and only the average volume between the detectable spots was reported. This is the case for 21 out of 224 spots. If no gel or only one gel showed detectable levels of a given spot, the spot was reported as ‘not observed’. The variance for these spots representing phosphoproteins was attributed to

Figure 40. *Spots demonstrating age-dependent phosphorylation differences in aging rat cerebellum. Image generated by Progenesis PG220.*

Pro-Q Diamond Image Analysis Results							
spot #	5 month Diamond Volume (CV)	34 month Diamond Volume (CV)	ratio 5 /34	spot #	5 month Diamond Volume (CV)	34 month Diamond Volume (CV)	ratio 5/34
500	4,064,361.877669 (76%)	1,603,556.360568 (75%)	2.5	3821	1,404,515.866264 (75%)	541,745.555094 (61%)	2.6
666	1,222,869.225225 (55%)	488,719.863467 (102%)	2.5	3822	5,553,475.435877 (83%)	2,441,801.275623 (11%)	2.3
694	448,357.652535 (133%)	669,782.345709 (106%)	0.7	3826	245,254.052099 (24%)	509,516.739384 (88%)	0.5
783	6,127,091.636713 (139%)	838,172.000000 (--)	7.3	3828	1,643,360.700000 (44%)	173,274.445688 (62%)	9.5
793	958,550.137442 (11%)	307,651.490909 (77%)	3.1	3845	854,458.875776 (121%)	623,690.113131 (101%)	1.4
804	1,723,462.931507 (--)	293,771.237511 (40%)	5.9	3848	1,623,888.227536 (24%)	2,763,044.138756 (119%)	0.6
863	1,061,922.787106 (54%)	182,787.285714 (42%)	5.8	3854	2,499,017.185383 (17%)	4,652,380.760000 (--)	0.5
907	2,004,158.904835 (133%)	1,639,460.368421 (26%)	1.2	3858	5,695,888.663082 (49%)	2,328,267.046584 (98%)	2.5
931	239,797.986842 (76%)	216,596.037506 (23%)	1.1	3860	2,680,125.376945 (26%)	1,024,515.578947 (--)	2.6
949	1,419,537.782033 (27%)	358,495.403020 (60%)	3.9	3862	8,178,216.060362 (83%)	6,852,281.002416 (29%)	1.2
978	2,752,532.161812 (--)	442,545.945089 (33%)	6.2	3864	1,063,611.371429 (39%)	1,087,583.135294 (15%)	1.0
988	238,812.139421 (26%)	1,086,718.505339 (80%)	0.2	3870	1,376,141.057471 (56%)	2,891,916.058646 (101%)	0.5
1033	648,986.666667 (126%)	362,003.838022 (125%)	1.8	3872	836,005.955857 (73%)	726,774.545455 (--)	1.2
1077	530,380.492424 (2%)	984,907.925225 (89%)	0.5	3877	1,892,187.322311 (14%)	4,773,334.140280 (41%)	0.4
1162	303695.703704 (--)	130,656.204301 (141%)	1.2	3884	2,753,293.548387 (72%)	3,259,172.672864 (41%)	0.8
1163	2,421,338.960030 (100%)	641,665.250794 (93%)	3.8	3885	2,541,116.093398 (50%)	1,903,958.796339 (22%)	1.3
1189	1,218,519.444445 (18%)	2,618,344.363636 (20%)	0.5	3906	1,878,711.457732 (82%)	2,235,627.728350 (70%)	0.8
1208	5,582,957.739683 (64%)	3,498,763.096774 (46%)	1.6	3912	372,911.625701 (135%)	346,403.290756 (92%)	1.0
1245	562,985.350480 (115%)	587,381.520202 (142%)	0.9	3950	754,086.980971 (87%)	789,958.026858 (15%)	1.0
1256	535,682.278572 (64%)	240,785.820000 (34%)	2.2	3953	2,905,499.821417 (76%)	1,416,583.860735 (38%)	2.1
1325	369,045.933824 (38%)	650,218.169231 (5%)	0.6	3954	1,043,235.812162 (138%)	21,851.010526 (--)	48
1335	2,180,833.286713 (123%)	540,434.772381 (19%)	4.0	3958	416939.665 (76%)	626436.782 (94%)	0.7
1366	1,121,760.406032 (105%)	554,844.981735 (49%)	2.0	3976	1,713,630.583271 (26%)	3,834,162.665627 (30%)	0.5
1395	393,096.291536 (94%)	1,501,863.901099 (48%)	0.3	3977	not observed	3,346,518.599290 (63%)	0.015
1424	6,336,353.483871 (25%)	3,991,485.671691 (77%)	1.6	3995	not observed	4,528,810.762240 (70%)	0.01
1437	1,862,695.470146 (73%)	505,831.975198 (56%)	3.7	3999	1,714,221.189263 (11%)	3,142,584.632763 (19%)	0.6
1439	2,109,870.046871 (99%)	1,154,070.138696 (14%)	1.8	4008	2,811,833.125177 (82%)	2,187,747.875363 (63%)	1.3
1456	62,438.857143 (--)	212,773.578947 (--)	0.3	4016	not observed	868,033.028171 (84%)	0.06
1460	1,348,082.794521 (70%)	669,019.755647 (26%)	2.0	4041	1,540,869.887654 (41%)	157,538.422360 (30%)	9.8
1531	3,736,137.999597 (55%)	2,013,913.383117 (13%)	1.9	4049	717,718.063008 (54%)	974,483.976699 (86%)	0.7
1545	2,580,572.422619 (2%)	1,546,742.565217 (141%)	0.8	4067	11,259,331.569542 (62%)	6,532,022.740741 (54%)	1.7
1633	1,592,432.180769 (61%)	394,073.824896 (91%)	4.0	4075	798,797.158249 (26%)	251,372.846154 (--)	3.2
1661	571,074.510000 (85%)	329,431.230920 (140%)	1.7	4083	not observed	782,489.904282 (154%)	0.03
1741	335,459.821818 (80%)	881,122.961683 (57%)	0.4	4084	2,171,240.944444 (12%)	1,195,278.477671 (6%)	1.8
1782	334,920.188502 (128%)	111,530.252190 (99%)	3.0	4088	317,202.858378 (104%)	462,686.83871 (--)	0.7
1783	1,440,680.504404 (66%)	742,456.678633 (26%)	1.9	4089	33,754.931774 (132%)	115,273.232527 (53%)	0.3
1813	4,093,999.125852 (10%)	1,249,306.055901 (108%)	3.3	4092	401,777.432367 (3%)	418,465.420635 (39%)	1.0
1951	522,120.248950 (75%)	277,332.774749 (50%)	1.9	4099	1,292,065.642857 (128%)	2,136,708.349445 (73%)	0.6
2042	187,011.907297 (5%)	1,410,818.153846 (--)	0.1	4105	2,072,643.544159 (56%)	2,846,532.607235 (93%)	0.7
2122	1,773,999.958909 (38%)	493,383.099855 (2%)	3.6	4111	not observed	1,682,946.070838 (132%)	0.03
2127	1,331,258.944179 (41%)	73,132.730769 (13%)	18	4121	76,155.635249 (2%)	1,066,815.311606 (6%)	0.1
2223	298,269.234043 (--)	928,472.831976 (47%)	0.3	4123	387,395.545455 (82%)	1,909,693.875000 (--)	0.2
2361	288,805.052085 (134%)	103,528.258720 (26%)	2.8	4158	274,825.500000 (27%)	277,429.022222 (60%)	1.0
2368	6332189.888889 (--)	1,826,930.161963 (58%)	3.5	4168	not observed	837,815.614136 (37%)	0.06
2488	644,922.706606 (120%)	189,810.172768 (48%)	3.4	4226	779,260.982564 (65%)	1,753,399.275556 (46%)	0.4
2563	908,620.782205 (56%)	1,029,921.803564 (7%)	0.9	4229	2,211,161.163743 (55%)	3,281,657.757199 (78%)	0.7
2861	125760.973913 (--)	446,515.080738 (13%)	0.3	4236	1,759,122.849673 (91%)	1,625,061.454699 (92%)	1.0
2918	2,074,494.851523 (15%)	4,076,697.161110 (18%)	0.5	4237	1,099,176.337607 (60%)	882,389.071429 (--)	1.3
3048	867,037.160567 (63%)	2,587,896.357143 (--)	0.3	4242	12,014,444.524743 (39%)	11,952,110.237282 (38%)	1.0
3087	426,911.052632 (--)	not observed	43	4271	1,915,629.543243 (88%)	969,160.370611 (47%)	2.0
3158	2,475,384.694547 (53%)	506,038.000000 (--)	4.9	4276	1,469,076.538655 (3%)	1,108,116.375000 (59%)	1.3
3671	1,002,978.726166 (129%)	3,814,667.198198 (73%)	0.3	4290	3,142,336.575661 (32%)	527,804.716038 (44%)	5.9
3701	3,203,756.113832 (5%)	2,779,802.491669 (85%)	1.1	4333	3,481,313.341644 (91%)	2,762,583.779082 (52%)	1.3
3774	1,474,028.413793 (80%)	575,929.144359 (51%)	2.6	4361	384,865.335632 (156%)	604,727.469136 (25%)	0.6
3775	1,556,314.177257 (72%)	1,257,207.460741 (119%)	1.2	4366	1,540,252.314741 (81%)	844,535.326784 (77%)	1.8
3810	1,090,782.672727 (19%)	371,954.836420 (44%)	2.9				

ratio 5/34: ratio of average spot volumes from 5 month old over 34 month old animals
CV: covariance
not observed: spot not observed or only present in one replicate
(--): CV not calculated where a spot was observed in only 2 of 3 replicates

Table 7. *Quantitative cerebellum results obtained by Pro-Q Diamond image analysis.*

Sypro Ruby Image Analysis Results							
spot	5 month Ruby	34 month Ruby	ratio	spot	5 month Ruby	34 month Ruby	Ratio
#	Volume (CV)	Volume (CV)	5 /34	#	Volume (CV)	Volume (CV)	5 /34
500	4,401,196.691746 (31%)	5,073,895.143350 (57%)	0.9	3821	8,553,675.683895 (77%)	8,540,550.066658 (7%)	1.0
666	802,404.215623 (71%)	1,009,028.292184 (25%)	0.8	3822	not observed	not observed	-
694	1,730,761.353837 (56%)	not observed	5.0	3826	not observed	not observed	-
783	not observed	1,067,024.399279 (36%)	0.009	3828	2,751,810.595556 (47%)	1,907,517.823980 (72%)	1.4
793	991,639.266145 (102%)	1,040,257.867554 (54%)	1.0	3845	1,638,553.043771 (71%)	1,266,602.657494 (7%)	1.3
804	909,476.941078 (62%)	3,946,665.478229 (31%)	0.2	3848	4,740,032.226310 (0%)	3,641,606.543781 (16%)	1.3
863	not observed	not observed	-	3854	33,900,613.055554 (11%)	28,712,973.314317 (50%)	1.2
907	not observed	1,558,312.281557 (22%)	0.006	3858	1,879,609.545604 (6%)	1,779,168.778540 (15%)	1.1
931	not observed	165,792.425000 (0%)	0.06	3860	2,202,703.509979 (23%)	1,748,432.247036 (50%)	1.3
949	not observed	1,165,122.442783 (20%)	0.009	3862	4,656,063.000000 (76%)	7,011,768.629219 (9%)	0.7
978	3,466,822.487222 (33%)	3,533,511.796912 (20%)	1.0	3864	3,904,128.390664 (67%)	428,032.302083 (51%)	9.1
988	225,041.921193 (44%)	684,008.830118 (80%)	0.3	3870	5,146,154.690396 (7%)	4,711,654.953782 (8%)	1.1
1033	not observed	661,305.445415 (48%)	0.015	3872	948,881.942702 (28%)	1,418,342.612899 (73%)	0.7
1077	891,771.448572 (40%)	768,767.434650 (15%)	1.2	3877	7,978,604.240299 (56%)	5,497,208.001150 (42%)	1.5
1162	1,592,015.695652 (69%)	1,889,584.934298 (9%)	0.8	3884	16,701,957.642157 (18%)	20,379,500.241558 (15%)	0.8
1163	not observed	not observed	-	3885	623,598.825960 (5%)	898,688.345803 (39%)	0.7
1189	1,642,279.094603 (9%)	1,877,399.911514 (9%)	0.9	3906	2,427,508.413723 (40%)	2,162,838.251768 (37%)	1.1
1208	2,667,680.517820 (49%)	2,603,231.000000 (24%)	1.0	3912	1,974,210.184800 (36%)	1,006,268.962514 (28%)	1.9
1245	891,702.286620 (14%)	1,332,129.315393 (125%)	0.7	3950	722,374.347439 (13%)	1,063,596.126566 (102%)	0.7
1256	1,630,202.056083 (6%)	1,379,775.375032 (18%)	1.2	3953	1,744,850.617326 (51%)	2,199,949.216895 (80%)	0.8
1325	1,344,532.522969 (42%)	1,205,346.798535 (21%)	1.1	3954	1,430,308.833342 (1%)	4,303,295.465649 (4%)	0.3
1335	6,580,542.179839 (3%)	7,054,895.283807 (18%)	0.9	3958	1,852,850.392 (13%)	1,445,378.212 (42%)	1.3
1366	2,356,852.336062 (37%)	1,030,526.499734 (69%)	2.3	3976	17,003,568.585006 (25%)	12,416,408.886731 (25%)	1.4
1382	4,404,940.262066 (34%)	7,269,563.144468 (31%)	0.6	3977	9,193,578.198532 (20%)	8,530,950.809452 (18%)	1.1
1424	4,970,430.219545 (33%)	3,159,600.843221 (4%)	1.6	3995	3,347,995.983395 (35%)	6,313,957.654660 (64%)	0.5
1437	16,991,281.210022 (1%)	11,489,434.751473 (45%)	1.5	3999	3,519,227.419510 (29%)	3,738,632.470808 (30%)	0.9
1439	1,248,523.437672 (42%)	972,246.789761 (57%)	1.3	4008	4,587,796.481204 (39%)	2,206,312.444186 (17%)	2.1
1456	13,389,967.745454 (16%)	14,465,152.112850 (2%)	0.9	4016	4,453,591.178803 (16%)	5,821,165.375858 (3%)	0.8
1460	2,156,122.676813 (52%)	1,592,689.574446 (48%)	1.4	4041	885,255.686881 (27%)	1,037,023.485350 (17%)	0.9
1531	9,992,368.182783 (25%)	12,588,935.033553 (11%)	0.8	4049	4,639,999.384708 (40%)	6,149,626.402062 (9%)	0.8
1545	4,609,641.506781 (130%)	8,013,091.468864 (23%)	0.6	4067	4,912,488.213580 (26%)	5,286,767.334523 (12%)	0.9
1633	8,387,130.643914 (24%)	8,053,094.294982 (5%)	1.0	4075	3,956,725.226800 (54%)	3,649,494.405949 (50%)	1.1
1661	9,720,144.020611 (16%)	12,577,868.311425 (23%)	0.8	4083	2,475,447.165824 (26%)	2,638,702.157886 (36%)	0.9
1741	1,358,436.419904 (18%)	1,625,454.995176 (12%)	0.8	4084	2,286,817.273516 (66%)	1,123,884.450000 (48%)	2.0
1783	1,133,754.259237 (37%)	1,576,776.411203 (9%)	0.7	4088	2,133,045.694617 (18%)	3,645,797.718993 (23%)	0.6
1782	6,512,573.031872 (25%)	6,659,335.942878 (23%)	1.0	4089	7,563,147.636501 (11%)	10,395,921.106418 (26%)	0.7
1813	886,216.183081 (10%)	1,054,354.990155 (63%)	0.8	4092	955,531.977289 (63%)	1,151,704.315376 (18%)	0.8
1951	14,944,647.304346 (14%)	15,992,872.126279 (10%)	0.9	4099	2,866,496.478242 (22%)	2,649,077.818670 (47%)	1.1
2042	2,039,425.128941 (44%)	2,553,471.089203 (43%)	0.8	4105	3,085,549.095266 (68%)	1,615,747.997861 (51%)	1.9
2122	4,283,605.732615 (28%)	5,356,223.964984 (26%)	0.8	4111	2,092,196.089421 (35%)	3,684,028.346374 (21%)	0.6
2127	7,214,168.444469 (2%)	6,403,723.860645 (2%)	1.1	4121	3,121,193.754647 (52%)	3,558,308.804470 (23%)	0.9
2223	3,173,646.836125 (20%)	1,859,080.964954 (130%)	1.7	4123	17,809,927.527017 (24%)	18,170,584.913115 (40%)	1.0
2361	11,486,442.097458 (9%)	6,255,387.279903 (2%)	1.8	4158	700,391.568027 (20%)	833,063.056604 (9%)	0.8
2368	3,345,558.228582 (45%)	3,933,419.049338 (61%)	0.9	4168	1,907,845.536088 (31%)	12,366,723.601100 (27%)	0.2
2488	10,893,734.304546 (49%)	12,590,515.315046 (0%)	0.9	4226	1,834,935.629630 (52%)	2,176,132.862130 (50%)	0.8
2563	6,322,723.051125 (9%)	5,114,224.056687 (38%)	1.2	4229	2,510,733.445220 (44%)	2,274,635.041457 (24%)	1.1
2861	5,388,725.281495 (14%)	4,169,184.558621 (9%)	1.3	4236	1,187,051.240030 (26%)	1,580,757.858472 (8%)	0.8
2918	2,048,135.930908 (9%)	10,248,009.113423 (29%)	0.2	4237	1,985,718.963415 (47%)	935,249.620432 (62%)	2.1
3048	6,554,809.739147 (13%)	5,748,298.347417 (49%)	1.1	4242	11,476,469.304348 (69%)	8,756,285.430416 (21%)	1.3
3087	7,245,405.106930 (58%)	4,700,013.082256 (27%)	1.5	4271	1,852,850.392130 (13%)	1,445,378.211889 (42%)	1.3
3158	432,248.030096 (45%)	739,184.510666 (16%)	0.6	4276	9,011,454.316819 (68%)	11,792,101.497153 (14%)	0.8
3671	568,671.393659 (31%)	not observed	57	4290	2,177,031.111262 (45%)	1,802,471.970843 (33%)	1.2
3701	764,726.382713 (46%)	747,660.473766 (45%)	1.0	4333	7,334,565.931550 (13%)	9,038,607.298738 (11%)	0.8
3774	1,881,244.323508 (21%)	2,254,459.470759 (18%)	0.8	4361	6,342,490.541075 (56%)	7,498,387.749602 (27%)	0.9
3775	2,241,694.578100 (74%)	582,444.206360 (89%)	3.9	4366	5,559,862.514286 (48%)	4,650,478.956814 (27%)	1.2
3810	6,939,049.191736 (35%)	5,471,158.502490 (26%)	1.3				

ratio 5/34: ratio of average spot volumes from 5 month old over 34 month old animals
CV: covariance
not observed: spot not observed or only present in one replicate
(--): CV not calculated where a spot was observed in only 2 of 3 replicates

Table 8. *Quantitative cerebellum results obtained by Sypro Ruby image analysis.*

biological variability and not the quality of the gels, since the variability was significantly reduced in the Sypro Ruby Image Analysis reported in **Table 8.** In the Sypro Ruby gels, there were no spots with only two of three triplicate values observed and no spots with only one of the three triplicate values observed; either the spot was present in all three triplicates or it was not. The covariances were much tighter in the Sypro Ruby staining with 80% of the spots showing a CV of 50% or less and 44% showing a CV of 25% or less compared with 37% and 17% respectively for the Pro-Q Diamond staining. The ratios between 5 month and 34 month volumes shown in **Tables 7** and **8** indicated that the more a value diverged from unity the more extreme the difference was between the values. Ratio values in the Pro-Q Diamond Image Analysis that approached unity were made much more meaningful when normalized to the ratio values from the Sypro Ruby Image Analysis. This was especially true when either the 5 month or the 34 month spot was absent, as is the case for spots 694, 783, 907, 931, 949, 1033, and 3671.

It is important to note that several of the spots in the tables do not show significant differences, but appeared to be part of a charge train containing a spot of interest and were selected for MS/MS analysis to assist in determining identity and/or phosphorylation state of that spot of interest. For spots listed as ‘not observed’, an area corresponding to the spot expected was manually created in the Progenesis software for each spot and averaged to obtain a background volume which was applied in the determination of the 5 month/34 month ratios for each spot. For the Pro-Q Diamond analysis, the average background spot volume was approximately 50,000 units and for the Sypro Ruby an average background spot volume of 10,000 units was applied in the ratio calculation for spots that were not observed.

The MS/MS analysis of 110 spots of interest yielded 20 phosphoproteins which were identified by peptide sequences and for which MS/MS spectra of specific phosphopeptides were obtained. These are listed in **Table 9.** In this table, the observed phosphopeptides are listed with the modified amino acid residues in lower case. In addition to phosphorylation of Ser, Thr and Tyr residues, acetoamidated cysteine and oxidized methionine residues are also noted.

In addition to the phosphoproteins identified from the 2D-PAGE samples, 6 unique phosphopeptides were identified after IMAC separation of a global digest of soluble cerebellar proteins (summarized in **Table 10**). One feature of note in this table, are the four missed cleavages observed for the neurofilament medium polypeptide (Nef3). This peptide has a relatively good SEQUEST score and low errors for its resultant fragments. Possible explanations for the missed cleavages include the phosphoserine residues adjacent to two of the lysine cleavage sites which could potentially inhibit trypsin due to their negative charge, and their general proximity to one another. The proline residues adjacent to three of the four lysine cleavage sites may also have an effect, although the dogma associated with trypsin and proline residues has been challenged[53]. Very little overlap is observed between the phosphoproteins observed using the 2D-PAGE methodology followed by NSI-MS/MS analysis versus the IMAC enrichment, with the exception being Nef3. This phosphoprotein was observed in both sets of experiments with overlapping peptidic fragments of the same phosphorylation site, p-Ser609. Both **Tables 9** and **10** contain literature references in which the phosphorylation site for the given peptide has been observed. An asterisk indicates that we could not find a literature citation for a given phosphorylation site.

spot #	Phosphoprotein	Primary IPI Accession number	Phosphopeptide sequence(s)	Scaffold Protein Probability	SEQUEST XCorr (charge)	references	MW (kD)	P ratio ^	E ratio Δ
694	Nef3 Neurofilament medium polypeptide	IPI00325609	s_{608}PVEEVKPKPEAK	100%	2.26 (+3)	37,38,39	96	0.7	5.0
863	Acadvl Very long-chain specific acyl-CoA dehydrogenase, mitochondrial precursor	IPI00213057	YYTLNGs_{246}KIWIR	95%	2.62 (+2)	*	71	5.8	ND
949	Syn2 Isoform IIa of Synapsin-2	IPI00210036	TPALs$_{426}$PQRPLTTQQPQSGTLK	100%	2.60 (+2)	40	63	3.9	0.009
978	Mark2 Serine/threonine-protein kinase MARK2	IPI00194773	PRPSADLt_{384}NSSAPSPSHKVQR	95%	2.37 (+3)	41	71	6.2	1.0
1077	Atp6v1a1_predicted;LOC685232 ATPase, H transporting, lysosomal V1 subunit A	IPI00373076	ESTFGYVHGVSGPVVt_{30}ACDMA-GAAMYELVR	100%	2.59 (+3)	*	68	0.5	1.2
1163	Gan Giant Axonal neuropathy	IPI00870043.1	FGAVAcGVAMELy$_{477}$VFGGVR	100%	3.15 (+2)	42	68	3.8	ND
1189	Pykm Isoform M1 of Pyruvate Kinase Isozymes M1/M2	IPI00231929.6	Gat$_{139}$LKITLDNAy$_{148}$MEK	98%	2.24 (+2)	*,43	58	0.5	0.9
2127	CalcB Calcitonin gene-related peptide 2 precursor	IPI00215106.1	SALESSLDLGt$_{41}$LSDQEK, and/or SALESSLDLGTLs$_{43}$DQEK	95%	2.72 (+2), 2.24 (+2)	*	15	18.2	1.1
2368	Spock1 Similar to Testican-1 precursor	IPI00782288.1	KQVt_6KNVLEDLLCVGGFVGK	90%	3.47 (+2)	*	37	3.5	0.9
2918	RGD1560112 similar to Urinary protein 2 precursor	IPI00366509.3	GTVENGGLt_{103}AK	95%	2.25 (+3)	*	13	0.5	0.2
3822	Bin1 Isoform AMPH2-1 of Myc box-dependent-interacting protein 1	IPI00196509	s_{297}PSPPPDGSPAATPEIR	100%	2.31 (+2)	40	65	2.3	ND
3848	Inexa Alpha-internexin	IPI00211936	LPAs$_{72}$DGLDLSQAAAR	100%	3.29 (+2)	40	56	0.6	1.3

^: phosphorylation ratio of average spot volumes from 5 month old over 34 month old animals from Pro-Q Diamond image analysis
Δ: expression ratio of average spot volumes from 5 month old over 34 month old animals from Sypro Ruby image analysis
* : no references for these phosphorylation sites were available
Scaffold Protein Probability determined by PeptideProphet[35, 36]

Table 9. *Cerebellum phosphoprotein IDs from 2D PAGE analysis.*

spot #	Phosphoprotein	Primary IPI Accession number	Phosphopeptide sequence(s)	Scaffold Protein Probability	SEQUEST XCorr (charge)	references	MW (kD)	P ratio ^	E ratio Δ
3858	Gfap Isoform 1 of Glial fibrillary acidic protein	IPI00190943	LRLDQLt$_{129}$t$_{130}$Ns$_{132}$AR	100%	2.22 (+3)	*	50	2.5	1.1
3862	Ndrg2 Isoform 2 of Protein NDRG2	IPI00326606	TAs$_{318}$LTSAASIDGSR	100%	2.30 (+2)	*	39	1.2	0.7
3877	HnRNP Heterogeneous Nuclear Ribonucleoprotein C	IPI00187860.3	RQRVSGNt$_{165}$s$_{166}$R	90%	2.23 (+2)	*	34	0.4	1.5
3953	Tpm3 33 kDa protein	IPI00393158	AISDELDHALNDmTs$_{283}$M	100%	2.92 (+2)	44	32	2.1	0.8
4099	Homer3 Homer protein homolog 3	IPI00210368	SQs$_{158}$ADAPGPTER	100%	3.17 (+2)	40	40	0.6	1.1
4123	Sytl2_predicted synaptotagmin-like 2	IPI00365777	RKt$_{736}$APVALEt$_{743}$ENR	88%	2.47 (+2)	*	103	0.2	1.0
4237	Atp5b ATP synthase subunit beta, mitochondrial precursor	IPI00551812	s$_{433}$LQDIIAILGMDELSEEDKLTVSR	100%	2.24 (+2)	*	56	1.3	2.1
4242	Tubb6 Tubulin, beta 6	IPI00195673	LTTPTYGDLNHLVSATMSGVt$_{237}$TSLR	100%	3.25 (+2)	50	1.0	1.3	50

^: phosphorylation ratio of average spot volumes from 5 month old over 34 month old animals from Pro-Q Diamond image analysis
Δ: expression ratio of average spot volumes from 5 month old over 34 month old animals from Sypro Ruby image analysis
* : no references for these phosphorylation sites were available
Scaffold Protein Probability determined by PeptideProphet[35, 36]

Table 9. *Cerebellum phosphoprotein IDs from 2D PAGE analysis. (continued)*

found in 5 month or 34 month	Phosphoproteins	Primary IPI Accession number	Phosphopeptide sequence(s)	Scaffold Protein Probability	SEQUEST XCorr (charge)	references	MW (kD)
5 month	Atp1a3 Sodium/potassium-transporting ATPase subunit alpha-3	IPI00231451	ILIFGLFEETALAAFLSy_{960}CPGMDVALR	100%	2.25 (+3)	*	112
34 month	Mbp Isoform 1 of Myelin basic protein S	IPI00231265	HGs_{13}KYLATASTMDHAR; NIVTPRt_{122}PPPSQGK	91%	2.51 (+2)	47; 40,48	17
34 month	Nef3 Neurofilament medium polypeptide	IPI00325609	AKs_{604}PVPKs_{609}PVEEVKPKPEAK	100%	2.42 (+2)	37,38,39,49	96
34 month	RGD1561178 similar to glyceraldehyde-3-phosphate dehydrogenase	IPI00369166	IVSNASCt_{158}IHCLAPLAK	76%	2.59 (+2)	*	20
34 month	Stx1b2 Syntaxin-1B	IPI00191730	SAKDs_{14}DDEEEVVHVDRDHFMDEFFE-QVEEIR	100%	4.75 (+4)	50,51	33
34 month	Syn1 Isoform IA of Synapsin-1	IPI00191335	DASPGRGS_{430}HSQTPSPGALPLGR	100%	1.25 (+3)	52	74

*** :** no references for these phosphorylation sites were available
Scaffold Protein Probability determined by PeptideProphet[35, 36]

Table 10. *Cerebellum phosphoprotein IDs from IMAC enrichment.*

An example of the quality of the mass spectra obtained is shown in **Figure 41** where the sequence coverage for the phosphorylated version of Bin1 Isoform AMPH2-1 of Myc box-dependent-interacting protein 1 is depicted. Additional examples of the quality of the spectra are shown in **Figure 42** depicting the tandem mass spectra and model error for the doubly charged, phosphorylated peptide **sPSPPPDGSPAATPEIR,** and **Figure 43** showing the tandem mass spectra and model error for the same peptide in its unphosphorylated state. The fragmentation tables for the respective peptides can be found in **Figures 44** and **45**.

The focused spectra in **Figure 46** of the phosphopeptide **sPSPPPDGSPAATPEIR** demonstrate the unique neutral loss of -98 Da from p-Ser_{297}. Several neutral loss peaks were observed, including neutral losses from the parent, the b_9, b_{12} and b_{13} fragments. The majority of the spots for which we observed phosphorylation differences by Pro-Q Diamond staining did not provide sufficient material for MS/MS sequencing of phosphopeptides. A true quantitative analysis of the specific proteins in each spot is difficult as many spots contain more than one protein. We assume that the phosphopeptides showing MS/MS are likely to be the most abundant phosphoprotein in the spot, suggesting that the protein from which they originate may represent the most abundant phosphoprotein in the spot. Hence, the following discussion is based on the assumption that the Pro-Q Diamond staining in the spot predominantly quantifies the phosphoprotein of which we obtained MS/MS data and that we can quantitate the phosphoprotein. Targeted purification and analysis of each individual phosphoprotein would be required to establish a more

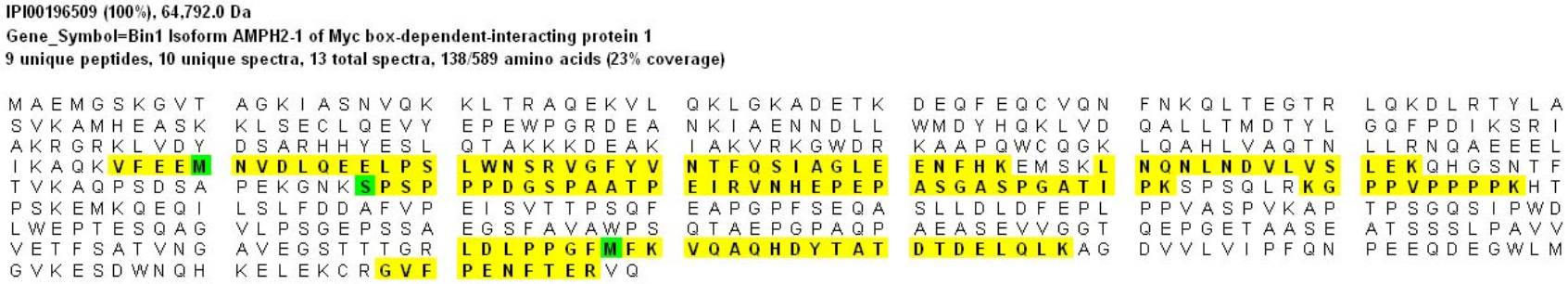

Figure 41. *Sequence coverage for Bin1 Isoform AMPH2-1 of Myc box-dependent-interacting protein 1.*

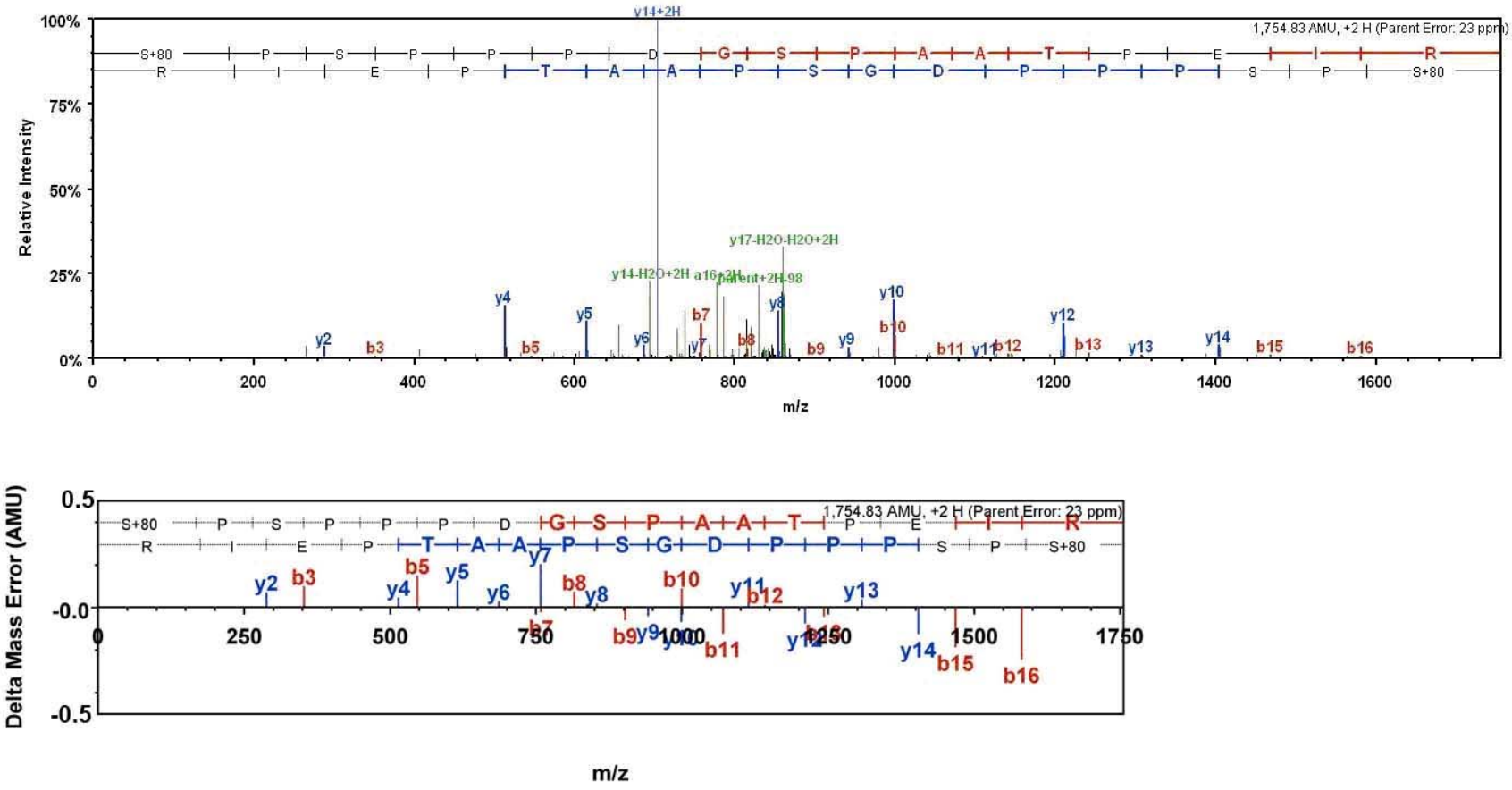

Figure 42. *Tandem mass spectra and model error for the doubly charged phosphorylated Bin1 peptide sPSPPPDGSPAATPEIR.*

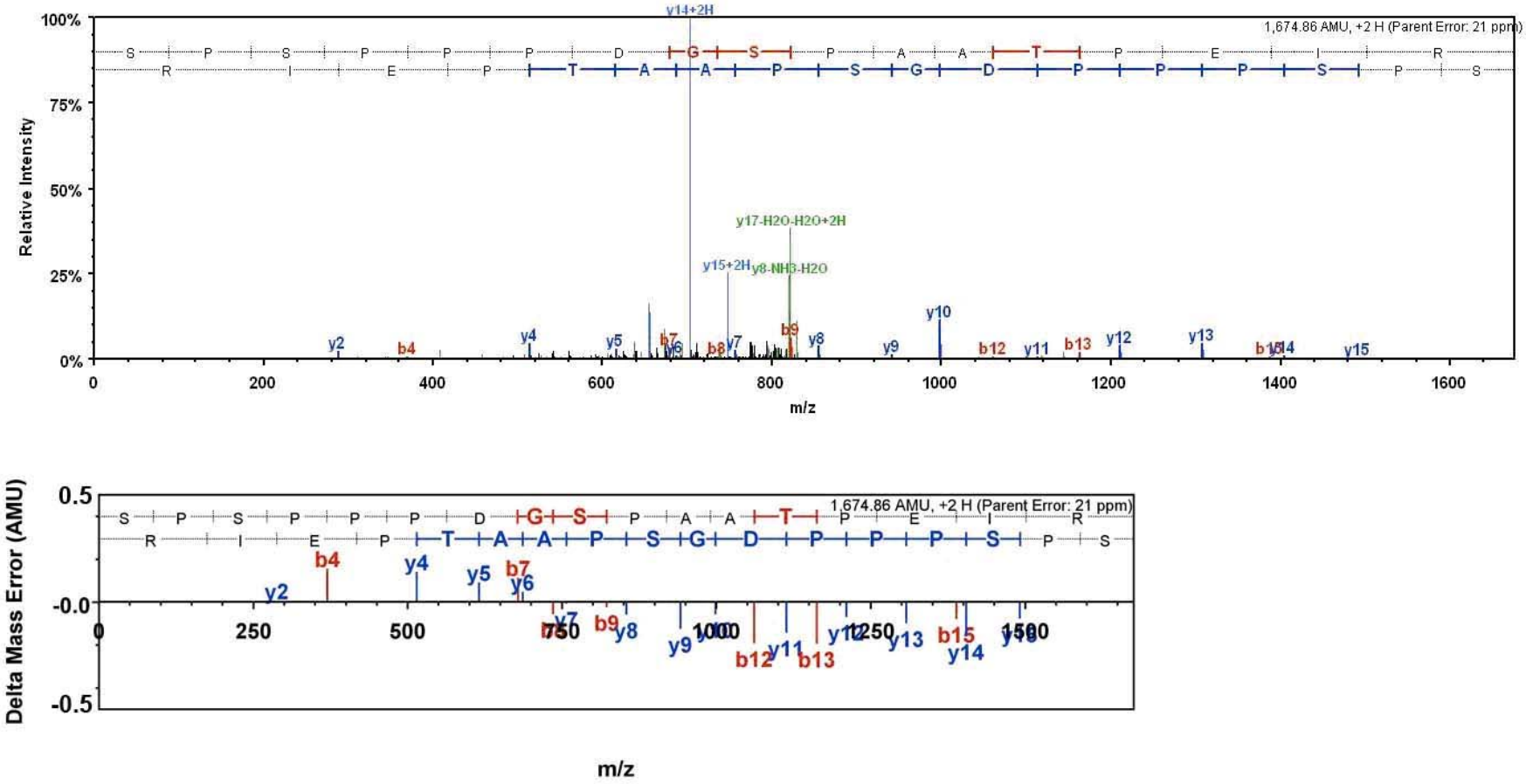

Figure 43. *Tandem mass spectra and model error for the doubly charged unphosphorylated Bin1 peptide SPSPPPDGSPAATPEIR.*

...	B Ions	B+2H	B-NH3	B-H2O	AA	Y Ions	Y+2H	Y-NH3	Y-H2O	...
1	168.0			150.0	S+80	1,755.8	878.4	1,738.8	1,737.8	17
2	265.1			247.0	P	1,588.8	794.9	1,571.8	1,570.8	16
3	352.1			334.1	S	1,491.7	746.4	1,474.7	1,473.7	15
4	449.1			431.1	P	1,404.7	702.9	1,387.7	1,386.7	14
5	546.2			528.2	P	1,307.7	654.3	1,290.6	1,289.6	13
6	643.2	322.1		625.2	P	1,210.6	605.8	1,193.6	1,192.6	12
7	758.3	379.6		740.3	D	1,113.6	557.3	1,096.5	1,095.5	11
8	815.3	408.2		797.3	G	998.5	499.8	981.5	980.5	10
9	902.3	451.7		884.3	S	941.5	471.3	924.5	923.5	9
10	999.4	500.2		981.4	P	854.5	427.7	837.4	836.5	8
11	1,070.4	535.7		1,052.4	A	757.4	379.2	740.4	739.4	7
12	1,141.5	571.2		1,123.4	A	686.4	343.7	669.4	668.4	6
13	1,242.5	621.8		1,224.5	T	615.3		598.3	597.3	5
14	1,339.6	670.3		1,321.5	P	514.3		497.3	496.3	4
15	1,468.6	734.8		1,450.6	E	417.2		400.2	399.2	3
16	1,581.7	791.3		1,563.7	I	288.2		271.2		2
17	1,755.8	878.4	1,738.8	1,737.8	R	175.1		158.1		1

Figure 44. *Fragmentation table for the doubly charged phosphorylated Bin1 peptide sPSPPPDGSPAATPEIR.*

...	B Ions	B+2H	B-NH3	B-H2O	AA	Y Ions	Y+2H	Y-NH3	Y-H2O	...
1	88.0			70.0	S	1,675.8	838.4	1,658.8	1,657.8	17
2	185.1			167.1	P	1,588.8	794.9	1,571.8	1,570.8	16
3	272.1			254.1	S	1,491.7	746.4	1,474.7	1,473.7	15
4	369.2			351.2	P	1,404.7	702.9	1,387.7	1,386.7	14
5	466.2			448.2	P	1,307.7	654.3	1,290.6	1,289.6	13
6	563.3	282.1		545.3	P	1,210.6	605.8	1,193.6	1,192.6	12
7	678.3	339.7		660.3	D	1,113.6	557.3	1,096.5	1,095.5	11
8	735.3	368.2		717.3	G	998.5	499.8	981.5	980.5	10
9	822.4	411.7		804.4	S	941.5	471.3	924.5	923.5	9
10	919.4	460.2		901.4	P	854.5	427.7	837.4	836.5	8
11	990.5	495.7		972.4	A	757.4	379.2	740.4	739.4	7
12	1,061.5	531.2		1,043.5	A	686.4	343.7	669.4	668.4	6
13	1,162.5	581.8		1,144.5	T	615.3		598.3	597.3	5
14	1,259.6	630.3		1,241.6	P	514.3		497.3	496.3	4
15	1,388.6	694.8		1,370.6	E	417.2		400.2	399.2	3
16	1,501.7	751.4		1,483.7	I	288.2		271.2		2
17	1,675.8	838.4	1,658.8	1,657.8	R	175.1		158.1		1

Figure 45. *Fragmentation table for the doubly charged unphosphorylated Bin1 peptide SPSPPPDGSPAATPEIR.*

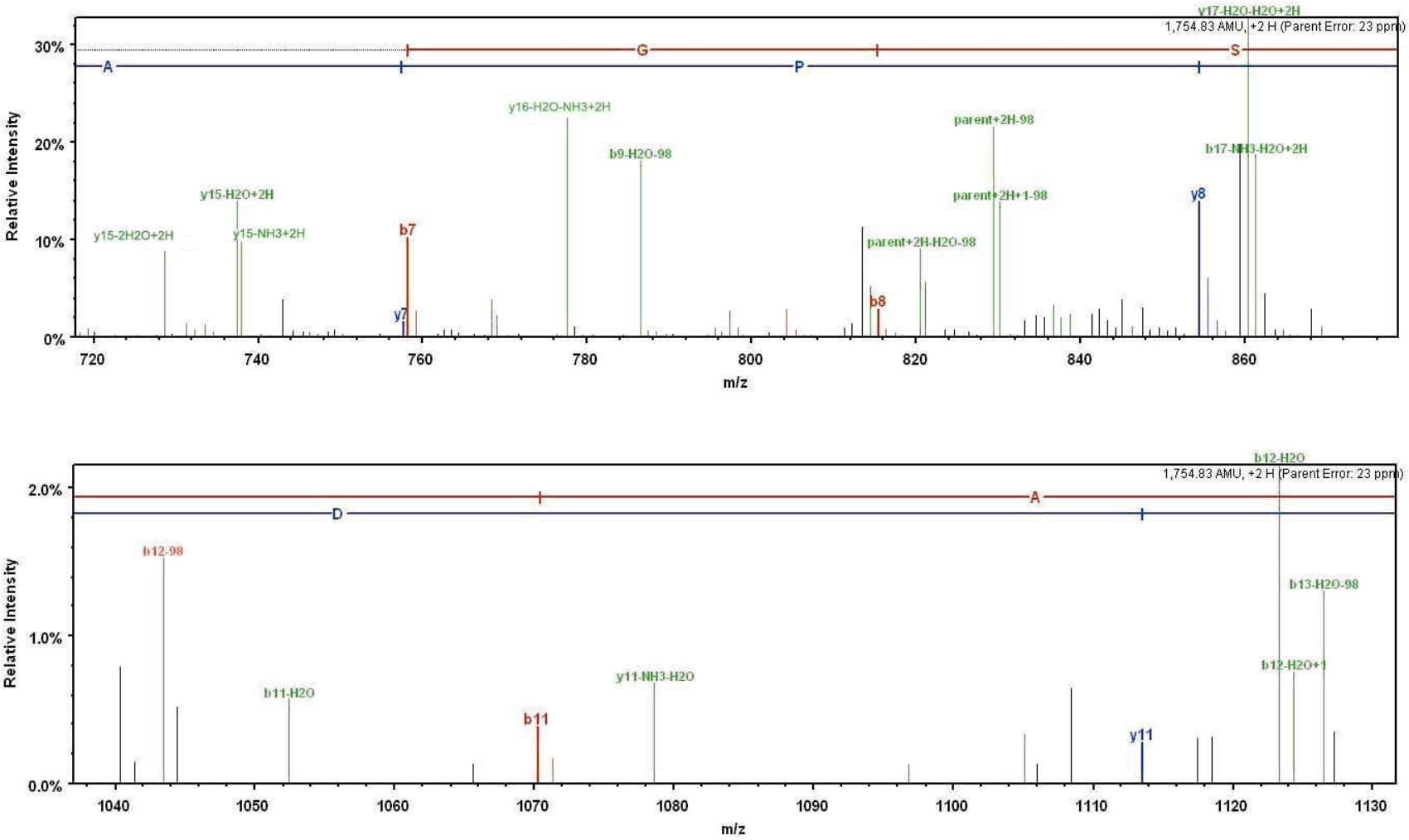

Figure 46. *Area zoom of tandem mass spectra for the doubly charged phosphorylated Bin1 peptide sPSPPPDGSPAATPEIR showing neutral losses.*

reliable quantitative analysis. Additional proteins that were positively identified but for which a quality phosphopeptide MS/MS spectrum was not acquired are summarized in **Table 11**. The phosphorylation ratios (P ratio) and expression ratios (E ratio) shown in **Tables 9** and **11** are derived from the image analysis results.

In an attempt to partially validate our findings, **Figure 47** shows a representative result from the immunoprecipitation (IP) and Western blotting experiments. The protein bands in Figure 10A were analyzed using the gel analysis functionality of ImageJ[54]. This analysis yielded the plot shown in Figure 10B. The numerical area values are shown in Figure 10C. In this example, the value obtained from the IP and Western blotting corresponds very well with the quantitative analytical data obtained from the 2D PAGE image analysis. A ratio of young/old of 0.56 was determined from the IP/WB and a ratio of 0.6 from the 2D PAGE image analysis. This result was only achieved by selecting a phosphoserine antibody (clone 4A9, Calbiochem) for IP that has been demonstrated to be specific for the RXXpS (calmodulin-dependent protein kinase II substrate motif) of the Homer-3 protein[55]. Experiments using broad range phospho-amino acid antibodies for IP proved to be inconsistent with the observed 2D PAGE image analysis from the Pro-Q Diamond/Sypro Ruby stained gels. As an example, the lack of antibodies for phosphoserine, where there may be a negatively charged amino acid near the epitope, makes it extremely difficult to observe phosphoproteins with this potential modification. When even a small part of the focus of the experiment is to find uncommon and aberrant phosphorylation, tools designed for the most common phosphorylation motifs don't seem to be the best tools to utilize.

Spot #	Proteins	Primary IPI Accession number	Scaffold Protein Probability	MW (kD)	P ratio^	E ratio^
500	Parg Poly(ADP-ribose) glycohydrolase	IPI00214269.3	100%	109	2.5	0.9
783	Hspca Heat shock protein HSP 90-alpha	IPI00210566	100%	85	7.3	0.009
804	Nefl Neurofilament light polypeptide	IPI00231302	95%	61	5.9	0.2
907	Hspa5 78 kDa glucose-regulated protein precursor	IPI00206624	100%	72	1.2	0.006
931	Hspa9a_predicted Stress-70 protein, mitochondrial precursor	IPI00363265	95%	74	1.1	0.06
931	Nefl Neurofilament light polypeptide	IPI00231302	100%	61	1.1	0.06
931	RGD1563803_predicted similar to Lamin-B2	IPI00366190	95%	69	1.1	0.06
931	Tuba4a Tubulin alpha-4A chain	IPI00362927	100%	49	1.1	0.06
931	Vim Vimentin	IPI00230941	100%	54	1.1	0.06
949	Lmna Lamin-A	IPI00201060	100%	74	3.9	0.009
949	Stip1 Stress-induced-phosphoprotein 1	IPI00213013	100%	63	3.9	0.009
1245	Eno1 Alpha-enolase	IPI00464815	95%	47	0.9	0.7
1633	RGD1561029 similar to RIKEN cDNA 4930434E21	IPI00363509.4	100%	39	4.0	1.0
2563	RGD1304704 LRRGT00192	IPI00421395	100%	34	0.9	1.2
3775	Dpysl2 Dihydropyrimidinase-related protein 2	IPI00870112	90%	62	1.2	3.9
3860	Uqcrc1 Cytochrome b-c1 complex subunit 1, mitochondrial precursor	IPI00471577	100%	53	2.6	1.3
3864	Ckb Creatine kinase B-type	IPI00470288	100%	43	1.0	9.1
3864	Eno2 Gamma-enolase	IPI00326412	100%	47	1.0	9.1
3950	MGC109519 Isoform 2 of Tropomyosin beta chain	IPI00187731	90%	33	1.0	0.7
3950	Npm1 Isoform B23.1 of Nucleophosmin	IPI00197553	95%	33	1.0	0.7
3954	- similar to Charged multivesicular body protein 4b	IPI00763972	95%	29	48	0.3
3954	Apoe Apolipoprotein E precursor	IPI00190701	100%	36	48	0.3
3954	Efhd2 EF-hand domain-containing protein 2	IPI00200410	95%	27	48	0.3
3954	Txnl1 Thioredoxin-like protein 1	IPI00200601	95%	32	48	0.3
3995	Ywhae 14-3-3 protein epsilon	IPI00325135	100%	29	0.01	0.5
4084	pur-beta Transcriptional activator protein Pur-beta	IPI00189358	100%	34	1.8	2.0
4084	Tmod2 Tropomodulin-2	IPI00189722	100%	39	1.8	2.0
4105	Efhd2 EF-hand domain-containing protein 2	IPI00200410	95%	27	0.7	1.9
4105	Tpm1 Isoform 5 of Tropomyosin alpha-1 chain	IPI00391997	100%	28	0.7	1.9
4111	Ywhae 14-3-3 protein epsilon	IPI00325135	100%	29	0.03	0.6

^: phosphorylation ratio of average spot volumes from 5 month old over 34 month old animals from Pro-Q Diamond image analysis
Δ: expression ratio of average spot volumes from 5 month old over 34 month old animals from Sypro Ruby image analysis
Scaffold Protein Probability determined by PeptideProphet[35, 36]

Table 11. *Identified proteins where a quality phosphopeptide MS/MS was not obtained.*

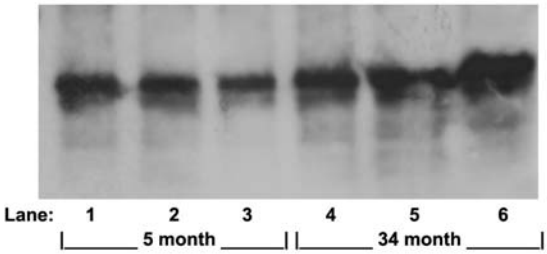

A) **Western blot of Homer-3 phosphoprotein after immunoprecipitation with phosphospecifc Ab and detection with anti-Homer-3 Ab.**

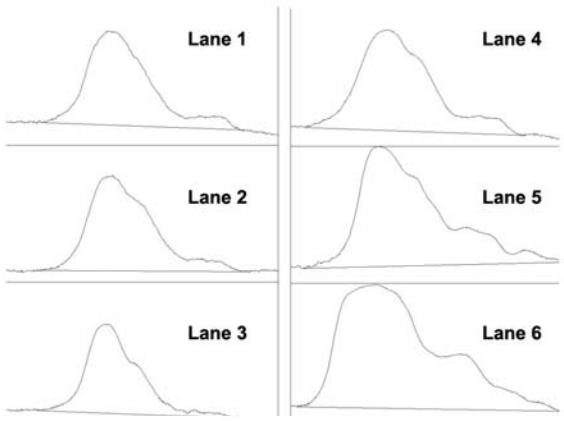

B) **Area plots of Homer-3 bands created using the densiometry gel functions of ImageJ software.**

Lane	Area		
1	36059		Average Lanes 1-3
2	37058		33840
3	28403		
4	44997		Average Lanes 4-6
5	58534		59902
6	76174		

C) **Area values for each lane and average values determined from ImageJ software.**

Figure 47. *Results from immunoprecipitation and Western blot of Homer-3.*

5.4 Discussion

A KEGG pathway analysis (see **Figures 24** and **25**, pages 70 and 71 respectively) was conducted on the identified proteins including those for which no phosphopeptides were detected by MS/MS sequencing. Assuming that all of these proteins are differentially phosphorylated, several pathways demonstrated significant perturbations most notably the carbohydrate and energy metabolism pathways. Examples of these pathways included pyruvate metabolism, the TCA cycle, glycolysis/gluconeogenesis, and oxidatative phosphorylation. However, we also established indicators for various neurodegenerative diseases and the potential for disruptions in cell communication and in the function of the immune system. Nevertheless, there are enough examples of proteins involved in these pathways for which we have direct evidence of the presence of phosphopeptides that allow us to restrict our discussion to these proteins alone.

Proteins involved in metabolism

Very long-chain specific acyl-CoA dehydrogenase (mitochondrial precursor), ATP synthase subunit beta (mitochondrial precursor), ubiquinol-cytochrome-c reductase complex core I (mitochondrial), and the M1 isoform of pyruvate kinase were all identified as differentially phosphorylated in our study. The protein poly(ADP-ribose) glycohydrolase [PARG] showed a normalized age-dependent phosphorylation reduction of nearly three-fold with only a marginal difference in expression. There is extensive evidence that oxidative stress, specifically peroxynitrite, causes damage to DNA which in turn activates the production of poly(ADP-ribose) [PAR] to correct the damage.[56]

High levels of the poly(ADP-ribose) polymerase [PARP] have been found in AD, ALS, and PD patients as well as in stroke victims. One hypothesis is that PARP activation, followed by necrosis and the release of cellular content into the extracellular space, renders PAR and poly(ADP-ribosylated) proteins immunogenic.[57] PARG is the major enzyme implicated in the catabolism of PAR[58] and an abnormality in its phosphorylation state may contribute to an immunogenic response. Inhibitors to PARG have been demonstrated to reduce the rate of PAR turnover, thus reducing the overall levels of necrosis and are under investigation as therapeutics.[59]

Another differentially phosphorylated protein involved in the metabolic pathways is the very long-chain specific acyl-CoA dehydrogenase, mitochondrial precursor, where nearly a six-fold reduction in phosphorylation was found. Mutants of this protein have been studied to observe defective fatty acid oxidation[60], but a structural aberration due to phosphorylation could cause similar effects with diminished levels of energy available and be responsible for a diminution of cerebellar function.

Another protein potentially contributing to metabolic defects is ATP synthase subunit beta, mitochondrial precursor. A two-fold greater level of expression in the 5 mo vs. 34 mo rats was observed without a corresponding increase in phosphorylation. ATP synthase is involved in oxidative phosphorylation and a reduction in the phosphorylated isoform of ATP synthase subunit beta has been implicated in type-2 diabetes as a possible source of insulin resistance.[61]

Another protein in the same family, ubiquinol-cytochrome-c reductase complex core I, mitochondrial, demonstrated a reduction in phosphorylation level in the aged population with nearly a two-fold change between 5 month and 34 month old rats. The

reduction in phosphorylation levels for proteins during the aging process could again be responsible for structural and functional losses and potentially lead to deficiencies in oxidative phosphorylation. A substantial number of patients with neurological conditions that exhibit gross deficiencies in oxidative phosphorylation capabilities lack any genetic abnormalities[62]. A change in post-translational modifications, such as the phosphorylation of ATP synthase may result in the deficiencies of oxidative phosphorylation observed in these patients.

The last protein involved in metabolism and which shows a differential level of phosphorylation was the M1 isoform of pyruvate kinase where a two-fold increase in phosphorylation was observed with no discernible increase in expression levels. Pyruvate kinase is a glycolytic enzyme that catalyzes the transfer of a phosphoryl group from phosphoenolpyruvate to ADP, thus producing ATP. This particular isoform of pyruvate kinase has been identified as an antigen associated with Tourette syndrome and associated disorders[63] and may be involved in microtubule dynamics.[64]

Structural Proteins

A number of structural proteins were identified in our study as differentially phosphorylated, including an analogue of the Cdc42 effector protein 4, neurofilament medium polypeptide, alpha-internexin, beta-synuclein, giant axonal neuropathy protein, tropomyosin 3, Homer protein homolog 3, and several tubulins. Microtubules are cytoskeletal scaffolds formed from dimers of tubulin, a protein for which there is evidence of a slight age-dependent increase in phosphorylation for various isoforms including the alpha 1-B, beta-2C, beta-3 and beta-6. Increased phosphorylation of the

alpha isoform has been previously correlated with aging and oxidative stress[65] and the phosphorylation of beta-3 tubulin, which is expressed exclusively in neurons, has been proposed as a marker for drug resistance in human cancer.[66] Other cytoskeletal proteins, the neurofilament medium polypeptide (Nef3) and an associated neurofilament, alpha-internexin, displayed an age-dependent increase in phosphorylation. Both proteins have been associated with neurodegenerative disorders where neurofilament accumulation correlated with the hyperphosphorylation of Nef3.[67]

Several other structural proteins were observed to suffer an age-dependent two-fold or greater loss in phosphorylation levels. These proteins were: tropomyosin 3 [TPM3], an analogue of the Cdc42 effector protein 4 (LOC689752), isoform 1 of the glial fibrilliary acidic protein [GFAP], and the giant axonal neuropathy protein, gigaxonin [GAN]. TPM3 and the Cdc42 effector protein 4 are both associated with the actin microfilament structure within the cell, stabilizing the shape of the cell for TPM3 and inducing change in the cell shape for the Cdc42 effector protein. GFAP, a class-III intermediate filament, is a cell-specific marker that distinguishes astrocytes from other glial cells during the development of the central nervous system. A mutant form of this protein has been correlated with Alexander's disease, the first known example of a primary genetic disorder of astrocytes. The mutant form of GFAP blocks the assembly of intermediate filaments within the astrocyte and deposited proteins known as Rosenthal fibers accumulate which disrupt the interaction of the astrocytes with other specialized cells in the brain. The disrupted interactions result in the inability to maintain or form myelin or to maintain the blood-brain barrier. Recent evidence is suggestive of GFAP requiring phosphorylation in order to preserve the plasticity of

astrocytes, a process that is necessary for maintaining their function.[68] Gigaxonin is a ubiquitin scaffolding protein that controls microtubule-associated protein 1B light chain degradation[69]. Mutations in the gigaxonin gene have been correlated with giant axonal neuropathy.[70] The age-dependent loss of phosphorylation of gigaxonin may cause deleterious effects similar to the mutation through the accumulation of intermediate filament proteins in neurons.

Another important protein is beta-synuclein [Sncb], which was both differentially phosphorylated and differentially expressed in 5 mo vs. 34 mo-old rat cerebella. This protein has been classified as an adaptor/scaffolding protein typically found in the nerve terminal and may be involved in neuronal plasticity. In a potentially more significant role, Sncb has been observed to prevent the aggregation of alpha-synuclein [Snca], which has been found to accumulate in Lewy bodies, the pathological neuronal inclusion bodies present in several neurodegenerative disorders.[71]

With regard to possible age-associated changes in the synaptic structure and function we detected a near two-fold increase in phosphorylation for Homer protein homolog 3 [Homer 3] in the aged samples with no significant change in expression level. Homer 3 is a postsynaptic density scaffolding protein that aids in coupling surface receptors to intracellular calcium release and may play an important role in maintaining plasticity at glutamatergic synapses.[72] Its phosphorylation state has been correlated with the regulation of postsynaptic architecture in response to synaptic activity.[73]

Signaling

A number of proteins that showed differential phosphorylation between 5 month and 34 month-old rat cerebella have been detected: Ser/Thr protein kinase MARK2, protein phosphatase 3 regulatory subunit B alpha 1, heterogenous nuclear ribonucleoprotein C, Isoform IIa of synapsin-2, calcitonin gene-related peptide 2 precursor, glypican-3 precursor, synaptotagmin-like 2 protein, isoform 2 of NDRG2 , two isoforms of the Myc box-dependent-interacting protein 1, and the protein similar to testican-1 precursor.

The Ser/Thr protein kinase MARK2 displayed a six-fold reduction in phosphorylation with no apparent change in expression level. This protein is considered to perform a crucial role in cell polarity and its phosphorylation state is important for the regulation of microtubule dynamics.[74] Another signaling protein is protein phosphatase 3 regulatory subunit B alpha 1 [Ppp3r1]. Ppp3r1 is a regulatory subunit of calcineurin, and is a calcium-dependent, calmodulin-stimulated protein phosphatase, that plays a critical role in coupling Ca^{2+} signals to cellular responses.[75] It is a protein whose altered function has been invoked in explaining a diminished learning capacity in aging brain.[19] Ppp3r1 was marginally more highly expressed in the cerebellum of aged rats while less than a two-fold difference in phosphorylation was observed. The normalization of the two signals shows a significant reduction in phosphorylation levels, potentially coupled to a change in function.

Heterogenous nuclear ribonucleoprotein C [HnRNP] is a phosphoprotein that has been demonstrated to undergo rapid phosphorylation in response to the presence of peroxide[76] and a greater than two-fold increase in phosphorylation level was observed

in the 34 month old rats with a small reduction in the expression level for the particular isoform observed in the 2D PAGE images. HnRNP has been associated with aspects of mRNA maturation/turnover and in telomere and telomerase regulation[77]. Isoform IIa of synapsin-2 (Syn2), calcitonin gene-related peptide 2 precursor (Calcb), and the protein similar to testican-1 precursor (Spock1) were all observed to show rather large reduction of phosphorylation in the cerebellum of 34 month old rats. Syn2 represents the most extreme example with nearly a four fold higher level of phosphorylation in the cerebellum of 5 month old rats compared to 34 month old rats as determined by imaging of the Pro-Q Diamond stained gels. There was no measurable evidence of expression in the 5 month sample compared to over a million counts for the same spot in the 34 month gel. Syn2 is a known neuronal phosphoprotein that may function in the regulation of neurotransmitter release and synaptogenesis.[78] Mutations in the gene have been associated with abnormal presnyaptic function and schizophrenia[79].

Calcb was observed to show an 18-fold reduction in phosphorylation in the aged samples without a significant change in expression. The expression of Calcb has been correlated with a response to inflammation and as a drug development target for the treatment of migraine[80]. To our knowledge, the phosphorylation state of Calcb has not been previously reported and no information concerning the relevance of this potential finding is currently available.

A greater than three-fold loss in phosphorylation was observed for the proteoglycan Spock1 in the aged rat cerebellum samples. This protein may contribute to neuronal development through its role in cell-cell and cell-matrix interactions through adhesion. Several functions of this protein have been demonstrated in vitro including

membrane-type matrix metalloproteinase inhibition, cathepsin L inhibition, and low-affinity calcium binding. It has also been shown to inhibit cell attachment and neurite extensions in culture[81].

The glypican-3 precursor [Gpc3] is another proteoglycan, and it has recently been reported to inhibit Hedgehog protein signaling[82]. This protein was curiously found to show a two-fold reduction in phosphorylation in the aged sample analyzed by Pro-Q Diamond imaging, but the spot was not observed in the young gel images using the Sypro Ruby stain.

The predicted synaptotagmin-like 2 protein [Sytl2] was observed to increase by a factor of five-fold in phosphorylation level in the aged cerebellum with no appreciable difference in expression level. Studies of synaptotagmin 2 in transgenic knockout mice have demonstrated the function of this protein in both spontaneous and Ca^{2+} initiated neurotransmitter release.[83,84] In the initial study, a single amino acid substitution (I377N) caused a delay and decrease in Ca^{2+} initiated neurotransmitter release. An aberrant and disadvantageous phosphorylation could potentially cause similar results by altering the conformation of the protein.

NDRG2 is a pro-apoptotic protein that may be involved in neuron differentiation.[85] Isoforms 1 and 2 are present in brain neurons and up-regulated in Alzheimer disease.[86] Expression of Isoform 2 increased in the aged rat cerebellum but exhibited a conversely proportional reduction in phosphorylation. Normalized for its expression, this isoform showed an approximate two-fold decrease in phosphorylation level. Two isoforms of the Myc box-dependent-interacting protein 1 (Bin1), isoform AMPH2-1 and AMPH2-3 were recovered from the same spot and shown to suffer just over a two fold loss in

phosphorylation in the 34 month rat samples, but no data were obtained for expression levels since the spot could not be detected in the 5 month or 34 month Sypro Ruby stained gels. Bin1 has been associated with the regulation of synaptic vesicle endocytosis, actin function and signaling that links the cortical cytoplasm to nuclear function.[87] Bin1 has also been demonstrated to perform as an inhibitor to malignant cell growth and as a tumor suppressor.[88] A number of phosphorylation sites have been reported including the one observed in this study, Ser296, but no functional study on the effects of phosphorylation was found by the authors.

5.5 Conclusions

The objective of the experiment was to catalogue proteins that show distinct differential phosphorylation in the cerebellum of 5 month compared to 34 month old rats, that could potentially be correlated to age-dependent dysfunction and pathologies. This objective was achieved for several classes of proteins with several structural, metabolic and signaling proteins identified as differentially phosphorylated in the cerebellum. The potential implications of the change in function of these proteins due to changes in phosphorylation state have been individually outlined in the discussion. Taken as a whole, these age-dependent changes can be seen as potentially contributing to the development of cerebellar disorders in an aged populace. A single feature, such as the loss in neuronal plasticity, which has been correlated to many of the described phosphorylation differences in the structural proteins, could possibly be a cause for deterioration of fine motor skills in and of itself. The phosphorylation differences observed in metabolic and signaling proteins would only aggravate this degeneration and provide contributing evidence for the importance of protein phosphorylation as a possible cause and a potential target for the therapeutic intervention of cerebellar disorders.

5.6 References

[1] Glickstein, M., Doron, K., Cerebellum: connections and function., Cerebellum, 2008;7(4):589-94

[2] Ellble R.J., The role of aging in the clinical expression of essential tremor., Exp. Gerontol., 1995 May-Aug;(3-4):337-47

[3] Holtzer, R., Friedman, R., Lipton, R.B., Katz, M., Xue, X., Verghese, J., The relationship between specific cognitive functions and falls in aging., Neuropsychology, 2007 Sep; 21(5):540-8

[4] Siu, K.C., Lugade, V., Chou, L.S., van Donkelaar, P., Woollacott, M.H., Dual-task interference during obstacle clearance in healthy and balance-impaired older adults., Aging Clin. Exp. Res. 2008 Aug;20(4):349-54

[5] Finkel, T. and Holbrook, N.J., Oxidants, oxidative stress and the biology of ageing. Nature 2000 Nov 9;408(6809):239-47

[6] Barnham, K.J., Masters, C.L., and Bush, A.I., Neurogenerative diseases and oxidative stress. Nat. Rev. Drug Discov. 2004 Mar:3(3):205-14

[7] Mariani, E., Polidori, M.C., Cherubini, A., and Mecocci, P., Oxidative stress in brain aging, neurogenerative and vascular diseases: an overview., J. Chromatogr B 2005 Nov15; 827(1):65-75

[8] Hekimi, S., and Guarente, L., Genetics and the specificity of the aging process. Science 2003 Feb 28;299(5611):1351-4

[9] Holzer, M., Holzapfel, H.P., Krohn, K. Gertz, H-J, and Arendt, T., Alterations in content and phosphorylation state of cytoskeletal proteins in the sciatic nerve during ageing and in Alzheimer's disease. J Neural Transm. 1999;106(7-8):743-55

[10] Wang X., Zaidi A., Pal R., Garrett A.S., Braceras R., Chen X.W., Michaelis M.L., Michaelis E.K. Genomic and biochemical approaches in the discovery of mechanisms for selective neuronal vulnerability to oxidative stress. BMC Neurosci. 2009 Feb 19;10:12

[11] Miura, Y., Kano, M., Abe, K., Urano,S., Suzuki, S., and Toda, T., Age-dependent variations of cell response to oxidative stress: proteomic approach to protein expression and phosphorylation. Electrophoresis 2005 Jul;26(14):2786-96

[12] Reynolds M.R., Berry R.W., Binder L.I., Site specific nitration and oxidative dityrosine bridging of the tau protein by peroxynitrite: implications for Alzheimer's disease, Biochemistry. 2005 Feb 8;44(5):1690-700

[13] Derkinderen P., Scales T.M., Hanger D.P., Leung K.Y., Byers H.L., Ward M.A., Lenz C., Price C., Bird I.N., Perera T., Kellie S., Williamson R., Noble W., Van Etten R.A., Leroy K., Brion J.P., Reynolds C.H., Anderton B.H., Tyrosine 394 is phosphorylated in Alzheimer's paired helical filament tau and in fetal tau with c-Abl as the candidate tyrosine kinase.J Neurosci. 2005 Jul 13;25(28):6584-93.

[14] Barghorn S., Mandelkow E., Toward a unified scheme for the aggregation of tau into Alzheimer paired helical filaments. Biochemistry. 2002 Dec 17;41(50):14885-96.

[15] Gow, A.J., Duran, D., Malcolm, S. and Ischiropoulos, H. Effects of peroxynitrite-induced protein modifications on tyrosine phosphorylation and degradation. FEBS Lett. 1996 Apr 29;385:63-6

[16] Di Stasi, A.M., Mallozzi, C., Macchia, G., Petrucci, T.C., and Minetti, M. Peroxynitrite induces tyrosine nitration and modulates tyrosine phosphorylation of synaptic proteins. J. Neurochem. 1999 Aug; 73(2):727-35.

[17] Cohen, P., The origins of protein phosphorylation., Nat. Cell Biol., 2002 May 4(5):E127-130.

[18] Kandel E.R. The molecular biology of memory storage: a dialog between genes and synapses. Biosci Rep. 2004 Aug-Oct;24(4-5):475-522.

[19] Norris C.M, Halpain S., and Foster T.C. Alterations in the balance of protein kinase/phosphatase activities parallel reduced synaptic strength during aging. J Neurophysiol. 1998 Sep;80(3):1567-70.

[20] Zhang, H., Zha, X., Tan, Y., Hornbeck, P.V., Mastrangelo, A.J., Alessi, D.R., Polakiewicz, R.D., Comb, M.J., Phosphoprotein analysis using antibodies broadly reactive against phosphorylated motifs., J. Biol. Chem. 2002 Oct 18; 277(42):39379-87

[21] Kersten, B., Agrawal, G.K., Iwahashi, H., and Rakwal, R., Plant phosphoproteomics: a long road ahead. Proteomics 2006 Oct;6(20):5517-28

[22] Manning G., Whyte, D.B., Martinez, R., Hunter, T., and Sudarsanam, S., The protein kinase complement of the human genome., Science, 2002 Dec 6; 298(5600):1912-34

[23] Andersen, J.N., Mortensen, O.H., Peters, G.H., Drake, P.G., Iversen, L.F., Olsen, O.H., Jansen, P.G., Andersen, H.S., Tonks, N.K., and Møller, N.P., Structural and evolutionary relationships among protein tyrosine phosphatase domains. Mol. Cell Biol. 2001Nov;21(21):7117-36

[24] Svenningsson, P., Tzavara, E.T., Carruthers, R., Rachleff, I., Wattler, S., Nehls, M., McKinzie, D.L., Fienberg, A.A., Nomikos, G.G., Greengard, P., Diverse psychotomimetics act through a common signaling pathway. Science 2003 Nov 21;302(5649):1412-5.

[25] Bodenmiller, B., Mueller, L.N., Mueller, M., Domon, B., and Aebersold, R., Reproducible isolation of distinct, overlapping segments of the phosphoproteome. Nat. Methods 2007 Mar;4(3): 231-7 (supplementary methods, IMAC)

[26] Wessel, D., and Flügge, U.I., A method for the quantitative recovery of protein in dilute solution in the presence of detergents and lipids. Anal Biochem. 1984 Apr;138(1):141-3.

[27] Leimgruber, R.M., Malone, J.P., Radabaugh, M.R., LaPorte, M.L., Violand, B.N. and Monahan, J.B. Development of improved cell lysis, solubilization and imaging approaches for proteomic analyses. Proteomics 2002 Feb;2(2):135-44.

[28] Lowry, O.H., Rosbrough, N.J., Farr, A.L., and Randall, R.J., Protein measurement with the Folin phenol reagent. J. Biol. Chem. 1951 Nov;193(1):265-75

[29] Görg A., Boguth, G., Obermaier, C., Posch, A. and Weiss, W., Two-dimensional polyacrylamide gel electrophoresis with immobilized pH gradients in the first dimension (IPG-Dalt): the state of the art and the controversy of vertical versus horizontal systems. Electrophoresis 1995 Jul;16(7):1079-86.

[30] Olsen, J.V., Ong, S.E. and Mann, M. Trypsin cleaves exclusively C-terminal to arginine and lysine residues. Mol. Cell. Proteomics 2004 Jun;3(6):608-14

[31] Mann, M., Ong, S.E., Grønborg, M., Steen, H., Jensen, O.N. and Pandey, A., Analysis of protein phosphorylation using mass spectrometry: deciphering the phosphoproteome. Trends Biotechnol. 2002 Jun;20(6):261-8

[32] Eng, J., McCormack, A.L., and Yates, J.R. An approach to correlate tandem mass spectral data of peptides with amino acid sequences in a protein database. J. Am. Soc. Mass Spectrom. 5, 976-989 (1994).

[33] Perkins, D.N., Pappin, D.J., Creasy, D.M., and Cottrell, J.S., Probability-based protein identification by searching sequence databases using mass spectrometry data. Electrophoresis 1999 Dec;20(18) 3551-67

[34] Craig, R. and Beavis, R.C., A method for reducing the time required to match protein sequences with tandem mass spectra. Rapid Commun. Mass Spectrom. 2003;17(20):2310-16

[35] Keller, A., Nesvizhskii, A.I., Kolker, E., and Aebersold, R., Empirical statistical model to estimate the accuracy of peptide identifications made by MS/MS data search. Anal. Chem. 2002 Oct 15;74(20):5383–92.

[36] Nesvizhskii, A.I., Keller, A., Kolker, E., and Aebersold, R. A statistical model for identifying proteins by tandem mass spectrometry. Anal Chem. 2003 Sep 2;75(17):4646–58.

[37] Cleverley KE, et al. Identification of novel in vitro PKA phosphorylation sites on the low and middle molecular mass neurofilament subunits by mass spectrometry. Biochemistry. 1998. 37, 3917-30

[38] Betts JC, Blackstock WP, Ward MA, Anderton BH Identification of phosphorylation sites on neurofilament proteins by nanoelectrospray mass spectrometry. J Biol Chem. 1997. 272, 12922-7

[39] Xu ZS, Liu WS, Willard MB Identification of six phosphorylation sites in the COOH-terminal tail region of the rat neurofilament protein M. J Biol Chem. 1992. 267, 4467-71

[40] Trinidad JC, et al. Comprehensive identification of phosphorylation sites in postsynaptic density preparations. Mol Cell Proteomics. 2006. 5, 914-22

[41] Daub H, et al. Kinase-selective enrichment enables quantitative phosphoproteomics of the kinome across the cell cycle. Mol Cell. 2008. 31, 438-48

[42] Wang Y, et al. Proteomic analysis reveals novel molecules involved in insulin signaling pathway. J Proteome Res. 2006. 5, 846-55

[43] Ballif BA, Carey GR, Sunyaev SR, Gygi SP Large-scale identification and evolution indexing of tyrosine phosphorylation sites from murine brain. J Proteome Res. 2008. 7, 311-8

[44] Dai J, et al. Protein phosphorylation and expression profiling by Yin-yang multidimensional liquid chromatography (Yin-yang MDLC) mass spectrometry. J Proteome Res. 2007. 6, 250-62

[45] Olsen JV, et al. Global, in vivo, and site-specific phosphorylation dynamics in signaling networks. Cell. 2006. 127, 635-48

[46] Edbauer D, et al. Identification and characterization of neuronal mitogen-activated protein kinase substrates using a specific phosphomotif antibody. Mol Cell Proteomics. 2009. 8, 681-95

[47] Collins MO, et al. Proteomic analysis of in vivo phosphorylated synaptic proteins. J Biol Chem. 2005. 280, 5972-82

[48] Atkins CM, Yon M, Groome NP, Sweatt JD Regulation of myelin basic protein phosphorylation by mitogen-activated protein kinase during increased action potential firing in the hippocampus. J Neurochem. 1999. 73, 1090-7

[49] Yang SD, Huang JJ, Huang TJ Protein kinase FA/glycogen synthase kinase 3 alpha predominantly phosphorylates the in vivo sites of Ser502, Ser506, Ser603, and Ser666 in neurofilament. J Neurochem. 1995. 64, 1848-54

[50] Wu CC, MacCoss MJ, Howell KE, Yates JR A method for the comprehensive proteomic analysis of membrane proteins. Nat Biotechnol. 2003. 21, 532-8

[51] Foletti DL, Lin R, Finley MA, Scheller RH Phosphorylated syntaxin 1 is localized to discrete domains along a subset of axons. J Neurosci. 2000. 20, 4535-44

[52] DeGiorgis JA, et al. Phosphoproteomic analysis of synaptosomes from human cerebral cortex. J Proteome Res. 2005. 4, 306-15

[53] Rodriguez J, Gupta N, Smith RD, Pevzner PA. Does trypsin cut before proline? J Proteome Res. 2008 Jan;7(1):300-5.

[54] Rasband, W.S., ImageJ, U. S. National Institutes of Health, Bethesda, Maryland, USA, http://rsb.info.nih.gov/ij/, 1997-2008.

[55] F. Zang, Y. Hu, P. Huang, C.A. Toleman, A.J. Paterson, and J.E. Kudlow Proteasome Function Is Regulated by Cyclic AMP-dependent Protein Kinase through Phosphorylation of Rpt6. J Biol Chem 2007 282: 22460-22471.

[56] Ying, W., Sevigny, M.B., Chen, Y., and Swanson, R.A., Poly(ADP-ribose) glycohydrolase mediates oxidative and excitotoxic neuronal death. Proc. Natl. Acad. Sci. U.S.A. 2001 Oct 9;98(21):12227-32.

[57] Pacher, P. and Szabo, C., Role of peroxynitrite-poly(ADP-ribose) polymerase pathway in human disease. Am. J. Pathol. 2008 Jul;173(1):2-13

[58] Davidovic, L., Vodnicharov, M., Affar, E.B., and Poirier, G.G., Importance of poly(ADP-ribose) glycohydrolase in the control of poly(ADP-ribose) metabolism. Exp. Cell Res. 2001 Aug 1;268(1):7-13.

[59] Ying, W., Swanson, R.A., The poly(ADP-ribose) glycohydrolase inhibitor gallotannin blocks oxidative astrocyte death. Neuroreport. 2000 May 15;11(7):1385-8.

[60] Gregersen, N., Andresen, B.S., Corydon, M.J., Corydon, T.J., Olsen, R.K., Bolund, L. and Bross, P., Mutation Analysis in mitochondrial fatty acid defects: Exemplified by acyl-CoA dehydrogenase deficiencies, with a special focus on genotype-phenotype relationship. Hum. Mutat. 2001 Sep;18(3):169-89.

[61] Højlund, K., Wrzesinski, K., Larsen, P.M., Fey, S.J., Roepstorff, P., Handberg, A., Dela, F., Vinten, J., McCormack, J.G., Reynet, C., and Beck-Nielsen, H., Proteome analysis reveals phosphorylation of ATP synthase beta subunit in human skeletal muscle and proteins with potential roles in type 2 diabetes. J. Biol. Chem. 2003 Mar 21;278(12):10436-42

[62] Coenen, M.J., van den Heuvel, L.P., Smeitink, J.A., Mitochondrial oxidative phosphorylation system assembly in man: recent achievements. Curr. Opin. Neurol. 2001 Dec;14(6):777-81.

[63] Kansy, J.W., Katsovich, L., McIver, K.S., Pick, J., Zabriskie, J.B., Lombroso, P.J., Leckman, J.F., and Bibb, J.A. Identification of pyruvate kinase as an antigen associated with Tourette syndrome. J Neuroimmunol. 2006 Dec;181(1-2):165-76.

[64.] Vértessy, B.G., Bánkfalvi, D., Kovács, J., Löw, P., Lehotzky, A. and Ovádi, J., Pyruvate kinase as a destabilizing factor in vitro. Biochem. Biophys. Res. Commun. 1999 Jan 19;254(2):430-5.

[65] Miura, Y., Kano, M., Abe, K. Urano, S., Suzuki, S. and Toda, T. Age-dependent variations of cell response to oxidative stress: proteomic approach to protein expression and phosphorylation. Electrophoresis. 2005 Jul;26(14):2786-96.

[66] Cicchillitti, L., Penci, R., Di Michele, M., Filippetti, F., Rotilio, D., Donati, M.B., Scambia, G. and Ferlini, C., Proteomic characterization of cytoskeletal and mitochondrial class III beta-tubulin. Mol. Cancer Ther. 2008 Jul;7(7):2070-9.

[67] Al-Chalabi, A. and Miller, C.C. Neurofilaments and neurological disease. Bioessays. 2003 Apr;25(4):346-55.

[68] Takemura, M., Gomi, H., Colucci-Guyon, E. and Itohara, S. Protective role of phosphorylation in turnover of glial fibrilliary acidic protein in mice. J. Neurosci. 2002 Aug 15;22(16):6972-9.

[69] Allen, E., Ding, J., Wang, W., Pramanik, S., Chou, J., Yau, V. and Yang, Y. Gigaxonin-controlled degradation of the MAP1B light chain is critical to neuronal survival. Nature. 2005 Nov 10;438(7065):224-8.

[70] Bomont, P., Cavalier, L., Blondeau, F., Ben Hamida, C., Belal, S., Tazir, M., Demir, E., Topaloglu, H., Korinthenberg, R., Tüysüz, B., Landrieu, P., Hentati, F. and Koenig, M., The gene encoding gigaxonin, and new member of the cytoskeletal BTB/kelch repeat family, is mutated in giant axonal neuropathy. Nat. Genet. 200 Nov;26(3):370-4.

[71] Windisch, M., Hutter-Paier, B., Rockenstein, E., Hashimoto, M., Mallory, M. and Masliah, E. Development of a new treatement for Alzheimer's disease and Parkinson's disease using anti-aggregatory beta-synuclein-derived peptides. J. Mol. Neurosci. 2002 Aug-Oct;19(1-2):63-9.

[72] Ehrengruber, M.U., Kato, A., Inokuchi, K. and Hennou S. Homer/Vesl proteins and their role in CNS neurons. Mol. Neurobiol. 2004 Jun;29(3):213-27.

[73] Mizutani, A., Kuroda, Y., Futatsugi, A., Furuichi, T. and Mikoshiba, K. Phosphorylation of Homer3 by calcium/calmodulin-dependent kinase II regulates a coupling state of its target molecules in Purkinje cells. J. Neurosci. 2008 May 14;28(20):5369-82.

[74] Terabayashi, T., Funato, Y. and Miki, H. Dishevelled-induced phosphorylation regulates membrane localization of Par1b. Biochem. Biophys. Res. Commun. 2008 Oct 31;375(4):660-5.

[75] Klee, C.B., Hao, R. and Wang, X. Regulation of the calmodulin-stimulated protein phosphatase, calcineurin. J. Biol. Chem. 1998 May;273(22):13367-70.

[76] Stone, J.R. and Collins, T. Rapid phosphorylation of heterogeneous nuclear ribonucleoprotein C1/C2 in response to physiologic levels of hydrogen peroxide in human endothelial cells. J. Biol. Chem. 2002 May 3;277(18):15621-8.

[77] Ford, L.P., Wright, W.E. and Shay, J.W. A model for heterogeneous nuclear ribonucleoproteins in telomere and telomerase regulation. Oncogene. 2002 Jan 21;21(4):580-3.

[78] Hilfiker, S., Pieribone, V.A., Czernik, A.J., Kao, H.T., Augustine, G.J. and Greengard, P. Synapsins as regulators of neurotransmitter release. Philos. Trans. R. Soc. Lond. B. Biol. Sci. 1999 Feb 28;354(1381):269-79.

[79] Saviouk, V., Moreau, M.P., Tereshchenko, I.V. and Brzustowicz, L.M. Association of synapsin 2 with schizophrenia in families of Northern European ancestry. Schizophr. Res. 2007 Nov;96(1-3):100-11.

[80] Limmroth, V., Katsarava, Z., Liedert, B., Guehring, H., Schmitz, K., Diener, H.C. and Michel, M.C. An in vivo rat model to study calcitonin gene related peptide release following activation of the trigeminal vascular system. Pain. 2001 May;92(1-2):101-6.

[81] Edgell, C.J., BaSalamah, M.A. and Marr, H.S. Testican-1: a differentially expressed proteoglycan with protease inhibiting activities. Int. Rev. Cytol. 2004;236:101-22.

[82] Capurro, M.I., Xu, P., Shi, W., Li, F., Jia, A. and Filmus, J. Glypican-3 inhibits Hedgehog signaling during development by competing with patched for Hedgehog binding. Dev. Cell. 2008 May;14(5):700-11.

[83] Pang, Z.P., Sun, J., Rizo, J., Maximov, A. and Südhof, T.C. Genetic analysis of synaptotagmin 2 in spontaneous and Ca2+-triggered neurotransmitter release. EMBO J. 2006 May 17;25(10):2039-50. Epub 2006 Apr 27.

[84] Pang, Z.P., Melicoff, E., Padgett, D., Liu, Y., Teich, A.F., Dickey, B.F., Lin, W., Adachi, R. and Südhof, T.C. Synaptotagmin-2 is essential for survival and contributes to Ca2+ triggering of neurotransmitter release in central and neuromuscular synapses. J. Neurosci. 2006 Dec 27;26(52):13493-504.

[85] Nichols, N.R., Agolley, D., Zieba, M. and Bye, N. Glucocorticoid regulation of glial responses during hippocampal neurodegeneration and regeneration. Brain Res. Brain Res. Rev. 2005 Apr;48(2):287-301.

[86] Mitchelmore, C., Büchmann-Møller, S., Rask, L., West, M.J., Troncoso, J.C. and Jensen, N.A., NDRG2: a novel Alzheimer's disease associated protein. Neurobiol. Dis. 2004 Jun;16(1):48-58.

[87] Butler, M.H., David, C., Ochoa, G.C., Freyberg, Z., Daniell, L., Grabs, D., Cremona, O. and De Camilli, P. Amphiphysin II (SH3P9; BIN1), a member of the amphiphysin/Rvs family, is concentrated in the cortical cytomatrix of axon initial segments and nodes of ranvier in brain and around T tubules in skeletal muscle. J. Cell Biol. 1997 Jun 16;137(6):1355-67.

[88] Elliott, K., Sakamuro, D., Basu, A., Du, W., Wunner, W., Staller, P., Gaubatz, S., Zhang, H., Prochownik, E., Eilers, M. and Prendergast, G.C. Bin1 functionally interacts with Myc and inhibits cell proliferation via multiple mechanisms. Oncogene. 1999 Jun 17;18(24):3564-73.

Chapter Six

Conclusions and Future Direction

6.1 Summary and Conclusions

As a differential tool, mass spectrometry-based proteomic technologies have been applied to investigate relative changes in biomarkers resulting from a specific disease state compared to control population or to find biomarkers resulting from a specific therapy compared to a diseased and/or a control population. There are a wide variety of approaches to proteomics and each approach has its inherent advantages and disadvantages. Whether the approach is 'top-down' with intact isolated proteins or 'bottom-up' with enyzymatically digested proteins or mixtures of proteins, the experiments involved are complex.

In order to reduce this complexity, the sample preparation can be refined to isolate and prefractionate specific organelles or cellular compartments. A variety of affinity separation methods have also been employed to either enrich or deplete specific proteins or protein modifications. These latter approaches of enrichment and depletion open the possibility of introducing new biases and compromise the experimental results with either poor quantitative data or with poor specificity for the target of depletion or enrichment. The research that has been described in this dissertation has attempted to both quantify and identify changes in phosphorylation level and changes in total protein level in specific tissues without prefractionation. We have made every effort to reduce and/or eliminate both intentional and unintentional experimental bias, but it must be acknowledged that the 2D-PAGE methodology utilized for this research also has inherent biases against membrane proteins and high molecular weight proteins.

In Chapter Two, we began with the development of the analytical methods, data handling and data analysis procedures that would be utilized in all of the following

experiments. We initially began with attempts at phosphoprotein enrichment using immunoaffinity techniques, but difficulties in sample pre-treatment and concerns with the potential pitfalls of nonspecific binding associated with the technique led us to investigate the phosphoprotein-specific gel stain Pro-Q Diamond using 2D-PAGE methods. A great deal of effort was made in optimizing the conditions for isoelectric focusing to maximize both the resolution and the total mass of protein in each gel. These efforts were further refined by investigating various alcohols and zwitterionic detergents in order to reduce the method's bias against membrane proteins. With a maximized signal level, the course of development proceeded to the optimization of the phosphoprotein stain. Previously published work with the Pro-Q Diamond stain,[1-3] had shown a high background and correspondingly poor signal using the manufacturer's protocol. The staining procedure was optimized by lengthening the first destaining step in the protocol to remove excess stain from the gel matrix and reduce the background signal. The most significant achievement described in Chapter Two was the successful implementation of nanoelectrospray ionization (NSI) coupled to the FT-ICR mass spectrometer in the Analytical Proteomics Laboratory. While the optimization of sample preparation, separation and gel staining all provided marginal improvements which were difficult to quantify, the sensitivity gains of NSI were easily quantifiable and improved by an order of magnitude over the existing method and greatly improved the quality of data as a result.

Chapter Three described the application of the methods developed in Chapter Two on a model system of C2C12 myoblasts treated with hydrogen peroxide. The lack of quality results for these experiments is a major disappointment since any

phosphorylation differences observed in this model could be directly attributed to the oxidation effects of the peroxide. Much of the discussion in phosphorylation changes due to aging revolves around discussing the effects and not the causes.[4-6] The most convincing hypothesis behind the cause of differences in protein phosphorylation levels in aged compared to young subjects continues to be due to the accumulation of oxidized biomolecules.

In Chapter Four we saw the application of the phosphoproteomic methodology in a differential experiment comparing thirty four month old rat skeletal muscle against five month old rat skeletal muscle. The process of aging appears to produce a number of changes in the phosphorylation status of skeletal muscle proteins. We observed that many metabolic enzymes appear to have differential phosphorylation levels between muscle from young and old animals, with some proteins demonstrating stable and some showing differential expression levels. Overall, the phosphorylation states of these proteins in tandem with the observed levels of total protein seem to support the observation of a metabolic shift associated with sarcopenia without providing direct evidence of the cause of this shift. Several other proteins involved in various functions such as skeletal muscle function, cell cycle, maintenance, structural proteins, transporter proteins, catabolic proteins and proteins responsive to oxidative stress were also observed to be differentially phosphorylated. The activities of several of the proteins identified in this study have been demonstrated to be directly influenced by their phosphorylation state and may be worthy targets for additional attention.

Chapter Five describes a series of differential experiments comparing thirty four month old rat cerebellum against five month old rat cerebellum. Several classes of

proteins including structural, metabolic and signaling proteins were identified as differentially phosphorylated in the cerebellum and can be seen as potentially contributing to the development of cerebellar disorders in an aged populace. The chapter contains references to previous work describing the changes in activity associated with a change in phosphorylation state for several of the identified proteins.

Overall, the experiments described in this dissertation show a number of biologically relevant proteins to be differentially phosphorylated. Many of the phosphorylation differences observed in both senescent rat skeletal muscle and cerebellum have been previously investigated, which not only gives credence to the results, but also highlights the novel targets that have been generated by the research conducted here. Moreover, the previous work conducted on many of these phosphoproteins for other disease states, confirms the relevance of protein phosphorylation as a target for therapeutic intervention in age-related disorders.

6.2 Future Directions

The lack of convincing results in the form of phosphopeptidic tandem MS/MS evidence from the peroxide treated C2C12 cells proved to be a disappointment and the experiment is in the process of being modified and repeated. The importance of this experiment in establishing the effects of oxidation on phosphorylation state could potentially lead to widespread use of phosphoproteomics as an indirect method to determine novel targets for further exploration in gerontological research.

As mentioned previously, there are many different approaches within the field of proteomics and the subfield of phosphoproteomics that could be used to study the

changes in protein phosphorylation due to aging. Each individual approach has its own advantages and disadvantages, and the selection of the best approach requires an understanding of the instrumentation available and the skills of the researchers involved. One inherent difficulty found in all approaches is sample complexity. In the cerebellum study more than 3500 protein spots were evident which greatly increased the difficulty of the image analysis in our experiments. Where sample enrichment alone is not likely to greatly improve upon these results, enrichment in combination with a series of organelle and sub-cellular compartment isolations may provide the best means to improve on the results of this dissertation.

As a final note, it must be repeated that the results provided in this dissertation are a starting point, not an ending point. Each of the phosphoproteins identified as being differentially phosphorylated requires further study for changes in activity or function.

6.3 References

[1] Gannon J, Staunton L, O'Connell K, Doran P, Ohlendieck K. Phosphoproteomic analysis of aged skeletal muscle. Int J Mol Med. 2008 Jul;22(1):33-42.

[2] Hopper R.K., Carroll S., Aponte A.M., Johnson D.T., French S., Shen R.F., Witzmann F.A., Harris R.A., Balaban R.S. Mitochondrial matrix phosphoproteome: effect of extra mitochondrial calcium. Biochemistry. 2006 Feb 28;45(8):2524-36.

[3] Wang M, Xiao GG, Li N, Xie Y, Loo JA, Nel AE. Use of a fluorescent phosphoprotein dye to characterize oxidative stress-induced signaling pathway components in macrophage and epithelial cultures exposed to diesel exhaust particle chemicals. Electrophoresis. 2005 Jun;26(11):2092-108.

[4] Xu A, Narayanan N. Effects of aging on sarcoplasmic reticulum Ca2+-cycling proteins and their phosphorylation in rat myocardium. Am J Physiol. 1998 Dec;275(6 Pt 2):H2087-94.

[5] Holzer M, Holzapfel HP, Krohn K, Gertz H-J, Arendt T. Alterations in content and phosphorylation state of cytoskeletal proteins in the sciatic nerve during ageing and in Alzheimer's disease. J Neural Transm. 1999;106(7-8):743-55.

[6] Højlund K, Wrzesinski K, Larsen PM, Fey SJ, Roepstorff P, Handberg A, Dela F, Vinten J, McCormack JG, Reynet C, Beck-Nielsen H. Proteome analysis reveals phosphorylation of ATP synthase beta -subunit in human skeletal muscle and proteins with potential roles in type 2 diabetes. J Biol Chem. 2003 Mar 21;278(12):10436-42. Epub 2003 Jan 16.